Organic Geochemical Biosignatures in Alkaline Hydrothermal Ecosystems

by

Alexander Smith Bradley

A.B. Earth and Planetary Sciences
Harvard College, 1998

M.S. Geological Sciences
University of Michigan, 2001

SUBMITTED TO THE DEPARTMENT OF
EARTH ATMOSPHERIC AND PLANETARY SCIENCES
IN PARTIAL FULFILLMENT OF THE REQUIREMENTS FOR THE DEGREE OF

DOCTOR OF PHILOSOPHY IN GEOCHEMISTRY

FEBRUARY 2008

Signature of Author……
Department of Earth Atmospheric and Planetary Sciences
January 15, 2008

Certified by……....
Roger E. Summons
Professor of Geobiology
Thesis Supervisor

Accepted by……...
Maria T. Zuber
E.A. Griswold Professor of Geophysics
Head, Department of Earth Atmospheric and Planetary Sciences

THIS PAGE INTENTIONALLY LEFT BLANK

Organic Geochemical Biosignatures in Alkaline Hydrothermal Ecosystems

by

Alexander Smith Bradley

Submitted to the Department of Earth Atmospheric and Planetary Sciences
on January 15, 2007 in partial fulfillment of the
requirements for the Degree of Doctor of Philosophy in Geochemistry

ABSTRACT

The ^{13}C content of microbial products are controlled by many factors, including the ^{13}C content of the growth substrate, growth rate, the flux of carbon through various parts of the biochemical network, and the isotopic fractionation imposed by the enzymes of that network. We analyzed the ^{13}C content of products of the methanogen *Methanosarcina barkeri* and found that fractionation varied strongly with substrate availability.

These results inform our analysis of methanogen lipids from carbonates of the Lost City Hydrothermal Field. This ultramafic ecosystem produces methane highly enriched in ^{13}C relative to most biotic methane. We find that the ^{13}C enrichment in methanogen lipids is even stronger – demonstrating that the Methanosarcinales in active vents are methane producers, and that they are likely carbon-limited. Archaea in other parts of the vent field at Lost City are methanotrophs. The application of lipid biomarkers helps unravel the multiple biological and abiotic sources of methane at Lost City.

Closer examination of lipids from Lost City shows that most are ether-type glycolipids. The dominance of glycolipids over phospholipids may be a phosphorus-conservation strategy in waters that are likely phosphorus-poor. Ether core lipids are similar to those produced by sulfate-reducing bacteria in environments where methane is oxidized anaerobically. Insoluble residues in Lost City carbonates contain proteinaceous organic material and have end-member $\delta^{15}N$ values near 0‰, suggesting active nitrogen fixation is occurring.

Biomass and lipids from Yellowstone hot springs also showed surprising enrichments in ^{13}C. The common factor is high pH; unusual ^{13}C enrichment may be common in alkaline hydrothermal systems.

Organisms in terrestrial and marine alkaline hydrothermal systems produced organic carbon with $\delta^{13}C$ outside of the usual biological range. This informs our application of carbon isotopes as biosignatures, and suggests that biological and abiotic organic carbon may sometimes have ^{13}C contents that are indistinguishable.

Thesis Supervisor: Roger E. Summons
Title: Professor of Geobiology

THIS PAGE INTENTIONALLY LEFT BLANK

Acknowledgements

Thoughts are but dreams till their effects be tried

A Ph.D. thesis, like any creative endeavor, is directed by the author but is executed by a large supporting cast. Without the commitment and generous support of my extended community of coworkers, advisors, family, and friends, this work would have remained an unrealized aspiration. Thank you.

The foremost thanks go to my advisor, Roger Summons. Roger's steadfast encouragement and assistance are the foundation on which my work of the last five and a half years has rested. His infectious enthusiasm for new ideas and directions has given me the confidence to undertake a research career. He will remain a valued collaborator.

The generosity of John Hayes with his time, assistance, criticism, and friendship has been an inspiration. John's eager anticipation of new results, clear insight, and sound advice, have all been tremendously helpful. I am grateful for his backing, for the warm welcome he extended to me at Woods Hole, and for the cold bucket of seawater he dunked on me after my first dive in *Alvin*.

Thanks also go to my other two committee members, Dan Rothman and Ed Boyle, for their help through the thesis defense process. Funding for much of my work at MIT came from a NASA Graduate Student Research Program fellowship. Linda Jahnke and Tori Hoehler were my benefactors at NASA, and both contributed financially and intellectually throughout the process. In particular, Linda opened her lab at NASA Ames to me on several occasions and taught me laboratory techniques that served me well. The support is most appreciated.

A variety of people provided me with the opportunity to do field work at hydrothermal sites. Deb Kelley made space available to me on the *R/V Atlantis* in 2003 and invited me to participate in the 'virtual' cruise to Lost City in 2005. Everett Shock encouraged me to join his team for several summers in Yellowstone, and the work and interaction there was enjoyable and instructive. Kathleen Londry and her students were essential collaborators in the experimental work on isotope fractionation in *Methanosarcina*, and got that project off the ground and running.

The geochemical work in this thesis can be understood only with an awareness of microbiology. Geobiology merges these fields, and my appreciation for this multidisciplinary approach was sparked on Catalina Island at the Agouron Geobiology course. Will Berelson, Frank Corsetti, and all the instructors there perform a unique and valuable service to our discipline.

I've been fortunate to have a number of outstanding coworkers at MIT and beyond

who have provided everything from advice on writing, to late-night help with instruments, to ice cream. Research demands a fire in the belly. It takes long hours and patience. It commands passion and exacts continual sweat from both hands. My coworkers at MIT have these traits: Gordon Love, Emma Grosjean, Yanek Hebting, D'Arcy Meyer-Dombard, Dave Fike, Amy Kelly, Sara Lincoln, Jake Waldbauer, James Saenz, Augusta Dibbell, Julie Maresca, and Neal Gupta have all contributed to any success or insight that might be found in these pages. Alla Skorokhod, Rick Kayser, and Carolyn Colonero provided logistical support in the (thankfully) now-demised E34 and in our new space in E25. Beyond MIT, generous advice was supplied by Alison Olcott, Matt Schrenk, Billy Brazelton, Steven Hallam, Jan Amend, Tom McCollom, Marcus Elvert, and Jaap Sinninghe Damsté. Peter Girguis was extremely helpful in discussing Lost City and archaeal methanotrophy. Susy Cote has been a devoted friend and a faithful confidant. Kai Hinrichs kindly made his LC-MS available, and Al Gagnon helped with TOC analyses. Sean Sylva and Helen Fredricks not only provided exceptionally skilled technical support, but also taught me the importance of understanding the theoretical and practical aspects of gas and liquid chromatography and mass-spectrometry. These skills were among the most important I have learned.

The most important thanks are for my family and close friends, who kept me grounded over this long process. My appreciation for them is the most deeply experienced and perhaps most poorly expressed. Mom, Dad, Andrew, Ben, Sam, Dana, and especially Marianna: Thank you. You have never wavered. My friends and extended family all have my gratitude, including two who are gone. Tadeusz Wellenger and Al Bradley turned dust into gold. Their inspiration will be remembered.

A final word of thanks: Dave Roberts, thank you for stealing second base!

Table of Contents

List of Figures and Tables

Chapter 5

Figures

Tables

Chapter 6

Figures

Tables

Chapter 7

Figures

Tables

Chapter 1

Introduction

This thesis examines the organic geochemical signatures of organisms inhabiting alkaline hydrothermal ecosystems. It focuses on two environments: a marine system driven by serpentinization – the Lost City Hydrothermal Field, and a terrestrial system in Yellowstone National Park. In comparing these two systems a few common patterns emerge. Archaea are dominant members of both microbial communities, but their phylogenetic affinities and metabolic strategies vastly differ. In both systems bacteria synthesize ether lipids. Microbes may be fixing nitrogen in each of the systems. Perhaps most significantly, each system contains biologically-derived organic carbon that is surprisingly enriched in ^{13}C.

At Lost City methane is being produced biologically, and probably also abiotically. Methanogenesis proceeds without any electron acceptors derived from oxygenic photosynthesis, and so in some ways Lost City may be a good analogue for an Archaean seafloor biosphere. Disentangling the complex methane production here will be important to students of the Archaean.

Much attention has been given to the fact that some abiotic reactions, particularly in experimental hydrothermal systems, produce abiotic carbon that is depleted by 25‰ to 60‰ relative to its source. This result confounds the use of ^{13}C-depleted carbon as an isotope biosignature. The concept of an isotope biosignature is further damaged by the work presented herein, which demonstrates that organic carbon may be biologically derived, yet have $\delta^{13}C$ near 0‰ vs. VPDB. This may be particularly true in the very types of environments often considered analogues for early Earth or extraterrestrial ecosystems. An important result of this study is that ranges of $\delta^{13}C$ for biological and abiotic organic carbon overlap: identification of the source of organic carbon must come from other approaches.

1.1 Alkaline hydrothermal systems and early life on Earth

Hydrothermal environments require three ingredients for their existence: heat, water, and rock. They may be expected anywhere these three ingredients are mixed, and hydrothermal systems are widespread along the mid-ocean ridges (Kelley et al., 2002; Wilcock et al., 2004), at volcanic hotspots such as Iceland and Yellowstone (Brock, 1978). The first hydrothermal systems likely appeared on Earth as soon as the surface was cool enough to allow liquid water. Their presence on other terrestrial planets such as Mars (Bock and Goode, 1996) and Europa (Lowell and DuBose, 2005) is a subject of extensive speculation.

As fluids are heated at depth, water-rock interaction alters their chemistry and can significantly modify the concentrations of dissolved species contained within. Ever-changing fluid chemistry, temperature, and kinetic barriers to reactions ensure that a hydrothermal fluid is rarely in chemical equilibrium. In some cases kinetic barriers to reactions may be overcome by mineral catalysts. In other cases biology supplies enzymes to take advantage of the thermodynamic gradient. Upon emergence at the surface, hydrothermal water mixes with cool surface fluids and the resultant disequilibrium may drive a new set of reactions, with or without the catalysis of biologically supplied enzymes.

Thermodynamic modeling has suggested that spontaneous reactions driven by the mixture of hydrothermal fluid and seawater can include the synthesis of organic acids, alcohols, and ketones (Shock, 1996; Shock and Schulte, 1998), amino acids (Keefe et al., 1995), and the constituents of nucleotides (Holm et al., 2006). The potential for abiotic synthesis of organic compounds in these settings has advanced the idea hydrothermal settings are candidate locations for the origin of life (Russell, 2003; Shock, 1996; Skophammer et al., 2007).

Alkaline hydrothermal systems are particularly interesting in that regard. Under warm (~100 ºC) alkaline conditions, amino acids can be converted to peptides on an iron-nickel catalyst (Huber and Wachtershauser, 1998). Addition of the mineral brucite

– a mineral commonly found in alkaline ultramafic hydrothermal systems – allows a continuous cycle of peptide formation and recycling (Huber et al., 2003). Gradients in pH under similar alkaline conditions can drive the formation of lipid vesicles (Hanczyc et al., 2003) – perhaps from fatty acids that had been synthesized abiotically (Shock and Schulte, 1998). Brucite may also play a role in scavenging phosphate and borate from seawater, both of which can contribute to the abiotic synthesis of nucleotides (Holm et al., 2006; Ricardo et al., 2004).

The universal tree of life has been cited in support of a hydrothermal origin of life. In universal phylogenies based on sequences of 16S small-subunit DNA from across the three domains of life, thermophiles occupy the deepest branches (Barns et al., 1996; Stetter, 1996). Other approaches to tree construction result in a different topology for the universal phylogeny, but preserve the notion of a thermophilic universal ancestor. For example Ciccarelli et al. (2006) use a concatenated gene set of 31 genes, mainly encoding for ribosomal proteins, with orthologs occurring in each of the 191 fully sequenced organisms present in their database. This produces a tree with thermophilic Firmicutes and archaea near the root. However, the very existence of a universal tree of life is controversial and subject to challenge (Doolittle and Bapteste, 2007). Furthermore, even if a valid universal tree of life is indeed recoverable through molecular methods it will inform our understanding of the last universal common ancestor, and not necessarily the first common ancestor at the origin of life. One plausible explanation for the position of thermophiles on the tree is that the Hadean late heavy bombardment created an evolutionary bottleneck through which only thermophiles survived (Nisbet and Sleep, 2001). In either case, investigating the organisms inhabiting these settings has the potential, at least, to shed some light on evolutionary history.

1.2. Serpentinization – a source of H_2, CH_4 and Ni

A large part of this thesis focuses on an environment in which chemistry is

controlled by serpentinization. Serpentinization is the hydration of olivine to a mineral of the serpentine group plus brucite and magnetite (Schroeder et al., 2002). It produces highly alkaline fluids found at the Lost City Hydrothermal Field. Three reactions describe the major pathways of serpentinization below 500˚C (Schroeder et al., 2002):

$$\underset{\text{olivine}}{6(Mg,Fe)_2SiO_4} + 7H_2O \rightarrow \underset{\text{serpentine}}{3(Mg,Fe)_3Si_2O_5(OH)_4} + \underset{\text{magnetite}}{Fe_3O_4} + H_2$$

$$\underset{\text{olivine}}{4(Mg,Fe)_2SiO_4} + 6H_2O \rightarrow \underset{\text{serpentine}}{2(Mg,Fe)_3Si_2O_5(OH)_4} + \underset{\text{brucite}}{2Mg(OH)_2} + H_2$$

$$\underset{\text{olivine}}{(Mg,Fe)_2SiO_4} + \underset{\text{orthopyroxene}}{(Mg,Fe)SiO_3} + 2H_2O \rightarrow \underset{\text{serpentine}}{(Mg,Fe)_3Si_2O_5(OH)_4} + H_2$$

These hydrogen produced by these reactions accumulates to millimolar levels. Additionally, under conditions of serpentinization pyroxenes become unstable and decompose:

$$\underset{\text{diopside}}{3CaMgSi_2O6} + 6H^+ \rightarrow \underset{\text{serpentine}}{Mg_3Si_2O_5(OH)_4} + 3Ca^+ + H_2O + 4SiO_2(aq)$$

These reactions produce exceptionally reducing fluids with enhanced calcium ion concentrations and high pH. The conditions produced are reducing enough that they may stabilize nickel-iron alloys such as awaruite ($FeNi_3$), that would decompose under more oxidizing conditions (Sleep et al., 2004). A detailed description of serpentinization reactions is given by Frost and Beard (2007). Serpentinization reactions are exothermic and in principle could give rise to a warm, alkaline, reducing hydrothermal fluid without a magmatic heat source (Lowell and Rona, 2002).

Serpentinization has attracted the attention of many geochemists because the abundant H_2 it produces is a biologically attractive electron donor, and because the magnetite and nickel-iron alloys produced by the reaction can catalyze the abiotic formation of methane, and perhaps other organic compounds in laboratory settings (Foustoukos and Seyfried, 2004; Horita and Berndt, 1999; McCollom and Seewald, 2001; McCollom and Seewald, 2007). The abiotic organic carbon produced in these experiments can have a ^{13}C content with δ values in the range that is usually typical of biological organic carbon (Horita and Berndt, 1999; McCollom and Seewald, 2006). This result restricts the use of

^{13}C-deletion in organic carbon as an isotope biosignature in ancient rocks or elsewhere in the solar system.

Serpentinization of peridotite is rare on Earth today, occurring only where mantle rock is exposed at the Earth's surface in ophiolites or through faulting and mantle uplift at sites like the Atlantis massif (Blackman et al., 2002). However, ultramafic rock would likely have been common on the Archean seafloor (Nisbet and Fowler, 2004), and serpentinization reactions would have been correspondingly more important. The hydrogen and methane supplied either abiotically by serpentinization, or biologically by the microbial communities inhabiting serpentinizing fluids, would have contributed to the Archaean atmosphere and biosphere. Constraints on the concentrations of hydrogen (Catling, 2006; Tian et al., 2006; Tian et al., 2005) and methane (Pavlov et al., 2000) in the Archaean atmosphere are highly contentious. The source of methane in the Archaean atmosphere has been equally contentious (Sherwood Lollar and McCollom, 2006; Ueno et al., 2006a; Ueno et al., 2006b). Understanding the sources and quantities of hydrogen and methane supplied by hydrothermal environments should contribute to the resolution of these controversies.

In the context of alkaline hydrothermal settings as possible locations for the orgin or early evolution of life, it is interesting to note the importance of the availability of nickel in ultramafic hydrothermal settings. As previously mentioned, nickel alloys can catalyze the abiotic synthesis of methane, but nickel is also essential for biological methanogenesis. Carbon monoxide dehyrogenase and hydrogenase, both key enzymes in methanogenesis are nickel dependent in many methangogens. Perhaps even more importantly, the key final step methanogenesis - in which energy is conserved and methane produced - is the activity of methyl-coenzyme M reductase. This enzyme is absolutely dependent on coenzyme F_{430}, the only nickel tetrapyrrole known in nature, as a cofactor. F_{430} is also the most reduced tetrapyrrole known, containing only five double bonds (Thauer, 1998). Methanogens are absolutely dependent on this nickel enzyme. In archaeal methanotrophs where this enzyme comprises 7% the total extractable protein, the dependence appears even greater (Krueger et

al., 2003). The relationship between apparent requirement for nickel in both biological and abiotic methanogenesis remains unexplored, but opens intriguing evolutionary questions. In this thesis we focus intensely on the biological signatures of methanogens, both in laboratory (Chapter 2) and field (Chapter 3) settings.

1.3 The Lost City Hydrothermal Field

The Lost City hydrothermal field is the best known example of a low-temperature hydrothermal system driven by serpentinization reactions (Kelley et al., 2001; Kelley et al., 2005). It is located on the ultramafic Atlantis Massif at 30˚N near the inside corner intersection of the Mid-Atlantic Ridge and the left-lateral Atlantic Transform Fault (Figure 1-1, Figure 1-2). The massif is approximately 15 km west of the Mid-Atlantic Ridge, and magnetic anomaly patterns suggest the local crust is 1.5 Mya (Kelley et al., 2001).

Topographic highs are common at inside corners of transform offsets along the Mid-Atlantic Ridge, and are likely to be the result of low-angle detachment faulting between the lower crust and upper mantle (Cann et al., 1997). The Atlantis Massif is interpreted as mantle material exhumed by an associated detachment fault. It is ~15 km across and bounded on its southern face by an escarpment with ~3,800 m of relief relative to the Atlantis Fracture Zone. (Schroeder et al., 2002) calculate the volume of peridotite of the Atlantis massif as ~30 km^3. The summit of the massif at ~700 m water depth consists of foliated serpentinites, overlain by carbonate cemented sedimentary breccias and a well lithified, bedded carbonate. The breccias include hydrothermal and bedded carbonate material, and are overlain with pelagic ooze. (Figure 1-3**)**

The LCHF rests on a terrace of the Atlantis massif at 750-850 m water depth and is underlain by altered mafic and ultramafic rocks. The field consists of active and inactive hydrothermal structures, the largest of which is 60 m tall (Kelley et al., 2005). Carbonate chimneys are largely composed of aragonite and brucite, and are precipitatied upon the admixture of alkaline vent water (up to 30 mM Ca^{2+}, pH 9-11) with ambient seawater

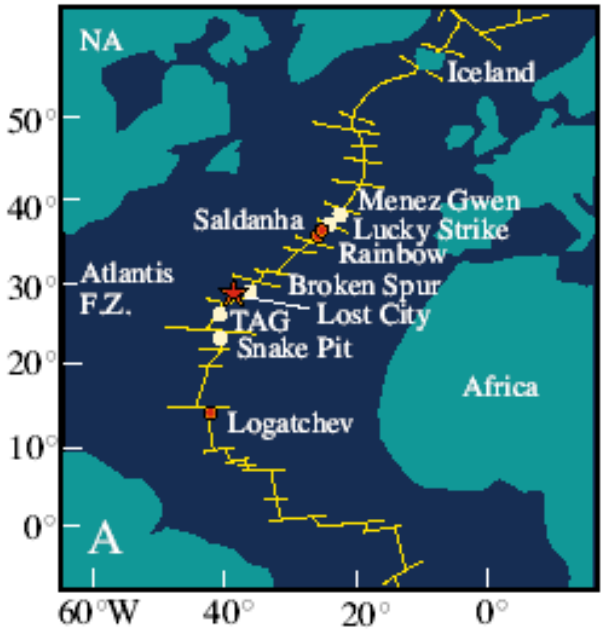

Figure 1-1: Location of Lost City and other vent fields along the Mid-Atlantic Ridge

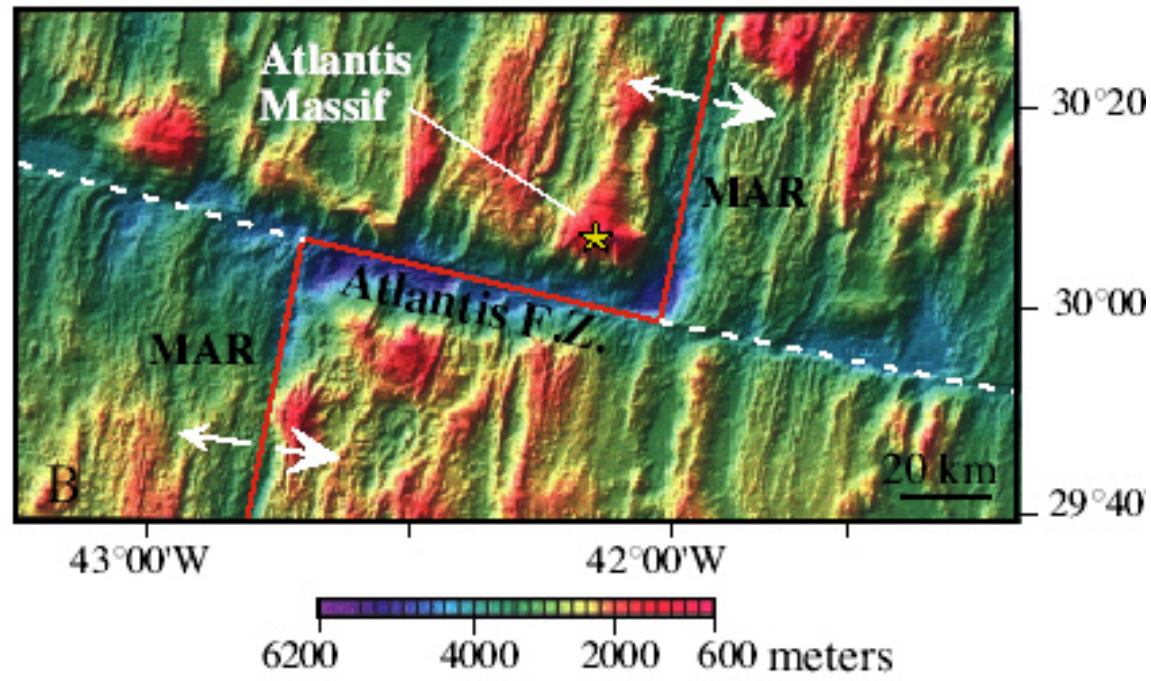

Figure 1-2: Location of the Atlantis Massif relative to Atlantis Fracture Zone and Mid-Atlantic Ridge

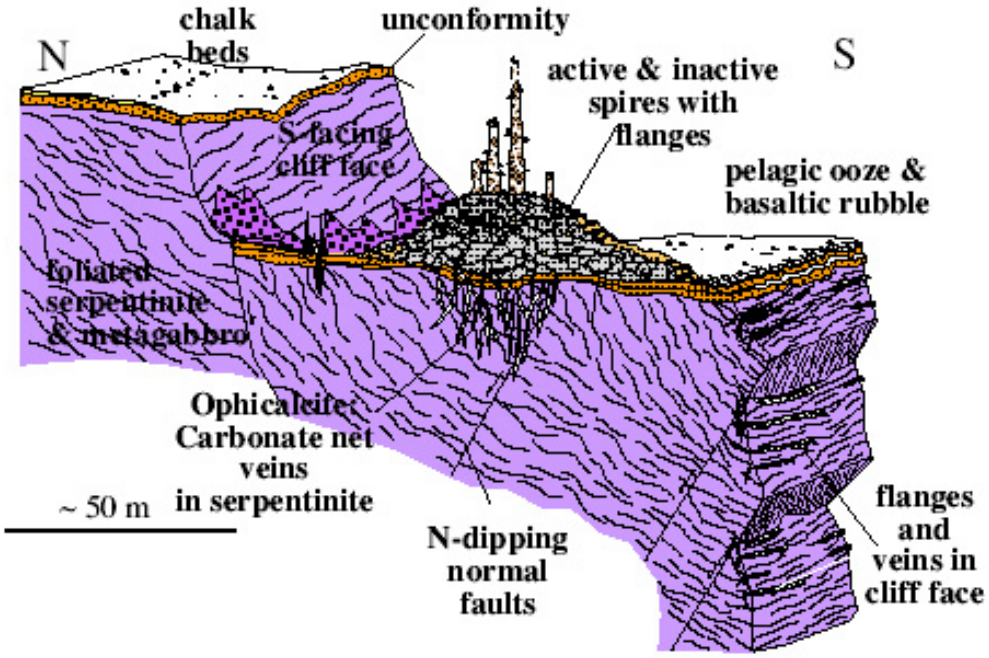

Figure 1-3: Schematic of the Lost City Hydrothermal Field on the flank of the Atlantis Massif

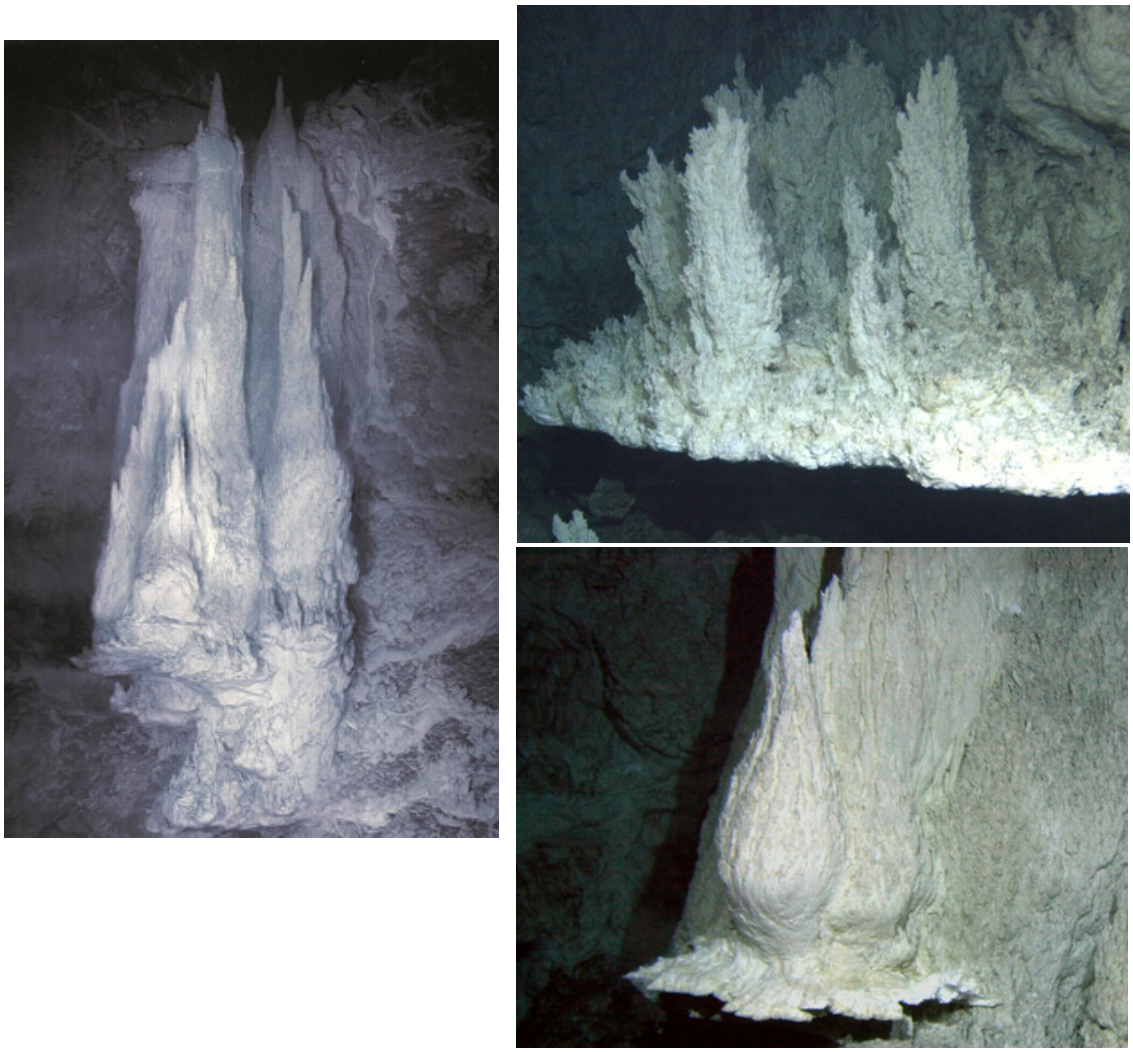

Figure 1-4: Active carbonate towers precipitating at the Lost City Hydrothermal Field

(Ludwig et al., 2006). Active venting in most cases occurs at the tops of these chimneys where fresh white aragonite is being precipitated as delicate "fingers" and dendritic growth (Kelley et al., 2001; Kelley et al., 2005; Ludwig et al., 2006). Representative structures are shown in Figure 1-4.

Inactive chimneys are composed of aragonite and calcite, with or without brucite (Fruh-Green et al., 2003) and range widely in porosity, friability and texture, although they are commonly more consolidated than active structures. The differences between active and inactive structures may be largely attributed to the conversion of aragonite to calcite, dissolution of brucite, and precipitation of new calcite in the inactive structures by reaction with seawater. The interpretation of recrystallization of carbonate in inactive structures is supported by $^{87}Sr/^{86}Sr$ values, which in active chimneys are indicative of basement rock values, but in inactive chimneys reflects the $^{87}Sr/^{86}Sr$ value of seawater (Fruh-Green et al., 2003). The hydrothermal structures overlie and postdate the cap carbonate, and lack pelagic cover, suggesting that they are relatively young (Kelley et al., 2001). Accelerator mass spectrometry (AMS) ^{14}C age-dating of carbonate vent structure suggests that they range in age from modern to a minimum of 25 ky (Fruh-Green et al., 2003). Vent-fluid precipitated carbonate is also found in abundant veins in the peridotite and as breccia and fracture infillings. AMS ^{14}C age-dating of these carbonates suggest that they are up to 32 ky.

At Lost City the possibility that exothermic serpentinization reactions are supplying the heat to vent fluids is excluded by heat balance models (Allen and Seyfried, 2004). By examination of the salinity of vent fluids, this study demonstrated that the ratio of water to rock interaction is high, and that heat supplied by hydration of olivine insufficient to reach the temperatures measured in vent fluids. Heat supplied by a steep geothermal gradient or a magmatic source is required. This finding is important when considering the kinetic barriers that must be overcome for the generation of abiotic methane, and the utility of Lost City as an analog for ultramafic Archaean seafloor.

Figure 1-5: Bison Spring, Lower Geyser Basin, Yellowstone National Park

1.4 Yellowstone

Terrestrial alkaline hot springs in Yellowstone National Park are chemically distinct from the serpentinite-hosted ecosystem at Lost City. Alkalinity in these systems is carbonate-buffered, but and pH varies between 7.5 and 9. Yellowstone also contains sulfuric acid springs with pH between 2 and 4, and this thesis presents a small amount of data on these as well. We focus our study here on a spring in the Lower Geyser Basin, unofficially dubbed 'Bison Pool' (Figure 1-5).

There are vast chemical, environmental, and microbial differences between the Lower Geyser Basin of Yellowstone and the hydrothermal chimneys of Lost City. We investigated the ecosystem at Yellowstone to determine if common organic geochemical signatures of alkaline hydrothermal settings would emerge from two very different environments.

1.5 Thesis outline

Chapter 2 presents the results of experiments designed to understand the extent of carbon isotope fractionation in a methanogen *Methanosarcina barkeri*. These experiments attempted to constrain the how isotope fractionation would change as a function of substrate availability. These data were useful in interpreting the results of **Chapter 3**, where we examined the ^{13}C content of lipids from carbonate chimneys at the Lost City Hydrothermal Field. These data suggest that the ecosystem at this location is dominated by methanogenic archaea, but that these archaea are carbon-limited, resulting in a surprising enrichment in ^{13}C in their lipids. In **Chapter 4** we attempt to do decipher the multiple origins of methane at Lost City. Serpentinization in this ecosystem is driving abiotic methane production at high temperature, while the activity of methanogenic archaea is supplying methane in lower temperature environments. At least some of the archaea at Lost City are consuming methane, and the ^{13}C content of their lipids suggests this methane may derive from a source that has not yet been identified. **Chapter 5** presents detailed data on the structure of bacterial and archaeal diether lipids. Notably, most of the lipids at Lost

City are glycolipids. We suggest that this may be a strategy for conserving phosphorus, and we note that there are unusual similarities between the archaeal and bacterial lipids. These may have evolutionary relevance. **Chapter 6** presents the results of analysis of insoluble residues from Lost City carbonates. This filament-like debris appears to be largely derived from protein, and contains enough organic nitrogen to measure its ^{15}N content. The values of $\delta^{15}N$ imply that active nitrogen fixation is occurring in the carbonate towers. In **Chapter 7** we present data regarding the ^{13}C and ^{15}N contents of pink streamer communities in Yellowstone National Park, and find that these alkaline hydrothermal environments also produce organic carbon unusually enriched in ^{13}C.

1.6 References

Allen, D.E., Seyfried, W.E., 2004. Serpentinization and heat generation: Constraints from Lost City and Rainbow hydrothermal systems. Geochimica Et Cosmochimica Acta 68(6), 1347-1354.

Barns, S.M., Delwiche, C.F., Palmer, J.D., Pace, N.R., 1996. Perspectives on archaeal diversity, thermophily and monophyly from environmental rRNA sequences. Proceedings of the National Academy of Sciences of the United States of America 93(17), 9188-9193.

Blackman, D.K., Karson, J.A., Kelley, D.S., Cann, J.R., Fruh-Green, G.L., Gee, J.S., Hurst, S.D., John, B.E., Morgan, J., Nooner, S.L., Ross, D.K., Schroeder, T.J., Williams, E.A., 2002. Geology of the Atlantis Massif (Mid-Atlantic Ridge, 30. N): Implications for the evolution of an ultramafic oceanic core complex. Marine Geophysical Researches 23, 443-469.

Bock, G.R., Goode, J.A., 1996. Evolution of hydrothermal ecosystems on Earth (and Mars?), pp. 334. Wiley, Chichester.

Brock, T.D., 1978. *Thermophilic Microorganisms and Life at High Temperatures*. Springer-Verlag, New York.

Cann, J.R., Blackman, D.K., Smith, D.K., McAllister, E., Janssen, B., Mello, S., Avgerinos, E., Pascoe, A.R., Escartin, J., 1997. Corrugated slip surfaces formed at ridge-transform intersections on the Mid-Atlantic Ridge. Nature (London) 385(6614), 329-332.

Catling, D.C., 2006. Comment on “A hydrogen-rich early Earth atmosphere”. Science 311(5757), 38; author reply 38.

Ciccarelli, F., D., Doerks, T., von Mering, C., Creevey Christopher, J., Snel, B., Bork, P., 2006. Toward automatic reconstruction of a highly resolved tree of life. Science 311(5765), 1283-7.

Doolittle, W.F., Bapteste, E., 2007. Pattern pluralism and the tree of life hypothesis. Proceedings of the National Academy of Sciences of the United States of America 104(7), 2043-2049.

Foustoukos, D.I., Seyfried, W.E., Jr., 2004. Hydrocarbons in hydrothermal vent fluids: The role of chromium-bearing catalysts. Science (Washington, DC, United States) 304(5673), 1002-1005.

Frost, B.R., Beard, J.S., 2007. On silica activity and serpentinization. Journal of Petrology 48(7), 1351-1368.

Fruh-Green, G.L., Kelley, D.S., Bernasconi, S.M., Karson, J.A., Ludwig, K.A., Butterfield, D.A., Boschi, C., Proskurowski, G., 2003. 30,000 years of hydrothermal activity at the Lost City vent field. Science 301(5632), 495-498.

Hanczyc, M.M., Fujikawa, S.M., Szostak, J.W., 2003. Experimental Models of Primitive Cellular Compartments: Encapsulation, Growth, and Division. Science 302, 618-622.

Holm, N.G., Dumont, M., Ivarsson, M., Konn, C., 2006. Alkaline fluid circulation in ultramafic rocks and formation of nucleotide constituents: a hypothesis. Geochemical Transactions 7, 1-7.

Horita, J., Berndt, M.E., 1999. Abiogenic Methane Formation and Isotopic Fractionation Under Hydrothermal Conditions. Science 285, 1055-1057.

Huber, C., Eisenreich, W., Hecht, S., Wachtershauser, G., 2003. A possible primordial peptide cycle. Science 301(5635), 938-40.

Huber, C., Wachtershauser, G., 1998. Peptides by activation of amino acids with CO on (Ni,Fe)S surfaces: implications for the origin of life. Science 281(5377), 670-2.

Keefe, A.D., Miller, S.L., McDonald, G., Bada, J., 1995. Investigation of the prebiotic synthesis of amino acids and RNA bases from CO2 using FeS/H2S as a reducing agent. Proceedings of the National Academy of Sciences of the United States of America 92(25), 11904-6.

Kelley, D.S., Baross, J.A., Delaney, J.R., 2002. Volcanoes, fluids, and life at mid-ocean ridge spreading centers. Annual Review of Earth and Planetary Sciences 30, 385-491, 2 plate.

Kelley, D.S., Karson, J.A., Blackman, D.K., Fruh-Green, G.L., Butterfield, D.A., Lilley, M.D., Olson, E.J., Schrenk, M.O., Roe, K.K., Lebon, G.T., Rivizzigno, P., 2001. An off-axis hydrothermal vent field near the Mid-Atlantic Ridge at 30 degrees N. Nature 412(6843), 145-149.

Kelley, D.S., Karson, J.A., Fruh-Green, G.L., Yoerger, D.R., Shank, T.M., Butterfield, D.A., Hayes, J.M., Schrenk, M.O., Olson, E.J., Proskurowski, G., Jakuba, M., Bradley, A., Larson, B., Ludwig, K., Glickson, D., Buckman, K., Bradley, A.S., Brazelton, W.J., Roe, K., Elend, M.J., Delacour, A., Bernasconi, S.M., Lilley, M.D., Baross, J.A., Summons, R.E., Sylva, S.P., 2005. A Serpentinite-Hosted Ecosystem: The Lost City Hydrothermal Field. Science 307(5714), 1428-1434.

Krueger, M., Meyerdierks, A., Gloeckner, F.O., Amann, R., Widdel, F., Kube, M., Reinhardt, R., Kahnt, J., Boecher, R., Thauer, R.K., Shima, S., 2003. A conspicuous nickel protein in microbial mats that oxidize methane anaerobically. Nature (London, United Kingdom) 426(6968), 878-881.

Lowell, R.P., DuBose, M., 2005. Hydrothermal systems on Europa. Geophysical Research Letters 32, LB05202.

Lowell, R.P., Rona, P.A., 2002. Seafloor hydrothermal systems driven by the serpentinization of peridotite. Geophysical Research Letters 29(11), -.

Ludwig, K.A., Kelley, D.S., Butterfield, D.A., Nelson, B.K., Frueh-Green, G., 2006. Formation and evolution of carbonate chimneys at the Lost City Hydrothermal Field. Geochimica et Cosmochimica Acta 70(14), 3625-3645.

McCollom, T.M., Seewald, J.S., 2001. A reassessment of the potential for reduction of dissolved CO2 to hydrocarbons during serpentinization of olivine. Geochimica et Cosmochimica Acta 65(21), 3769-3778.

McCollom, T.M., Seewald, J.S., 2006. Carbon isotope composition of organic compounds produced by abiotic synthesis under hydrothermal conditions. Earth and Planetary Science Letters 243(1-2), 74-84.

McCollom, T.M., Seewald, J.S., 2007. Abiotic Synthesis of Organic Compounds in Deep-Sea Hydrothermal Environments. Chemical Reviews (Washington, DC, United States) 107(2), 382-401.

Nisbet, E.G., Fowler, C.M.R., 2004. The early history of life. In: W.H. Schlesinger (Ed.), *Biogeochemistry 8*, *Treatise on Geochemistry*, pp. 1-40. Elsevier, Oxford.

Nisbet, E.G., Sleep, N.H., 2001. The habitat and nature of early life. Nature 409(6823), 1083-1091.

Pavlov, A.A., Kasting, J.F., Brown, L.L., Rages, K.A., Freedman, R., 2000. Greenhouse warming by CH4 in the atmosphere of early Earth. Journal of Geophysical Research, [Planets] 105(E5), 11981-11990.

Ricardo, A., Carrigan, M.A., Olcott, A.N., Benner, S.A., 2004. Borate minerals stabilize ribose. Science (Washington, DC, United States) 303(5655), 196.

Russell, M.J., 2003. The importance of being alkaline. Science 302, 580-581.

Schroeder, T., John, B., Frost, B.R., 2002. Geologic implications of seawater circulation through peridotite exposed at slow-spreading mid-ocean ridges. Geology 30(4), 367-370.

Sherwood Lollar, B., McCollom, T.M., 2006. Biosignatures and abiotic constraints on early life. Nature (London, United Kingdom) 444(7121), E18.

Shock, E.L., 1996. Hydrothermal systems as environments for the emergence of life. In: G.R. Bock, J.A. Goode (Eds.), *Evolution of hydrothermal ecosystems on Earth (and Mars?)*, pp. 40-60. Wiley, Chichester.

Shock, E.L., Schulte, M.D., 1998. Organic synthesis during fluid mixing in hydrothermal systems. Journal of Geophysical Research, [Planets] 103(E12), 28513-28527.

Skophammer, R.G., Servin, J.A., Herbold, C.W., Lake, J.A., 2007. Evidence for a Gram Positive, Eubacterial Root of the Tree of Life. Mol Biol Evol, msm096.

Sleep, N.H., Meibom, A., Fridriksson, T., Coleman, R.G., Bird, D.K., 2004. H2-rich fluids from serpentinization: geochemical and biotic implications. Proceedings of the National Academy of Sciences of the United States of America 101(35), 12818-23.

Stetter, K.O., 1996. Hyperthermophiles in the history of life. In: G. Bock, J. Goode (Eds.), *Evolution of hydrothermal ecosystems on Earth (and Mars?)*, pp. 1-18. Wiley, Chichester.

Thauer, R.K., 1998. Biochemistry of methanogenesis: a tribute to Marjory Stephenson. Microbiology 144, 2377-2406.

Tian, F., Toon, O.B., Pavlov, A.A., 2006. Response to Comment on “A Hydrogen-Rich Early Earth Atmosphere”. Science (Washington, DC, United States) 311(5757), 38.

Tian, F., Toon, O.B., Pavlov, A.A., De Sterck, H., 2005. A Hydrogen-Rich Early Earth Atmosphere. Science 308(5724), 1014-1017.

Ueno, Y., Yamada, K., Yoshida, N., Maruyama, S., Isozaki, Y., 2006a. Biosignatures and abiotic constraints on early life (Reply). Nature (London, United Kingdom) 444(7121), E18-E19.

Ueno, Y., Yamada, K., Yoshida, N., Maruyama, S., Isozaki, Y., 2006b. Evidence from fluid inclusions for microbial methanogenesis in the early Archaean era. Nature 440(7083), 516-9.

Wilcock, W.S.D., DeLong, E.F., Kelley, D.S., Baross, J.A., Cary, S.C., 2004. The Subseafloor Biosphere at Mid-Ocean Ridges *Geophysical Monograph 144*, pp. 399. AGU Books, Washington D.C.

Chapter 2

Stable carbon isotope fractionation between substrates and products of *Methanosarcina barkeri*

Abstract

Stable carbon isotope ratios are an important tool for understanding methanogenesis in the environment. When applied to biological methanogenesis, interpretation of carbon isotope ratios requires a thorough understanding of how the availability of different substrates affects the eventual $\delta^{13}C$ of methane, biomass and lipids. *Methanosarcina barkeri* was grown on four substrates: methanol, trimethylamine (TMA), acetate, and H_2/CO_2, under variable conditions in which the substrate was either present in excess or limited in availability. The extent of isotopic fractionation between the carbon substrate and the products of *M. barkeri* was dependent on the substrate type and availability.

Growth on unlimited substrate resulted in a range of observed isotope fractionation, with growth on methanol yielding methane, biomass, and lipids most depleted in ^{13}C relative to substrate, and growth on acetate yielding the least depleted products. Autotrophic fractionations were intermediate. Substrate limited growth afforded smaller depletions in ^{13}C on all substrates.

There were large differences in the $\delta^{13}C$ among the *M. barkeri* lipids produced within each experiment, with the notable exception of growth on acetate. The ^{13}C content of lipids was generally well correlated with that of biomass, with archaeol showing the strongest relationship. The ^{13}C content of individual lipids varied with substrate availability in some cases, but did not show patterns that could be used to identify the growth substrate of methanogens in natural environments.

2.1. Introduction

Methane is an important component of the Earth's carbon cycle, not least because of its role as a greenhouse gas. Despite this, there is still insufficient quantitative understanding of the various sources of methane to the atmosphere and hydrosphere. These include abiotic CO_2 reduction, thermogenic cracking of hydrocarbons, and microbial production by methanogens. Biological methanogenesis is carried out by a subset of Euryarchaeota, which use a distinct biochemical pathway to transform CO_2 or organic compounds to biomass, energy, and methane (Conrad, 2005; Thauer, 1998; Whiticar, 1999).

Stable isotopes can be employed as tracers of methane through the global carbon cycle. Methane is often attributed to biological or abiotic sources based on little more than $\delta^{13}C$ values, or with a combination of $\delta^{13}C$ and δD values. But the multitude of factors controlling ^{13}C fractionation suggests that the use of $\delta^{13}C$ values of methane alone does not always uniquely constrain its source.

Interpretation of the isotopic signatures of methanogens and their metabolic products requires a solid foundation that can only be achieved with controlled laboratory experiments. Isotopic data have been used to determine whether biological methanogenesis is principally autotrophic (using H_2 and CO_2) or heterotrophic (Conrad, 2005; Whiticar et al., 1986). Heterotrophic methanogenesis occurs in only a subset of methanogens, principally the Methanosarcinaceae. These organisms are thought to use acetate as their primary substrate during heterotrophic growth, but a variety of other small compounds may serve as substrates, including methanol, methylated amines and methyl sulfides. In marine environments, these compounds may be of high enough abundance to serve as significant substrates for methanogens (Summons et al., 1998).

For isotopic measurements to play a role in understanding the substrates used in methanogenesis, it is important to define the difference in isotopic fractionations associated with autotrophic and heterotrophic methanogenesis. A common rule of thumb is that biological methane with $\delta^{13}C_{PDB}$ between -110‰ and -60‰ is derived from autotrophic

methanogenesis (Conrad, 2005; Whiticar et al., 1986), while methane with $\delta^{13}C$ between -60‰ and -50‰ is derived from acetoclastic methanogenesis (Whiticar et al., 1986). However, there are very few studies that constrain these ranges, and research in this area remains limited. More definitive understanding is in great demand (Conrad, 2005).

Most studies of the isotope biogeochemistry of methane cycling have focused on methane. Several recent reports have examined the ^{13}C content of the lipids of methane cycling Archaea in environmental samples to understand their ecological role (Hinrichs et al., 1999; Pancost et al., 2000; Schouten et al., 2001; Thiel et al., 2001). In these studies, archaeal lipids with large ^{13}C depletions relative to Vienna Pee Dee belemnite (VPDB) (generally with $\delta^{13}C \leq$ -60‰) are considered to be of methanotrophic origin, while those with $\delta^{13}C \geq$ -30‰ are considered to represent inputs of methanogens. However, there are few data to inform us about the relationship between the ^{13}C content of substrates and that of products: the lipids, biomass, and methane produced by methanogens. To date, only one study (Summons et al., 1998) has reported fractionations between the substrate and lipids of methanogens, in this case grown on trimethylamine (TMA). Methane produced by *Methanosarcina barkeri* was depleted by 50.2‰, biomass by 20.9‰, and lipids by up to 36.8‰ relative to the source TMA (Summons et al., 1998). Fractionation in *Methanococccoides burtonii* was slightly larger. The impact of Archaeal physiology and environmental conditions on the isotopic signatures of methanogen products must be better constrained to improve understanding of the flow of carbon through environments where methane is cycled.

Fractionation of carbon in methanogenesis results from the preferential use of the lighter isotope (^{12}C) over the heavier isotope (^{13}C) during methane production. This can be observed as the difference between the delta values ($\delta^{13}C$) of the substrate carbon source and the product:

$$\Delta\delta^{13}C = \delta^{13}C_{substrate} - \delta^{13}C_{product}$$

When substrate is in abundant supply for a given set of conditions, the observed

fractionation is maximized. Magnitude of fractionation depends on many factors, including temperature, growth phase, the hydrogen supply, the species of methanogen and the isotope effects associated with the enzymes in its carbon acquisition pathways (Botz et al., 1996; Conrad, 2005; Games et al., 1978; House et al., 2003; Penning et al., 2005; Valentine et al., 2004). Organic substrates are rarely abundant in nature, and it is unlikely that the full magnitude of isotope discrimination is commonly expressed during heterotrophic methanogenesis. Inorganic carbon is more frequently abundant, although there may be cases in which it is limited.

The fractionation between substrate and product also depends on the topology of the biosynthetic network involved in methane production. This network has many branch points that shuttle carbon to various biological products. The relative fluxes of carbon to various products at any branch point, the fractionations imposed by each enzyme, and the reversibility of each of the enzymes are all important factors in determining the isotopic difference between substrate and any particular product (Hayes, 2001). Depending on the biological product being examined, the carbon source and the number of enzymes by which it has been processed may be different.

The multiple substrates for biological methanogenesis are metabolized differently. Each substrate enters the biochemical network and is quickly converted to the intermediate that most closely resembles its redox state and chemical composition: acetate is immediately processed to acetyl-CoA, methanol and TMA to methyl-S-CoM, and CO_2 to formylmethanofuran. The relative fluxes of carbon through the biochemical network to methane or biomass are in principle dependent on the standard free energy yield of the methanogenesis reaction for that substrate, and on the substrate concentration. In practice, the fluxes may depend on more complex biological requirements.

The core biosynthetic pathways of methanogenesis and biomass production (Thauer, 1998) lead to the production of methane and biomass, including lipids. Simplified schematics are shown for each substrate in Figure 2-1. The network of intermediates is

similar in each case, but the direction and magnitude of carbon flow differs among them. All methanogens, with the exception of those growing on acetate, require CO_2 for the synthesis of the carboxyl group of acetyl-CoA. All methanogens require CO_2 for pyruvate synthesis. Methylotrophic and acetotrophic methanogens also produce CO_2 from their substrates during catabolism (Figure 2-1b,c). The acetotrophic pathway produces CO_2 as a byproduct of the dissociation of acetyl-CoA while methane is derived exclusively from the acetate methyl group. It is possible that CO_2 required for anabolism could be derived from the CO_2 pool produced catabolically, but this has not been investigated.

During autotrophic growth, CO_2 is initially reduced by the enzyme formylmethanofuran dehydrogenase and will end up as methane or biomass (Figure 2-1). A second carbon fixing enzyme, carbon monoxide dehydrogenase, is involved in the synthesis of acetyl-CoA for autotrophic and methylotrophic methanogens. A third CO_2 fixing step is required for pyruvate synthesis from acetyl-CoA. Thus, for autotrophic growth, three carbon fixing steps are involved in biomass production, whereas only one is required for methane production. Recognizing the differences in the metabolic pathways to the production of biomass, methane, and lipids is essential for understanding the differences in the carbon isotopic composition of these products.

We sought to examine the variability of the $\delta^{13}C$ of *M. barkeri* biomass, methane, and lipids (PMI, archaeol, and *sn*-2 hydroxyarchaeol) as functions of growth substrate and substrate availability. The isotopic compositions of these products can vary substantially for different methanogens. There can be isotopic differences between products formed under laboratory conditions and those produced in the natural environment. We chose to study *Methanosarcina barkeri* because of its ability to utilize various substrates (CO_2/H_2, acetate, TMA, and methanol). *M. barkeri* is the type species of the genus *Methanosarcina*. The species of this genus are environmentally diverse, existing in both marine and nonmarine ecosystems. Some species within the group are halophilic (Zinder, 1993). *Methanosarcina* species are also detected in sewage sludge and animal rumens (Balch et al., 1979). *M.*

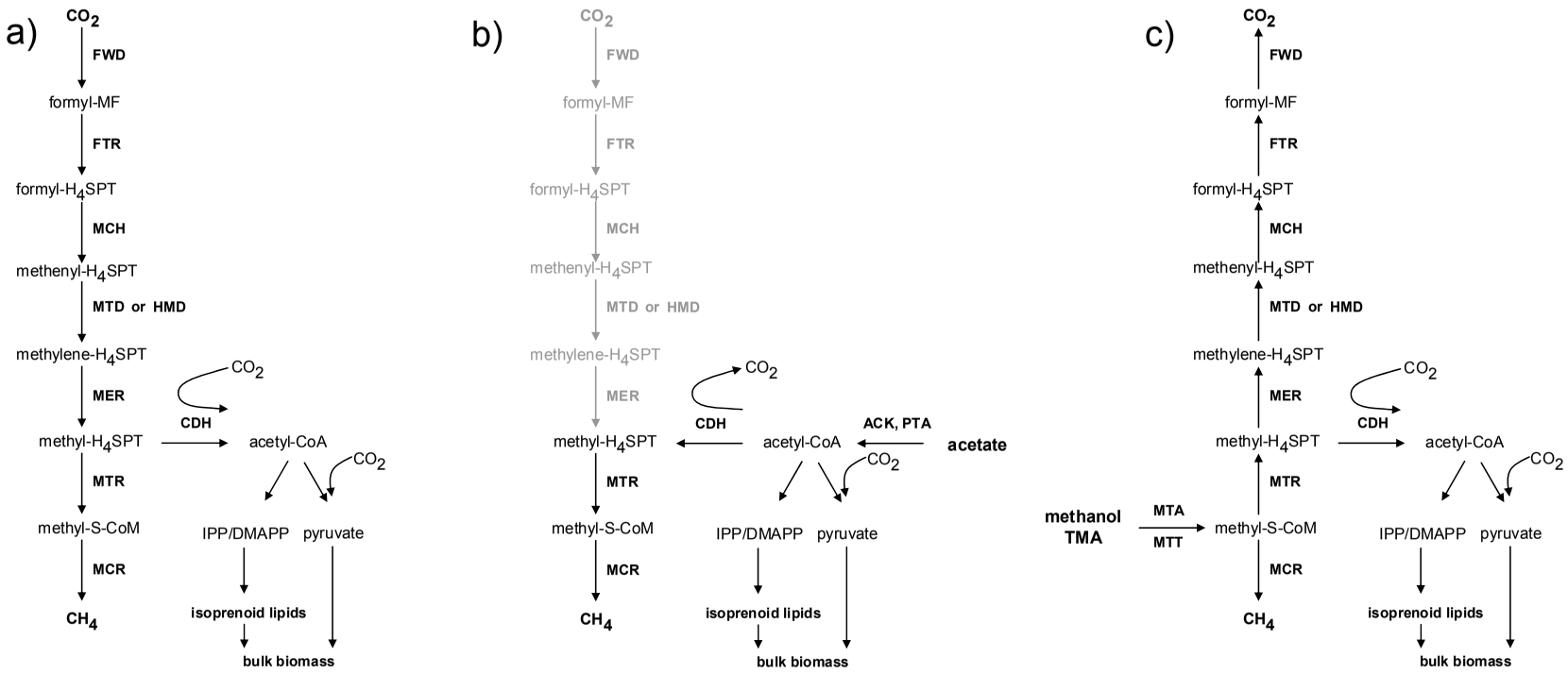

Figure 2-1: Schematic of carbon assimilation and dissimilation pathways in methanogens (after Thauer, 1998). Pathways are shown for growth on CO_2 (a), acetate (b) and methanol or TMA (c). In each case methyl-H_4SPT is the branch point between methane production and biomass production. CO_2 is in each case fixed or produced by cdh and there is an additional CO_2 fixation step in the production of pyruvate. This step is used in biomass production but not in lipid production.

Enzyme Abbreviations: ACK: acetate kinase; CDH: carbon monoxide dehydrogenase/acetyl-CoA synthase; FTR: formylmethanofuran:H_4SPT formyltransferase; FWD: formylmethanofuran dehydrogenase; HMD: H_2-dependent methylene-H_4SPT dehydrogenase; MCH: methenyl- H_4SPT cyclohydrolase; MCR: methyl-coenzyme M reductase; MER: F_{420}-dependent methylene-H_4SPT reductase; MTA: methanol:coenzyme M methyltransferase; MTD: F_{420}-dependent methylene H_4SPT dehydrogenase; MTR: methyl-H_4SPT:coenzyme M methyltransferase; MTT: trimethylamine:coenzyme M methyltransferase; PTA: phosphotransacetylase. Intermediate abbreviations: CO_2: carbon dioxide; formyl-MF: formyl-methanofuran; formyl-H_4SPT: formyl-tetrahydrosarcinapterin; methenyl-H_4SPT: methenyl-tetrahydrosarcinapterin; methylene-H_4SPT: methylene-tetrahydrosarcinapterin; methyl-H_4SPT: methyl-tetrahydrosarcinapterin; methyl-S-CoM: methyl-coenzyme M; CH_4: methane.

barkeri is mesophilic with a maximum growth temperature of 40 ºC (Zinder et al., 1985). *Methanosarcina* species are closely related to the ANME-2 group of methane oxidizing Archaea (Orphan et al., 2001a), commonly found at cold seeps.

Previous studies have shown that the isotope fractionation between substrate and methane in *M. barkeri* varies substantially, with intermediate fractionation under autotrophic growth, small fractionation during growth on acetate (Gelwicks et al., 1994; Krzycki et al., 1987; Penning et al., 2006), and large fractionation during growth on methylated substances (Krzycki et al., 1987; Summons et al., 1998). We sought to obtain a better understanding of the nature of carbon isotope fractionation in methanogens and of the effects of substrate concentration. This information will be useful in evaluating carbon isotope data in methanogenic environments.

2.2. Experimental

2.2.1 Culturing

The methanogen *Methanosarcina barkeri* strain Fusaro was grown on medium modified from Kandler and Hippe (1977) with pH adjustment to 6.7, and addition of 0.125 mg resazurin, 2 mM Na_2S, and 0.05 g/l yeast extract (cultures with acetate received 0.1 g/l yeast extract). *M. barkeri* stock cultures were maintained in 165 ml glass bottles sealed with butyl rubber stoppers, which contained approximately 100 ml culture, and a N_2:CO_2 (80:20) headspace at a pressure of 75 kPa. Cultures of *M. barkeri* were grown separately on three organic substrates: methanol (250 mM), sodium acetate (200 mM) or TMA (100 mM). The substrate concentrations used during these experiments had been determined to be the highest possible concentration that could be used without causing growth inhibition. Autotrophically grown cultures received no organic substrates and were provided H_2:CO_2 (80:20 at 100 kPa) with a smaller liquid to volume ratio (50 ml culture in a 165 ml bottle) in order to supply larger amounts of gaseous substrate. All cultures were incubated without agitation at 37 ºC in the dark.

Cultures were prepared as inocula for isotope fractionation experiments on a similar medium but with a higher salt content to reduce clumping, as per Summons et al. (1998). Inocula were prepared individually in 1.4 l capacity bottles with butyl rubber stoppers adapted to fit stoppered severed Balch tubes. The cultures were prepared to a final volume of 700 ml with 70 ml (10% v/v) inoculum, and grown until analysis of methane in the headspace (440 ml) indicated that the substrate had just been entirely consumed, as close to the end of exponential growth as possible. Inoculum for the acetate amended experimental cultures did not consume all the substrate, such that 2.16 mmol acetate was transferred with the 140 ml inoculum. The ^{13}C contents of biomass and lipids were determined for each inoculum culture by the same methods used for samples.

2.2.2 Isotope fractionation experiments

Parallel series of *M. barkeri* cultures were established from inoculum cultures for each of the three organic substrates. One set was allowed to consume only a small fraction (~5%) of the substrate, which was provided in abundance at the beginning of the experiment, in order to maximize isotope fractionation. By allowing consumption of only 5% of carbon, the effects of Raleigh isotope distillation of the substrate were minimized. The second set of cultures was designed to consume 100% of the substrate provided in limited 10 mM intervals throughout the experiment, to minimize isotope fractionation. Increments of substrate were added when cultures were determined to have used most of the substrate available from earlier additions, based on methane production in identical substrate monitoring cultures. Cultures grown with hydrogen as a substrate were provided with H_2:CO_2 in a headspace (100 kPa) at the beginning of the experiment (abundant hydrogen), or this gas mix was added in increments that amounted to 5% of the headspace volume (headspace was N_2:CO_2) at two day intervals (limited hydrogen). Growth data for cultures analyzed for biomass are reported in Table 1. Growth data for parallel cultures of larger size for H_2/CO_2 and TMA biomarker isotope analysis are reported in Table 2. In the

acetate and methanol experiments the same material was used for both biomass and lipid analysis, and all relevant growth parameters are reported in Table 1. This table includes data on methane-production rates for the growth-monitoring cultures that were run in parallel with the separate cultures for biomass and biomarkers.

All cultures were grown in triplicate. Each experiment included at least one sterile (autoclaved) control. Triplicate cultures were also established with medium that did not receive substrate (organic or hydrogen) in order to measure methane production associated with substrate carried over from the inoculum. It was not possible to measure the course of substrate conversion to methane in the experimental cultures because any sampling of those bottles could lead to isotope fractionation of the gases. Accordingly, a set of growth monitor cultures was prepared and inoculated. Sampling of methane from these cultures continued throughout the experiment in order to approximate substrate conversion to methane in the cultures used to determine isotopic fractionation. Finally, small cultures were also established in 25 ml Balch tubes (15 ml cultures) which were autoclaved after set intervals to stop activity, and which were exclusively used to measure the $\delta^{13}C$ of methane and carbon dioxide over the course of each experiment. These values were measured at or regressed to time zero to estimate the initial $\delta^{13}C$ of methane for each experiment, which was used to approximate the maximum fractionation ε. A true measure of ε was not possible as we did not monitor substrate consumption over time due to the potential for isotope fractionation caused by routine sampling. For each culture we report both the initial estimated $\delta^{13}C$ of methane and the $\delta^{13}C$ at the end of the experiment. All cultures for each experiment were inoculated at the same time from a single inoculum to reduce variability.

2.2.3 Methane analysis

Methane was quantified by gas chromatography (GC). Methane production in inoculum cultures was monitored by extracting 0.1 ml gas samples from culture headspace with a N_2 flushed gastight syringe and analyzing methane content on a Shimadzu mini-

GC equipped with a flame ionization detector. Injections were repeated in triplicate and peak areas were compared to a standard curve that related peak area to μmol methane in external standards prepared daily by injecting methane into sealed serum bottles. Methane production was converted to substrate consumption by means of Buswell's equation (Suflita et al., 1997).

The pressure in the cultures was measured with a pressure gauge (Cole-Parmer) and used to calculate the total methane in each culture, taking temperature and atmospheric pressure into account. The amount of organic substrate that had been converted to methane was calculated based on the expected yield of methane from each substrate as per equations 1-4.

(1) $4\ CH_3OH \rightarrow 3\ CH_4 + CO_2 + 2\ H_2O$ $\Delta G^{o'} = -106$ kJ/mol CH_4

(2) $CH_3COOH \rightarrow CH_4 + CO_2$ $\Delta G^{o'} = -36$ kJ/mol CH_4

(3) $4\ (CH_3)_3N + 6\ H_2O \rightarrow 9\ CH_4 + 3\ CO_2 + 4\ NH_3$ $\Delta G^{o'} = -76$ kJ/mol CH_4

(4) $CO_2 + 4\ H_2 \rightarrow CH_4 + 2H_2O$ $\Delta G^{o'} = -130$ kJ/mol CH_4

2.2.4 Harvesting of experimental cultures

Once experimental cultures were estimated to have reached the intended substrate consumption (based on the monitoring cultures), the headspace pressure, methane, and pH for each culture were measured. The biomass was then collected via centrifugation at 6000 x g for 30 minutes. Cells were washed with phosphate buffer (pH 7.4), and the cell pellet after centrifugation was collected, frozen, lyophilized, and the dry weight was determined. The molar yield of biomass was estimated assuming the biomass was 45% C (Weimer and Zeikus, 1978). The flow to biomass was calculated as the percent of substrate carbon incorporated into biomass relative to the total moles of substrate carbon produced as methane or biomass, where the measured biomass was divided by three to account for the fact that only a third of the carbon comes directly from these substrates, with the rest coming from subsequent carboxylation reactions.

2.2.5 Lipid Analysis

Lipids were extracted from up to 10-15 mg dry cell material using the method of Bligh and Dyer (Bligh and Dyer, 1959). All glassware for lipid analysis was pre-combusted at 450 ºC. Total lipid extracts were derivatized with N,O-bis(trimethylsilyl) trifluoroacetamide (BSTFA) + 1% trimethylchlorosilane (TMCS) in pyridine. Analysis of derivatized samples took place on one of two instruments. The first was a Varian Saturn 2000 gas chromatograph/mass spectrometer equipped with a 30 m DB5-MS column with the oven temperature program 70 ºC for one minute, followed by a ramp of 25 ºC/minute to 165 ºC, held at 165 ºC for 4 minutes and then raised at 20 ºC/minute to 320 ºC followed by a final hold of 43 minutes. The second was an Agilent 6890 gas chromatograph equipped with a J&W DB-1MS column (60 m x 0.32 mm, 0.25 μm film) and an Agilent 5971 mass selective detector. Chromatographic conditions were initially 60 ºC for 2 minutes, then 60-320 ºC at 8 ºC/min.

2.2.6 Isotope Analysis

Gas samples (methane and CO_2), methanol, and TMA were injected on an Agilent 6890 gas chromatograph equipped with an AT-Q column (30 m x 0.32 mm, Alltech) with a constant temperature of 40 ºC and a helium carrier flow of 3 ml/minute. The GC was coupled to a combustion furnace interfaced to a Finnigan MAT DeltaPlus isotope ratio monitoring mass spectrometer operated with IsodatNT. Precision of isotope results was determined using standards and found to be better than 1‰ vs. VPDB. Growth on methanol and acetate produced methane very slowly. As a result we were unable to reliably determine the initial $\delta^{13}C$ of methane produced at the initial time points of these experiments.

Biomass and sodium acetate were analyzed using a Fisons NA 1500 Elemental analyzer operated with an oxidation furnace at 1030 ºC and a reduction furnace at 650 ºC coupled to a Finnigan MAT DeltaPlus XP isotope ratio monitoring mass spectrometer

operated with Isodat 2.0. Precision of isotope results were measured with standards and found to be better than 0.3‰ vs. VPDB. Biomass results were corrected for the inoculum by mass balance.

Compound specific isotope results for lipids were obtained with a ThermoFinnigan TraceGC equipped with a J&W DB-1MS column (60 m x 0.32 mm, 0.25 μm film). Chromatographic conditions were initially 60 ºC for 2 minutes, then 60-320 ºC at 8 ºC/min. The GC was coupled to a combustion furnace interfaced to a Finnigan MAT DeltaPlus XP isotope ratio monitoring mass spectrometer operated with Isodat 2.0. Precision of isotope results were measured with standards and found to be better than 0.3‰ vs. VPDB, and sample replicates produced variations less than 0.5‰ vs. VPDB. Isotope results were corrected for the TMS derivative by mass balance where appropriate. The isotopic composition of a heptadecanol standard was measured by GC-IRMS, then derivatized with the BSTFA reagent used for sample derivatization. We measured the $\delta^{13}C$ value of the resultant heptadecanol-TMS. Comparison of these two $\delta^{13}C$ values allowed us to calculate the $\delta^{13}C$ of the TMS group by mass balance. Lipid $\delta^{13}C$ values were then corrected for the presence of one (archaeol) or two (hydroxyarchaeol) TMS groups by mass balance. Mass balance calculations were then applied to correct for the presence of the inoculum.

2.3. Results and Discussion

2.3.1 Growth and metabolism

M. barkeri grew on acetate, CO_2, TMA and methanol but failed to grow on formate or dimethylsulfide. Initial measurements of growth cultures indicated that the amount of methane carried over with the inoculum was ≤ 0.033 mmol and that sterile controls did not produce methane. Data for growth parameters are given in Table 1.

2.3.1.1. CO_2

Autotrophic growth produced methane more slowly than any other substrate with

abundantly supplied H_2 and even more slowly with limited H_2 (Table 1). The ratio of produced biomass to methane (mg/mmol) was higher under abundant H_2 than limited H_2 for one set of cultures (Table 2) as well as growth monitoring cultures (data not shown). In the other set (Table 1), the values were not significantly different, and the yield under abundant conditions only appeared low due to a poor yield in a single culture. Under both growth conditions, the organisms had sufficient CO_2 for growth, and the increased diversion of carbon to biomass with abundant hydrogen suggests that *M. barkeri* was growing more efficiently under this condition. This may reflect a shift in the metabolic priorities whereby, during growth at low hydrogen partial pressures, the metabolism of *M. barkeri* optimizes for efficient hydrogen use for energy generation by methanogenesis whereas under high hydrogen availability the organism optimizes for some other parameter, possibly growth rate.

2.3.1.2 Acetate

Cultures grown on acetate grew sluggishly, with a seven day lag time before growth began. Cultures provided with abundant acetate produced methane about 3-5 times faster than autotrophic cultures, and the methane production rates were similar under conditions of abundant and limited supplies of substrate. Therefore, differences in carbon flows and isotopic fractionation are due to the extent of carbon usage, not the kinetics. The ratio of carbon diverted to biomass versus methane in the culture grown on limited acetate was the lowest of any of the experiments. This suggests that these cultures were energy starved. Acetate limited methanogenesis is expected to be the least thermodynamically favored condition examined (Zinder, 1993), so under those conditions it is expected that a high proportion of substrate will be diverted to energy generation leading to a low biomass yield. However, in general we did not observe any correlation of growth yield with free energy of reaction.

2.3.1.3 Methanol

When supplied with abundant methanol, *M. barkeri* metabolized the substrate without a lag period and the rate of methanogenesis was very fast, allowing harvesting of cultures in only three days. Carbon dioxide production was indicated by the declining $\delta^{13}C$ value of headspace CO_2. Initial headspace CO_2 was -13‰ vs. VPDB, and decreased linearly over four days to -36.6‰, a value approaching the substrate δ value of -46.2‰. Production of CO_2 caused the pH of the growth media to drop to 6.25. The flow of carbon to biomass versus methane was higher for abundantly supplied methanol than for acetate or H_2/CO_2.

When grown on limiting methanol, the methanogenesis rate was nearly an order of magnitude slower than on abundant methanol. Growth ceased after 30 days, without complete consumption of substrate, most likely due to the drop in pH to 6.01 (in our studies, methanogenesis in *M. barkeri* was inhibited at pH < 6.2). The flux of carbon to biomass versus methane was approximately half of that observed for growth on abundant methanol. This higher relative flux of carbon to methane with limited substrate may be indicative of the lower free energy yield of methanogenesis under limited substrate concentrations.

2.3.1.4 Trimethylamine

Methanogens inoculated into cultures with abundant TMA as a carbon substrate displayed an initial growth lag, followed by a methanogenesis rate that was the fastest observed for any abundant substrate culture. The ratio of carbon flow to biomass versus methane was the highest measured for any experiment, despite the fact that the free energy yield per mole of methane produced is not as high for growth on TMA as it is for growth on CO_2 or methanol.

Growth on limited TMA continued until 81% of the substrate was consumed, at which point the pH had decreased below 6.2. The methanogenesis rate was the highest of any set of experimental conditions, and yielded one of the highest percentages of carbon

flow to biomass, despite the limited substrate availability; although it was significantly less than with abundant substrate, as with the other organic substrates.

2.3.2 Fractionation in biosynthetic pathways

2.3.2.1 CO_2

Carbon dioxide undergoes the most complex transformation of any substrate in order to become methane. The transformation of CO_2 to methane requires seven enzymatic steps (Figure 2-1a). The first five of these enzymes are common to both the catabolic and anabolic pathways with methyl-tetrahydrosarcinapterin (methyl-H_4SPT) occupying the position of the biosynthetic branch point. The methyl group of this intermediate can be reduced to methane with the conservation of energy or it may be transferred to another carbon, forming acetyl-CoA. The ^{13}C content of the products of autotrophic methanogenesis therefore depend on the degree to which each of these enzymes discriminates against ^{13}C as well as the flux through the critical branch-point. Autotrophic methanogenesis yields methane that is 17‰ (House et al., 2003) to 71‰ (Botz et al., 1996) more depleted in ^{13}C than the substrate.

Isotopic results of autotrophic growth experiments are given in Table 3. They are consistent with two previous studies that showed fractionations of 45-46‰ between CO_2 and methane (Krzycki et al., 1987), but were higher than the 17‰ fractionation reported in a recent study (House et al., 2003). Growth on the higher partial pressure of hydrogen showed less carbon isotopic fractionation between substrate and methane than did growth on low partial pressures of hydrogen, consistent with the previous work of Valentine et al. (2004). That study suggested that the difference in isotope discrimination between high and low hydrogen pressures could be due to "differential reversibility" of the enzymes – that under low hydrogen pressures several steps of the pathway were reversible and that this reversibility allows full expression of the isotope fractionation associated with each step. In contrast, under high hydrogen pressures, enzymatic steps were highly exothermic and

irreversible, yielding quantitative transfer of carbon from each biosynthetic intermediate to the next and limiting the observed isotope fractionation.

The two experiments show differences in isotope discrimination between substrate and lipids, supporting the notion of differential reversibility. The isotopic composition of lipids is closely related to the isotopic composition of the lipid precursor acetyl-CoA (Hayes, 2001). The results (Table 3) show that each lipid in the H_2-limited cultures is more depleted in ^{13}C than the corresponding lipid in the H_2–abundant cultures. Both lipids and methane show differences in $\delta^{13}C$ of 20‰ or more between H_2-abundant and H_2-limited growth. This suggests that the large ^{13}C depletion during growth on limited H_2 occurs in their shared intermediate – methyl-H_4SPT – and is present in at least the methyl position of acetyl-CoA. The large difference in ^{13}C content between abundant and limited H_2 growth conditions was not observed in bulk biomass, for reasons that are not yet understood.

We detected significant differences among the isotopic compositions of individual isoprenoid lipids produced within each H_2/CO_2 growth experiment. At face value, all isoprenoid lipids should have the same isotopic composition, since all are synthesized from isopentenyl diphosphate (IPP) by the mevalonate pathway (Koga and Morii, 2007). In fact, under both substrate limited and substrate abundant conditions *sn*-2 hydroxyarchaeol was depleted in ^{13}C by about 3‰ relative to co-occurring archaeol. PMI was in both cases depleted in ^{13}C relative to the archaeols and this depletion was more pronounced in the fast growing cultures (≤11.1‰) than in the slow growing cultures (≤2.3‰).

The reason for the differences in the isotopic compositions of these lipids remains unknown, but one possibility is that the differences may reflect the timing of lipid production during growth. If PMI were synthesized during early growth while the substrate is more depleted in ^{13}C, and the archaeols were synthesized later in growth, their difference in $\delta^{13}C$ could be explained by progressive enrichment of the substrate. However, we do not have direct evidence for differential synthesis of these compounds over the course of growth. The magnitude of change in $\delta^{13}C$ of methane throughout the course of growth (Table 3) is

also a result of the ^{13}C enrichment of substrate, and is greater than the difference in $\delta^{13}C$ between lipids. However, the small difference in ^{13}C content between archaeol and *sn*-2 hydroxyarchaeol even in the slow growing culture may suggest another explanation for the differences between these two compounds, perhaps because they are coupled as precursor and product.

2.3.2.2 Acetate

Acetate could be considered the simplest substrate for assimilation since it is a direct precursor of acetyl-CoA. In *M. barkeri*, acetate is converted to acetyl-CoA by the enzymes acetate kinase and phosphotransacetylase. Acetyl-CoA is located at a crucial branch point in the metabolic network (Figure 2-1b) and undergoes one of two fates. The first is the disproportionation of acetyl-CoA by carbon monoxide dehydrogenase with the production of CO_2 from the carboxyl group of the acetate and the transfer of the methyl group to methyl-tetrahydrosarcinapterin from which it is subsequently reduced to methane in the energy conserving pathway. Thus methane is derived from the methyl group of acetate only. The other possible fate for acetyl-CoA is that the whole molecule serves as the raw material for biomass production entering into lipids or total biomass.

Results of isotope experiments, shown in Table 3, are consistent with the relatively simple incorporation of acetate into biomass. Fractionations between substrate and total biomass are small, the lowest for any substrate tested. Similarly, the fractionation between substrate and methane is the lowest for any substrate tested but greater than the values of 22‰ (Krzycki et al., 1987), 24‰ (Gelwicks et al., 1994), and 27‰ (Zyakun et al., 1988) determined in previous studies. Fractionations between substrate and lipids are small in the case of abundant substrate and negative in the case of limited substrate. Together, these data imply that the fractionation imposed by the enzymes in the catabolic pathway is larger than those in the anabolic pathway, and ^{13}C is preferentially diverted to the anabolic branch and to lipids. Acetate is the only substrate on which growth results in lipids being enriched

in ^{13}C relative to both substrate and bulk biomass. This relationship could be useful in environmental samples for distinguishing between autotrophic and acetoclastic growth if the $\delta^{13}C$ of the substrates is constrained.

2.3.2.3 Methanol and trimethylamine

The methylated substrates methanol and TMA are processed in a very similar manner by *M. barkeri*. Methanol is introduced to the methanogenic pathway by a transfer of the substrate methyl group to methyl-S-CoM by the enzyme methylcobalamin:coenzyme M methyltransferase. This intermediate has two potential fates, the first being the reduction of the methyl group to methane by methyl-coenzyme M reductase. This step is associated with the production of energy. The second possible fate for the methyl group is incorporation into biomass by being transferred to tetrahydrosarcinapterin by methyl-H_4SPT:coenzyme M methyltransferase. The methyl-H_4SPT can be oxidized to CO_2 via the five enzymatic steps between formylmethanofuran dehydrogenase and F_{420}-dependent methylene-H_4SPT reductase, or it can be combined with a molecule of CO_2 by carbon monoxide dehydrogenase into acetyl-CoA and subsequently to lipids and other biomass.

TMA is incorporated into the biochemical network by the enzyme trimethylamine:coenzyme M methyltransferase producing dimethylamine and transferring one methyl group to methyl-S-CoM. This is metabolically processed in the same manner as methanol.

Results from carbon isotope experiments with *M. barkeri* grown on methanol are summarized in Table 3. These experiments show that despite the entrance of methanol into the biosynthetic network only two enzymatic steps away from the production of methane, the difference in ^{13}C content between substrate and methane was larger for methanol than for any other substrate, and was the same as that determined in a previous study (Krzycki et al., 1987). Similarly, differences in $\delta^{13}C$ between substrate and total biomass were larger for growth on methanol than for any other substrate.

Under limited substrate conditions, the isotopic fractionation between methanol and lipid was approximately equal for PMI, archaeol and *sn*-2 hydroxyarchaeol. With abundant substrate, however, the differences are manifest: archaeols were depleted in ^{13}C by about 15‰ relative to PMI.

Isotope discrimination between TMA and methane in these experiments was greater than for growth on acetate, similar in magnitude to growth on methanol or slow growth on CO_2 and greater than that determined in a previous study (Summons et al., 1998). Isotopic discrimination between TMA and total biomass was large, like the discriminations seen between methanol and biomass.

Isotope discriminations between TMA and individual lipids showed deviations from the pattern observed in methanol growth cultures. Under substrate abundant conditions, archaeols were depleted by about 4‰ relative to PMI, which is a smaller difference than seen in the methanol cultures. Under substrate limited conditions, the fractionation between substrate and lipid increased by 4-5‰ from archaeol to PMI to *sn*-2 hydroxyarchaeol, much greater differences than in the methanol cultures.

Differences in $\delta^{13}C$ values between the substrate and methane, and substrate and biomass or lipids, were similar for the substrates methanol and TMA. During growth on abundant substrate, fractionations were slightly larger between substrate and the biomass and methane products when the substrate was methanol than when it was TMA. This seems to suggest that methanol:coenzyme M methyltransferase discriminates against ^{13}C more strongly than trimethylamine:coenzyme M methyltransferase. However, if this were true we would expect *all* the products of growth on methanol to be more depleted relative to substrate than the products of growth on TMA. This is not the case for PMI. Furthermore we would expect to see products of growth on methanol more depleted than products of growth on TMA even at low substrate concentrations. The reverse is true. This suggests that the differences in fractionation among products, between substrates, and between substrate concentrations is the result of a complex interplay of enzymes. The biosynthetic network

may respond to different conditions by using different enzymes (in the case of TMA vs. methanol) and moving carbon around its biosynthetic network in different ways.

2.3.2.4 General trends and correlations

Figure 2-2a plots the difference in carbon isotopic composition of substrate and biomass versus that between substrate and initially produced methane for each of the four abundant-substrate experiments. The result from each experiment plots to the right of the 1:1 line (illustrated by the dashed line), indicating that methane is more depleted in ^{13}C than biomass. Remarkably, in spite of the multiple pathways involved, the substrate-initial methane and substrate-biomass fractionations (for abundant substrate conditions) are well correlated. Further experiments under different conditions, such as continuous culture, are therefore warranted.

Figure 2-2b plots the difference in carbon isotopic composition between substrate and final biomass and methane for the four abundantly supplied substrates, and a compilation of comparable data (open symbols) from several previous studies (Balabane et al., 1987; Belyaev et al., 1983; Fuchs et al., 1979; House et al., 2003; Summons et al., 1998). These studies were performed primarily with H_2/CO_2 as the substrate under conditions of abundant substrate supply and varying degrees of substrate consumption. These confirm the general trend that methane appears depleted relative to biomass, although in most cases the extent of this difference is not as pronounced as it is in our experiments.

Figure 2-3 plots the difference in $\delta^{13}C$ between substrate and individual lipids versus that between substrate and biomass for each experiment. This plot shows that growth on acetate is unique in producing lipids that are uniformly less depleted than biomass, relative to substrate. Growth on other substrates usually produces lipids which are more depleted in ^{13}C than total biomass, with varying degrees of deviation from the 1:1 line.

The wide range of fractionation between substrate and lipid with variation in substrate availability will probably frustrate attempts to make precise predictions of the $\delta^{13}C$

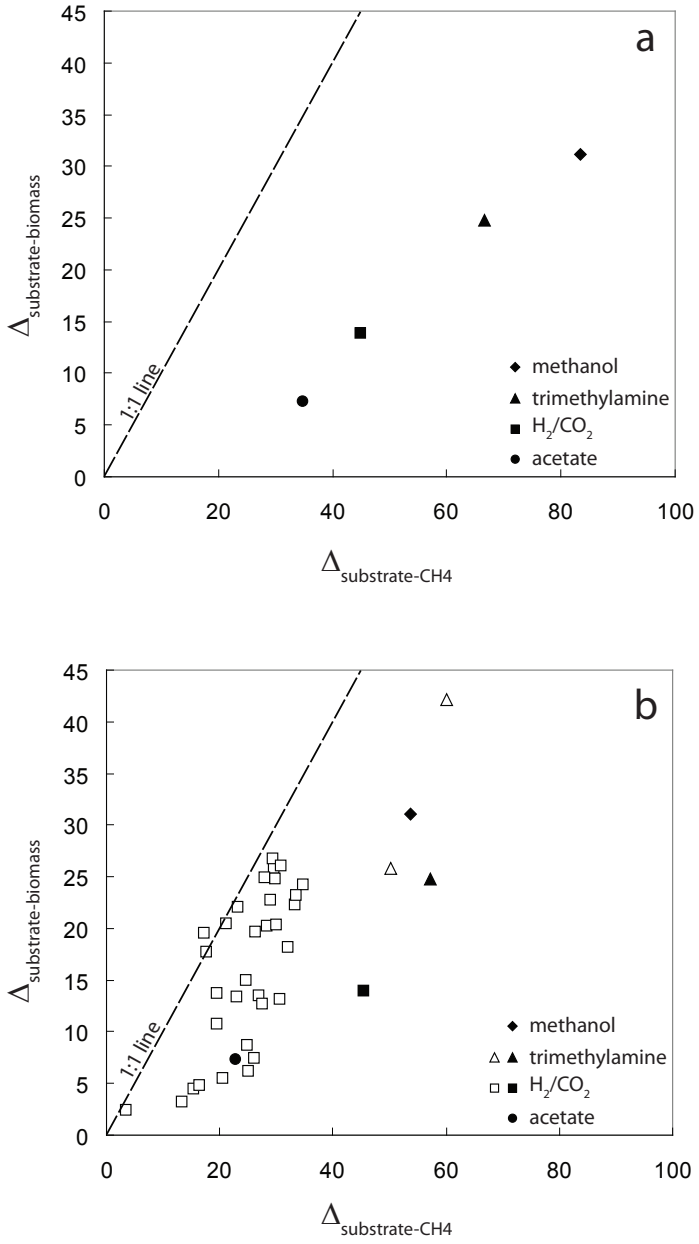

Figure 2-2: a) Plot of the difference in $\delta^{13}C$ between substrate and biomass ($\Delta_{substrate\text{-}biomass}$; y-axis) vs. $\Delta_{substrate\text{-}CH4}$ between substrate and initial methane (x-axis) for each of the four experiments with abundantly provided substrate. b) Plot of the $\Delta_{biomass\text{-}substrate}$ versus the Δ between substrate and final methane produced in experiments conducted in this study (solid symbols) and from abundant substrate experiments from a survey of literature data (open symbols). Dashed lines are 1:1 lines.

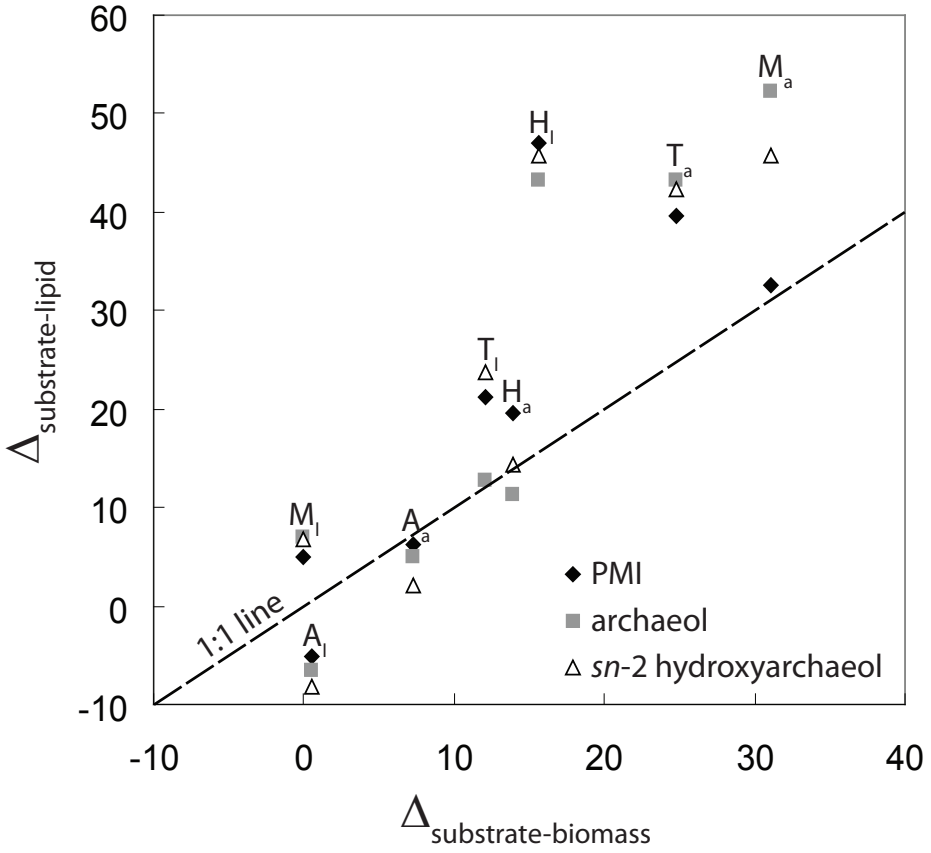

Figure 2-3: Plot of the $\Delta_{substrate\text{-}biomass}$ versus the Δ between substrate and individual lipids for each experiment. Symbols indicate the lipid type: PMI, archaeol or *sn*-2 hydroxyarchaeol. Results from each experiment are identified by a letter (A: acetate, H: H_2/CO_2, M: methanol, T: trimethylamine) and a subscript (a: abundant, l: limited) placed above the cluster of its three lipid points. The dashed line is a 1:1 line.

of methanogen lipids in natural environments, even in cases where the $\delta^{13}C$ of substrates is well constrained. It may be more feasible to suggest ranges into which lipids are expected to fall relative to substrate, with acetate showing the smallest deviations (< 20‰) and other substrates displaying much larger ranges.

We detected variations in the patterns of $\delta^{13}C$ values among the various individual lipids produced under different growth conditions. In general, differences in ^{13}C content of individual lipids were greater when the organisms grew on abundant substrate than when grown on limited substrate, but this rule was not universal (see growth on TMA, Table 2-3 and Figure 2-3). Growth on acetate yielded lipids that were generally most similar to each other in ^{13}C content while growth on abundant methanol yielded large differences between PMI and archaeols. No pattern emerged of $\delta^{13}C$ relationships among the individual lipids that could usefully be employed to distinguish the growth substrate of a methanogen *in situ* by examination of lipid isotopes.

A previous study of isotopic fractionation between methylated substrates and lipids noted the large difference in ^{13}C content of the methane and lipid products (Summons et al., 1998). The authors of that study predicted that under conditions of substrate limitation, the larger ^{13}C depletion in methane might result in lipids that were enriched relative to the methylated substrate. Another study (Fuchs et al., 1979) found methanogen biomass enriched relative to substrate during growth on limited CO_2. Mass balance requires the production of a ^{13}C enriched product if another product is ^{13}C depleted and the consumption is quantitative. However we note a complicating factor: methanogens fix CO_2 even when growing on methylated substrates (Figure 2-1). Fractionation imposed on CO_2 assimilated by carbon monoxide dehydrogenase will manifest itself in the $\delta^{13}C$ of lipids. This study indicates that even under substrate limited conditions, lipids are always depleted relative to the methylated substrates. This was much more pronounced during growth on TMA than on methanol. In these experiments however, substrate consumption did not reach 100 percent (Tables 2-1 and 2-2).

In environmental samples, lipids derived from methanogens can not be distinguished from those derived from Archaeal methanotrophs on the basis of their structure. The diagnostic criteria is usually the $\delta^{13}C$ value; when lipid $\delta^{13}C$ is less than around -60‰ the lipids are interpreted to derive from methanotrophs (Blumenberg et al., 2004; Hinrichs et al., 1999; Pancost et al., 2000; Thiel et al., 2001). In many cases this assumption has been supported by other evidence (Blumenberg et al., 2005; Boetius et al., 2000; Orphan et al., 2001b; Raghoebarsing et al., 2006). Our results suggest that such interpretations should continue to be made cautiously, as there may be some overlap between the $\delta^{13}C$ of lipids produced by methanogenic and methanotrophic archaea. We have shown that methylotrophic *M. barkeri* can produce lipids that are depleted in ^{13}C by more than 50‰ relative to substrate. Methylated substrates are likely to derive from primary producers (Summons et al., 1998) and could have $\delta^{13}C$ as depleted as -30‰ vs. VPDB in natural environments. It follows that lipids produced by methanogens using those substrates could have $\delta^{13}C$ as negative as -80‰. It is unlikely that the largest possible fractionations for methylated substrates will be expressed since compounds such as TMA and methanol are not likely to be abundant in natural environments. But even with growth on limited TMA *M. barkeri* produced lipids nearly 30‰ depleted relative to substrate. The expected $\delta^{13}C$ values for lipids produced by this organism could reasonably be expected to reach -60‰ in natural environments, overlapping with values that are often considered diagnostic for methanotrophy. Among pathways examined here, methylotrophic methanogenesis is the most likely to produce lipids strongly depleted in ^{13}C, although other pathways might also in cases where extreme ^{13}C depletion in substrates is a possibility. We do not suggest that previous reports of methanotrophy are incorrect, but stress that the possible range of $\delta^{13}C$ values of methanogens may extend to more negative values than commonly realized.

2.4. Conclusions

Experimental cultures of *M. barkeri* grown on four different substrates under

substrate limited and substrate abundant conditions revealed considerable variation in the ^{13}C content of the various biological products. Variation is extensive enough that knowledge of the isotopic composition of a substrate does not allow prediction of the isotopic composition of products in natural environments. Discrimination against the heavier isotope in the production of methane was similar for the methylated substrates and CO_2, and much lower with acetate as a substrate. In the production of lipids, growth on methylated substrates discriminated against ^{13}C most significantly, followed by CO_2 and acetate.

	Substrate Provided (mmol)	Incubation time (days)	Lag time (days)	CH_4 production rate (umol/day)[1]	Final pH	Calculated substrate converted to methane (%)	CH_4 produced (mmol)	Biomass (mg)	Yield biomass(mg)/ methane(mmol)	Flow to biomass (%)
H_2/CO_2										
abundant H_2	NA[2]	14	0	35.7 ± 0.7	6.59 ± 0.02	NA	0.53 ± 0.02	2.9 ± 1.2	5.4 ± 2.4	6.3 ± 2.7
limited H_2	NA[2]	23	0	20.7 ± 0.8	6.30 ± 0.07	NA	0.50 ± 0.00	4.3 ± 1.0	8.6 ± 2.0	9.6 ± 2.0
Acetate										
abundant	16	14	7	104 ± 13	6.94 ± 0.01	6.5 ± 0.7	1.18 ± 0.12	6.6± 0.6	5.7± 1.1	6.7 ± 1.2
limited	4	30	7	101 ± 4	7.20 ± 0.05	97 ± 7	6.00 ± 0.42	8.7 ± 2.3	1.4 ± 0.3	1.8 ± 0.4
Methanol										
abundant	22.5	3	0	502 ± 101	6.25 ± 0.01	9.9 ± 1.1	1.68 ± 0.19	15.4 ± 5.5	9.2 ± 3.4	10.2 ± 3.5
limited	5	30	0	81 ± 2	6.01 ± 0.02	68.1 ± 2.9	2.55 ± 0.11	9.8 ± 3.7	3.8 ± 1.3	4.5 ± 1.5
TMA										
abundant	25	5	4	660 ± 250	6.28 ± 0.04	1.25 ± 0.03	0.73 ± 0.02	22.7 ± 6.9	31.3 ± 9.0	27.7 ± 6.0
limited	3.5	12	4	1050 ± 50	6.06 ± 0.02	80.6 ± 1.4	6.34 ± 0.11	49.4 ± 2.3	7.8 ± 0.3	8.9 ± 0.3

[1] Calculated from linearized methane concentration during exponential growth

[2] Not applicable - carbon dioxide supplied in excess

Table 2-1: Growth parameters for cultures used in biomass fractionation measurements and methanogenesis rates for growth monitoring cultures. Biomass for methanol and acetate experiments was also used for lipid measurements.

	Substrate Provided (mmol)	Final pH	Calculated substrate converted to methane (%)	CH4 produced (mmol)	Biomass (mg)	Yield biomass (mg)/CH4 (mmol)	Flow to biomass (%)
H_2/CO_2							
abundant H_2	NA	7.18 ± 0.13	NA	2.29 ± 0.05	88.2 ± 9.1	38.5 ± 4.6	32.3 ± 2.7
limited H_2	NA	6.37 ± 0.04	NA	2.83 ± 0.04	15.0 ± 3.8	5.3 ± 1.3	6.2 ± 1.5
TMA							
abundant	178	6.33 ± 0.01	1.00 ± 0.07	4.03 ± 0.27	80.1 ± 3.7	19.9 ± 2.0	20.3 ± 1.6
limited	3.5	6.14 ± 0.04	75.8 ± 9.3	5.96 ± 0.73	55.6 ± 4.5	9.3 ± 0.4	10.5 ± 0.4

NA = not applicable
Note: "abundant" cultures grown in large bottles

Table 2-2: Growth parameters for cultures measuring fractionation for lipids for H_2/CO_2 and TMA experiments.

	Substrate $\delta^{13}C$	Biomass $\delta^{13}C$	$\delta^{13}C$ initial CH_4	$\delta^{13}C$ final CH_4	$\delta^{13}C$ PMI	$\delta^{13}C$ archaeol	$\delta^{13}C$ sn-2	$\Delta_{S\text{-}CH4}$ [1]	$\Delta_{S\text{-}biomass}$ [2]	$\Delta_{S\text{-}PMI}$ [3]	$\Delta_{S\text{-}archaeol}$ [4]	$\Delta_{S\text{-}sn2}$ [5]
H_2/CO_2												
abundant H	-31.2	-45.1	-76.6	-71.5	-50.7	-42.5	-45.6	45.4	13.9	19.5	11.3	14.4
limited H_2	-28.5	-44.1	-108.0	-79.6	-75.5	-71.7	-74.3	79.5	15.6	47.0	43.2	45.8
Acetate												
abundant	-30.9	-38.2	-65.7	-53.8	-37.2	-35.8	-33.0	34.8	7.3	6.3	4.9	2.1
limited	-30.9	-31.4			-25.7	-24.3	-22.7		0.5	-5.2	-6.6	-8.2
Methanol												
abundant	-46.2	-77.3	-129.6	-100	-78.7	-98.4	-92.0	83.4	31.1	32.5	52.2	45.8
limited	-46.2	-46.1			-51.2	-53.1	-53.0		-0.1	5.0	6.9	6.8
TMA												
abundant	-29.5	-54.3	-96.0	-86.8	-69.2	-72.8	-71.9	66.5	24.8	39.7	43.3	42.4
limited	-29.5	-41.6	-96.1		-50.7	-42.2	-53.2	66.6	12.1	21.2	12.7	23.7

[1]Difference between $\delta^{13}C$ substrate and $\delta^{13}C$ for initially produced methane
[2]Difference between $\delta^{13}C$ substrate and $\delta^{13}C$ biomass
[3]Difference between $\delta^{13}C$ substrate and $\delta^{13}C$ PMI
[4]Difference between $\delta^{13}C$ substrate and $\delta^{13}C$ archaeol
[5]Difference between $\delta^{13}C$ substrate and $\delta^{13}C$ *sn*-2 hydroxyarchaeol

Table 2-3: Summary of ^{13}C contents and discriminations

2.5 References

Balabane, M., Galimov, E., Hermann, M., Letolle, R., 1987. Hydrogen and carbon isotope fractionation during experimental production of bacterial methane. Organic Geochemistry 11(2), 115-9.

Balch, W.E., Fox, G.E., Magrum, L.J., Woese, C.R., Wolfe, R.S., 1979. Methanogens: reevaluation of a unique biological group. Microbiol Rev FIELD Full Journal Title:Microbiological reviews 43(2), 260-96.

Belyaev, S.S., Wolkin, R., Kenealy, W.R., DeNiro, M.J., Epstein, S., Zeikus, J.G., 1983. Methanogenic bacteria from the Bondyuzhskoe oil field: general characterization and analysis of stable-carbon isotopic fractionation. Applied and Environmental Microbiology 45(2), 691-7.

Bligh, E.G., Dyer, W.J., 1959. A rapid method of total lipid extraction and purification. Canadian journal of biochemistry and physiology 37(8), 911-7.

Blumenberg, M., Seifert, R., Nauhaus, K., Pape, T., Michaelis, W., 2005. In vitro study of lipid biosynthesis in an anaerobically methane-oxidizing microbial mat. Applied and Environmental Microbiology 71(8), 4345-51.

Blumenberg, M., Seifert, R., Reitner, J., Pape, T., Michaelis, W., 2004. Membrane lipid patterns typify distinct anaerobic methanotrophic consortia. Proceedings of the National Academy of Sciences of the United States of America 101(30), 11111-11116.

Boetius, A., Ravenschlag, K., Schubert, C.J., Rickert, D., Widdel, F., Gieseke, A., Amann, R., Jorgensen, B.B., Witte, U., Pfannkuche, O., 2000. A marine microbial consortium apparently mediating anaerobic oxidation of methane. Nature 407, 623-626.

Botz, R., Pokojski, H.-D., Schmitt, M., Thomm, M., 1996. Carbon isotope fractionation during bacterial methanogenesis by CO_2 reduction. Org. Geochem. 25, 255-262.

Conrad, R., 2005. Quantification of methanogenic pathways using stable carbon isotopic signatures: a review and a proposal. Organic Geochemistry 36(5), 739-752.

Fuchs, G., Thauer, R., Ziegler, H., Stichler, W., 1979. Carbon isotope fractionation by Methanobacterium thermoautotrophicum. Archives of Microbiology 120(2), 135-9.

Games, L.M., Hayes, J.M., Gunsalus, R.P., 1978. Methane-producing bacteria: natural fractionations of the stable carbon isotopes. Geochim. Cosmochim. Acta 42, 1295-1297.

Gelwicks, J.T., Risatti, J.B., Hayes, J.M., 1994. Carbon isotope effects associated with aceticlastic methanogenesis. Applied and Environmental Microbiology 60, 467-472.

Hayes, J.M., 2001. Fractionation of carbon and hydrogen isotopes in biosynthetic processes. Reviews in Mineralogy & Geochemistry 43, 225-277.

Hinrichs, K.-U., Hayes, J.M., Sylva, S.P., Brewer, P.G., DeLong, E.F., 1999. Methane-consuming archaebacteria in marine sediments. Nature 398, 802-805.

House, C.H., Schopf, J.W., Stetter, K.O., 2003. Carbon isotopic fractionation by Archaeans and other thermophilic prokaryotes. Organic Geochemistry 34, 345-356.

Kandler, O., Hippe, H., 1977. Lack of peptidoglycan in the cell walls of *Methanosarcina*

barkeri. Arch. Microbiol. 113, 57-60.
Koga, Y., Morii, H., 2007. Biosynthesis of ether-type polar lipids in archaea and evolutionary considerations. Microbiol Mol Biol Rev FIELD Full Journal Title:Microbiology and molecular biology reviews : MMBR 71(1), 97-120.
Krzycki, J.A., Kenealy, W.R., DeNiro, M.J., Zeikus, J.G., 1987. Stable carbon isotope fractionation by *Methanosarcina barkeri* during methanogenesis from acetate, methanol, or carbon dioxide-hydrogen. Applied and Environmental Microbiology 53(2597-2599).
Orphan, V.J., Hinrichs, K.U., Ussler, W., III, Paull, C.K., Taylor, L.T., Sylva, S.P., Hayes, J.M., Delong, E.F., 2001a. Comparative analysis of methane-oxidizing archaea and sulfate-reducing bacteria in anoxic marine sediments. Applied and Environmental Microbiology 67(4), 1922-1934.
Orphan, V.J., House, C.H., Hinrichs, K.-U., McKeegan, K.D., DeLong, E.F., 2001b. Methane-Consuming Archaea Revealed by Directly Coupled Isotopic and Phylogenetic Analysis. Science 293, 484-487.
Pancost, R.D., Sinninghe Damste, J.S., de Lint, S., van der Maarel, M.J.E.C., Gottschal, J.C., Party, M.S.S., 2000. Biomarker Evidence for Widespread Anaerobic Methane Oxidation in Mediterranean Sediments by a Consortium of Methanogenic Archaea and Bacteria. Applied and Environmental Microbiology 66(3), 1126-1132.
Penning, H., Claus, P., Casper, P., Conrad, R., 2006. Carbon isotope fractionation during acetoclastic methanogenesis by Methanosaeta concilii in culture and a lake sediment. Applied and Environmental Microbiology 72(8), 5648-52.
Penning, H., Glugge, C.M., Galand, P., Conrad, R., 2005. Variation of carbon isotope fractionation in hydrogenotrophic methanogenic microbial cultures and environmental samples at different energy status. Global Change Biol. 11, 2103-2113.
Raghoebarsing, A.A., Pol, A., van de Pas-Schoonen Katinka, T., Smolders Alfons, J.P., Ettwig Katharina, F., Rijpstra, W.I.C., Schouten, S., Damste Jaap, S.S., Op den Camp Huub, J.M., Jetten Mike, S.M., Strous, M., 2006. A microbial consortium couples anaerobic methane oxidation to denitrification. Nature 440(7086), 918-21.
Schouten, S., Rupstra, W.I.C., Kok, M., Hopmans, E.C., Summons, R.E., Volkman, J.K., Damste, J.S.S., 2001. Molecular organic tracers of biogeochemical processes in a saline meromictic lake (Ace Lake). Geochimica et Cosmochimica Acta 65(10), 1629-1640.
Suflita, J.M., Londry, K.L., Ulrich, G.A., 1997. Determination of anaerobic biodegradation activity. In: C.J. Hurst, G.R. Knudson, M.J. McInerny, L.D. Stetzenbach, M.V. Walter (Eds.), *Manual of Environmental Microbiology*, pp. 790-801. ASM Press, Washington D.C.
Summons, R.E., Franzmann, P.D., Nichols, P.D., 1998. Carbon isotopic fractionation associated with methylotrophic methanogenesis. Organic Geochemistry 28(7/8), 465-475.
Thauer, R.K., 1998. Biochemistry of methanogenesis: a tribute to Marjory Stephenson. Microbiology 144, 2377-2406.
Thiel, V., Peckmann, J., Schmale, O., Reitner, J., Michaelis, W., 2001. A new straight-

chain hydrocarbon biomarker associated with anaerobic methane cycling. Organic Geochemistry 32, 1019-1023.
Valentine, D.L., Chidthaisong, A., Rice, A., Reeburgh, W.S., Tyler, S.C., 2004. Carbon and hydrogen isotope fractionation by moderately thermophilic methanogens. Geochimica et Cosmochimica Acta 68(7), 1571-1590.
Weimer, P.J., Zeikus, J.G., 1978. One carbon metabolism in methanogenic bacteria. Archives of Microbiology 119, 49-57.
Whiticar, M.J., 1999. Carbon and hydrogen isotope systematics of bacterial formation and oxidation of methane. Chemical Geology 161(1-3), 291-314.
Whiticar, M.J., Faber, E., Schoell, M., 1986. Biogenic methane formation in marine and freshwater environments: CO2 reduction vs. acetate fermentation- Isotope evidence. Geochimica et Cosmochemica Acta 50, 693-709.
Zinder, S.H., 1993. Physiological Ecology of Methanogens. In: J.G. Ferry (Ed.), *Methanogenesis: ecology, physiology, biochemistry, & genetics*, pp. 128-206. Chapman & Hall, New York.
Zinder, S.H., Sowers, K.R., Ferry, J.G., 1985. Methanosarcina thermophila sp. nov., a thermophilic, acetotrophic, methane-producing bacterium. Int. J. Syst. Bacteriol. 35, 522-523.
Zyakun, A.M., Bondar, V.A., Laurinavichus, K.S., Shipin, S.S., Belyaev, S.S., Ivanov, M.V., 1988. Fractionation of carbon isotopes under the growth of methane-producing bacteria on various substrates. Mikrobiologiceskij Zhurnal 50, 16-22.

THIS PAGE INTENTIONALLY LEFT BLANK

Chapter 3

Extraordinary ^{13}C enrichment of diether lipids at the Lost City Hydrothermal Field suggests a carbon-limited ecosystem

Abstract

Active and inactive carbonate chimneys from the Lost City Hydrothermal Field contain up to 0.6% organic carbon with diverse lipid assemblages. The $\delta^{13}C$ values of total organic carbon range from -21.5‰ vs. VPDB at an extinct carbonate chimney to -2.8‰ at a 70˚C actively venting carbonate chimney near Marker 7 (Figure 3-1). Samples collected at locations with total organic carbon having $\delta^{13}C$ values > -15‰ also contained high abundances of isoprenoidal and nonisoprenoidal diether lipids. Samples with TOC more depleted in ^{13}C lacked or contained lower amounts of these diethers.

The relationship between high $\delta^{13}C$ values for TOC and the presence of diethers is supported by compound-specific isotopic analysis. Isoprenoidal and nonisoprenoidal diethers have extraordinary ^{13}C enrichments for biological lipids. The lipid biomarkers *sn*-2 hydroxyarchaeol, *sn*-3 hydroxyarchaeol, and dihydroxyarchaeol, which are characteristic of methanogenic Archaea, have $\delta^{13}C$ values that range from -2.9 to +6.7‰ vs. VPDB. Diethers and monoethers with non-isoprenoidal side chains are also present, are of presumed bacterial origin, and have structures similar to those produced by sulfate reducing bacteria in culture and found in natural communities at cold seeps. Diethers have $\delta^{13}C$ values between -11.8‰ and +3.6‰ in samples that also contained abundant hydroxyarchaeols. In samples without abundant hydroxyarchaeols, the nonisoprenoidal diethers were more depleted in ^{13}C, with $\delta^{13}C$ as low as -28.7‰.

The lipid assemblage of hydroxyarchaeols and nonisoprenoidal glycerol diethers that characterizes the active chimneys is typical of natural environments in which methane is oxidized anaerobically. In contrast to the latter, the $\delta^{13}C$ values of the Lost City lipids are heavy. At Lost City, these lipids are likely produced by hydrogen-consuming methanogens.

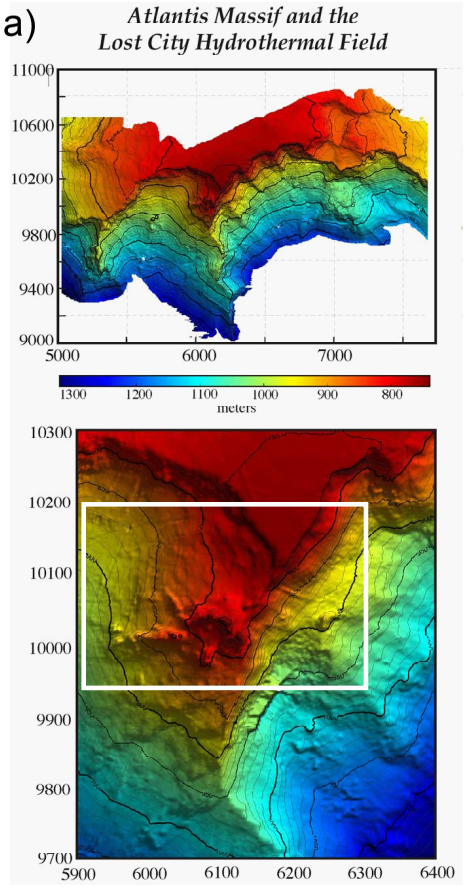

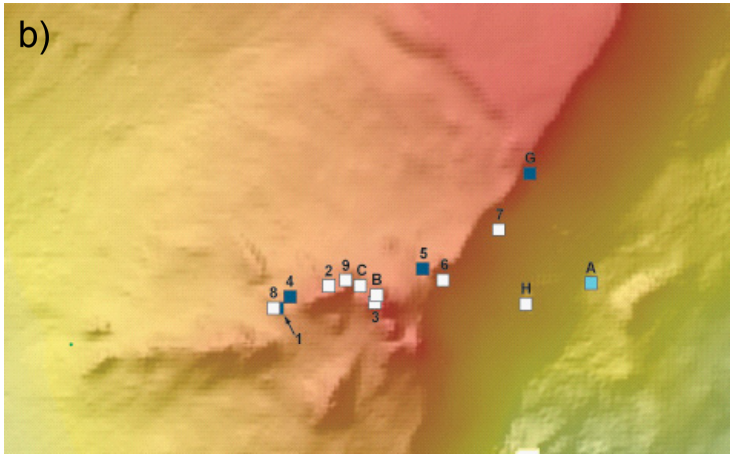

Figure 3-1: Map of the Lost City Hydrothermal Field. a) shows bathymetry of southern edge of Atlantis Massif as mapped by Autonomous Benthic Explorer (ABE). b) is area delineated by box in (a) showing relative locations of sampling sites at Lost City Hydothermal Field. Letters and numbers refer to Marker numbers.

Hydrogen concentrations in some vent fluids exceed 14 mmol/kg and they are in all cases greater than 1 mmol/kg (Proskurowski et al. *Chem. Geol.* 229 (2006), 331). High hydrogen concentrations create the thermodynamic drive that favors methane generation over methane oxidation. Lipids specific for methane-cycling archaea are enriched in ^{13}C relative to the methane in vent fluids, thereby excluding methane as their carbon source. In combination, these lines of evidence show that Methanosarcinales inhabiting Lost City carbonate chimneys are methanogens and not methane-oxidizing methanotrophs.

The Lost City ecosystem is biogeochemically important because it is driven by serpentinization – a reaction that can be expected wherever ultramafic rock interacts with water. Hydrogen and methane from such environments may have been important components Earth's early biosphere. However the presence of abundant methanogenic archaea complicates efforts to understand the relative contributions of biotic and abiotic methanogenesis in these environments.

3.1 Introduction

The discovery of the Lost City Hydrothermal Field (LCHF) in 2000 (Kelley et al., 2001; Kelley et al., 2005) marked the first recognition of an ocean-floor ecosystem driven by the serpentinization of ultramafic rock. Ultramafic rocks are a significant component of the oceanic lithosphere (Fruh-Green et al., 2004b). They may have been widespread on early Earth (Shock and Schulte, 1998), and can be expected on other terrestrial planets (Sleep et al., 2004) and on Europa (McCollom, 1999). Because of the alkalinity and reducing power produced abundantly by serpentinization, the alteration of ultramafic rocks by water has important geochemical and biological consequences. Study of these environments may bear on prebiotic chemistry, early Earth evolution, and the potential for life elsewhere.

The LCHF is located on the peridotitic Atlantis massif 15 km west of the mid-Atlantic ridge at a depth of 750 to 900 m. Fluids are alkaline and reducing, and cool relative to magma-driven hydrothermal systems at mid-ocean ridges. The heat source driving

hydrothermal circulation at Lost City has been proposed to derive entirely from exothermic serpentinization reactions (Kelley et al., 2001; Kelley et al., 2005). However, this view has been challenged on the basis of heat-balance calculations showing that this source may be inadequate (Allen and Seyfried, 2004) and that geothermal heat must also be important. Hydrothermal fluid temperatures range from <40 to 90˚C with pH between 9 and 11, Ca^{2+} concentrations up to 30 mmol/kg, CH_4 concentrations up to almost 2 mmol/kg, and H_2 concentrations up to nearly 15 mmol/kg.

Hydrogen is a preferred electron donor for many microbes. Autotrophic methanogenesis couples oxidation of H_2 to reduction of CO_2 with the production of methane and is predicted to be thermodynamically favorable in the H_2-rich fluids produced by serpentinization (Sleep et al., 2004). Autotrophic methanogenesis requires no direct or indirect byproducts of oxygenic photosynthesis and may be one of the more ancient metabolic strategies on Earth. There is evidence for methanogenesis as far back in Earth history as the Archaean (Hayes, 1994; Ueno et al., 2006), although this some of this evidence has been subsequently challenged (Sherwood Lollar and McCollom, 2006), and some biologists dispute the early evolution of methanogenic archaea (Cavalier-Smith, 2006). Microbes that use other terminal electron acceptors such as sulfate are also capable of using H_2 as an electron donor and, when these electron acceptors are present, such organisms generally outcompete methanogens (Hoehler et al., 1998; Kristjansson et al., 1982).

The most spectacular features of the LCHF are massive calcium carbonate and brucite chimneys which grow up to 60 meters tall from the peridotite seafloor. Radiocarbon measurements indicate that the carbonate has been precipitating at its present location for at least 30 ky (Fruh-Green et al., 2003). The carbonate has $\delta^{13}C$ between +1.4‰ and +2.9‰ and $\delta^{18}O$ between +1.5‰ and +5.2‰ relative to VPDB, while $^{87}Sr/^{86}Sr$ values are between 0.70760 and 0.70908. These data indicate a source dominated by seawater, and suggests that precipitation of calcium carbonate occurs upon mixing of seawater with vent fluids. The Ca^{2+} source is dominantly hydrothermal, while the CO_3^{2-} derives predominantly from

seawater (Fruh-Green et al., 2003; Ludwig et al., 2006). Measurements of Sr isotopes and wt% Mg in carbonate chimneys have shown that mixing ratios of seawater and vent fluids vary between chimneys (Ludwig et al., 2006).

The carbonate towers host a rich microbial ecosystem. Analyses of 16S rDNA and cell counts by fluorescence in situ hybridization (FISH) show that active vent structures contain a predominance of archaea (Brazelton et al., 2006; Kelley et al., 2005) , with Methanosarcinales prevalent in active, high-temperature vent structures and ANME-1 group methanotrophs present in two samples from lower-temperature carbonate veins, and one active vent (Brazelton et al., 2006; Kelley et al., 2005). Studies of bacterial diversity indicate that Firmicutes are present in higher-temperature, active vent fluids, along with methane-oxidizing and sulfur-oxidizing bacteria (Brazelton et al., 2006; Kelley et al., 2005). The coexistence of obligate aerobes and obligate anaerobes in the same samples suggests that different microbial communities inhabit different environments around the vents, possibly an anaerobic community inhabiting reducing anaerobic hydrothermal fluid within carbonate structures and aerobic microbes inhabiting zones on carbonate surfaces where hydrothermal fluid mixes with oxygenated seawater.

Here we report on the chemical and isotopic composition of organic matter in the carbonate chimneys at the LCHF. This data sheds light on the nature of the Lost City Methanosarcinales and on the biological production of methane. Understanding of the source of methane at Lost City is significant in informing our understanding of the evolution of the biosphere. Methane is an important trace gas in the modern atmosphere and was probably abundant in the atmosphere during the first two billion years of Earth history (Catling et al., 2001; Kasting and Ono, 2006) when it may have played an important role in regulating global temperature (Lowe and Tice, 2004; Pavlov et al., 2001). The role of methanogens in moderating the H_2 level in the atmosphere is an important component of Precambrian climate models (Kasting, 2005) and the abundance of H_2 in the Precambrian atmosphere is hotly debated (Catling, 2006; Tian et al., 2006; Tian et al., 2005). Methane

has been detected in the Martian atmosphere (Formisano et al., 2004) where its source is unknown. Understanding systems such as Lost City should shed light on these issues.

3.2. Methodology

Carbonate samples were collected during Atlantis cruise AT-7-41 using the submersible *Alvin* and stored in Teflon containers at -20°C until processing. Subsamples were freeze-dried and crushed to a fine powder, then ultrasonically extracted three times (ca. 30 min) in a mixture of dichloromethane (DCM):methanol (3:1, v/v) and all three extracts were combined. Extracts were centrifuged at 2000 rpm for 15 minutes to remove residual carbonate particles and then the bulk of solvent was evaporated at 35°C under a stream of dry nitrogen. Elemental sulfur was removed from the extracts by passing over a column of activated copper, followed by filtration of the extract through a 40 μm combusted glass Buchner funnel. Total lipid extracts were weighed and are reported as μg of lipid per gram of dry rock extracted.

Aliquots of lipid extracts were analyzed as their trimethylsilyl ethers and esters by reacting with *N,O*-bis(trimethylsilyl)trifluoro-acetamide (BSTFA + 1% TMCS) in pyridine at 60°C for thirty minutes. The remainder of the total lipid extract was separated over silica gel into five fractions using an elution scheme of solvents of increasing polarity: aliphatic hydrocarbons 1⅜ dead column volume (DV, measured by slow addition of the first eluent with calibrated syringe) hexane, aromatic hydrocarbons 2 DV 4:1 hexane:DCM, ketones 2 DV DCM, alcohols 2 DV 4:1 DCM:ethyl acetate, fatty acids and diols 2 DV 7:3 DCM:methanol. Individual lipids were identified using a HP 6890 gas chromatograph fitted with a PTV injector operated in splitless mode and equipped with a Varian CP-Sil-5 (60-m length, 0.32 mm inner diameter, and 0.25-um film thickness) fused silica capillary column and coupled to an Agilent 5973 mass-selective detector. Lipids were identified by comparisons of mass spectra and retention times with authentic standards or samples where these compounds have previously been characterized. Diether lipids were identified by

comparison to similar authentic standards, and we report their masses without attempting to solve their detailed structures. Lipids were quantified relative to coinjected standards.

In some cases the side chains of ether lipids were cleaved by reaction with 1.0 M boron tribromide (BBr_3, Aldrich) in dichloromethane (DCM). Approximately 200 µl BBr_3 was added to lipid extracts in dry vials under a stream of argon, after which vials were sealed and heated to 60ºC for 2 hours. After the reaction was complete, the resulting bromides were reduced to hydrocarbons by adding the DCM solution containing bromides to approximately 1 ml of Super-Hydride solution (1.0 M lithium triethylborohydride in tetrahydrofuran, Aldrich) in dry vials under a stream of argon and reacting at 60ºC for 2 hours. Samples were cleaved and reduced in parallel with an ether lipid standard to confirm quantitative cleavage of side chains to hydrocarbons.

Carbon-isotopic compositions of individual lipids were determined using a TraceGC gas chromatograph fitted with a PTV injector and equipped with a Varian DB-1 (60-m length, 0.32 mm inner diameter, and 0.25-um film thickness) fused-silica capillary column and coupled to a ThermoFinnigan Deltaplus XL isotope-ratio-monitoring mass spectrometer via a combustion interface at 850°C. Column temperatures were programmed from 60°C at 10°C/min to 100°C, to 320°C at 4°C/min, and then held isothermal for 20 minutes. Carbon isotope ratios were determined relative to an external CO_2 standard that was regularly calibrated relative to a reference mixture of *n*-alkane (Mixture B) provided by Arndt Schimmelmann (Indiana University). All lipid isotope values were corrected by mass balance for the carbon present in the TMS derivative.

Total organic carbon contents of carbonates were determined by weighing freeze-dried and finely crushed carbonate samples (20-40 mg) in triplicate into clean silver capsules. The silver capsules were placed in an evacuated chamber for seven days with vapor in equilibrium with concentrated HCl and several grams of P_2O_5 which served as a dessicant. Complete removal of carbonate was verified by addition of 50 – 100 µl of concentrated HCl directly to the silver capsules at 60°C. Samples were dried at 60°C

overnight, and residual $CaCl_2$ was allowed to remain with the samples. Silver capsules were burned in a Fisions Elemental Analyzer at 1030°C coupled to a ThermoFinnigan Delta Plus XL isotope ratio monitoring mass spectrometer. Inspection of the resulting CO_2 traces with ThermoFinnigan IsoDat software confirmed the absence of carbonate remaining in the samples. Total organic carbon contents were calculated by integration of peak areas compared to an external standard with known carbon content. Stable carbon isotope ratios were determined with an external CO_2 standard calibrated to international reference materials NBS-22 oil, CH-6 sucrose and an internal lab standard (acetanilide) and reported in Vienna Pee Dee Belemnite (VPDB) notation.

3.3. Results and Discussion

3.3.1 Total Organic Carbon

Thirty-seven carbonate samples had total organic carbon contents averaging about 0.2% and varying between approximately 0.05% and 0.5% TOC (Table 3-1). The ^{13}C content of the organic carbon was widely variable with $\delta^{13}C$ from -27.7‰ to -2.8‰. TOC and $\delta^{13}C$ are uncorrelated (Figure 3-2a**)**. As will be discussed below, the enhanced ^{13}C contents are consistent with the ^{13}C contents seen in individual lipids. Diether lipids are the most ^{13}C enriched components and samples with the highest concentrations of diether lipids also tend to have the highest $\delta^{13}C_{TOC}$ **(**Figure 3-3**)**. Samples taken from various parts of the same carbonate tower have values of $\delta^{13}C_{TOC}$ varying by up to 14.4‰ . Replicate measurements for a single sample yield variations < 0.5‰. Accordingly, larger variations reflect natural heterogeneity of microbial communities within a tower.

Exceptional enrichment in ^{13}C is most prevalent in actively venting structures. (Table 3-1). Of samples that are characterized as active or inactive, only active structures contained total organic carbon with $\delta^{13}C > -10$‰, and inactive structures all contained TOC with $\delta^{13}C < -15$‰. A histogram (Figure 3-4) shows the distribution of $\delta^{13}C$ values for TOC with regard to vent activity.

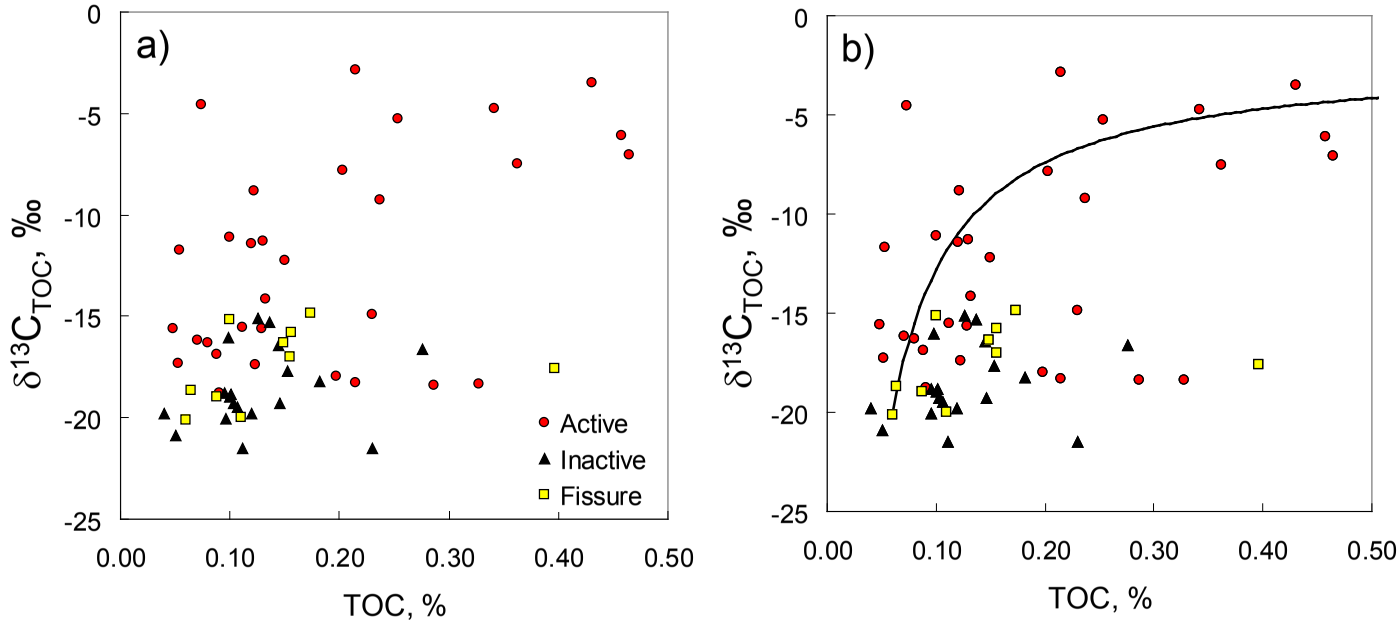

Figure 3-2: a) Plot of total organic carbon and $\delta^{13}C_{TOC}$ for all carbonate chimney samples, grouped as active, inactive, and fissure samples. B) same plot as (a) but with a hypothetical mixing line of two end members: 0.06% marine organic carbon applied to all vents ($\delta^{13}C$ = -20‰) and a varying amount of vent organic carbon with ($\delta^{13}C$ = -2‰).

Table 3-1: Total organic carbon content and $\delta^{13}C_{TOC}$ for all collected carbonate samples. Marker location and carbonate type (after Ludwig et al., 2006) are denoted Type A: active, I: inactive, F: fissure. Samples were analyzed in two batches at the Woods Hole Oceanographic Institue (w) and at the Massachusetts Institute of Technology (m).

Marker	Sample	$\delta^{13}C$	% TOC	Type	
3	LC 3862-1219	-12.2	0.15	A	m
3	LC 3862-1219	-11.4	0.12	A	w
2	LC 3864-1524	-15.5	0.11	A	m
2	LC 3864-1537	-8.8	0.12	A	m
1	LC 3864-1647	-18.2	0.18	I	m
1	LC 3864-1647	-15.3	0.14	I	w
fracture fill near mkr 7	LC 3865-1322	-15.1	0.10	F	m
7	LC 3867-1225	-3.5	0.43	A	m
7	LC 3867-1225	-6.1	0.46	A	m
7	LC 3867-1225	-5.2	0.25	A	w
7	LC 3867-1228	-7.5	0.36	I	m
7	LC 3867-1228	-2.8	0.21	I	w
Under Poseidon	LC 3867-1308	-19.8	0.12	I	m
Under Poseidon	LC 3867-1308	-19.0	0.10	I	w
C	LC 3869-1404	-7.8	0.20	A	m
C	LC 3869-1404	-14.9	0.23	A	m
C	LC 3869-1404	-9.2	0.24	A	w
C	LC 3869-1443	-7.0	0.47	A	m
C	LC 3869-1443		0.40	A	w
C	LC 3869-1446	-4.7	0.34	A	m
8	LC 3871-1147	-11.3	0.13	A	w
8	LC 3871-1147	-11.1	0.10	A	w
C	LC 3871-1319		0.60	A	w
C	LC 3871-1319	-18.4	0.33	A	w
2	LC 3871-1442	-18.8	0.09	I	m
2	LC 3871-1442	-19.3	0.10	I	m
2	LC 3871-1442	-17.7	0.15	I	m
below W part vent field	LC 3871-1512	-20.9	0.05	I	m
extinct carbonate	LC 3872-1544	-21.5	0.23	I	m
lithified carbonate	LC 3873-1203	-19.8	0.04	I	m
	LC 3873-1413	-17.6	0.40	F	m
9	LC 3875-1244	-16.1	0.10	I	w
B	LC 3875-1409	-18.4	0.29	A	w
hump spire	LC 3876-1104	-18.0	0.20	A	w
hump spire	LC 3876-1104	-18.3	0.22	A	m
on serpentinite basement	LC 3876-1113	-20.1	0.10	I	m
X1	LC 3876-1133	-16.3	0.15	F	m
X1	LC 3876-1133	-14.9	0.17	F	w
carbonate growing on serpentinite	LC 3876-1219	-15.8	0.16	F	m
B	LC 3876-1427	-18.7	0.06	F	w
B	LC 3876-1436	-16.2	0.07	A	w
carbonate sediment	LC 3877-1214	-21.5	0.11	I	m
old ext. chimney	LC 3877-1501	-19.3	0.15	I	m
extinct carbonate	LC 3877-1501	-19.5	0.11	I	w
Nature cover	LC 3877-1606	-18.8	0.09	A	m
Nature cover	LC 3877-1606	-17.3	0.05	A	w
Poseidon	LC 3878-1630	-16.4	0.14	I	m
Poseidon edifice	LC 3878-stow	-6.9	0.37	?	m
Poseidon edifice	LC 3878-stow	-21.3	0.10	?	w
H	LC 3879-1216	-11.7	0.05	A	w
carbonate close to serpentinite	LC 3879-1258	-20.1	0.06	F	m
2	LC 3879-1500	-4.6	0.07	A	w
7	LC 3879-1605	-3.1	0.28	A	w
7	LC 3879-slurp	-6.5	0.44	A	m
carbonate assoc. w black rock	LC 3880-1353	-17.0	0.16	F	m
active, below Nature tower	LC 3880-1532	-16.3	0.08	A	m
X2	LC 3880-1557	-19.0	0.09	F	w
X2	LC 3880-1557	-20.0	0.11	F	m
flange at H	LC 3881-1201	-17.4	0.12	A	m
H	LC 3881-1225		0.36	A	w
H	LC 3881-1228	-14.1	0.13	A	w
H	LC 3881-1228	-16.9	0.09	A	m
mussel acres at H	LC 3881-1256	-16.6	0.28	I	m
mussel acres at H	LC 3881-1256	-15.1	0.13	I	w
H - inactive	LC 3881-1325	-18.8	0.10	I	m
3	LC 3881-1408	-15.6	0.13	A	m
3	LC 3881-1408	-15.6	0.05	A	w

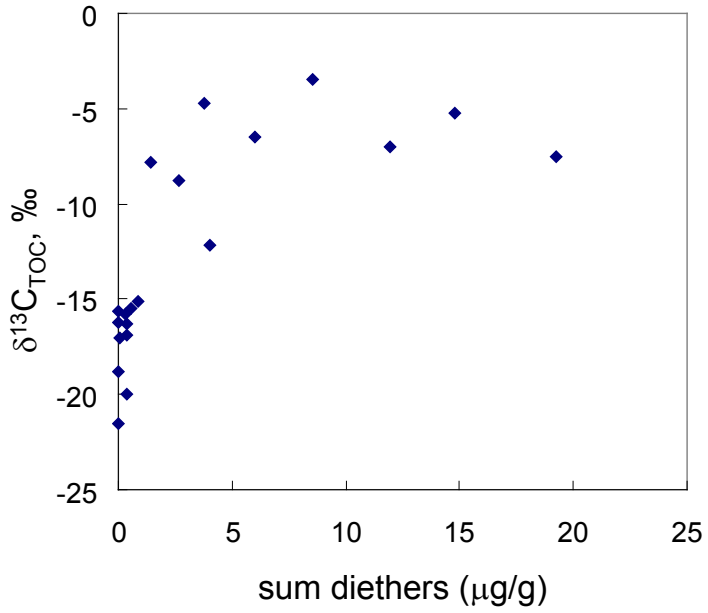

Figure 3-3: Plot of diether content vs. $\delta^{13}C_{TOC}$ for samples with lipid analyses, showing that TOC highly enriched in ^{13}C contain higher amounts of isoprenoidal and non-isoprenoidal diether lipids.

The ^{13}C content of total organic carbon in Lost City carbonates can be loosely modeled as a mixture between two end-members. One end-member is marine carbon incorporated from the water column, that can be estimated to have $\delta^{13}C$ = -20‰ (Goericke and Fry, 1994). Vent organisms comprise the second end-member $\delta^{13}C$ near -2‰. If TOC_{marine} is assumed to be near constant at 0.06%, and TOCvent varies from 0 to 0.5%, it produces the curve shown in Figure 3-2b.

3.3.2 Archaeal lipid distribution and ^{13}C content

To estimate the relative inputs of archaeal biomass at various LCHF vent sites, we measured the abundances of lipids diagnostic for archaea. We sampled carbonates from active and inactive vent structures from several locations that spanned the range of fluid temperatures at Lost City.

Archaeol, a lipid unique to archaea, was detected in approximately one-half of the

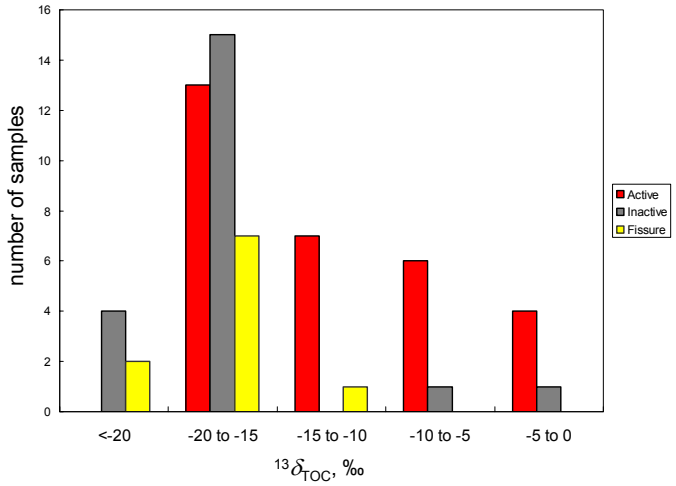

Figure 3-4: Histogram showing frequency of $\delta^{13}C_{TOC}$ for samples classified as "active", "inactive" and "fissure" after Ludwig et al., 2006. Samples enriched in ^{13}C are dominantly from active carbonate chimneys.

samples (Table 3-2). Concentrations ranged from below detection limit up to 600 ng of archaeol per gram of dry carbonate. In most cases archaeol was enriched in ^{13}C relative to typical phytoplanktonic products, with δ values up to +6.0‰. The average value of $\delta_{archaeol}$ in carbonate chimneys was +1.5‰. In only one case did a sample contain archaeol with a δ <-4.2‰. That sample, with $\delta_{archaeol}$ = -77‰ was an inactive carbonate collected 30 meters E of marker H (marker X2, sample 3880-1557). The low value of $\delta_{archaeol}$ implies that archaea at this site consume methane. Correspondingly, a microbiological survey of 16S rDNA (Brazelton et al., 2006) has detected ANME-1 methanotrophic archaea at this location.

All other samples containing archaeol also contained *sn*-2 hydroxyarchaeol, *sn*-3 hydroxyarchaeol, and a putative dihydroxyarchaeol. Both *sn*-2 hydroxyarchaeol and dihydroxyarchaeol were more abundant than archaeol in each case. The concentrations and $\delta^{13}C$ values of archaeol and *sn*-2 hydroxyarchaeol are strongly co-variant in Lost City carbonates. (Figure 3-5a, 3-5b). Concentrations of archaeol strongly correlate with those of dihyxroxyarchaeol (Figure 3-5c), but the δ values are unrelated (Figure 3-5d). The

Table 3-2: Individual lipid abundances and $\delta^{13}C$ value listed by sample. For each sample examined the Marker locations is noted, along with the $\delta^{13}C_{TOC}$ and information about vent activity and temperature where known. All lipid concentrations are in µg lipid per gram of dry rock.

Marker	B		X2		X1		C		3		C		C		7		nd	
Temperature	90		-		-		70		81		70		70		34		-	
Type	A		F		F		A		A		A		A		A		F	
TOC	0.07		0.11		0.15		0.47		0.13		0.20		0.34		0.25		0.16	
d TOC	-16.2		-20.0		-16.3		-7.0		-15.6		-7.8		-4.7		-5.2		-15.8	
	3876-1436		3880-1557		3876-1133		3869-1443		3881-1408		3869-1404		3869-1446		3867-1225		3876-1219	
total lipid (ug/g)	6		105		76		131		67		53		91		235		75	
	conc (ug/g)	$\delta^{13}C$	conc (ug/g)	$\delta^{13}C$ [3]	conc (ug/g)	$\delta^{13}C$	conc (ug/g)	$\delta^{13}C$	conc (ug/g)	$\delta^{13}C$	conc (ug/g)	$\delta^{13}C$	conc (ug/g)	$\delta^{13}C$	conc (ug/g)	$\delta^{13}C$	conc (ug/g)	$\delta^{13}C$
archaeol			0.01	-77.0			0.11	3.0			0.03	6.7	0.10	5.7	0.61	0.7		
sn-2							2.22	2.8			0.39	5.1	0.97	4.8	5.94	1.3		
sn-3							0.22	1.6			0.03	0.8	0.12	6.0	1.25	-2.1		
diOH							0.85	2.4			0.11	6.6	0.40	5.3	3.47	-0.4		
PMI											0.12	7.1	0.22	10.0				
16:1 FA					0.39	-21.5	0.05	-			0.02	-27.3	0.08	-17.0	0.28	-25.4	0.02	-16.5
16 FA	0.01	-31.4			0.12	-27.4	0.20	-14.7			0.04	-25.7	0.52	-4.3	1.56	-7.5	0.13	-19.8
18:1 FA					0.16	-27.5	0.12	-16.7			0.04	-25.4	0.14	-20.3	0.41	-22.5	0.17	-26.1
18 FA	0.01	-30.2			0.02	-25.0	0.11	-9.7			0.02	-15.3	0.21	-8.0	0.51	-1.1	0.03	-24.2
cholesterol	0.01	-27.7	0.09	-28.6	0.58	-27.0	0.21	-23.8	0.01	-26.1	0.06	-26.3	0.49	-27.5	0.29	-26.1	0.10	-23.2
C28:2			0.01	-28.1	0.12	-28.2					0.03	-20.1	0.09	-25.9			0.05	-21.9
C29:2				-27.7							0.04	-27.0	0.20	-24.6			0.09	-20.2
C29			0.05	-26.4	0.09	-28.6	0.08	-			0.02		0.15	-22.3			0.09	-19.8
cycloartenol			0.02	-29.8	0.27	-27.5			0.03	-16.0	0.04	-25.1		-			0.15	-24.3
diploptene			0.03		0.03						0.03	-21.4	0.14				0.09	
tetrahymanol			0.04	-26.5	0.06	-16.9	0.09		0.002	-23.5			0.08		trace		0.07	-15.1
diplopterol			0.12	-22.0	0.7	-18.2	0.08		0.16	-16.7	0.04		0.23		trace		0.67	-15.0
C19:1 GME			0.02	-23.9	0.06	-26.4	0.04	-12.4			0.003	-6.1	0.04	-6.7			0.06	-24.9
C21 GME			0.03	-27.7	0.08	-23.3	0.04	-14.0			0.004	-10.6	0.06	-3.9	0.03	-11.5	0.06	-22.2
GDE 556																		
GDE 570																		
GDE 582			0.02	-30.3			1.50	2.6			0.06	-1.1	0.47	2.6	0.33	-5.0	0.05	-14.3
GDE 582			0.05	-32.4														
GDE 582																		
GDE 584			0.04	-36.2			0.24	-0.4			0.05	0.8	0.14	-2.2	0.25	-6.4	0.05	-18.8
GDE 584													0.21	-3.3	0.09	-7.9		
GDE 584																		
GDE 584																		
GDE 596											0.02	-3.8	0.25	-4.9				
GDE 596											0.03	0.0						
GDE 596											0.02	-10.6						
GDE 598											0.02	3.6			0.21	-4.9	0.06	-22.3
GDE 598															0.58	-5.4		
GDE 608			0.20	-41.3	0.19	-22.1	6.02	-1.0			0.05	-5.3	1.03	-1.4	0.93	-6.0	0.07	-19.4
GDE 608											0.37	0.1						
GDE 608																		
GDE 610	0.003	-4.4							0.01	-5.4								
GDE 610																		
GDE 612							0.29	1.7	0.01	-3.6	0.03	2.2			0.19	-3.4	0.06	-19.5
GDE 622			0.01	-45.0														
GDE 624			0.01	-36.4			0.23	-3.7					0.15	-0.9				
GDE 626					0.12	-17.3					0.03	1.5			0.21	-10.1		
GDE 626											0.04	0.3			0.45	-7.6		
GDE 636			0.03	-36.9			0.21	-11.8										
GDE 636			0.02	-42.7							0.06	-9.3						
GDE 636																		
GDE 638									0.01	-7.7	0.06	-11.2			0.24	-9.0		
GDE 640					0.05	-18.9					0.03	1.4						
GDE 652							0.08	-5.0										
GDE 664																		

Table 3-2 (cont.): Individual lipid abundances and $\delta^{13}C$ value listed by sample. For each sample examined the Marker locations is noted, along with the $\delta^{13}C_{TOC}$ and information about vent activity and temperature where known. All lipid concentrations are in µg lipid per gram of dry rock.

Marker	near 7		H		7		-		2		7		H		2		3	
Temperature	-		46		52		-		64		-		-		53.5		59	
Type	F		I		+		F		A		I		I		A		A	
TOC	0.10		0.10		0.44		no data		0.11		0.36		0.09		0.12		0.15	
d TOC	-15.1		-18.8		-6.5		no data		-15.5		-7.5		-16.9		-8.8		-12.2	
	3865-1322		3881-1325		3879-1605		3881-1132		3864-1524		3867-1228		3881-1228		3864-1537		3862-1219	
total lipid (ug/g)	35		3		364		4		304		217		36		253		92	
	conc (ug/g)	$\delta^{13}C$	conc (ug/g)	$\delta^{13}C$	conc (ug/g)	$\delta^{13}C$	conc (ug/g)	$\delta^{13}C$	conc (ug/g)	$\delta^{13}C$	conc (ug/g)	$\delta^{13}C$	conc (ug/g)	$\delta^{13}C$	conc (ug/g)	$\delta^{13}C$	conc (ug/g)	$\delta^{13}C$
archaeol					0.16	1.3			0.02	-0.4	0.42	6.0	0.01	-4.2	0.12	-0.8	0.01	-2.5
sn-2			0.01	-2.2	1.80	0.7			0.15	2.4	6.66	4.2	0.18	0.6	0.21	0.2	0.07	1.3
sn-3					0.39	0.5			0.03	1.9	0.67	-1.5	0.08	4.8		-	0.01	0.2
diOH					1.09	0.5			0.05	3.8	1.97	3.8	0.09	-2.9	0.09	1.1	0.02	1.2
PMI																		
16:1 FA	0.17	-13.2	0.00		0.10	-20.7	0.00		0.02	-12.9	0.06	-19.5	0.24	-14.7	0.11	-13.5	0.26	-28.3
16 FA	0.15	-13.4	0.01		0.73	-9.1	0.01	-24.1	0.06	-7.3	0.09	-8.6	0.33	-12.0	1.62	-6.8	0.75	-8.8
18:1 FA	0.08	-20.1	0.01		0.18	-16.8	0.00		0.06	-13.3	0.03	-26.5	0.85	-12.0	0.47	-13.4	0.15	-17.6
18 FA	0.01	-20.4	0.01		0.21	-8.7	0.01	-26.7	0.02	-8.7	0.10	-2.2	0.11	-12.4	0.53	-8.9	0.10	-5.4
cholesterol	0.10	-24.7	0.06	-23.3	0.17	-27.8	0.02	-25.4	0.04	-27.7	0.10	-26.1	0.01	-26.4	0.35		0.25	-28.5
C28:2	0.05		0.02	-21.7			0.01											
C29:2	0.03	-20.3	0.01	-25.5			0.01				0.13	-24.9						
C29	0.10	-25.8	0.01	-23.4			0.01	-26.5			0.09							
cycloartenol	0.15	-17.6							0.10	-15.4							0.49	-15.9
diploptene	0.08						0.01				0.04	-19.2						
tetrahymanol	0.04	-15.8	0.01	-15.7	0.04		0.03	-11.8	0.03	-4.5	0.04		0.14	-4.6	0.15	-3.5		
diplopterol	0.74	-18.5	0.02	-19.3	0.03		0.07	-19.0	0.01	-3.2	0.07		0.10	-20.4				
C19:1 GME	0.01	-21.4	0.00		0.01	-13.5	0.00	-26.7	0.01	-6.0	0.03	-9.3	0.04	-14.0	0.15	-6.0		
C21 GME	0.02	-19.6	0.00		0.01	-12.9	0.00	-19.6	0.02	-10.6	0.07	-19.2	0.13	-9.7	0.14	-8.1		
GDE 556											0.11	-6.8						
GDE 570											0.13	-5.6						
GDE 582					0.26	-5.6					2.37	-2.0			0.14	-4.3	0.42	-4.9
GDE 582																		
GDE 582																		
GDE 584			0.00	-18.2	0.08	-6.1					0.12	-5.5	0.01	-6.8	0.16	-6.0		
GDE 584					0.17	-6.8					0.15	-7.5						
GDE 584											0.22	-3.9						
GDE 584											0.75	-6.0						
GDE 596					0.25	-5.6					0.31	-6.2						
GDE 596											0.32	-8.8						
GDE 596											0.17	-3.7						
GDE 598																	0.15	-8.9
GDE 598																	0.17	-2.5
GDE 608	0.07	-19.8	0.02	-25.6					0.03	-4.6	3.50	-3.5			0.17	-2.9		
GDE 608	0.18	-28.4																
GDE 608	0.35	-28.7																
GDE 610					0.35	-5.7			0.07	-5.2					0.54	-4.4	0.30	-4.6
GDE 610					0.76	-8.8			0.11	-4.5								
GDE 612											0.33	-1.3	0.02	-7.3	0.47	-5.0	2.06	-4.7
GDE 622											0.34	-4.6						
GDE 624					0.48	-7.2			0.02	-3.6	0.17	-1.9			0.08	-2.1	0.32	-4.2
GDE 626					0.10	-11.0							0.004	-10.6	0.14	-3.7	0.09	-8.5
GDE 626																		
GDE 636	0.12	-18.9							0.03	-6.4	0.24	-7.7			0.28	-2.5		
GDE 636											0.25	-7.5						
GDE 636											0.09	-5.0						
GDE 638					0.11	-8.7			0.04	-6.1					0.20	-5.1	0.15	-7.4
GDE 640	0.14	-16.9															0.25	-5.4
GDE 652									0.01	-0.4								
GDE 664									0.01	-5.3								

concentration of *sn*-2 hydroxyarchaeol averages 2.6 times that of dihydroxyarchaeol, and both of these compounds are more abundant than *sn*-3 hydroxyarchaeol (Figure 3-6). This pattern, which might not be expected with mixed inputs from various species, is suggestive that all of the hydroxyarchaeol compounds are synthesized by a single archaeal strain, although the isotope data suggest a that dihydroxyarchaeol may have multiple sources. Two other compounds with spectra similar to hydroxyarchaeols are also common at Lost City – one eluting after *sn*-3 hydroxyarchaeol and one just after dihydroxyarchaeol **(**Figure 3-6**)**. These compounds are probably similar in structure to hydroxyarchaeols. Compounds with similar retention times and spectra have been detected in sediments at the Haakon Mosby Mud Volcano (M. Elvert, pers. comm.), which contains ANME-3 methanotrophs. The ANME-3 group is very closely related to the methanogens found at Lost City (Losekann et al., 2007). These compounds may be specific to this clade.

In environmental samples, detection of hydroxyarchaeols is usually related to the presence of the archaeal orders Methanosarcinales or Methanococcales, including the ANME-2 group and the closely related ANME-1 archaeal methanotrophs (Blumenberg et al., 2004; Hinrichs et al., 2000; Pancost et al., 2001). There are a few exceptions to this rule, however. Within the Methanobacteriales, *Methanosphaera* species have been reported to synthesize hydroxyarchaeol (Koga et al., 1998; Sprott et al., 1999), as has *Methanobrevibacter* (Sprott et al., 1999). One halophilic archaeon, *Natronobacterium*, is also reported to synthesize the compound (Upasani et al., 1994). In many Lost City carbonates, *sn*-2 hydroxyarchaeol is the single most abundant extractable lipid.

Microbiological studies suggest that hydroxyarchaeols indeed derive from Methanosarcinales. Examination of 16S rRNA sequences from Lost City carbonates has shown that archaeal diversity is low and dominated by a phylotype of Methanosarcinales denoted as Lost City Methanosarcinales (Brazelton et al., 2006). LCMS was the sole archaeal phylotype in most carbonate chimneys with the exception of samples from Marker C, characterized by sequences corresponding to both LCMS and ANME-1. Two samples

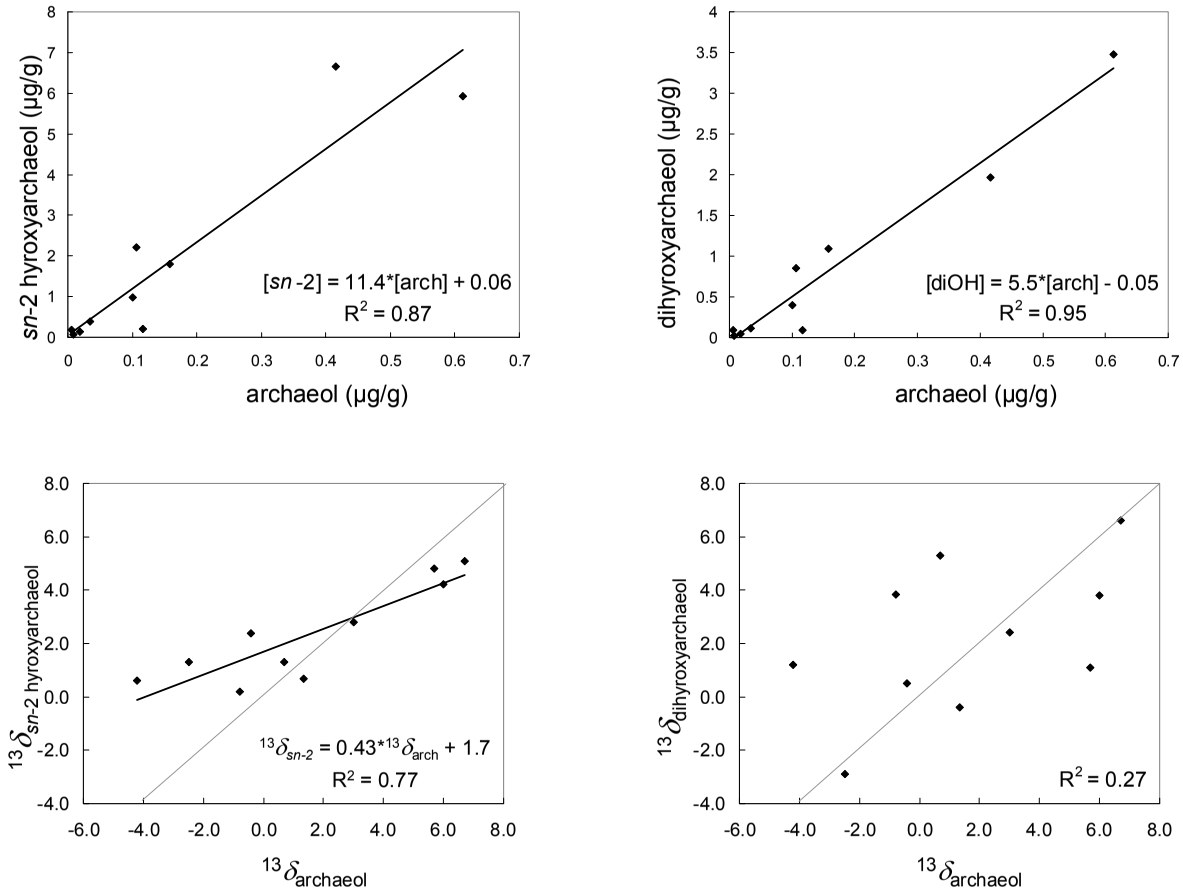

Figure 3-5: Correlations of a) the concentrations of archaeol and *sn*-2 hydroxyarchaeol in samples in which both were detected, b) $\delta^{13}C$ values of archaeol and *sn*-2 hydroxyarchaeol, c) concentrations of archaeol and dihydroxyarchaeol, d) $\delta^{13}C$ values of archaeol and dihydroxyarchaeol. Black lines in (a), (b), and (c) are regression lines. Grey lines in (b) and (d) are 1:1 lines.

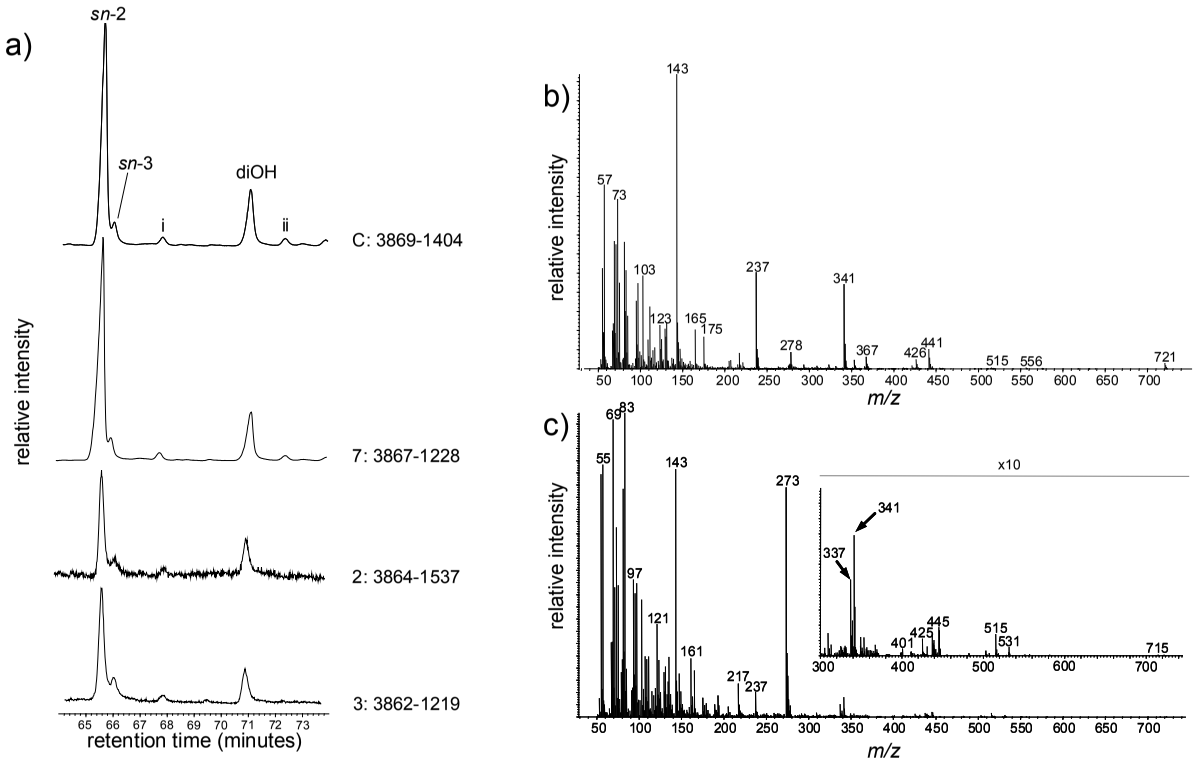

Figure 3-6: a) TIC chromatograms showing constant relative peak areas among samples of *sn*-2 hydroxyarchaeol (*sn*-2), *sn*-3 hydroxyarchaeol (*sn*-3), dihydroxyarchaeol (diOH), and two unidentified compounds (i, ii) that are presumed to be structurally related to hydroxyarchaeols. b) mass spectrum of compound i. c) mass spectrum of compound ii.

from carbonate veins hosted in serpentinite (marked X1 and X2) contained ANME-1 only (X2) or ANME-1 dominated with a very small amount of LCMS (X2).

Ether-cleavage reactions (BBr_3/SH, see methods) did not yield any C_{40} products. Accordingly, GDGTs must be absent. Such compounds are commonly detected in methanogens and in anaerobic archaeal methanotrophs (Blumenberg et al., 2004; Hinrichs et al., 1999; Hinrichs et al., 2000; Pancost et al., 2001). The hydrocarbon 2,6,10,16,19-pentamethylicosane (PMI) was present in two samples. Its $\delta^{13}C$ value was between +7‰ and +10‰ (Table 3-2).

When hydroxyarchaeols are detected in methanotrophic archaea, typically they are extremely depleted in ^{13}C with δ values of -80 to -100‰ (Hinrichs et al., 2000). At Lost City, hydroxyarchaeols are uniformly highly enriched in ^{13}C, with an average $\delta^{13}C$ near +2‰ (Table 3-2). Lipids with such high ^{13}C enrichments are rare. Lipids with $\delta^{13}C$ = +4‰ have been detected in a geothermal sinter in New Zealand (Pancost et al., 2006), but the Lost City PMI, with $\delta^{13}C$ = +10‰ establishes a new record for enrichment of ^{13}C in a natural lipid.

Such a striking enrichment in ^{13}C suggests that the assimilation of carbon by Methanosarcinales at Lost City must be unusual. The LCMS phylotype has in some cases been included in the newly defined ANME-3 group, apparently on the basis of the close correspondence of its 16S rDNA sequence to sequences from environments where methane is being oxidized anaerobically such as the Haakon Mosby Mud Volcano (Knittel et al., 2005). The ANME-3 group has been defined as a methanotroph on the basis of its association with zones of methane consumption and sulfide production, and archaeol and *sn*-2 hydroxyarchaeol highly depleted in ^{13}C (Niemann et al., 2006). Later reports have defined the ANME-3 clade more narrowly, and exclude the LCMS (Losekann et al., 2007). Our findings support the latter view, and suggest that the LCMS phylotype is not methanotrophic. Three convergent lines of evidence support this view.

First, the $\delta^{13}C$ of methane at Lost City is reported to be -13.6‰ to -8.8‰ (Kelley

et al., 2005). Lipids are significantly more enriched in ^{13}C than methane, therefore methane is excluded as a viable carbon source for these organisms. In AOM environments Methanosarcinales lipids are exceedingly depleted relative to methane, often by amounts up to 60‰ (Hinrichs et al., 1999). Second, DIC is lower in abundance than methane but more enriched in ^{13}C. This pattern would not occur if large amounts of methane were being oxidized to DIC. Third, the concentrations of hydrogen within the vent fluids are up to nearly 15 mM. These high hydrogen concentrations provide a strong thermodynamic drive for methanogenesis but not for the reverse reaction. Under the millimolar hydrogen concentrations at Lost City, anaerobic oxidation of methane would be thermodynamically difficult, favored only if an H_2-consuming syntroph were available to remove large amounts of hydrogen over short distances within the consortium (see Appendix 1). However ANME-1 organisms were detected at Marker C (Brazelton et al., 2006) where hydrogen concentrations are higher than 7 mmol/kg (Proskurowski et al., 2006).

If not methanotrophic, the LCMS phylotype is likely methanogenic. Methanosarcinales are physiologically diverse and capable of producing methane from a variety of substrates including CO_2, acetate, methanol, and trimethylamine. The extraordinary abundance of hydrogen in Lost City vent fluids suggests that it is the most viable electron donor for methanogenesis.The methanogenesis is therefore likely autotrophic, although heterotrophic methanogenesis using substrates such as formate or methanol can not be absolutely excluded. Formate or methanol might form by reduction of CO formed from CO_2 under some hydrothermal conditions, but the pH at Lost City limits CO_2 availability and these substrates are unlikely to be available in abundance (Seewald et al., 2006).

The isotope discrimination between CO_2 and hydroxyarchaeols produced by autotrophic Methanosarcinales varies with a number of conditions and particularly hydrogen concentration (Chapter 2). At high concentrations of H_2 carbon-isotopic differences between CO_2 and lipids are smaller than at low concentrations, probably due to differential reversibility of the enzymes in the methanogenic pathway (Valentine et

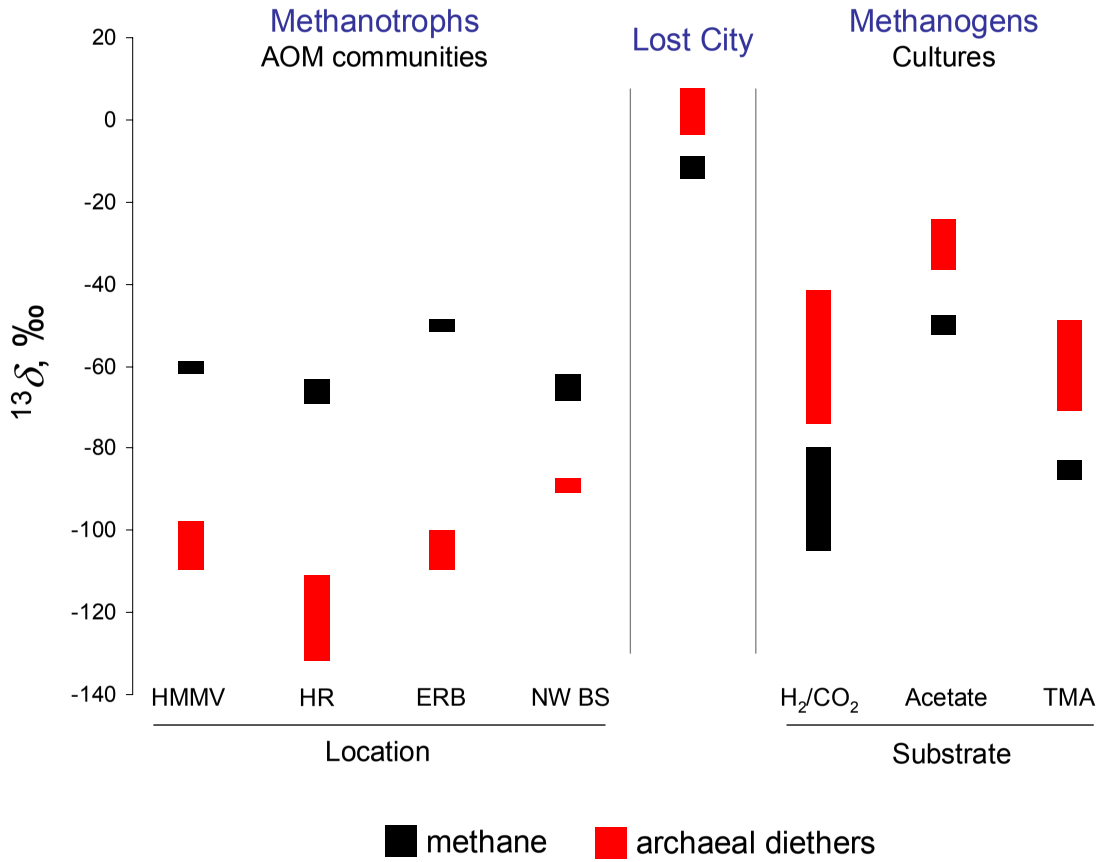

Figure 3-7: Ranges of the $\delta^{13}C$ values of archaeal diethers and of methane in AOM communities (HMMV: Haakon Mosby Mud Volcano (Losekann et al., 2007; Niemann et al., 2006); HR: Hydrate Ridge (Boetius et al., 2000; Elvert et al., 1999; Heeschen et al., 2005; Teichert et al., 2005); ERB: Eel River Basin (Hinrichs et al., 1999); NW BS: Dniepr Canyon, Northwest Black Sea (Michaelis et al., 2002)), Lost City (this study) and methanogen cultures grown on several substrates (Chapter 2; Summons et al., 1998).

al., 2004). In parallel investigations, we have found that the fractionation between CO_2 and *sn*-2 hydroxyarchaeol in *Methanosarcina barkeri* at high hydrogen concentrations is approximately 12‰, compared to more than 40‰ at low hydrogen concentrations (Chapter 2).

Values of $\delta^{13}C$ of inorganic carbon in Lost City vent fluids range between -8‰ to +3‰ (Kelley et al., 2005). The similar ^{13}C contents between lipids and DIC can be explained by carbon limitation. If available inorganic carbon is consumed nearly completely, isotopic discrimination will be minimized. Seawater contains approximately 2 mmol DIC/kg and the high concentrations of reductants, produced by serpentinization are, in principle, of sufficient abundance to reduce all DIC to biomass and methane. End-member vent fluids have methane concentrations that approach, but do not exceed 2 mmol/kg (Bouloubassi et al., 2006; Pancost et al., 2001; Proskurowski et al., 2006), suggesting that a large proportion of the DIC in the starting fluid is reduced to methane. Concentrations of inorganic carbon at Lost City are indeed estimated to be very low. Carbonate alkalinity is reported to be below one-third that of seawater (Proskurowski et al., 2006). At a pH of 11 and temperature of 70 ºC that suggests the DIC concentration is less than 0.4 mmol/kg.

We propose that the LCMS organisms inhabiting the carbonate towers at Lost City are fixing inorganic carbon and that they are carbon-limited. This limitation results from two factors. The first is the abundance of reductants, which allows the conversion of most of the DIC to biomass and methane. Residual carbonate alkalinity is slightly enriched in ^{13}C from seawater DIC. The second factor is the high pH and temperature, which results in limited concentrations of bioavailable CO_2 and bicarbonate. At pH 11 and 70 ºC more than 99% of DIC is carbonate.

CO_2 limitation has been shown to limit the growth rate of phytoplankton under optimal growth conditions (Riebesell et al., 1993) leading to enriched values of $\delta^{13}C_{phytoplankton}$ (Rau et al., 1989). In that case phytoplankton remove CO_2 from seawater resulting in a shortfall in CO_2 concentration at their cell surface. Equilibrium concentrations are restored

by diffusion of CO_2 towards the cell surface and by the reaction that converts bicarbonate to CO_2. The relative importance of diffusion and reaction can be estimated by comparing the size of the diffusive boundary layer surrounding a cell (equivalent to the cell radius for cells with a radius of less than 1 mm) to the reacto-diffusive length scale (Riebesell et al., 1993). In surface seawater (pH = 8.1) the reacto-diffusive length scale varies between approximately 300 μm at temperatures slightly above 15 ºC, to 800 μm at temperatures near 0 ºC (Riebesell et al., 1993). Since the reacto-diffusive length scale is much larger than the diffusive boundary layer of phytoplankton (~15 μm), only diffusion is significant: conversion of bicarbonate does not contribute significant CO_2 to the cell (Riebesell et al., 1993).

At the hydrothermal conditions in Lost City vent fluids, the reacto-diffusive length scale is on the order of 1 μm (Appendix 2). This length scale is similar to the size of a bacterial or archaeal cell. Under such conditions equilibrium reactions transforming bicarbonate to CO_2 are important and may supply most carbon to the cell surface. At high pH and temperature however, the equilibrium isotope fractionation between CO_2 and bicarbonate is minimized. At 70 ºC and pH 11 he two species have δ values within 2‰. This may help to explain the high ^{13}C content of biological products at Lost City.

It is also possible that the inorganic carbon source is bicarbonate, which is biologically converted to CO_2 with carbonic anhydrase. At the temperature and pH of Lost City vent fluids, bicarbonate is also very limiting, and is enriched in 13C relative to CO_2. Conversion of carbonate to CO_2 is not enzymatically catalyzed.

Whether the carbon source is bicarbonate or CO_2, the high pH and tempertature limit their availability. It is likely that these conditions result in lipids with ^{13}C contents similar to that of the inorganic carbon. Studies of complementary systems could help to resolve controls on ^{13}C content. At the Rainbow field, for example, concentrations of H_2 are similar to those at Lost City but vent fluids are acidic (Charlou et al., 2002).

3.3.3 Bacterial lipid distribution and ^{13}C content

We detected nonisoprenoidal ether lipids at Lost City in nearly all samples analyzed (Table 3-2). Diethers were most abundant and ranged in mass from 556 Da ($C_{31:2}$-TMS) to 652 Da ($C_{38:2}$-TMS) with saturated and unsaturated side chains ranging in length from C_{13} to C_{18}. A detailed description of these diether structures is provided in Chapter 5. The range of structures is similar to that described in cold-seep carbonate crusts associated with Mediterranean mud volcanoes (Bouloubassi et al., 2006; Pancost et al., 2001), including the Series I, II, and III components, and several additional series of diethers that do not fall into the categories described from the Mediterranean cold seeps. There was no apparent pattern to the variety of diether structures between samples, although diethers with masses of 584 Da and 608 Da (TMS derivatives) were particularly common. Multiple chromatographic peaks yield identical mass spectra, suggesting that isomeric structures are present. Several samples also contain glycerol monoethers, with $C_{16:1}$ and C_{18} nonisoprenoidal side chains being most abundant.

Ether lipids, which are common in archaea, are rare in bacteria. They are, however, produced by *Aquificales*, *Ammonifex*, *Thermodesulfobacterium* and several sulfate-reducing δ-proteobacteria (Huber et al., 1992; Langworthy et al., 1983). In all cases, the known bacterial diethers have nonisoprenoidal carbon chains. Archaeal diethers have isoprenoidal side chains, with few exceptions (Nishihara et al., 2000). A tetraether lipid containing putative isoprenoidal and nonisoprenoidal carbon chains and with an unknown microbial source has been reported in low abundance in marine and lacustrine sediments (Schouten et al., 2000), but further reports of such lipids are lacking. For these reasons we interpret the nonisoprenoidal lipids at Lost City as bacterial in nature.

It is common to find isoprenoidal and nonisoprenoidal ether lipids co-occurring in marine sediments with values of $\delta^{13}C$ so low that the carbon source can only be methane. A combination of geochemical and microbiological techniques has confirmed that the nonisoprenoidal lipids are produced by sulfate-reducing bacteria that are the syntrophic

partner of methane-oxidizing archaea that oxidize methane anaerobically (Blumenberg et al., 2004; Hinrichs et al., 1999; Hinrichs et al., 2000; Orphan et al., 2001; Orphan et al., 2002). The archaeal members of these consortia belong to the ANME-1 or ANME-2 phylogenetic clusters. The bacterial members belong to the sulfate-reducing *Desulfosarcina*/*Desulfococcus* group.

If Lost City Methanosarcinales are methanogens, methane-oxidizing consortia are unlikely to be a dominant part of the community in active carbonate chimneys. Microbiological studies fail to detect the presence of known syntrophic partners to such consortia (Brazelton et al., 2006). No δ-proteobacterial sulfate-reducers or other known ether-lipid producers were detected, so the source of the nonisoprenoidal diether lipids is enigmatic. Diverse Firmicutes related to the sulfate reducer *Desulfotomaculum* were detected in the Lost City carbonates and are presumed to be the sulfate reducers which, in these environments, use H_2 as an electron donor (Brazelton et al., 2006). Accordingly, Clostridia are candidates for producers of the non-isoprenoidal diethers. Clostridia commonly produce ether-lipid plasmalogens and incorporate them in their cellular membranes (Goldfine, 1997). However, studies of *Desulfotomaculum* have not detected diethers (Londry et al., 2004; Pikuta et al., 2000). At least one Clostridium, *Ammonifex*, does produce diethers (Huber et al., 1996), and the Firmicute lipid biosynthesis pathway shares many characteristics with archaea (Skophammer et al., 2007). However, Firmicutes were undetected in two carbonate vein samples (X1, and X2) (Brazelton et al., 2006) containing nonisoprenoidal diethers, seemingly ruling them out as the sole source for these lipids.

Regardless of their source, nonisoprenoidal ether lipids, like the isoprenoidal diethers, are in many cases unusually enriched in ^{13}C. The most extreme enrichments are found where hydroxyarchaeols are also abundant. In samples with both *sn*-2 hydroxyarchaeol and dihydroxyarchaeol, the $\delta^{13}C$ of nonisoprenoidal diethers ranged from -11.8‰ to +3.6‰ (Table 3-2, Figure 3-8) and that of monoethers ranged from -19.2‰ to

-3.9‰. The nonisoprenoidal diethers were typically a 2-10‰ more depleted in ^{13}C than hydroxyarchaeols. In many cases nonisoprenoidal monoethers were still more depleted. We propose that the low availability of DIC is responsible for the ^{13}C enrichment in non-isoprenoidal ether lipids, just as it is for the archaeal diethers.

In carbonate tower samples where hydroxyarchaeols were not abundant, nonisoprenoidal diethers were more depleted in ^{13}C, with $\delta^{13}C$ ranging from -14.3‰ to -28.7‰. Values of δ for monoethers ranged from -19.6‰ to -26.7‰. There was one exception: a sample from Marker 3 (3881-1408) in which archaeal lipids were absent had nonisoprenoidal diethers with δ averaging near -6‰. Although archaeal lipids were absent, the LCMS phylotype was detected in this sample by presence of its 16S rRNA genes (Brazelton et al., 2006).

The availability of carbon is apparently limited only in carbonate chimneys containing LCMS organisms. The $\delta^{13}C$ values found in samples at X1 and X2 range from those typical of carbon-fixing microbes to values sufficiently negative to suggest methane as a carbon source (-45‰). At site X2, diethers with the most positive values of $\delta^{13}C$ are enriched relative to archaeol by slightly less than 50‰ – a difference that is within the range found between archaeal and bacterial diethers at AOM sites (Hinrichs et al., 2000). However, no bacterial syntrophic partners or sulfate-reducing Firmicutes are found in the carbonate vein sites (Brazelton et al., 2006), so the source of the non-isoprenoidal ether lipids remains unclear. Conceivably, the ANME-1 organisms at these sites are operating without a syntrophic partner (Orphan et al., 2002).

The C_{30} hopanoids diploptene and diplopterol were also detected in a number of the vent chimney samples and are unambiguously bacterial products. Their $\delta^{13}C$ values (-26‰ to -2‰; Table 3-2) resembled those of bacterial diethers.

3.3.4 Eukaryotic lipid distribution and ^{13}C content

Sterols were detected in all analyzed samples. Cholesterol was most common

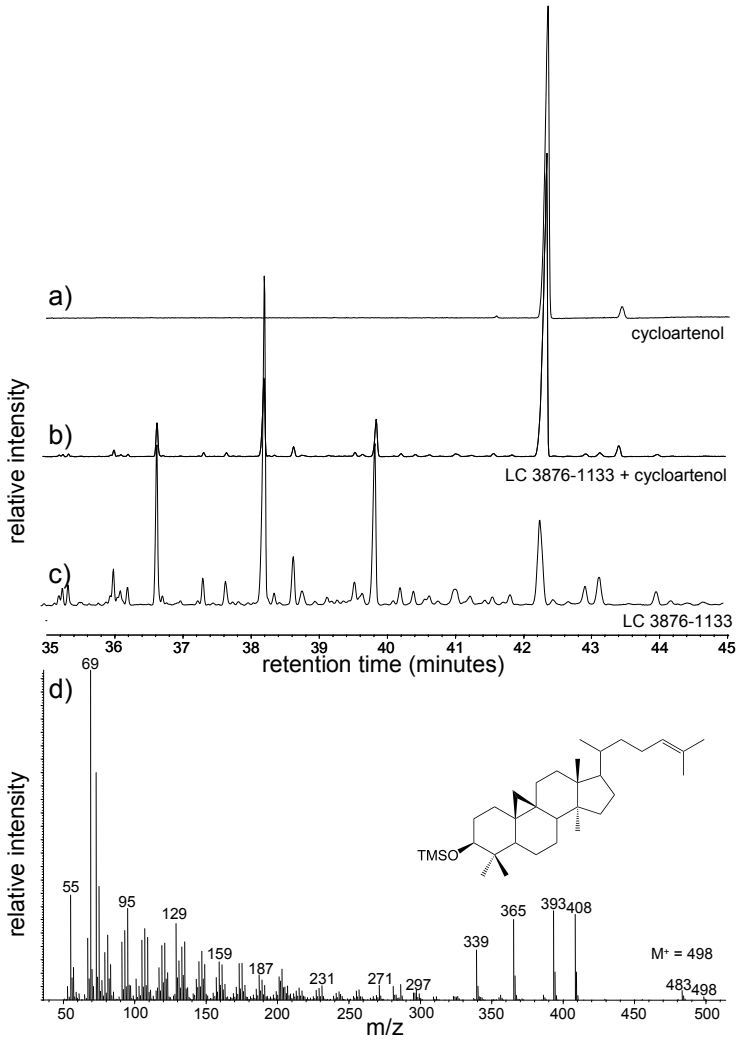

Figure 3-8: Coinjection experiment demonstrating the presence of cycloartenol. a) TIC chromatogram of cycloartenol authentic standard, b) TIC chromatogram of cycloartenol authentic standard coinjected with extract from carbonate chimney sample 3876-1133, c) extract from carbonate chimney sample 3876-1133, d) mass spectrum of tms derivative of cycloartenol in 3876-1133.

probably derived from input from animals inhabiting the surfaces of the carbonate chimneys (DeChaine et al., 2006; Kelley et al., 2005) and from detritus trapped from the water column. Stigmasterol and β-sitosterol were also common and are likely sourced from eukaryotic phytoplankton. Many samples contained both unsaturated and saturated C_{28} and C_{29} sterols likely to have derived from phytoplankton or other eukaryotic inputs. Ergosterol was detected in trace amounts in some samples and is likely to be a product of one of the two fungal lineages detected at Lost City (Lopez-Garcia et al., 2007).

Cycloartenol was commonly detected in concentrations approaching 500 ng per gram of dry rock. Its identity was confirmed by mass spectrum and coinjection with an authentic standard (Figure 3-8**)**. Cycloartenol is a 'protosterol' (Summons et al., 2006) that is known to be the immediate product of the cyclization of oxidosqualene in plants and algae as well as in several groups of protists. To date it has been reported as the accumulating final product in only one organism, the myxobacterium *Stigmatella aurantiaca* Sg a15 (Bode et al., 2003). In other organisms concentrations detected in cellular extracts are typically minor, reflecting its role as a biosynthetic intermediate. Its accumulation can be enhanced by accumulation of metabolic inhibitors (Hata et al., 1987; Haughan et al., 1988) or by genetic mutation of the downstream sterol modification pathway.

At Lost City, cycloartenol is the most abundant sterol in some samples. This implies that it is being accumulated in an organism without subsequent modification to a demethylated sterol. Given that the animal protosterol is always lanosterol and that C_{28} and C_{29} phytosterols are dominant in marine algae, these groups can probably be excluded as the source. Myxobacteria are not detected in 16S rDNA surveys at Lost City (Brazelton et al., 2006). The most probable source of abundant cycloartenol is a protist inhabiting the carbonate chimneys.

A diverse population of protists has been detected in Lost City carbonates, with ciliates being the most dominant, other alveolates, fungi, heterokonts, radiolaria and other cercozoa, and heterolobosea also detected (Lopez-Garcia et al., 2007). Detailed information

about sterol biosynthetic pathways in these groups of protists is sparse. Most non-opisthokont protists with a known sterol synthetic pathway make cycloartenol as a protosterol. The two known exceptions that make lanosterol, trypanosomatids and dinoflagellates, do not occur in Lost City carbonates, although a more deeply-branching relative of each of these groups is present (kinetoplastids and ciliates, respectively). However, only the opisthokonts can be conclusively ruled out as possible sources for cycloartenol.

Given the abundance of cycloartenol in some carbonates, its source is likely to be an important part of the microbial ecology. The triterpenoid tetrahymenol (Harvey and McManus, 1991; Ten Haven et al., 1989), commonly attributed to ciliates, was detected several Lost City vent carbonates. This is not unexpected, due to the detection of gene sequences representative of ciliates (Lopez-Garcia et al., 2007). The ^{13}C content of tetrahymanol ranged from -3.5 to -26.5, similar to the range in bacterial lipids. Ciliates may be consuming bacterial biomass; marine bacteriovorous ciliates commonly produce tetrahymanol (Harvey et al., 1997; Harvey and McManus, 1991). Consumption of bacteria in AOM environments at the Kazan mud volcano has been previously reported (Werne et al., 2002).

Sterols are not in any case as exceptionally ^{13}C-enriched as diethers. However, variability in $\delta^{13}C$ is greater than would be expected if all inputs were marine. Cholesterol ranges in $\delta^{13}C$ from approximately -28‰, near the expected value for a marine sterol, to -23.2‰, which may reflect input by animals with a dietary composition that includes ^{13}C enriched vent microbes. Cycloartenol varies even more, with $\delta^{13}C$ near -30‰ in the carbonate vein X2, which has diethers relatively depleted in ^{13}C. Cycloartenol in carbonate chimneys with abundant archaeol lipids has $\delta^{13}C$ as high as -15.4‰. This large range of $\delta^{13}C$ values is consistent with cycloartenol begin derived from protists feeding in part on archaea and bacteria in the carbonate chimneys. C_{28} and C_{29} sterols are also enriched in some samples with $\delta^{13}C$ up to a maximum of near -20‰ at Marker C, suggesting that their sources are not entirely from the water column. Synthesis of a sterol such that it is

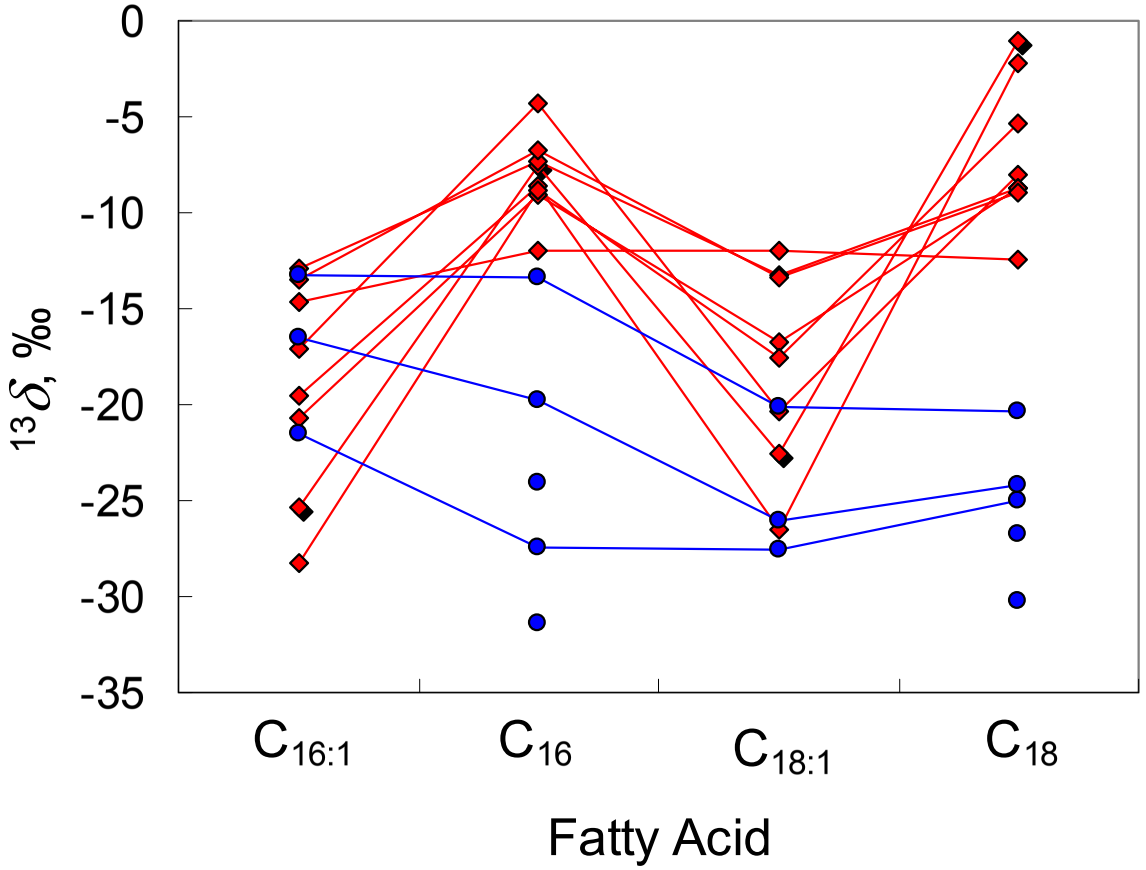

Figure 3-9: Plot of individual fatty acid $\delta^{13}C$ values for C_{16} and C_{18} saturated and monounsaturated fatty acids. Fatty acids from hydroxyarchaeol-rich samples (Table 3) are denoted as red diamonds, while those from hydroxyarchaeol-poor samples are denoted as blue circles. Saturated fatty acids show a strong enrichment in ^{13}C over monounsaturated fatty acids in hydroxyarchaeol-rich samples, while there is little difference in the hyroxyarchaeol-poor samples.

fully demethylated on its α-face, such as stigmasterol, requires 11-12 molecules of O_2. But synthesis of cycloartenol requires only one molecule of O_2 (Summons et al., 2006). We speculate that cycloartenol might be a favored sterol from a microaerophilic eukaryote inhabiting vent fluids with only sporadic access to oxygenated seawater.

Free fatty acids, potentially derived from both eukaryotes and bacteria, were detected in nearly all samples. Concentrations ranged to over 1500 ng per gram of dry rock. Abundances and $\delta^{13}C$ values of fatty acids are listed in Table 3-2. Like the diethers, fatty acids have highly variable contents of ^{13}C, spanning a range from approximately -1‰ to -27‰. The most ^{13}C-depleted fatty acids were found in the carbonate veins, where all

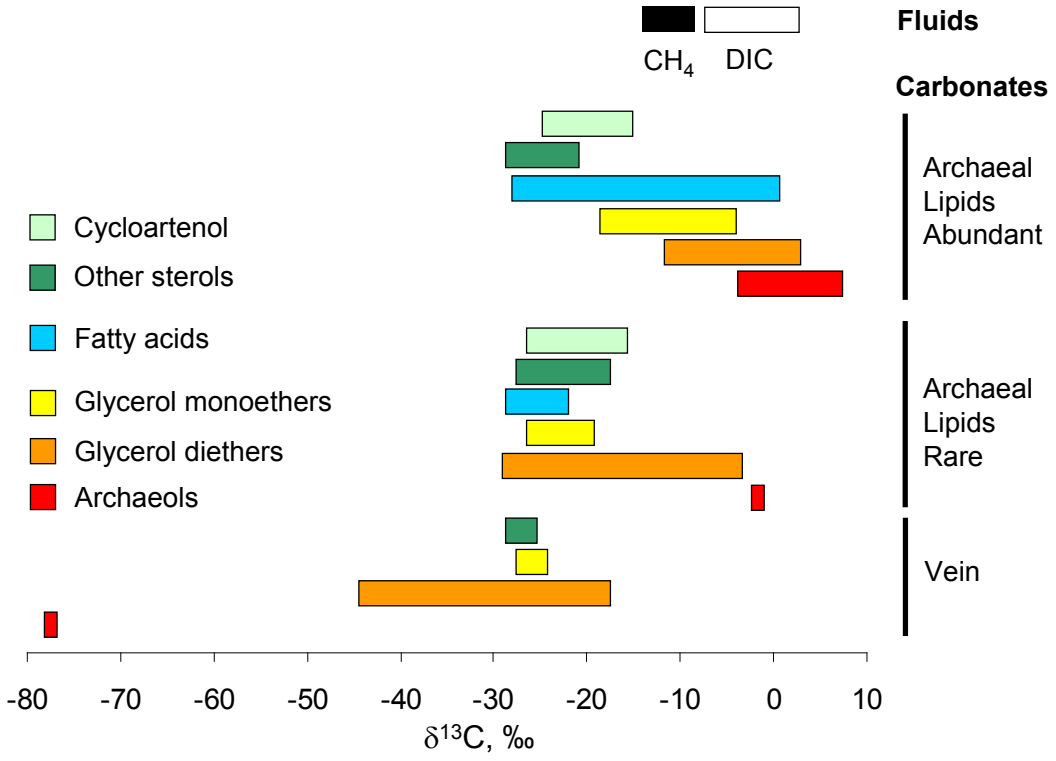

Figure 3-10: Ranges of carbon isotopic compositions for different compound classes at Lost City. Ranges for methane and DIC are measured from fluid samples over the entire field (Kelley et al., 2005). Ranges for lipids are reported by grouping samples into those with abundant archaeal lipids (3862-1219, 3864,1524, 3864-1537, 3867-1225, 3867-1228, 3869-1404, 3869-1443, 3869-1446, 3879-slurp), rare archaeal lipids (3865-1322, 3876-1133, 3876-1219, 3876-1436, 3881-1132, 3881-1325, 3881-1408), and the vein sample at marker X2 (3880-1557).

detected lipids had $\delta^{13}C < -15‰$. Similarly, the most ^{13}C-enriched fatty acids were found in the samples containing abundant hydroxyarchaeols, where carbon-limitation is evident by virtue of the exceptional ^{13}C enrichment in common with the ether lipids. Many of the most ^{13}C enriched samples displayed a pattern where saturated fatty acids were notably more enriched in ^{13}C than monounsaturated fatty acids (Figure 3-9). This is interpreted to mean that saturated fatty acids in these samples are predominantly derived, along with the ether lipids, from the carbon-limited anaerobic environment inside the carbonate chimneys. Mono-unsaturated fatty acids probably originate both from this environment and from organisms inhabiting the chimney exterior and overlying water column. At first glance this pattern is consistent with a requirement for oxygen in fatty acid desaturation. However, we note that there are two types of fatty acid desaturases in nature. The first is an aerobic pathway that occurs in both bacteria and eukaryotes, and the second is an anaerobic pathway that is restricted to bacteria (Bloch, 1969; Shanklin and Cahoon, 1998). In principle this should mean that both saturated and monounsaturated fatty acids should reflect mixed inputs from the anaerobic carbon limited environment inside the vent chimneys, and the aerobic carbon-replete external environment. The extraordinary ^{13}C enrichment in saturated fatty acids suggests they predominantly derive from inside the vent chimneys, but the precise reasons for this are unknown.

Isotopic compositions of the various biomarker classes detected at Lost City are summarized in Figure 3-10.

3.3.5 Biological sulfate reduction

Sulfate reduction is inferred at Lost City on the basis that vent fluids have sulfate concentrations of 1 to 4 mmol/kg, significantly lower than ambient seawater but higher than would be expected if precipitation of anhydrite were dominant (Kelley et al., 2005). Sulfate in low-Mg end-member fluids is enriched in ^{34}S relative to seawater by up to 10‰. Sulfate concentrations are strongly negatively correlated with sulfide concentrations (Kelley et

al., 2005). While all of these observations point to biological sulfate-reduction, the sulfur cycle at Lost City is not fully defined. Sulfide has $\delta^{34}S$ between +34‰ and +37‰ (Fruh-Green et al., 2004a) and concentrations do not exceed 2.8 mM. Enrichment of ^{34}S in sulfide relative to sulfate is not expected during biological sulfate reduction (Canfield, 2001) and the summed concentrations of sulfide plus sulfate are significantly less than the 28 mM found in the seawater from which vent fluids are derived. Serpentinites are a net sink for sulfur (Alt and Shanks III, 2003) and may contain the 'missing' sulfur. Given these results, the best evidence for biological sulfate reduction at Lost City is the presence of the sulfate-reducing Firmicute *Desulfotomaculum*.

The coexistence of sulfate-reducing bacteria and methanogens is unusual. In marine sediments, sulfate-reducing bacteria outcompete methanogens for H_2 due to the higher energy yield of sulfate reduction compared to CO_2 reduction (Hoehler et al., 1998) and the greater substrate affinity of sulfate-reducer enzymes for H_2 (Kristjansson et al., 1982). However, under very high hydrogen concentrations methanogens and sulfate-reducing bacteria can coexist. Enzymatic affinities for hydrogen are in the micromolar range for both sulfate-reducers and methanogens (Kristjansson et al., 1982); the millimolar hydrogen concentrations at Lost City exceed this threshold and allow coexistence.

Biological sulfate reduction has been invoked to explain the wide variation in hydrogen concentrations among fluids that differ only slightly in temperature. There are no obvious correlations between the concentrations of non-isoprenoidal diether lipids in vent carbonates and the hydrogen concentrations in vent fluids at the same location. –However, only small portions of any given carbonate chimney were sampled, and we have not positively linked the non-isoprenoidal diether lipids to sulfate-reducing bacteria. Therefore we do not exclude the possibility that sulfate reduction is a strong control on hydrogen concentration.

3.3.6 Implications for Earth history and astrobiology

The anaerobic ecosystem within the carbonate towers at Lost City may be particularly relevant as an analogue for some early Earth ecosystems. In particular, autotrophic methanogenesis using CO_2 or bicarbonate as an electron acceptor proceeds exergonically without need for any products of oxygenic photosynthesis. This is in contrast to many other anaerobic ecosystems which usually require indirect byproducts of photosynthesis such as sulfate or nitrate. The bacterial component of the ecosystem at Lost City likely relies on sulfate, but it is also possible that sulfate was sometimes present very early on in Earth history (Shen and Buick, 2004).

The alkaline conditions at Lost City are favorable for some aspects of prebiotic chemistry (Russell, 2003). Intriguingly, recent attempts to root the universal tree of life based on analyses of insertions and deletions within paralogous genes have suggested that the widely accepted root between archaea and bacteria may be an artifact of long branch attraction (Skophammer et al., 2007). Instead, several alternative sites for the root have been proposed within the Gram Positive Bacteria, including a root on the branch leading to the Firmicutes plus Archaea. The particular importance of these two groups at Lost City (Brazelton et al., 2006) points to the potential importance of Lost City type environments may have had to early microbial evolution.

The fluxes of microbially derived and abiotic methane at Lost City will be important in constraining the composition of the early atmosphere. Methane is often invoked to solve the faint young sun problem (Kasting, 2005), but models applying this to the Hadean and Archean Earth require an accurate understanding of whether off-axis vent systems can supply abundant methane before the evolution of archaeal methanogens. Furthermore, the possibility of the production of abundant biological methane that is enriched in ^{13}C complicates the understanding of the timing of the evolution of biological methanogenesis. These questions should be illuminated by an isotopic analysis of the light hydrocarbons at Lost City.

Organic carbon or methane in hydrothermal deposits can not be distinguished as biotic or abiotic based solely on a $\delta^{13}C$ value of less than -25‰ (McCollom and Seewald, 2006; Sherwood Lollar and McCollom, 2006). The isotope results at Lost City extend this concept to the full range of ^{13}C contents found in nature. If ultramafic ecosystems rich in H_2 were important on the early Earth, preserved organic compounds of biological origin detected in those systems may not have the characteristic ^{13}C depletion that is commonly associated with life.

3.4. Conclusions

The H_2-rich fluid chemistry of Lost City vent fluids and the isotopic compostions of the archaeal and bacterial diether lipids lead us to conclude that the Lost City Methanosarcinales phylotype is a methanogen. Similar ^{13}C enrichments in non-isoprenoidal diethers demonstrate that the conditions causing unusual $\delta^{13}C$ values are not restricted to archaea. The most plausible explanation for these data is that the vent communities are carbon-limited and the full extent of fractionation between DIC and biomass is not being expressed.

Conditions of CO_2 limitation are rare on Earth. As a result, depletion in ^{13}C is usually necessary (but not sufficient) evidence that preserved organic carbon is biological in origin. The results from Lost City suggest that even this bias may not be appropriate for all environments. Ultramafic ecosystems may have been important on early Earth, and may be present elsewhere in the solar system. The results presented here suggest that biological organic carbon in such systems may have a wide range of ^{13}C contents. Many investigations have emphasized that ^{13}C-depleted organic carbon is not necessarily a signature for biology. Similarly, our results show that detection of organic carbon with ^{13}C contents near or greater than mantle CO_2 may in some cases be biologically derived.

3.5 References

Allen, D.E., Seyfried, W.E., Jr., 2004. Serpentinization and heat generation: Constraints from Lost City and Rainbow hydrothermal systems. Geochimica et Cosmochimica Acta 68(6), 1347-1354.

Alt, J.C., Shanks III, W.C., 2003. Serpentinization of abyssal peridotites from the MARK area, Mid-Atlantic Ridge: Sulfur geochemistry and reaction modeling. Geochimica et Cosmochimica Acta 67(4), 641-653.

Bloch, K., 1969. Enzymatic synthesis of monounsaturated fatty acids. Accounts of Chemical Research 2(7), 193-202.

Blumenberg, M., Seifert, R., Reitner, J., Pape, T., Michaelis, W., 2004. Membrane lipid patterns typify distinct anaerobic methanotrophic consortia. Proceedings of the National Academy of Sciences of the United States of America 101(30), 11111-11116.

Bode, H.B., Zeggel, B., Silakowski, B., Wenzel, S.C., Reichenbach, H., Muller, R., 2003. Steroid biosynthesis in prokaryotes: Identification of myxobacterial steroids and cloning of the first bacterial 2,3(S)-oxidosqualene cyclase from the myxobacterium Stigmatella aurantiaca. Molecular Microbiology 47(2), 471-481.

Bouloubassi, I., Aloisi, G., Pancost, R.D., Hopmans, E., Pierre, C., Sinninghe Damste, J.S., 2006. Archaeal and bacterial lipids in authigenic carbonate crusts from eastern Mediterranean mud volcanoes. Organic Geochemistry 37(4), 484-500.

Brazelton, W.J., Schrenk, M.O., Kelley, D.S., Baross, J.A., 2006. Methane- and sulfur-metabolizing microbial communities dominate the lost city hydrothermal field ecosystem. Applied and Environmental Microbiology 72(9), 6257-6270.

Canfield, D.E., 2001. Biogeochemistry of sulfur isotopes. In: J.W. Valley, D.R. Cole (Eds.), *Stable Isotope Geochemistry 43*, *Reviews in Mineralogy & Geochemistry*. Mineralogical Society of America.

Catling, D.C., 2006. Comment on "A hydrogen-rich early Earth atmosphere". Science 311(5757), 38; author reply 38.

Catling, D.C., Zahnle, K.J., McKay, C.P., 2001. Biogenic methane, hydrogen escape, and the irreversible oxidation of early Earth. Science (Washington, DC, United States) 293(5531), 839-843.

Cavalier-Smith, T., 2006. Cell evolution and Earth history: stasis and revolution. Philosophical Transactions of the Royal Society of London, Series B: Biological Sciences 361(1470), 969-1006.

Charlou, J.L., Donval, J.P., Fouquet, Y., Jean-Baptiste, P., Holm, N., 2002. Geochemistry of high H2 and CH4 vent fluids issuing from ultramafic rocks at the Rainbow hydrothermal field (36 Deg14'N, MAR). Chemical Geology 191(4), 345-359.

DeChaine, E.G., Bates, A.E., Shank, T.M., Cavanaugh, C.M., 2006. Off-axis symbiosis found: characterization and biogeography of bacterial symbionts of Bathymodiolus mussels from Lost City hydrothermal vents. Environmental Microbiology 8(11), 1902-1912.

Formisano, V., Atreya, S., Encrenaz, T., Ignatiev, N., Giuranna, M., 2004. Detection of methane in the atmosphere of Mars. Science 306(5702), 1758-61.

Fruh-Green, G.L., Bernasconi, S.M., Butterfield, D.A., Kelley, D.S., 2004a. Sulfur Isotope Geochemistry of the Lost City Hydrothermal Vent Fluids. Eos Trans.

AGU 85(47), Fall meet. Suppl., Abstract B13A-0199.
Fruh-Green, G.L., Connolly, J.A.D., Plas, A., Kelley, D.S., Grobety, B., 2004b. Serpentinization of Oceanic Peridotites: Implications for Geochemical Cycles and Biological Activity. In: W.S.D. Wilcock, E.F. DeLong, D.S. Kelley, J.A. Baross, S.C. Cary (Eds.), *The Subseafloor Biosphere at Mid-Ocean Ridges 144*, *Geophysical Monograph Series*, pp. 119-136. American Geophysical Union, Washington D.C.
Fruh-Green, G.L., Kelley, D.S., Bernasconi, S.M., Karson, J.A., Ludwig, K.A., Butterfield, D.A., Boschi, C., Proskurowski, G., 2003. 30,000 years of hydrothermal activity at the Lost City vent field. Science 301(5632), 495-498.
Goericke, R., Fry, B., 1994. Variations of marine plankton d13C with latitude, temperature, and dissolved CO2 in the world ocean. Global Biogeochemical Cycles 8(1), 85-90.
Goldfine, H., 1997. Structure, biosynthesis, physical properties, and functions of the polar lipids of Clostridium. Advances in Lipobiology 2, 109-142.
Harvey, H.R., Ederington, M.C., McManus, G.B., 1997. Lipid composition of the marine ciliates Pleuronema sp. and Fabrea salina: shifts in response to changes in diet. Journal of Eukaryotic Microbiology 44(3), 189-193.
Harvey, H.R., McManus, G.B., 1991. Marine ciliates as a widespread source of tetrahymanol and hopan-3b-ol in sediments. Geochimica et Cosmochimica Acta 55(11), 3387-90.
Hata, S., Shirata, K., Takagishi, H., Kouchi, H., 1987. Accumulation of Rare Phytosterols in Plant Cells on Treatment with Metabolic Inhibitors and Mevalonic Acid. Plant Cell Physiol. 28(4), 715-721.
Haughan, P.A., Lenton, J.R., Goad, L.J., 1988. Sterol requirements and paclobutrazol inhibition of a celery cell culture. Phytochemistry 27(8), 2491-500.
Hayes, J.M., 1994. Global methanotrophy at the Archaean-Proterozoic transition. In: S. Bengston (Ed.), *Early Life on Earth*, pp. 220-236. Columbia University Press, New York.
Hinrichs, K.-U., Hayes, J.M., Sylva, S.P., Brewer, P.G., DeLong, E.F., 1999. Methane-consuming archaebacteria in marine sediments. Nature 398, 802-805.
Hinrichs, K.-U., Summons, R.E., Orphan, V., Sylva, S.P., Hayes, J.M., 2000. Molecular and isotopic analysis of anaerobic methane-oxidizing communities in marine sediments. Organic Geochemistry 31, 1685-1701.
Hoehler, T.M., Alperin, M.J., Albert, D.B., Martens, C.S., 1998. Thermodynamic control on hydrogen concentrations in anoxic sediments. Geochimica et Cosmochimica Acta 62(10), 1745-1756.
Huber, R., Rossnagel, P., Woese, C.R., Rachel, R., Langworthy, T.A., Stetter, K.O., 1996. Formation of ammonium from nitrate during chemolithoautotrophic growth of the extremely thermophilic bacterium *Ammonifex degensii* gen. Nov. sp. nov. Systematic and Applied Microbiology 19, 79-93.
Huber, R., Wilharm, T., Huber, D., Trincone, A., Burggraf, S., Konig, H., Rachel, R., Rockinger, I., Fricke, H., Stetter, K.O., 1992. Aquifex pyrophilus gen. nov. sp. nov., Represents a Novel Group of Marine Hyperthermophilic Hydrogen-Oxidizing Bacteria. System. Appl. Microbiol. 15, 340-351.

Kasting, J.F., 2005. Methane and climate during the Precambrian era. Precambrian Research 137(3-4), 119-129.
Kasting, J.F., Ono, S., 2006. Palaeoclimates: the first two billion years. Philosophical transactions of the Royal Society of London. Series B, Biological sciences 361(1470), 917-29.
Kelley, D.S., Karson, J.A., Blackman, D.K., Fruh-Green, G.L., Butterfield, D.A., Lilley, M.D., Olson, E.J., Schrenk, M.O., Roe, K.K., Lebon, G.T., Rivizzigno, P., 2001. An off-axis hydrothermal vent field near the Mid-Atlantic Ridge at 30 degrees N. Nature 412(6843), 145-149.
Kelley, D.S., Karson, J.A., Fruh-Green, G.L., Yoerger, D.R., Shank, T.M., Butterfield, D.A., Hayes, J.M., Schrenk, M.O., Olson, E.J., Proskurowski, G., Jakuba, M., Bradley, A., Larson, B., Ludwig, K., Glickson, D., Buckman, K., Bradley, A.S., Brazelton, W.J., Roe, K., Elend, M.J., Delacour, A., Bernasconi, S.M., Lilley, M.D., Baross, J.A., Summons, R.E., Sylva, S.P., 2005. A Serpentinite-Hosted Ecosystem: The Lost City Hydrothermal Field. Science 307(5714), 1428-1434.
Knittel, K., Losekann, T., Boetius, A., Kort, R., Amann, R., 2005. Diversity and distribution of methanotrophic archaea at cold seeps. Applied and Environmental Microbiology 71(1), 467-79.
Koga, Y., Morii, H., Akagawa-Matsushita, M., Ohga, M., 1998. Correlation of polar lipid composition with 16S rRNA phylogeny in methanogens. Further analysis of lipid component parts. Bioscience, Biotechnology, and Biochemistry 62(2), 230-236.
Kristjansson, J.K., Schoenheit, P., Thauer, R.K., 1982. Different Ks values for hydrogen of methanogenic bacteria and sulfate-reducing bacteria: an explanation for the apparent inhibition of methanogenesis by sulfate. Archives of Microbiology 131(3), 278-282.
Langworthy, T.A., Holzer, G., Zeikus, J.G., Tornabene, T.G., 1983. Iso- and anteiso-branched glycerol diethers of the thermophilic anaerobe Thermodesulfobacterium commune. System. Appl. Microbiol. 4, 1-17.
Londry, K.L., Jahnke, L.L., Des Marais, D.J., 2004. Stable Carbon Isotope Ratios of Lipid Biomarkers of Sulfate-Reducing Bacteria. Applied and Environmental Microbiology 70(2), 745-751.
Lopez-Garcia, P., Vereshchaka, A., Moreira, D., 2007. Eukaryotic diversity associated with carbonates and fluid-seawater interface in Lost City hydrothermal field. Environmental Microbiology 9(2), 546-554.
Losekann, T., Knittel, K., Nadalig, T., Fuchs, B., Niemann, H., Boetius, A., Amann, R., 2007. Diversity and abundance of aerobic and anaerobic methane oxidizers at the Haakon Mosby Mud Volcano, Barents Sea. Applied and Environmental Microbiology 73(10), 3348-3362.
Lowe, D.R., Tice, M.M., 2004. Geologic evidence for Archean atmospheric and climatic evolution: Fluctuating levels of CO2, CH4 , and O2 with an overriding tectonic control. Geology 32(6), 493-496.
Ludwig, K.A., Kelley, D.S., Butterfield, D.A., Nelson, B.K., Frueh-Green, G., 2006. Formation and evolution of carbonate chimneys at the Lost City Hydrothermal Field. Geochimica et Cosmochimica Acta 70(14), 3625-3645.
McCollom, T.M., 1999. Methanogenesis as a potential source of chemical energy for

primary biomass production by autotrophic organisms in hydrothermal systems on Europa. Journal of Geophysical Research 104(E12), 30729-30742.
McCollom, T.M., Seewald, J.S., 2006. Carbon isotope composition of organic compounds produced by abiotic synthesis under hydrothermal conditions. Earth and Planetary Science Letters 243(1-2), 74-84.
Niemann, H., Losekann, T., de Beer, D., Elvert, M., Nadalig, T., Knittel, K., Amann, R., Sauter Eberhard, J., Schluter, M., Klages, M., Foucher Jean, P., Boetius, A., 2006. Novel microbial communities of the Haakon Mosby mud volcano and their role as a methane sink. Nature 443(7113), 854-8.
Nishihara, M., Nagahama, S., Ohga, M., Koga, Y., 2000. Straight-chain fatty alcohols in the hyperthermophilic archaeon Pyrococcus furiosus. Extremophiles 4(5), 275-277.
Orphan, V.J., House, C.H., Hinrichs, K.-U., McKeegan, K.D., DeLong, E.F., 2001. Methane-Consuming Archaea Revealed by Directly Coupled Isotopic and Phylogenetic Analysis. Science 293, 484-487.
Orphan, V.J., House, C.H., Hinrichs, K.-U., McKeegan, K.D., DeLong, E.F., 2002. Multiple archaeal groups mediate methane oxidation in anoxic cold seep sediments. Proceedings of the National Academy of Sciences of the United States of America 99(11), 7663-7668.
Pancost, R.D., Hopmans, E.C., Sinninghe Damste, J.S., Party, M.S.S., 2001. Archaeal lipids in Mediterranean Cold Seeps: Molecular proxies for anaerobic methane oxidation. Geochimica et Cosmochimica Acta 65(10), 1611-1627.
Pancost, R.D., Pressley, S., Coleman, J.M., Talbot, H.M., Kelly, S.P., Farrimond, P., Schouten, S., Benning, L., Mountain, B.W., 2006. Composition and implications of diverse lipids in New Zealand geothermal sinters. Geobiology 4(2), 71-92.
Pavlov, A.A., Kasting, J.F., Eigenbrode, J.L., Freeman, K.H., 2001. Organic haze in Earth's early atmosphere: source of low-13C Late Archean kerogens? Geology 29(11), 1003-1006.
Pikuta, E., Lysenko, A., Suzina, N., Osipov, G., Kuznetsov, B., Tourova, T., Akimenko, V., Laurinavichius, K., 2000. Desulfotomaculum alkaliphilum sp. nov., a new alkaliphilic, moderately thermophilic, sulfate-reducing bacterium. International Journal of Systematic and Evolutionary Microbiology 50(1), 25-33.
Proskurowski, G., Lilley, M.D., Kelley, D.S., Olson, E.J., 2006. Low temperature volatile production at the Lost City Hydrothermal Field, evidence from a hydrogen stable isotope geothermometer. Chemical Geology 229(4), 331-343.
Rau, G.H., Takahashi, T., Des Marais, D.J., 1989. Latitudinal variations in plankton d13C: implications for CO2 and productivity in past oceans. Nature 341.
Riebesell, U., Wolf-Gladrow, D.A., Smetacek, V., 1993. Carbon dioxide limitation of marine phytoplankton growth rates. 361(6409), 249-251.
Russell, M.J., 2003. The importance of being alkaline. Science 302, 580-581.
Schouten, S., Hopmans, E.C., Pancost, R.D., Damste, J.S.S., 2000. Widespread occurrence of structurally diverse tetraether membrane lipids: Evidence for the ubiquitous presence of low-temperature relatives of hyperthermophiles. Proceedings of the National Academy of Sciences of the United States of America 97(26), 14421-14426.

Seewald, J.S., Zolotov, M.Y., McCollom, T., 2006. Experimental investigation of single carbon compounds under hydrothermal conditions. Geochimica et Cosmochimica Acta 70(2), 446-460.
Shanklin, J., Cahoon, E.B., 1998. Desaturation and related modifications of fatty acids. Annual Review of Plant Physiology and Plant Molecular Biology 49, 611-641.
Shen, Y., Buick, R., 2004. The antiquity of microbial sulfate reduction. Earth-Science Reviews 64(3-4), 243-272.
Sherwood Lollar, B., McCollom, T.M., 2006. Biosignatures and abiotic constraints on early life. Nature (London, United Kingdom) 444(7121), E18.
Shock, E.L., Schulte, M.D., 1998. Organic synthesis during fluid mixing in hydrothermal systems. Journal of Geophysical Research, [Planets] 103(E12), 28513-28527.
Skophammer, R.G., Servin, J.A., Herbold, C.W., Lake, J.A., 2007. Evidence for a Gram Positive, Eubacterial Root of the Tree of Life. Molecular Biology and Evolution 24(8), 1761-1768.
Sleep, N.H., Meibom, A., Fridriksson, T., Coleman, R.G., Bird, D.K., 2004. H2-rich fluids from serpentinization: geochemical and biotic implications. Proceedings of the National Academy of Sciences of the United States of America 101(35), 12818-23.
Sprott, G.D., Brisson, J., Dicaire, C.J., Pelletier, A.K., Deschatelets, L.A., Krishnan, L., Patel, G.B., 1999. A structural comparison of the total polar lipids from the human archaea Methanobrevibacter smithii and Methanosphaera stadtmanae and its relevance to the adjuvant activities of their liposomes. Biochim Biophys Acta FIELD Full Journal Title:Biochimica et biophysica acta 1440(2-3), 275-88.
Summons, R.E., Bradley, A.S., Jahnke, L.L., Waldbauer, J.R., 2006. Steroids, triterpenoids and molecular oxygen. Philosophical Transactions of the Royal Society of London, Series B: Biological Sciences 361(1470), 951-968.
Ten Haven, H.L., Rohmer, M., Rullkoetter, J., Bisseret, P., 1989. Tetrahymanol, the most likely precursor of gammacerane, occurs ubiquitously in marine sediments. Geochimica et Cosmochimica Acta 53(11), 3073-9.
Tian, F., Toon, O.B., Pavlov, A.A., 2006. Response to Comment on “A Hydrogen-Rich Early Earth Atmosphere”. Science (Washington, DC, United States) 311(5757), 38.
Tian, F., Toon, O.B., Pavlov, A.A., De Sterck, H., 2005. A Hydrogen-Rich Early Earth Atmosphere. Science 308(5724), 1014-1017.
Ueno, Y., Yamada, K., Yoshida, N., Maruyama, S., Isozaki, Y., 2006. Evidence from fluid inclusions for microbial methanogenesis in the early Archaean era. Nature 440(7083), 516-9.
Upasani, V.N., Desai, S.G., Moldoveanu, N., Kates, M., 1994. Lipids of extremely halophilic archaeobacteria from saline environments in India: a novel glycolipid in Natronobacterium strains. Microbiology 140(8), 1959-66.
Valentine, D.L., Chidthaisong, A., Rice, A., Reeburgh, W.S., Tyler, S.C., 2004. Carbon and hydrogen isotope fractionation by moderately thermophilic methanogens. Geochimica et Cosmochimica Acta 68(7), 1571-1590.
Werne, J.P., Baas, M., Damste, J.S.S., 2002. Molecular isotopic tracing of carbon flow and trophic relationships in a methane-supported benthic microbial community.

Limnology and Oceanography 47(6), 1694-1701.

Chapter 4

Multiple origins of methane at the Lost City Hydrothermal Field

Abstract

The Lost City hydrothermal field emits fluids rich in hydrogen and methane, with serpentinization reactions exerting a strong influence on fluid chemistry. Cycling of methane in these fluids is a complex interaction of biological and abiotic sources and sinks. Carbon isotope compositions of archaeal lipids suggest that there may be at least two isotopically distinct sources of methane at Lost City. The first source is a mixture of abiotic and biological methane, detected at actively venting sites with $^{13}\delta_{CH4}$ = -13.6‰ to -8.8‰. The second source has not been directly detected, but is inferred to be -27‰ to -70‰ on the basis of detection of archaeal lipids at one site with $^{13}\delta$ = -77‰.

The high hydrogen concentrations at Lost City create a thermodynamic drive for methane production. Kinetic inhibition for this reaction is overcome by catalysis, perhaps with NiFe alloys stabilized under reducing conditions, and by enzymatic activity. Abiotic methanogenesis may be dominant at Lost City, but this is probably not the case in all serpentinizing systems.

4.1 Introduction

The fluids of the Lost City Hydrothermal Field have been noted for their abundant hydrogen (~15 mmol/kg) and methane (~2 mmol/kg) contents (Kelley et al., 2005). Due to the serpentinization reactions that influence fluid chemistry, the source of methane in Lost City fluids is suspected to be partially or largely abiotic (Proskurowski et al., 2006). However, this interpretation is complicated by the fact that carbonate towers precipitating at Lost City are inhabited by abundant archaea (Brazelton et al., 2006) that are producing methane (Chapter 3) . Ultramafic rocks like those that host Lost City would likely have been an abundant component of the seafloor on a young hot Earth (Nisbet and Fowler,

2004), and low-temperature serpentinization reactions can be expected to have had a correspondingly larger influence on the chemistry of the Archaean atmosphere and ocean. Similarly, serpentinization might influence environmental chemistry or potentially even support microbial communities on other terrestrial planets that contain both ultramafic rock and water (Chapelle et al., 2002; McCollom, 1999). Therefore it is critical to understand the degree to which methane production in these systems requires biology.

The ^{13}C contents of methane in Lost City fluids is markedly greater than that produced by methanogenic archaea in typical sedimentary systems. At Lost City $\delta_{methane}$ ranges from -13.6‰ to -8.8‰ vs. VPDB (Kelley et al., 2005), while biological production usually results in $\delta_{methane} \leq$ -50‰ (Whiticar, 1999). The abundance of ^{13}C in Lost City methane is consistent with an abiotic source, but it does not exclude a biological origin if fractionation is minimized by limited availability of carbon substrate. Archaeal lipids at Lost City are enriched in ^{13}C relative to methane, consistent with biological production of methane from a limited substrate (Chapter 3). Lipids in both methanogenic and methanotrophic archaea are depleted in ^{13}C relative to their source of carbon. Comparison of δ_{lipid} to that of dissolved inorganic carbon and methane in vent fluids allows us to put constraints on carbon cycling in the hydrothermal fluids and begin to decipher the sources and sinks of methane.

Abundances of deuterium in methane and hydrogen might also be used to constrain methane sources. At high temperatures, the abundance of deuterium in these species approaches isotopic equilibrium. This equilibrium is temperature-dependent and has been used as a geothermometer at Lost City and at other hydrothermal vents (Proskurowski et al., 2006). Activity of methanogenic archaea can be expected to influence the deuterium contents of both hydrogen and methane. Hydrogenase, a key enzyme operating in autotrophic archaea, enhances the rate at which the deuterium content of hydrogen re-equilibrates with H_2O at temperatures below 110ºC. Microbial methane, which is thought to have deuterium content related primarily to that of water, contributes to the total methane pool. We present a deuterium-isotope model for the mixture of abiotic and microbial methane and suggest

criteria by which a dominantly biological input can be identified.

4.2 Abiotic Production of Methane

4.2.1 Natural and experimental evidence

The abundant hydrogen produced in serpentinization reactions leads to conditions that thermodynamically favor the reduction of CO_2 (Shock and Schulte, 1998). Several experimental studies have indicated that methane and higher hydrocarbons may be produced abiotically in ultramafic hydrothermal systems by Fischer-Tropsch type (FTT) processes (Berndt et al., 1996; Foustoukos and Seyfried, 2004; Horita and Berndt, 1999; McCollom and Seewald, 2001). Methane alone can also be produced by other processes at hydrothermal systems (McCollom and Seewald, 2007; Seewald et al., 2006). Indeed, the evidence at natural hydrothermal systems for abiotic synthesis of any compounds other than methane is equivocal. Where such evidence has been proposed in natural settings (Holm and Charlou, 2001), it has subsequently been challenged (Simoneit et al., 2004). In laboratory settings, some of the first experiments to investigate reduction of CO_2 to higher hydrocarbons under simulated serpentinization conditions initially appeared to be successful (Berndt et al., 1996). However, reassessments of this result have suggested that the hydrocarbons detected were contaminants in the experimental system (McCollom and Seewald, 2001). Later experiments (Foustoukos and Seyfried, 2004) suggested that abiotic synthesis of ethane and propane is possible with chromite as a catalyst, but the exact role of chromite in these reactions remains unclear (McCollom and Seewald, 2007).

The thermodynamic drive for methane production is a necessary but not sufficient condition for its abiotic synthesis. Kinetic inhibition may limit the amount of methane produced in a natural system regardless of the energetic drive to create it. All of the experimental investigations that have examined abiotic methane production under serpentinization conditions have yielded far less methane than would be predicted based on thermodynamics alone, suggesting that the reactions are kinetically inhibited (McCollom

and Seewald, 2007). The only experiment in which large amounts of methane have been created used a nickel-iron alloy (Horita and Berndt, 1999). These alloys are stable only under very reducing conditions, but ultramafic hydrothermal systems like Lost City may be reducing enough (McCollom and Seewald, 2007).

Abiotic methane has been reported from a number of hydrothermal systems, including the high temperature hydrothermal systems of the Mediterranean (Fiebig et al., 2007), the ultramafic Rainbow hydrothermal field (Charlou et al., 2002; Holm and Charlou, 2001) and potentially, the deep subsurface of the Precambrian Shields of Canada and South Africa (Sherwood Lollar et al., 2006; Sherwood Lollar et al., 2002). The criteria most commonly used to identify methane sources are its ^{13}C and deuterium contents, which are compared to empirically defined ranges (Figure 4-1). The range expected for abiotic methane is not precisely constrained. Abiotic methane is expected to be enriched in ^{13}C, primarily based on the reported δ values of methane at locations where abiotic methanogenesis is thought to be occurring (Abrajano et al., 1988; Charlou et al., 2002; Fritz et al., 1992). However, experiments have suggested that abiotic methanogenesis could discriminate against ^{13}C by up to 60‰ (Horita and Berndt, 1999).

The ^{13}C content of methane at Lost City falls does not fall within the range typically ascribed to biotic production; $\delta^{13}C$ ranges from -13.6‰ to -8.8‰ vs. VPDB (Kelley et al., 2005). δD is reported as -120‰ ± 12‰ vs. VSMOW (Proskurowski et al., 2006) with approximately 70% of the measurements falling within the usual biological range. Methane from Lost City plots at the extreme end of the thermogenic field; yet this methane is unlikely to be thermogenic. Lost City is an unsedimented hydrothermal field located on young crust near the center of the North Atlantic gyre with no obvious source of abundant organics. Methane, therefore, is likely to be produced by abiotic serpentinization or by biology.

4.2.2. Potential for abiotic methane production at Lost City

Methane concentrations in Lost City hydrothermal fluids are uniformly greater than

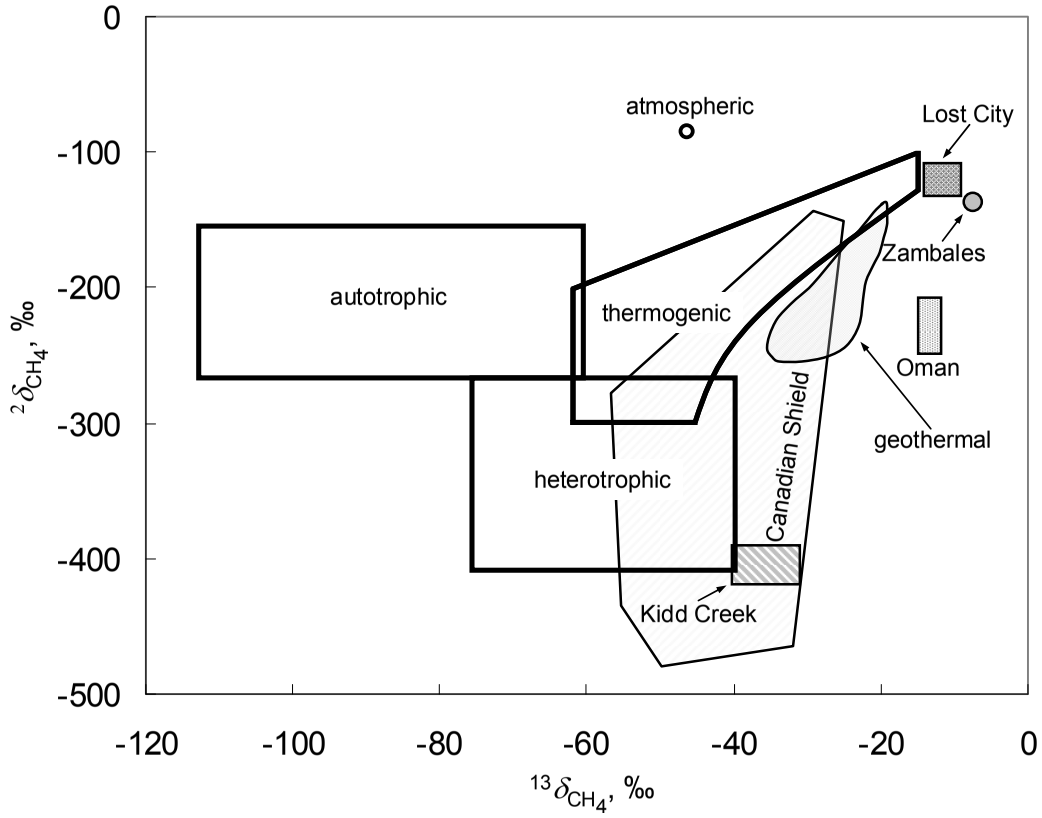

Figure 4-1: Ranges of $\delta^{13}C$ and δD detected in methane produced by a variety of sources. 'autotrophic' refers to methane produced by H_2/CO_2 methanogenesis, while 'heterotrophic' refers to methane produced by fermentation of acetate or consumption of methylated organic compounds. 'Thermogenic' refers to cracking of biologically-derived oils, while 'geothermal' refers to cracking of high molecular-weight organic compounds. Also included are observed variations at several locations where abiotic methane formation has been proposed: Canadian Shield gases (including Kidd Creek), the Oman ophiolite, Zambales ophiolite, and Lost City Hydrothermal Field. After Schoell, 1988.

1 mmol/kg (Proskurowski et al., 2006). The highest temperatures attained in the Lost City system are 110 – 150 ºC (Proskurowski et al., 2006) and considerably lower than temperatures at the Rainbow hydrothermal field (Holm and Charlou, 2001). The lack of anhydrite precipitation at Lost City has also been interpreted as evidence that serpentinization temperatures never exceed 150 ºC (Kelley et al., 2005).

Low maximum temperatures at Lost City raise significant questions about the conditions conducive to generation of abiotic methane. Experimental serpentinization studies have generally been carried out at temperatures higher than 150 ºC due to the slow reaction kinetics (McCollom and Seewald, 2001; Seewald et al., 2006). At Lost City abiotic formation of methane may be slow but attainable if residence times between fluid and the host-rock are very long.

Based on experimental data (McCollom and Seewald, 2001), Fiebig et al. (Fiebig et al., 2007) proposed the following equation (modified after (Giggenbach, 1997) for the chemical exchange between CO_2 and CH_4:

$$\log \tau_c = -5.06 + 4440 / T$$

where t_c is the half-time for chemical exchange in years, and T is the temperature (K). Fiebig et al. assume that chemical equilibrium should be approached after four half-times. In that case the equilibration of methane with CO_2 at Lost City, with a reaction temperature of 110 ºC to 150 ºC should take 13.6 My to 1.1 My, which spans the range of the 1.5 Ma crust at the Atlantis Massif (Kelley et al., 2001). Fiebig et al. note that equilibration of CH_4 and CO_2 at Mediterranean fumaroles is also much faster than predicted by equation 1, but suggest that this is due to the presence of a water-saturated vapor phase. Such a phase is unlikely to be present at a high-pressure low-temperature site such as Lost City. If Lost City methane is indeed being produced by reduction of CO_2 during serpentinization, then equation 1 suggests that maximum temperatures probably approach 150 ºC, although disequilibrium production might be reached at lower temperatures. Alternatively, lower temperature equilibrium could conceivably be due to the formation and catalytic action of

a nickel-iron phase (Horita and Berndt, 1999) which is stabilized under the highly reducing conditions, as previously noted.

However, it is worth noting that geochemical models suggest that redox equilibrium at Lost City is sluggish (Allen and Seyfried, 2004). Given the high hydrogen concentrations, sulfate in hydrothermal fluid should be quantitatively reduced to sulfide, but is not (Allen and Seyfried, 2004). The reduction of sulfate is thermodynamically more favorable than the reduction of CO_2 and its slow reduction implies that slower rates are indeed controlling abiotic chemical redox equilibrium. Furthermore, although experimental data suggests the potential for methane formation with olivine or nickel-iron phases as a catalyst, these experiments were not carried out in the presence of sulfide. The role of sulfur compounds in FTT synthesis is not well understood and could possibly poison the reaction (McCollom and Seewald, 2007). The role of sulfur in these reactions remains a topic for future experimental work.

4.3. Biological Production of Methane

Carbonates at Lost City contain abundant archaea containing 16S rDNA genes clustering within the Methanosarcinales (Brazelton et al., 2006; Kelley et al., 2005; Schrenk et al., 2004). These organisms fall within a large clade of methanogens, but also fall either within (Knittel et al., 2005) or very close (Losekann et al., 2007) to the ANME-3 methanotrophic clade. Lipids associated with these archaea are unusually enriched in ^{13}C (Kelley et al., 2005). The question of whether these archaea are operating as methanogens or methanotrophs is definitively resolved in favor of methanogenesis by the observation that at actively venting sites the ^{13}C content of archaeal lipids is greater than the ^{13}C content of methane (Chapter 3).

The activity of methane-producing archaea requires that at least some proportion of the methane at Lost City is biological. Indeed, the carbon-isotopic compositions of dissolved inorganic carbon, methane, and methanogen lipids do not exclude the possibility that all of

the methane at Lost City is biologically derived. Evidence for biological methanogenesis is extensively addressed in Chapter 3.

4.4 Archaeal methanotrophy

ANME-1 methanotrophs are also observed at a few sites at Lost City, particularly in cooler environments (Brazelton et al., 2006; Kelley et al., 2005). At one site, marker X2, the dominant Lost City Methanosarcinales phylotype was undetected, but ANME-1 was present. That site contained the methanogen lipid archaeol with $\delta_{archaeol}$ = -77‰, suggesting it is indeed derived from a methanotroph. Hydroxyarchaeols were not detected at this site.

At most locations at Lost City, *sn*-2 hydroxyarchaeol was more abundant than archaeol. This is seemingly a characteristic of the Lost City phylotype Methanosarcinales. However archaeol is typically more abundant than *sn*-2 hydroxyarchaeol in ANME-1 archaea (Blumenberg et al., 2004). Archaeol was detected in only small amounts at site X2, so if this site is indeed dominated by ANME-1 methanotrophs it is perhaps unsurprising that *sn*-2 hydroxyarchaeol was undetected.

Site X2 was located in an area where no fluid samples were collected, so $\delta_{methane}$ at this location is unknown. However, the extent of ^{13}C depletion in the lipid from this sample suggests that it may derive from a source of methane with ^{13}C contents outside the range that has previously been observed in Lost City fluids.

Examination of the fractionation between methane and lipids in methanotrophic archaea is understudied, probably because anaerobic methanotrophs are difficult to culture and have not been isolated in pure culture. The ^{13}C contents of both methane and lipids for have been reported at several locations where anaerobic methanotrophs dominate the archaeal community. Figure 4-2 shows the ranges of δ values for methane, archaeol, and *sn*-2 hydroxyarchaeol in several environments dominated by ANME-1 organisms. In samples from the Eel River Basin archaeol is depleted by approximately 50‰ relative to methane (Hinrichs et al., 1999). Other sites show lesser depletions. At each site *sn*-2

hydroxyarchaeol is more depleted in ^{13}C than archaeol.

If the methane constituting the carbon source for ANME-1 methanotrophs at marker X2 has $\delta_{methane}$ within the range measured in Lost City fluids, then the fractionation between methane and lipid falls outside the range previously observed in other ANME-1 organisms. Thus, Lost City ANME-1 may be exhibiting the largest fractionation yet observed in methanotrophic archaea. Alternatively, they are consuming a second, unsampled source of methane with lower ^{13}C content. The previously observed range of ^{13}C discrimination between methane and ANME-1 archaeol leads to the prediction that ANME-1 organisms at Lost City are consuming methane with $\delta^{13}C$ between -27‰ and -70‰ (Figure 4-2).

The precise location of site X2 is not well constrained. The cruise report states that this sample (3880-1557) was a fracture-filling carbonate recovered from an area up to 50 m to the east of Marker H (map, Chapter 3, Figure 3-1) at a depth of 860 meters. This description suggests that this sample was likely recovered outside of the main area of venting. If methane produced at Lost City consists of multiple inputs, both biological and abiotic, it is possible that the source dominating fluids at this edge of the field is not the same as that at the active high temperature vents. No fluids were collected here and this hypothesis will likely remain untested until a return expedition to Lost City is mounted.

4.5. Resolving mixed sources of methane

4.5.1. Patterns of Fischer-Tropsch products

Methane attributed to sources in the mantle is usually distinguished by three criteria. These are: $\delta^{13}C$ greater than -25‰, association with light hydrocarbons with $\delta^{13}C$ values that decreased with increasing molecular weight , and association with mantle values of $^{3}He/^{4}He$ (Sherwood Lollar et al., 2006). At hydrothermal systems such as the Rainbow Field at the mid-Atlantic ridge, the abiotic origin of methane is inferred because its carbon isotope ratios ($\delta^{13}C$ = -16 to -24) constitute enrichment in ^{13}C beyond the typical biogenic range (Charlou et al., 2002; Simoneit et al., 2004). Recent studies have demonstrated that

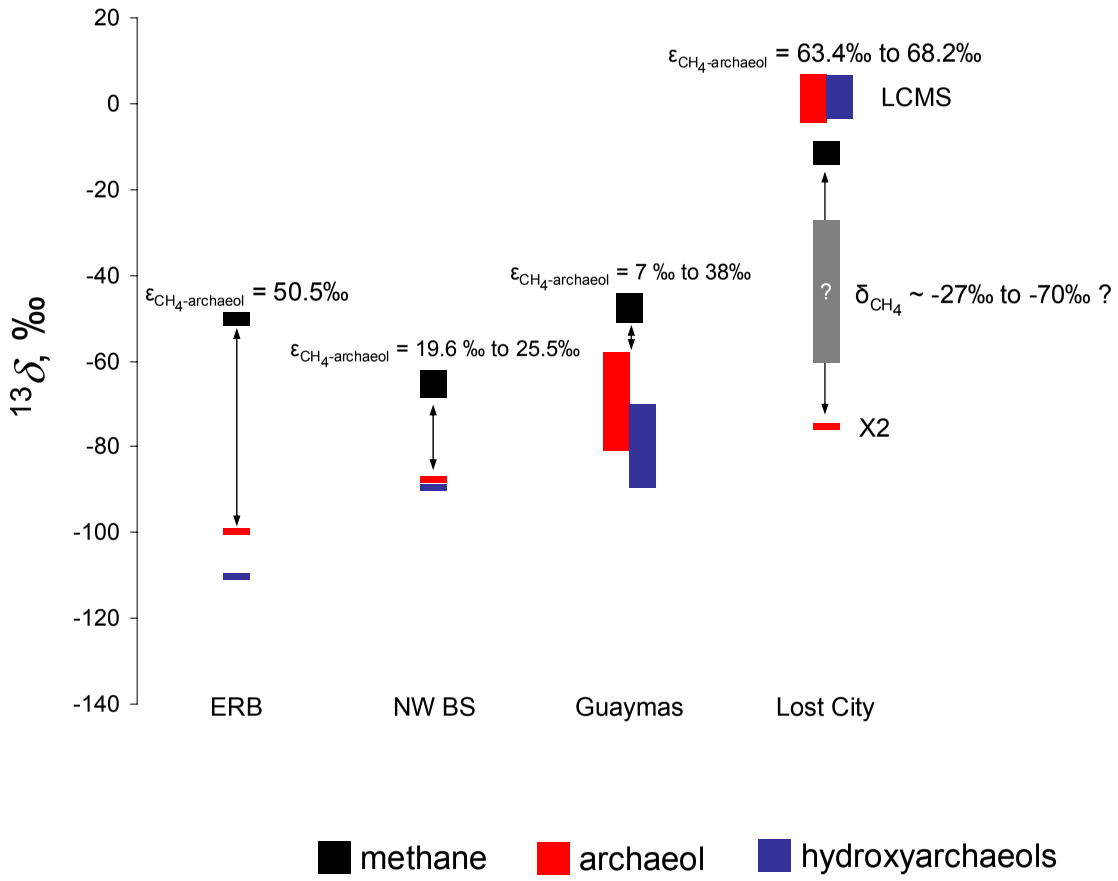

Figure 4-2: Ranges of $\delta^{13}C$ of methane, archaeol, and *sn*-2 hydroxyarchaeol at several sites where ANME-1 are the main archaeal contributors to biomass. ERB: Eel River Basin (Hinrichs et al., 1999); NW BS: Dniepr Canyon, northwest Black Sea (Michaelis et al., 2002); Guaymas: Guaymas Basin, Gulf of California (Teske et al., 2002); Lost City (Kelley et al., 2005)

methane produced by FTT processes be depleted in ^{13}C relative to DIC by 35‰ to 60‰, with larger depletions occurring at lower temperatures (Horita and Berndt, 1999; McCollom and Seewald, 2006). Thus, abiotic methane can have $\delta^{13}C$ values less than -25‰; ^{13}C depletion is not by itself a criterion by which biological methane can be identified (Schoell, 1988; Sherwood Lollar and McCollom, 2006) .

Sherwood Lollar et al. (2002) proposed criteria by which to identify abiotic hydrocarbons on the basis of stable isotopes. Geological FTT processes can produce higher hydrocarbons (ethane, propane, butane) along with methane. Abiotic ethane shows a depletion in ^{13}C but an enrichment in ^{2}H relative to abiotic non-thermogenic methane (Sherwood Lollar et al., 2002). However, this can be complicated in systems where archaeal methanogens provide an additional methane source (Sherwood Lollar et al., 2006; Sherwood Lollar et al., 2002). In several such cases examined by Sherwood Lollar et al.(2006) this pattern held for only the samples containing the most ^{13}C enriched methane at a given site. These ^{13}C enriched samples were considered to an abiotic end member, and the $\delta^{13}C$ of biological methane was inferred by comparing the $\delta^{13}C$ of methane to the ratio of methane to higher hydrocarbons (>1000 for biological methane) in samples from several sites. With the resulting two end members, a mixing model was constructed and used to estimate the relative inputs of biological and abiotic methane. Such a model holds promise at Lost City, where higher hydrocarbons have been detected (Proskurowski et al., 2005) but not yet analyzed isotopically. Sherwood Lollar et al. (2006) noted that the most ^{13}C-enriched (abiotic) methane at each site was consistently detected at the sites with the highest H_2 concentrations while lower H_2 concentrations were inferred to have been drawn down by methanogens operating at sites with higher proportions of biological methane.

One site showing this pattern is the deep fracture system under a mine in the Precambrian Shield of South Africa (Moser et al., 2005). Here, hydrogen gas is produced by radiolysis of water and drives the formation of both abiotic and biotic methane. Waters are alkaline, warm, with low DIC (between 100 and 200 μm) and the micromolar H_2 supports

communities of methanogens and *Desulfotomaculum*. These conditions and microbial community are analogous to the conditions at Lost City.

Lost City hydrogen concentrations are substantially higher (up to nearly 15 mM) compared to 0.16 to 165 μM in the South African system. The ^{13}C contents of the methane are also higher. Methane $\delta^{13}C$ values are -13.6‰ to -8.8‰ at Lost City and -42.2‰ to -39.5‰ in the South African system. This is consistent with the relationship between methane $\delta^{13}C$ and hydrogen concentrations described by Sherwood Lollar et al. (Sherwood Lollar et al., 2006). However we note that unlike in the South African mine, hydrogen concentrations at Lost City are at least one order of magnitude higher than DIC concentration. Furthermore, while the South African mine system shows differences in $\delta^{13}C$ between DIC and methane of 23.2‰ to 27.2‰, at Lost City the differences are smaller. The smaller differences are consistent with carbon limitation limiting isotope fractionation in methane production, be it biological or abiotic.

Other criteria can also be applied to distinguish abiotic from biological methane. For example both abiotic methane produced by FTT processes and methane produced by thermogenic cracking of higher-molecular-weight hydrocarbons have an Anderson-Shulz-Flory (AFS) distribution, defined as a log-linear relationship with decreasing concentration related to increasing length of the alkyl chain (Fiebig et al., 2007; Sherwood Lollar et al., 2002). Hydrocarbons produced by FTT reactions should be progressively depleted in ^{13}C and enriched in D with increasing molecular weight, because the lighter isotope of carbon is more readily incorporated into a growing polymer, while bonds between carbon and ^{1}H are weaker and more readily broken that those between carbon and deuterium (Des Marais et al., 1981). Such a hydrocarbon distribution, with compounds up to C_4 has been detected at Lost City (Proskurowski et al., 2005), although isotopic results have not yet been reported. The presence of higher hydrocarbons at Lost City is somewhat surprising, since the low temperatures and high pH of the LCHF fluids are likely to inhibit the production of CO from CO_2 (Seewald et al., 2006), and since low temperature catalysis of CO_2 reduction

has overcome kinetic barriers only with NiFe substrates (Horita and Berndt, 1999), which produce exclusively methane as a product (Anderson, 1984; Horita and Berndt, 1999) . CO has been postulated to be the critical intermediate for FTT synthesis of abiotic hydrocarbons and Lost City may provide a good test of that hypothesis. Still, the AFS distribution suggests that a proportion of the methane at Lost City is abiotic. Biological processes can also produce low molecular weight hydrocarbons, although compounds heavier than C_3 have not been detected (Hinrichs et al., 2006).

4.5.2. Deuterium isotope patterns

4.5.2.1 Deuterium isotope results

Methane at Lost City has δD values of -120 ± 12‰ (Proskurowski et al., 2006) and these can be compared to the δD of H_2 as a geothermometer. When this is done the results correlate linearly with the results from the H_2O-H_2 thermometer (Figure 4-3), suggesting serpentinization temperatures near 100 ºC (Proskurowski et al., 2006), but with the methane geothermometer consistently recording a temperature nearly 24ºC cooler than the hydrogen geothermometer.

The deuterium content does not immediately preclude a biotic source for methane. The δD of Lost City fluid waters is +2‰ to +7‰ (Proskurowski et al., 2006). Autotrophic methanogens produce methane with δD that is independent relative to δD-H_2 but dependent on δD-H_2O (Valentine et al., 2004). Deuterium fractionation between H_2O and autotrophic CH_4 was measured to have a wide range (127‰ - 275‰) for the methanogen *Methanothermobacter marburgensis* (Valentine et al., 2004) and other methanogens fractionate with similar magnitude (Whiticar, 1999). The difference in δD between water and methane at Lost City is of similar magnitude (100‰ - 150‰). These fractionations are all within or very close to the low end of fractionations that have been observed from a biological origin. They are plausibly biological; the isotopic signatures of methane at Lost City are therefore fully consistent with a biological source. Similarly, other ultramafic sites

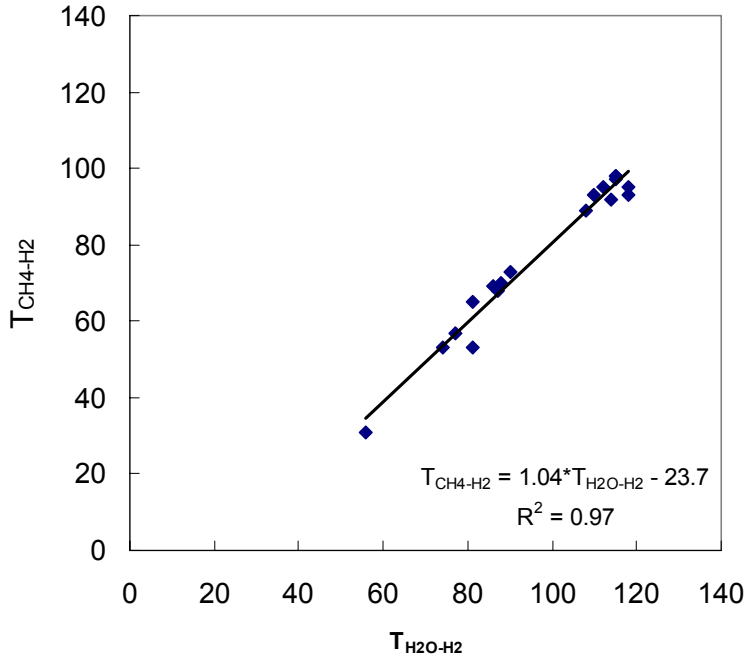

Figure 4-3: Strong correspondence of methane and hydrogen geothermometers, showing consistently lower temperatures predicted by CH_4-H_2 thermometer. Data is obtained from Table 1 in Proskurowski et al. (2006).

where ^{13}C enriched methane has been detected, such as the Oman and Zambales ophiolites, should be investigated for the possibility that some of the methane is biological.

4.5.2.2. Deuterium isotope mixing

We introduce the concept of isotopic concordance in geothermometry as a tool to consider the influence of methanogenic archaea on the deuterium content of hydrogen and methane. In a fluid that has previously equilibrated at higher temperatures microbial methanogenesis can alter the high temperature geothermometry signal, so that a concordant signal is no longer observed. While concordance is an ideal that is probably never observed in natural samples, understanding the causes of deviations from it can help us better constrain the sources of hydrothermal methane.

When H_2 and H_2O are in isotopic equilibrium at hydrothermal temperatures, H_2 is substantially depleted in deuterium relative to water. The magnitude of depletion is greater

at cooler temperatures. Several investigators have determined equilibrium fractionation factors between these species. The equation that most robustly aligns with experimental testing (Horibe and Craig, 1995) is:

$$\alpha_{H_2O\text{-}H_2} = 1.0473 + \frac{201{,}036}{T^2} + 2.060\frac{10^9}{T^4} + 0.180 * \frac{10^{15}}{T^6}$$

(Bardo and Wolfsberg, 1976).

Similarly, Horibe and Craig (1995) give an empirically-derived equation for the equilibrium between CH_4 and H_2:

.

$$\alpha_{CH_4\text{-}H_2} = 0.8994 + \frac{183{,}540}{T^2}$$

In principle, if full equilibrium in the CH_4-H_2-H_2O system were attained, the fractionation factors would lie on the curve in Figure 4-4a. The geothermometer has been calibrated for temperatures only above 200ºC, so it is unclear whether it is applicable at lower temperatures (dashed line). For the purposes of this argument we follow precedent (Proskurowski et al., 2006) and extrapolate the calibration to low temperature; the merit of this is discussed below.

Measurements of the deuterium content of methane and hydrogen in vent waters are plotted in Figure 4-4b (data from Prosukurowski et al.(2006)). Most are discordant, and that the deviation from the ideal is greater at the low temperature Lost City site than at the high temperature black smoker sites. The reasons for these discordant temperature results are beyond the scope of this investigation, but may be related to sluggish isotope equilibrium at low temperatures (Proskurowski et al., 2006). We draw attention only to its consistent pattern: with the exception of one sample from the Oman ophiolite (discussed in more detail below), all natural hydrothermal fluids plot above the concordance line (Figure 4-4b).

Activity of methanogenic archaea can be expected to affect the deuterium content of both hydrogen and methane in a fluid. This activity should produce deviations from

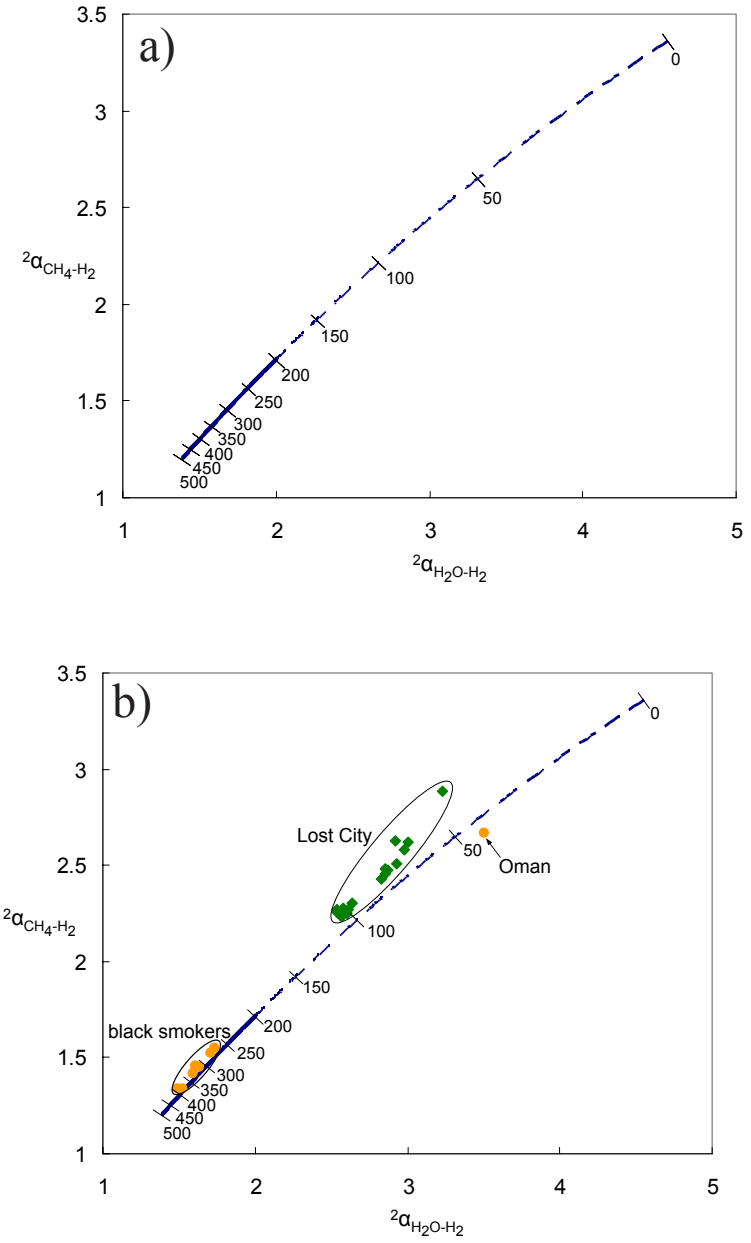

Figure 4-4: a) Theoretical temperature concordance diagram showing fractionation in the CH_4-H_2O-H_2 system. This concordance considers equations for CH_4-H_2 equilibrium (Horibe and Craig, 1995) and H_2O-H_2 equilibrium (Bardo and Wolfsberg, 1976).
b) same plot as a with data from black smokers, Oman ophiolite, and Lost City plotted (Proskurowski et al., 2005).

temperature concordance. Here we explore the manner in which this deviation should occur, in expectation that activity of methanogens can be identified where concurrent abiotic methane is present.

Autotrophic methanogens use the enzyme hydrogenase to activate molecular hydrogen for use as a biochemical reductant (Thauer, 1998). In order to synthesize one unit of methane, four units of hydrogen are required. However, experimental work has determined that hydrogenase is probably only about 50% efficient in methangogens (Valentine et al., 2004). Hydrogenase is a rapidly reversible enzyme, and catalyzes the isotopic equilibration of hydrogen with water (Valentine et al., 2004). Therefore, where autotrophic methanogens are active they can be expected to facilitate isotopic equilibration of hydrogen with water at ambient temperature.

Methanogens produce methane with a deuterium content that is primarily related to the deuterium content of water, although under high hydrogen partial pressures at least one-fourth of methane hydrogen may be directly derived from molecular hydrogen (Valentine et al., 2004). In one experimental study (Valentine et al., 2004) fractionation factors were found to range from 127‰ to 275‰ (α = 1.16 to 1.43), while another found a range of 170‰ to 250‰ (α = 1.20 to 1.33) (Whiticar, 1999). The smaller end of this range is probably not directly applicable to hydrothermal settings. This result was obtained by growing methanogens on a high partial pressure of hydrogen with a much higher deuterium content than that expected to be produced in equilibrium with H_2O (Valentine et al., 2004 Experiment D-2, $^2\delta_{H2}$ = -190). This experiment superbly demonstrated the potential for direct incorporation of deuterium from molecular hydrogen into methane under high hydrogen partial pressures. In natural settings $^2\delta_{H2}$ in this range is probably produced only by fermentation of organic material. In hydrothermal settings the natural range of methane deuterium depletion relative H_2O is probably in the range of 150‰ to 275‰.

Figure 4-5a shows the concordant temperature equilibrium curve for methane and hydrogen in natural water with $^2\delta_{H2O}$ = +5‰, which is approximately the value at Lost City

(Proskurowski et al., 2006). The red dots represent the expected $^{2}\delta$ values for methane and hydrogen that have equilibrated at 150 ºC. The lower red dot is placed directly on the concordance curve and the upper dot is placed off the curve in the discordant range generally observed in hydrothermal fluids.

Activity of methanogens can be expected to contribute to the reequilibration of hydrogen at lower temperatures. The highest temperature at which methanogens are known to grow is 110 ºC, the upper growth limit for *Methanopyrus kandleri* (Kurr et al., 1991). At 110 ºC the equilibrium $^{2}\delta_{H2}$ on this curve is approximately -610‰. This therefore constitutes an upper limit to the value of $^{2}\delta_{H2}$ supplied by hydrogenase-catalyzed reequilibration.

Methanogens are expected to produce methane with $^{2}\delta_{CH4}$ in the range -150‰ to -275‰, more negative than that produced abiotically at higher temperatures. The upper boundary of the grey box represents the maximum expected $^{2}\delta_{CH4}$ for biological methane.

The black dot shows a potential end member for deuterium content of microbial methane and hydrogen. This black dot can be expected to fall anywhere within the area delineated by the grey box, which is bounded as explained in the previous two paragraphs.

The dotted black lines denote potential mixing curves. Evolution of deuterium content of methane and hydrogen will move approximately along these curves as biological methanogenesis continues. The curves are drawn as linear lines for schematic purposes, but they need not be straight. The shape of these curves will depend on i) the ratio of biologically equilibrated hydrogen to biologically produced methane (estimated at 4:1 by Valentine et al., 2004, but note that additional hydrogenase activity can be contributed by organisms that are not methangens) and ii) the ratio of hydrogen concentration to methane concentration in hydrothermal fluids. If these two ratios are similar then the mixing line should be nearly straight. If the 'biologically produced' H_2/CH_4 ratio is greater than the concentrations in the environment, the curves will be concave up, where as they will be convex if the reverse is true.

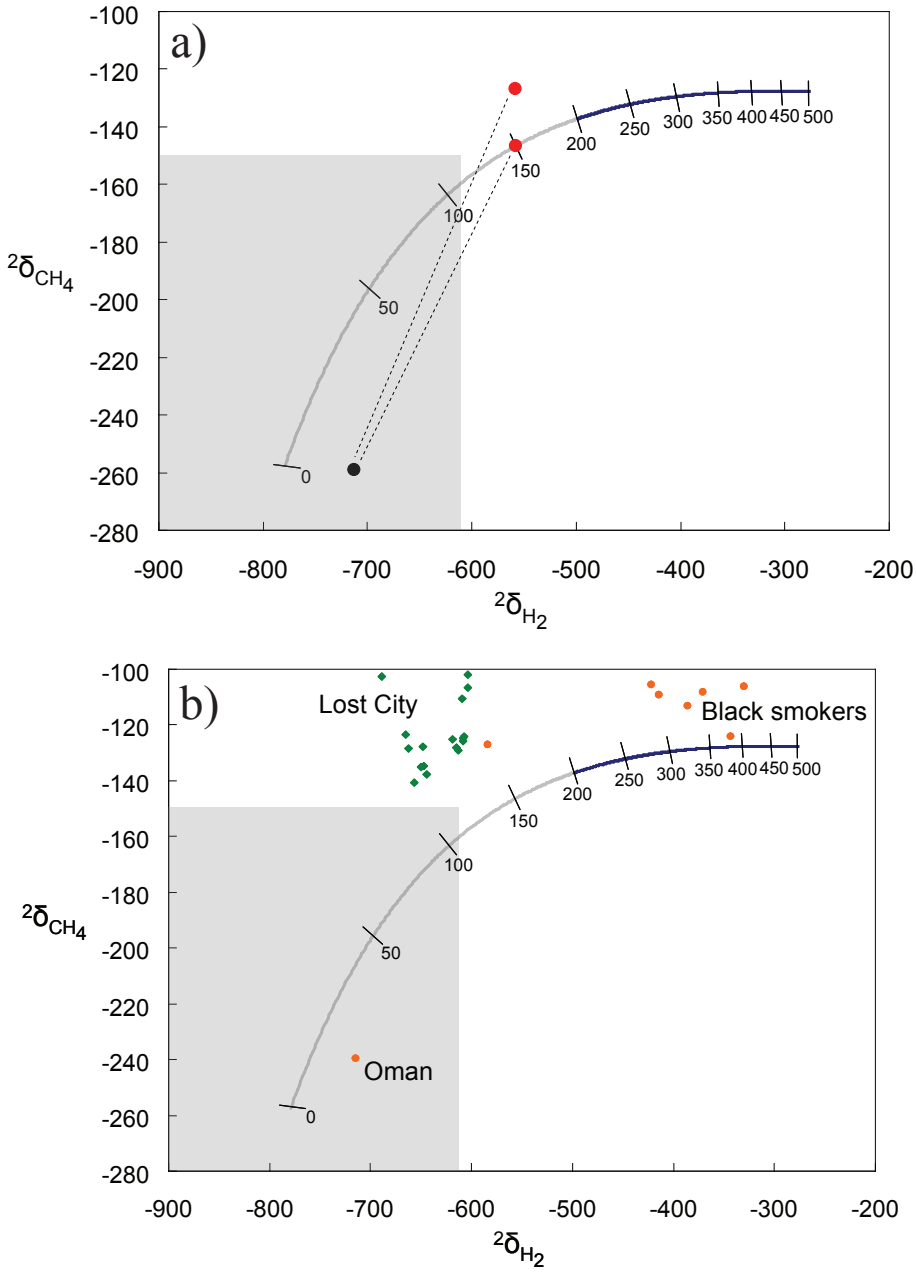

Figure 4-5: a) Theoretical temperature concordance diagram plotted as δ values from water with $^2\delta$ = +5‰. Red points are theoretical starting points for deuterium contents of methane and hydrogen in a fluid equilibrated at 150 ºC. Methane and hydrogen produced by activity of methanogens is expected to fall within the grey box. The upper bound of the box on the CH_4 axis is controlled by the minimum expected biological fractionation between deuterium contents of H_2O and biological CH_4 (~150‰). The upper bound of the box on the H2 axis is controlled by the isotope equilibrium between H_2O and H_2 at the maximum temperature that methanogens can survive (~110 ºC). The black point is an example of a potential biological end-member and could fall anywhere within the grey box. The dashed lines are potential mixing lines.
b) Same plot as (a) with data from natural hydrothermal settings plotted (Proskurowski et al., 2005). The only point clearly falling within the biological field is that from the Oman ophiolite.

In hydrothermal fluids dominated by biological methanogenesis we can expect $^{2}\delta$ values to approach or fall within the grey box. Figure 4-5b shows the same curve as Figure 4-5a, but with $^{2}\delta$ values for the hydrothermal fluids at Lost City and black smokers denoted (Proskurowski et al., 2006). This approach suggests that the activity of biological methanogenesis is not the dominant control on deuterium isotopic abundances in methane and hydrogen at Lost City, or any of the other hydrothermal sites. However, given that we know that some of the methane at active vents at Lost City is certainly biological (Chapter 3), there has undoubtedly been some movement of points along mixing lines. This may imply that the isotope geothermometer approach slightly underestimates maximum temperatures.

The deuterium contents of methane and hydrogen produced by the serpentinization of the Semail ophiolite in Oman suggests possible biological control of the isotopic equilibration at that site (Abrajano et al., 1988). A biological origin for the methane here has previously been excluded on the basis of its ^{13}C enrichment ($\delta^{13}C$ = -15‰ to -20‰) (Abrajano et al., 1988). However our work (Chapter 3) has suggested that under the high partial pressures of hydrogen produced by serpentinization, ^{13}C enrichment beyond the usual biological range may be expected. If methane at this site is not biologically produced, then equilibration there has occurred at very low temperatures. Further investigation of this site is required to ascertain the origin of methane in the Oman ophiolite.

4.6 Conclusions

Examination of the carbon isotope composition of methane and the deuterium contents of methane and hydrogen can shed light on the origins of methane and the relative contributions of biological and abiotic inputs. Our approach suggests that methane at the warmest vent fluids at Lost City are dominated by abiotic inputs.

Carbon isotope contents of archaeal lipids are consistent with a biological source of methane in actively venting chimneys. The contribution of biological methane to a

largely abiotic pool may lead to isotope geothermometry results that slightly underestimate maximum temperatures.

One site at the edge of the Lost City field had lipids recording archaeal methanotrophy, consistent with the work of others documenting ANME-1 methanotrophs there. The extreme depletion in ^{13}C of lipids relative to measured ^{13}C of methane invites the consideration of a methane source. This source should be depleted in ^{13}C relative to that of measured vent waters. The nature of this source (abiotic or biotic) is unknown, and can not be determined solely on the basis of estimated ^{13}C content.

The determination of a likely preponderance of abiotic methane at Lost City is instructive for our understanding of contributions of reduced carbon to the Archaean biosphere. But we must proceed with care. Although serpentinization at Lost City appears to be producing abiotic methane, fluid temperatures at this site require an external heat source (Allen and Seyfried, 2004). We do not yet know if serpentinization alone produces enough heat to overcome kinetic barriers to methane generation. One site where this may be better explored is in the ophiolite complex of Oman. The fluids there are cooler than at Lost City and heat might be supplied solely by serpentinization (Abrajano et al., 1988). However, that site might well be dominated by biological methane.

4.7 References

Abrajano, T.A., Sturchio, N.C., Bohlke, J.K., Lyon, G.L., Poreda, R.J., Stevens, C.M., 1988. Methane-hydrogen gas seeps, Zambales Ophiolite, Philippines: Deep or shallow origin? Chemical Geology 71(1-3), 211-22.

Allen, D.E., Seyfried, W.E., Jr., 2004. Serpentinization and heat generation: Constraints from Lost City and Rainbow hydrothermal systems. Geochimica et Cosmochimica Acta 68(6), 1347-1354.

Anderson, R.B., 1984. *The Fischer-Tropsch synthesis*. Academic Press, London.

Bardo, R.D., Wolfsberg, M., 1976. A theoretical calculation of the equilibrium constant for the isotope exchange reaction between H2O and HD. Journal of Physical Chemistry 80, 1068-1071.

Berndt, M.E., Allen, D.E., Seyfried, W.E., Jr., 1996. Reduction of CO (sub 2) during serpentinization of olivine at 300 degrees C and 500 bar. Geology (Boulder) 24(4), 351-354.

Blumenberg, M., Seifert, R., Reitner, J., Pape, T., Michaelis, W., 2004. Membrane lipid patterns typify distinct anaerobic methanotrophic consortia. Proceedings of the National Academy of Sciences of the United States of America 101(30), 11111-11116.

Brazelton, W.J., Schrenk, M.O., Kelley, D.S., Baross, J.A., 2006. Methane- and sulfur-metabolizing microbial communities dominate the lost city hydrothermal field ecosystem. Applied and Environmental Microbiology 72(9), 6257-6270.

Chapelle, F.H., O'Neill, K., Bradley, P.M., Methe, B.A., Ciufo, S.A., Knobel, L.L., Lovley, D.R., 2002. A hydrogen-based subsurface microbial community dominated bymethanogens. Nature 415, 312-315.

Charlou, J.L., Donval, J.P., Fouquet, Y., Jean-Baptiste, P., Holm, N., 2002. Geochemistry of high H2 and CH4 vent fluids issuing from ultramafic rocks at the Rainbow hydrothermal field (36 Deg14'N, MAR). Chemical Geology 191(4), 345-359.

Des Marais, D.J., Donchin, J.H., Nehring, N.L., Truesdell, A.H., 1981. Molecular carbon isotopic evidence for the origin of geothermal hydrocarbons. 292(5826), 826-828.

Fiebig, J., Woodland, A.B., Spangenberg, J., Oschmann, W., 2007. Natural evidence for rapid abiogenic hydrothermal generation of CH_4. Geochimica et Cosmochimica Acta 71(12), 3028-3039.

Foustoukos, D.I., Seyfried, W.E., Jr., 2004. Hydrocarbons in hydrothermal vent fluids: The role of chromium-bearing catalysts. Science (Washington, DC, United States) 304(5673), 1002-1005.

Fritz, P., Clark, I.D., Fontes, J.-C., Whiticar, M.J., Faber, E., 1992. Deuterium and 13C evidence for low temperature production of hydrogen and methane in a highly alkaline groundwater environment in Oman. In: Y.K. Kharaka, A.S. Maest (Eds.), *Proceedings of the 7th international symposium on Water-Rock Interaction; Volume 1, Low Temperature Environments*, pp. 793-796. Balkema, Rotterdam.

Giggenbach, W.F., 1997. Relative importance of thermodynamic and kinetic processes in governing the chemical and isotopic composition of carbon gases in high-heatflow sedimentary systmes. Geochimica et Cosmochemica Acta 61, 3763-3785.

Hinrichs, K.-U., Hayes, J.M., Bach, W., Spivack, A.J., Hmelo, L.R., Holm, N.G., Johnson, C.G., Sylva, S.P., 2006. Biological formation of ethane and propane in

the deep marine subsurface. Proceedings of the National Academy of Sciences of the United States of America 103(40), 14684-9.
Hinrichs, K.-U., Hayes, J.M., Sylva, S.P., Brewer, P.G., DeLong, E.F., 1999. Methane-consuming archaebacteria in marine sediments. Nature 398, 802-805.
Holm, N.G., Charlou, J.L., 2001. Initial indications of abiotic formation of hydrocarbons in the Rainbow ultramafic hydrothermal system, Mid-Atlantic Ridge. Earth and Planetary Science Letters 191, 1-8.
Horibe, Y., Craig, H., 1995. D/H fractionation in the system methane-hydrogen-water. Geochimica et Cosmochimica Acta 59(24), 5209-17.
Horita, J., Berndt, M.E., 1999. Abiogenic Methane Formation and Isotopic Fractionation Under Hydrothermal Conditions. Science 285, 1055-1057.
Kelley, D.S., Karson, J.A., Blackman, D.K., Fruh-Green, G.L., Butterfield, D.A., Lilley, M.D., Olson, E.J., Schrenk, M.O., Roe, K.K., Lebon, G.T., Rivizzigno, P., 2001. An off-axis hydrothermal vent field near the Mid-Atlantic Ridge at 30 degrees N. Nature 412(6843), 145-149.
Kelley, D.S., Karson, J.A., Fruh-Green, G.L., Yoerger, D.R., Shank, T.M., Butterfield, D.A., Hayes, J.M., Schrenk, M.O., Olson, E.J., Proskurowski, G., Jakuba, M., Bradley, A., Larson, B., Ludwig, K., Glickson, D., Buckman, K., Bradley, A.S., Brazelton, W.J., Roe, K., Elend, M.J., Delacour, A., Bernasconi, S.M., Lilley, M.D., Baross, J.A., Summons, R.E., Sylva, S.P., 2005. A Serpentinite-Hosted Ecosystem: The Lost City Hydrothermal Field. Science 307(5714), 1428-1434.
Knittel, K., Losekann, T., Boetius, A., Kort, R., Amann, R., 2005. Diversity and distribution of methanotrophic archaea at cold seeps. Applied and Environmental Microbiology 71(1), 467-79.
Kurr, M., Huber, R., Koenig, H., Jannasch, H.W., Fricke, H., Trincone, A., Krisjansson, J.K., Stetter, K.O., 1991. Methanopyrus kandleri, gen. and sp. nov. represents a novel group of hyperthermophilic methanogens, growing at 110 DegC. Archives of Microbiology 156(4), 239-47.
Losekann, T., Knittel, K., Nadalig, T., Fuchs, B., Niemann, H., Boetius, A., Amann, R., 2007. Diversity and abundance of aerobic and anaerobic methane oxidizers at the Haakon Mosby Mud Volcano, Barents Sea. Applied and Environmental Microbiology 73(10), 3348-3362.
McCollom, T.M., 1999. Methanogenesis as a potential source of chemical energy for primary biomass production by autotrophic organisms in hydrothermal systems on Europa. Journal of Geophysical Research 104(E12), 30729-30742.
McCollom, T.M., Seewald, J.S., 2001. A reassessment of the potential for reduction of dissolved CO2 to hydrocarbons during serpentinization of olivine. Geochimica et Cosmochimica Acta 65(21), 3769-3778.
McCollom, T.M., Seewald, J.S., 2006. Carbon isotope composition of organic compounds produced by abiotic synthesis under hydrothermal conditions. Earth and Planetary Science Letters 243(1-2), 74-84.
McCollom, T.M., Seewald, J.S., 2007. Abiotic Synthesis of Organic Compounds in Deep-Sea Hydrothermal Environments. Chemical Reviews (Washington, DC, United States) 107(2), 382-401.
Moser, D., P., Gihring, T., M., Brockman, F., J., Fredrickson, J., K., Balkwill, D., L.,

Dollhopf, M., E., Lollar Barbara, S., Pratt Lisa, M., Boice, E., Southam, G., Wanger, G., Baker, B., J., Pfiffner, S., M., Lin, L.-H., Onstott, T.C., 2005. Desulfotomaculum and Methanobacterium spp. dominate a 4- to 5-kilometer-deep fault. Applied and Environmental Microbiology 71(12), 8773-83.

Nisbet, E.G., Fowler, C.M.R., 2004. The early history of life. In: W.H. Schlesinger (Ed.), *Biogeochemistry 8*, *Treatise on Geochemistry*, pp. 1-40. Elsevier, Oxford.

Proskurowski, G., Lilley, M., Olsen, E., Kelley, D., Frueh-Green, G., 2005. Low Molecular Weight Hydrocarbon Production at the Lost City Hydrothermal Field. Eos Trans. AGU 86(52), Fall Meet. Suppl.. Abstract V51B-1485.

Proskurowski, G., Lilley, M.D., Kelley, D.S., Olson, E.J., 2006. Low temperature volatile production at the Lost City Hydrothermal Field, evidence from a hydrogen stable isotope geothermometer. Chemical Geology 229(4), 331-343.

Schoell, M., 1988. Multiple origins of methane in the Earth. Chemical Geology 71(1-3), 1-10.

Schrenk, M., O., Kelley Deborah, S., Bolton Sheryl, A., Baross John, A., 2004. Low archaeal diversity linked to subseafloor geochemical processes at the Lost City Hydrothermal Field, Mid-Atlantic Ridge. Environmental Microbiology 6(10), 1086-95.

Seewald, J.S., Zolotov, M.Y., McCollom, T., 2006. Experimental investigation of single carbon compounds under hydrothermal conditions. Geochimica et Cosmochimica Acta 70(2), 446-460.

Sherwood Lollar, B., Lacrampe-Couloume, G., Slater, G.F., Ward, J., Moser, D.P., Gihring, T.M., Lin, L.H., Onstott, T.C., 2006. Unravelling abiogenic and biogenic sources of methane in the Earth's deep subsurface. Chemical Geology 226(3-4), 328-339.

Sherwood Lollar, B., McCollom, T.M., 2006. Biosignatures and abiotic constraints on early life. Nature (London, United Kingdom) 444(7121), E18.

Sherwood Lollar, B., Westgate, T.D., Ward, J.A., Slater, G.F., Lacrampe-Couloume, G., 2002. Abiogenic formation of alkanes in the Earth's crust as a minor source for global hydrocarbon reservoirs. Nature (London, United Kingdom) 416(6880), 522-524.

Shock, E.L., Schulte, M.D., 1998. Organic synthesis during fluid mixing in hydrothermal systems. Journal of Geophysical Research, [Planets] 103(E12), 28513-28527.

Simoneit, B.R.T., Lein, A.Y., Peresypkin, V.I., Osipov, G.A., 2004. Composition and origin of hydrothermal petroleum and associated lipids in the sulfide deposits of the Rainbow field (Mid-Atlantic Ridge at 36 DegN). Geochimica et Cosmochimica Acta 68(10), 2275-2294.

Thauer, R.K., 1998. Biochemistry of methanogenesis: a tribute to Marjory Stephenson. Microbiology 144, 2377-2406.

Valentine, D.L., Chidthaisong, A., Rice, A., Reeburgh, W.S., Tyler, S.C., 2004. Carbon and hydrogen isotope fractionation by moderately thermophilic methanogens. Geochimica et Cosmochimica Acta 68(7), 1571-1590.

Whiticar, M.J., 1999. Carbon and hydrogen isotope systematics of bacterial formation and oxidation of methane. Chemical Geology 161(1-3), 291-314.

Chapter 5

Structural diversity of diether lipids in carbonate chimneys at the Lost City Hydrothermal Field

Abstract

Nonisoprenoidal diether lipids detected in carbonate chimneys at the Lost City hydrothermal field are glycolipids. Ether-linked glycolipids are common in archaea, but have no known bacterial source. Production of glycosyl headgroups might be an effective evolutionary strategy for conservation of phosphate in fluids that are likely to be phosphate-poor. The structural diversity of the diether core lipids is similar to inferred bacterial ether lipids detected in carbonate crusts at cold seeps where anaerobic oxidation of methane (AOM) is the dominant biogeochemical process. At Lost City, methane cycling is dominated by a single archaeal strain of Methanosarcinales that produces methane and several isoprenoidal diethers. The isoprenoidal diethers, derived from archaea, are bare lipids, having a hydroxyl in place of a large polar headgroup. The non-isoprenoidal glycolipid diethers are, by inference, bacterial in origin, and likely possess a *sn*-1,2-dialkylgylcerol stereochemistry.

5.1. Introduction

Differences in membrane lipids are a defining characteristic that separates the domains Archaea and Bacteria. Archaeal lipids are synthesized from a backbone of *sn*-glycerol-1-phosphate (G-1-P), while bacterial lipids are synthesized from *sn*-glycerol-3-phosphate (G-3-P), and some authors have suggested that this stereochemical difference led to the evolutionary divergence of bacteria and archaea (Koga et al., 1998; Pereto et al., 2004; Wachtershauser, 2003). If that is true, lipids may be a key to understanding early evolution. For example, one study has suggested that the root of the tree of life does not lie between the bacteria and archaea, that the earliest branching may group archaea with

Firmicutes, and predicts that Firmicutes should have lipids with archaeal traits (Skophammer et al., 2007). Indeed global phylogenies of fully sequenced organisms place thermophilic Firmicutes as the deepest branching bacteria (Ciccarelli et al., 2006).

Archaea typically have core lipids consisting of isoprenoidal side-chains linked to glycerol while bacterial core lipids are *n*-alkyl or modified *n*-alkyl side chains linked to glycerol. Archaeal core lipids contain ether linkages between glycerol and side-chains whereas bacteria, with few exceptions, have ester linkages. Archaea often synthesize membrane-spanning tetraethers, while bacterial membranes are nearly always composed of lipid bilayers.

Glycerol ether lipids have also been detected in a variety of thermophilic bacteria, such as *Thermodesulfobacterium* (Langworthy et al., 1983), *Thermotoga* (Sinninghe Damste et al., 2007) *Aquifex* (Huber et al., 1992), and *Ammonifex* (Huber et al., 1996). They are also inferred to be present in the membranes of sulfate-reducing Desulfosarcinales in consortia with methanotrophic archaea (Orphan et al., 2001). Tetraethers with non-isoprenoidal alkyl moieties have been reported in diverse marine and terrestrial environments (Schouten et al., 2000), and are likely bacterial in origin. Membrane-spanning lipids have been detected ether-linked to a single glycerol in *Thermotoga* (De Rosa et al., 1988). Some of these characteristics are well-conserved. There are no reported exceptions to the sterochemical distinction between bacterial and archaeal lipids. No bacteria have been reported to have glycerol-linked isoprenoids as core lipids, and only one archaeon, *Pyrococcus,* is known to synthesize straight-chain alcohols in its core lipid (Nishihara et al., 2000).

In this study we report the structures of a wide diversity of diether lipids in the carbonates of the Lost City hydrothermal field. The isoprenoidal diethers in these carbonates are predominantly derived from the single strain of Methanosarcinales that inhabits the carbonates (Chapter 3). The precise source of the non-isoprenoidal diethers is unknown, but they are presumed to be derived from bacteria. The non-isoprenoidal diethers are diverse, and include each of the three series reported to exist in cold-seep carbonate crusts

(Pancost et al., 2001), as well as structures that are similar but do not fall into these three categories. Our results suggest that bacterial diether lipids have a wider range of structural diversity than previously reported and that, at least at Lost City, they are glycolipids. Ether glycolpids are common in archaea, and so their presence in bacteria further blurs the distinction between the characteristics of bacterial and archaeal lipids.

5.2. Methods

Carbonate samples were collected from the Lost City Hydrothermal Field during Atlantis cruise AT-7-41 using the submersible *Alvin* and stored in Teflon containers at -20°C until processing. Subsamples were freeze-dried and crushed to a fine powder, then ultrasonically extracted three times (ca. 30 min) in a mixture of dichloromethane (DCM):methanol (3:1, v/v) and all three extracts were combined. Extracts were centrifuged at 2000 rpm for 15 minutes to remove residual carbonate particles and then the bulk of solvent was evaporated at 35°C under a stream of dry nitrogen. Elemental sulfur was removed from the extracts by passing over a column of activated copper, followed by filtration of the extract through a 40 μm combusted glass Buchner funnel.

To analyze total lipid extracts we performed analytical high-performance liquid chromatography following methods previously established (Sturt et al., 2004). Briefly, lipids were separated on a LiChrospher® Diol column (125 mm x 2mm, 5μm) with a linear solvent gradient and the HPLC was coupled to a ThermoFinnigan LCQ Deca XP ion-trap mass spectrometer. Solvents contained ammonia and formic acid to act as adducts that help ionization of polar lipids. The mass spectrometer scanned *m/z* 500 – 2000 and performed MS^n experiments in a data dependent acquisition mode where the base peak was fragmented up to MS^3 in both positive and negative ion modes. The MS^n data allowed us to gather information about the masses of the headgroup and core lipid by reference to standards previously published (Sturt et al., 2004).

For GC-MS analysis the total lipid extract was separated over silica gel into five

fractions using an elution scheme of solvents of increasing polarity. Most diethers eluted in the alcohol fraction (F4) with a mixture of 4:1 DCM:ethyl acetate. Diether diols such as hydroxyarchaeol eluted in fraction F5 with ethyl acetate.

Diethers were derivatized to their trimethylsilyl ethers and esters by reacting with *N,O*-bis(trimethylsilyl)trifluoro-acetamide (BSTFA + 1% TMCS) in pyridine at 60°C for thirty minutes, and analyzed with a HP 6890 gas chromatograph fitted with a PTV injector operated in splitless mode and equipped with a Varian CP-Sil-5 (60-m length, 0.32 mm inner diameter, and 0.25-um film thickness) fused silica capillary column and coupled to an Agilent 5973 mass-selective detector.

Cleavage of ether side chains was achieved by reaction with 1.0 M boron tribromide (BBr_3, Aldrich) in dichloromethane (DCM). Approximately 200 µl BBr_3 was added to lipid extracts in dry vials under a stream of argon, after which vials were sealed and heated to 60 ºC for 2 hours. After the reaction was complete, the resulting bromides were reduced to hydrocarbons by adding the DCM solution containing bromides to approximately 1 ml of Super-Hydride solution (1.0 M lithium triethylborohydride in tetrahydrofuran, Aldrich) in dry vials under a stream of argon and reacting at 60 ºC for 2 hours. This procedure was done in parallel on an ether lipid standard to confirm quantitative cleavage of side chains to hydrocarbons.

5.3. Results and discussion

5.3.1 HPLC-ESI-MS^n analysis

Identification of polar lipids by HPLC-ESI-MS^n followed methods previously established (Sturt et al., 2004). Compounds are separated primarily on the basis of the polarity of the headgroup. By monitoring the MS-MS reactions in both positive and negative mode, we can in many cases discern information about the identity of the polar headgroup and the nature of the links between the glycerol backbone and the apolar sidechains (i.e. ether or ester links) (Sturt et al., 2004).

The molecular ion (very abundant in the MS^1 spectrum) is selected for refragmentation to a daughter spectrum (the MS^2 spectrum). The mass difference between the molecular ion in MS^1 and its products in MS^2 in positive-ionization mode is particularly useful for identifying the nature of the headgroup. In many phosophlipids the polar headgroup is lost during this fragmentation. The mass loss determined by the difference in *m/z* between the molecular ion and the most abundant ion in the MS^2 spectrum usually corresponds to the mass of the headgroup (in some cases including the mass of an adduct introduced with the HPLC mobile phase). The details of fragmentation may differ between ether-linked and ester-linked lipids (Sturt et al., 2004). Glycolipids behave similarly, and show a pattern in the fragmentation of MS^1 to MS^2 that corresponds to loss of a C_6 sugar. (Sturt et al., 2004). There are variants on this rule based on the proton affinity of each fragment (McLafferty and Turecek, 1993); in some phospholipids such as phosphatidylcholine the headgroup retains the charge and is detected in the MS^2 spectrum. In such cases the mass difference between ions in MS^1 and MS^2 reveals information about the size of the core lipid. In some cases the fragmentation of MS^1 to MS^2 yields no mass difference that corresponds to any known polar headgroups. This may be interpreted as the detection of lipids containing unknown polar headgroups, or other compounds.

Negative ionization is especially useful for deducing the nature of the links in the core lipid between the glycerol and side chains, and in some cases the sizes of the individual chains. In many phospholipids the MS^2 spectrum includes *m/z* that corresponds to a fragment lacking both the headgroup and the *sn*-2 chain. This facilitates the calculation of the masses of both the *sn*-1 and *sn*-2 side chains (in bacterial lipids) or *sn*-2 and *sn*-3 in archaeal lipids. Glycolipids exhibit different behavior under negative ionization. Typically, negative-ion mass differences within the MS^1, MS^2 and MS^3 spectra of glycolipids reveal only fragmentation of the glycosyl headgroup (Sturt et al., 2004).

Figure 5-1 shows the positive-ionization-mode chromatogram of polar lipids from sample 3862-1219. The distribution of polar lipids is relatively simple, with four main

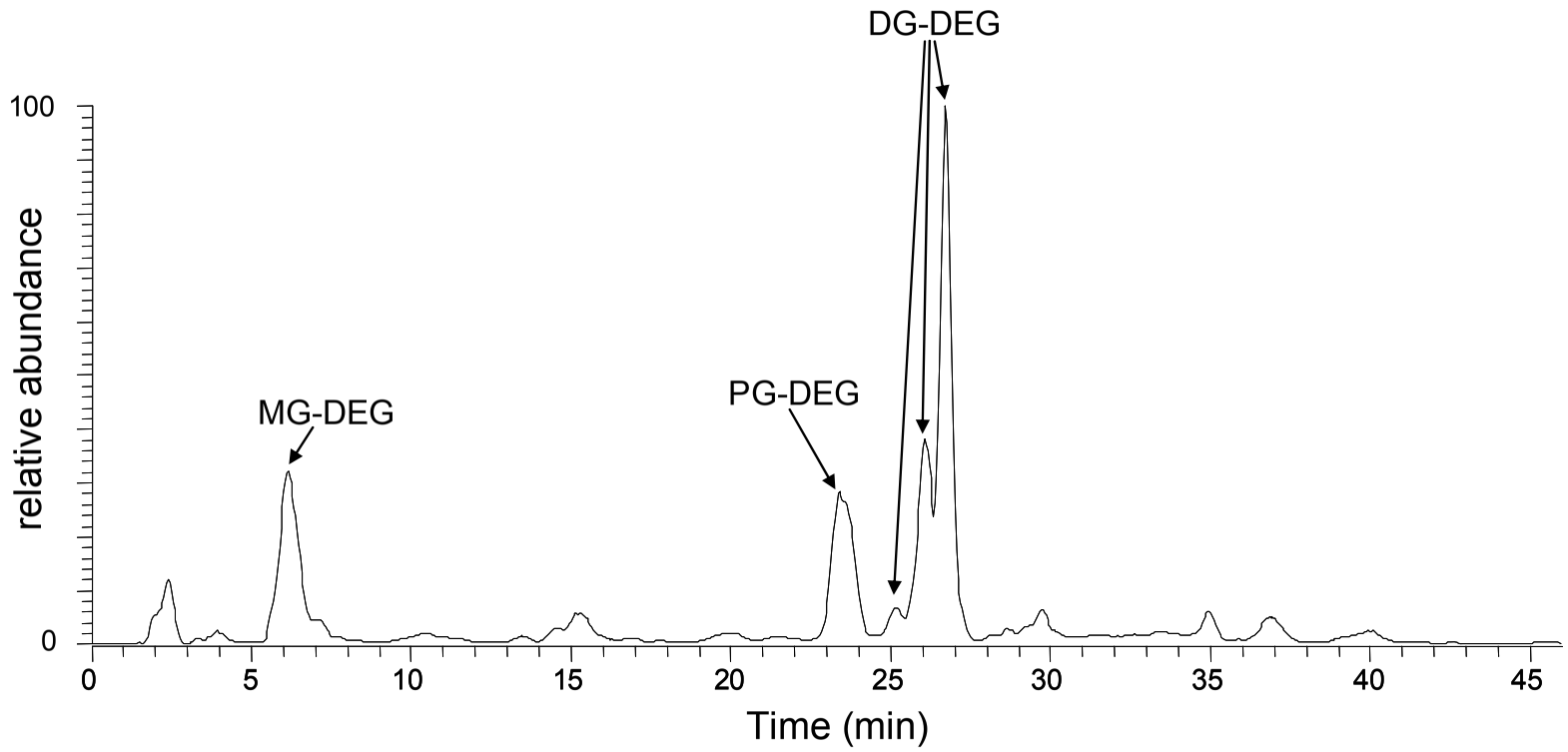

Figure 5-1: Positive ion chromatogram from sample 3862-1219. Main peaks are monoglycosyl diethers (MG-DEG), phosphatidylgylcerol diethers (PG-DEG), and digylocsyl diethers (DG-DEG).

Table 5-1: HPLC-ESI-MS^n mass retention time and mass transition data for samples analyzed in this study.

Time	+ MS^1	+ MS^2	MS^1 --> MS^2	Interpretation
3862-1219				
2.41	541	316	225	unknown 4
6.16	720	541	179	monoglycosyl + NH4
23.40	766	577	189	DAG PG
26.07	1116	400	716	unknown 2b
26.73	882	541	341	diglycosyl + NH4
25.16	868	527	341	diglycosyl + NH4
3867-1225				
2.75	686	557	129	hydroxyarchaeol
4.18	753	377	376	unknown
4.99	713	549	164	unknown
6.57	720	541	179	monoglycosyl + NH4
7.46	706	527	179	monoglycosyl + NH4
20.23	1004	412	592	unknown 2a
25.22	868	527	341	diglycosyl + NH4
26.84	894	553	341	diglycosyl + NH4
29.59	1129	nd		unknown
24.10	738	549	189	PG
23.55	764	575	189	PG
3867-1228				
2.58	670	373	297	archaeol
2.68	686	557	129	hydroxyarchaeol
5.56	832	653	179	monoglycosyl + NH4: monogylcosyl archaeol
11.24	718	511	207	unknown 1
18.23	686	557	129	hydroxyarchaeol
20.45	1004	412	592	unknown 2a
23.55	764	500	264	unknown 3
24.01	738	549	189	DAG PG
25.42	852	511	341	diglycosyl + NH4
27.08	878	537	341	diglycosyl + NH4
28.25	834	538	296	unknown
31.00	938	836	102	unknown
33.40	866	686	180	unknown

Time	+ MS^1	+ MS^2	MS^1 --> MS^2	Interpretation
3869-1404				
2.48	686	557		hydroxyarchaeol
4.48	713	658	55	unknown
6.55	732	553	179	monoglycosyl + NH4
6.95	690	511	179	monoglycosyl + NH4
7.77	690	511	179	monoglycosyl + NH4
9.04	730	551	179	monoglycosyl + NH4
14.61	550	450	100	unknown
17.16	623	508	115	unknown
19.90	1004	412		unknown 2a
23.19	792	603	189	DAG PG
25.32	894	553	341	diglycosyl + NH4
27.37	880	839	41	unknown
27.65	878	537	341	diglycosyl + NH4
28.16	834	538	296	unknown
28.17	834	538	296	unknown
29.87	1444	1241	203	unknown
30.16	850	554	296	unknown
34.12	866	669	197	unknown
34.12	866	nd		
3869-1446				
2.20	670	373		archaeol
2.48	686	557		hydroxyarchaeol
3.58	693	541	152	unknown
4.42	659	398	261	unknown
6.10	718	539	179	monoglycosyl + NH4
6.30	716	537	179	monoglycosyl + NH4
6.48	690	511	179	monoglycosyl + NH4
7.19	690	511	179	monoglycosyl + NH4
9.96	746	539	207	unknown
12.38	941	821	120	unknown
20.53	1004	412	592	unknown
23.52	792	603	189	DAG PG
24.76	894	553	341	diglycosyl + NH4
25.19	852	511	341	diglycosyl + NH4
25.90	1116	400	716	unknown
26.47	882	541	341	diglycosyl + NH4
26.94	878	537	341	diglycosyl + NH4
28.24	834	538	296	unknown
28.76	786	184	602	PC
30.22	850	554	296	unknown
32.79	894	697	197	unknown
33.31	866	669	197	unknown
3876-1133				
6.57	716	537	179	monoglycosyl + NH4
7.08	690	511	179	monoglycosyl + NH4
12.13	594	397	197	unknown
20.68	978	414	564	unknown
22.15	1010	444	566	unknown
23.59	764	500	264	unknown
24.24	736	547	189	DAG PG
25.12	1130	926	204	unknown
26.61	688	547	141	DAG PE
28.90	786	184	602	PC
30.56	1817	1299	518	unknown

components. The MS-MS spectra of the first (least polar) compound to elute does not correspond to a lipid polar headgroup that we could identify. The second compound (6.2 minutes) and the compound eluting at 26.7 minutes have MS-MS spectra that identify them as monoglycosyl and digylcosyl lipids, respectively, while the peak a 23.4 minutes is a polar lipid with a phosphatidylglycerol (PG) headgroup. The small peaks eluting just before 26.7 minutes are another digylcosyl headgroup, and an unidentified lipid (Table 5-1).

Both the monoglycosyl and diglycosyl headgroups are apparently associated with diether lipids. Figure 5-2 shows the positive- and negative-ion multidimensional mass spectra of the largest peak in the chromatogram (RT = 26.7 min). In positive ion mode the initial mass loss is 341 Da. This is consistent with the loss of a digylcosyl headgroup plus a NH_4^+ adduct as shown in Figure 5-2, and is similar to the loss of headgroup from archaeal ether lipids such as tetraethers (Sturt et al., 2004). We note that there is a 1 Da difference in the mass loss between the glycolipid tetraethers (Sturt et al., 2004) which show a loss of 342, and this sample. We interpret this as a rearrangement that transferrs a hydrogen atom between the headgroup and core lipid (Figure 5-2). The mass of the core lipid, 541 Da, is consistent with such a rearrangement operating on a diether lipid core that has saturated alkyl chains with a total of 32 carbon atoms. The data in negative ion mode are consistent with this interpretation. The initial mass loss in negative ion mode is consistent with a loss of the formate adduct. The mass of the MS^2 negative ion is 863.4 Da which is consistent with a digylcosyl glycerol diether lipid with 32 saturated carbon atoms in the side chains, having lost a single hydrogen. The MS^3 spectrum is consistent with a further fragmentation of the molecule within the glycolipid headgroup, with a bond breaking between the two sugar moieties.

The detailed multidimensional spectrum shows a number of glycolipid diethers of different molecular masses. These are detailed in Table 5-1. Similar analyses were repeated for the lipid extracts of a number of samples from Lost City. Chromatograms in Figure

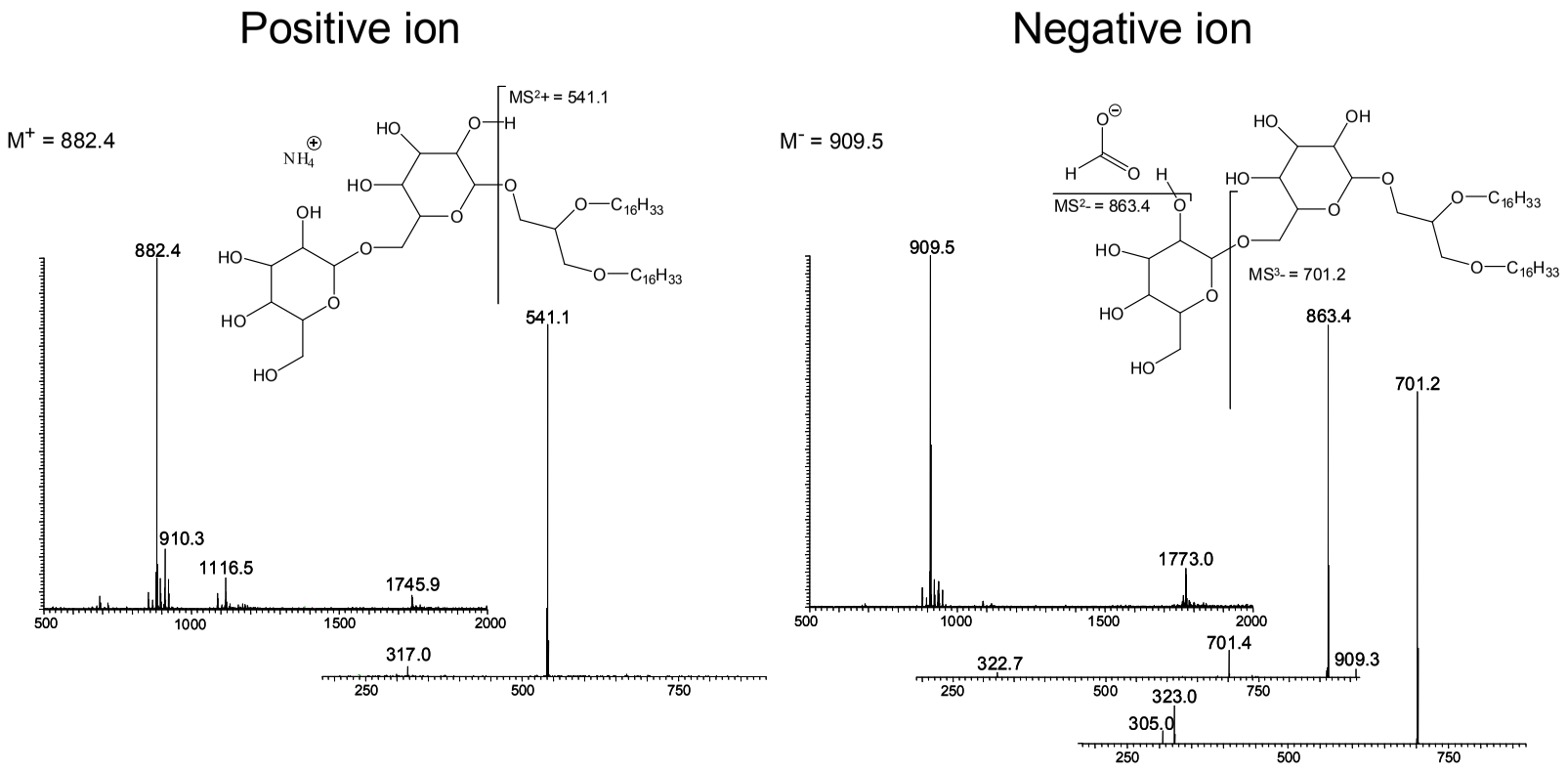

Figure 5-2: Positive ion and negative ion MS^1, MS^2, and MS^3 spectra for the largest peak in Figure 5-1, DG-DEG eluting at 26.7 minutes. The spectra are consistent with a digylcosyl diether structure.

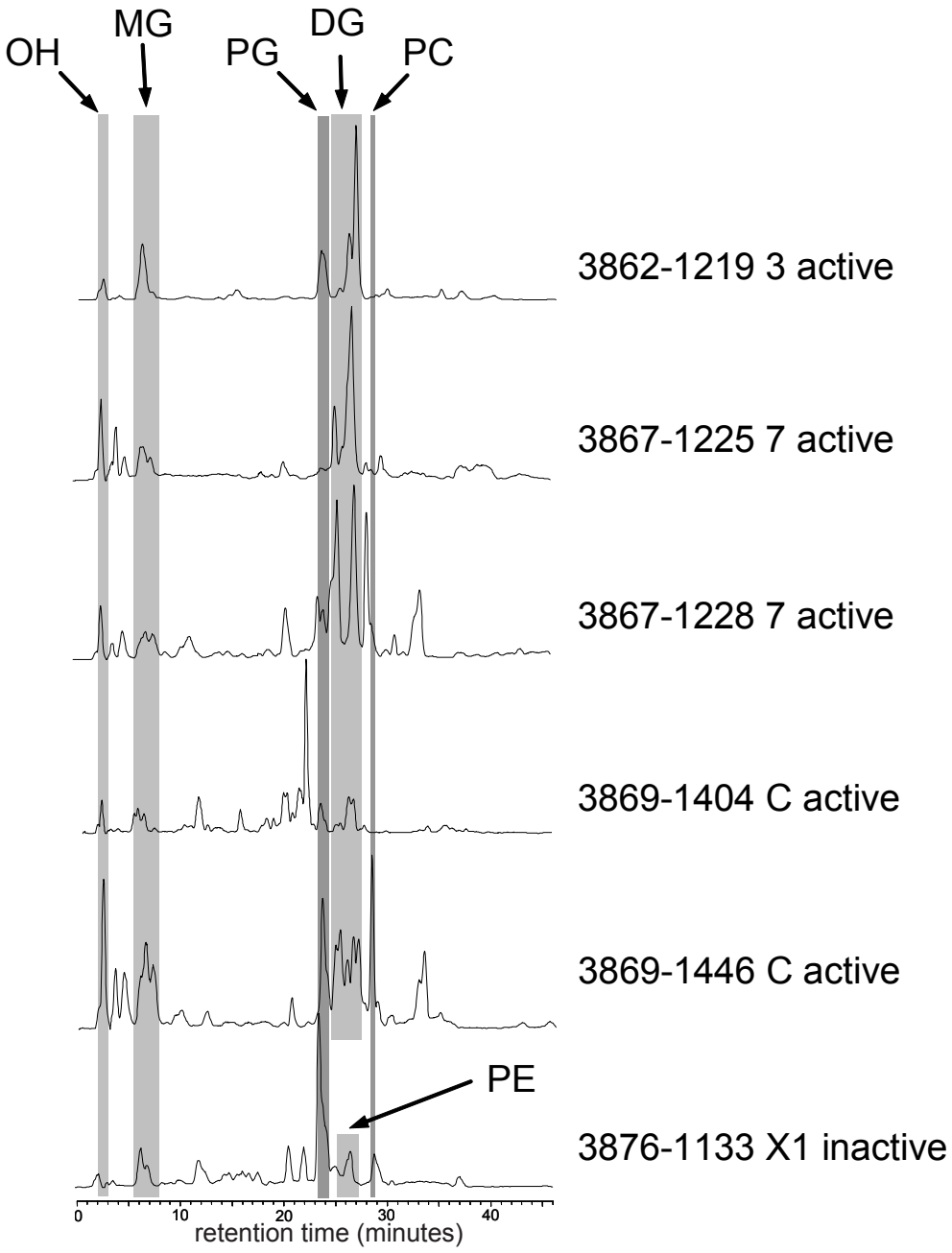

Figure 5-3: Positive ion chromatograms of lipid extracts from several active samples at Lost City, showing abundant glycolipids in all. Abbreviations: OH: hydroxyl (no polar headgroup); MG: monogylcosyl; PG: phosphatidylglycerol; DG: digylcosyl; PC: phosphatidylcholine; PE: phosphatidylethanolamine.

5-3 reveal that the dominant types of polar lipids are similar in all the active samples, which include abundant monogylcosyl and digylcosyl diethers, along with less abundant diacyl phosophatidyl glyceols and bare hydroxyarchaeol (containing only a hydroxyl instead of a polar headgroup on *sn*-1). The inactive sample (3876-1133) shows reduced amounts of monogylcosyl diethers and lacks digylcosyl diethers, but contains both diacyl phosphatidylgylcerol, diacyl phosphatidylethanolamine, and phosphatidylcholine lipids. It is the only sample to contain each of these three headgroup types.

All the inferred ether lipids detected in HPLC-ESI-MS^n data at Lost City have monoglyco- or digylco- headgroups, with the exception of the archaeol lipids archaeol and hydroxyarchaeol, which have hydroxyl headgroups. The core lipid masses associated with the gylcolipids are inconsistent with the side chains being C_{20} phytanyl groups, as are common in archaea. We propose, therefore, that these lipids are bacterial, an inference supported by GC-MS data. The significance of the lack of a polar headgroup is not known. While this could indicate that the lipids do not derive from living cells, that interpretation would be inconsistent with the results of 16S rDNA surveys (Brazelton et al., 2006; Schrenk et al., 2004). Bare lipids (lacking polar headgroups) are known to occur in living methanogens (Koga et al., 1993; Nishihara et al., 1989; Poulter et al., 1988) and the bare lipids detected at Lost City may well derive from living cells.

5.3.2 GC-MS analysis

GC-MS analyses of lipid extracts from Lost City reveal information complementary to that determined by analyses of polar lipids. Diether lipids are abundant in GC-MS traces, as would be expected given the abundance of diether glycolpids. Monoethers are detected in much lower abundances and are discussed in Chapter 3. Our analysis of alcohol fraction of total lipid extracts is complementary to the HPLC-ESI-MS^n data, and does not directly analyze glycolipid. However, since polar headgroups are easily lost after cell death (Sturt et al., 2004), we infer that these neutral lipids are closely related to the glycolipids.

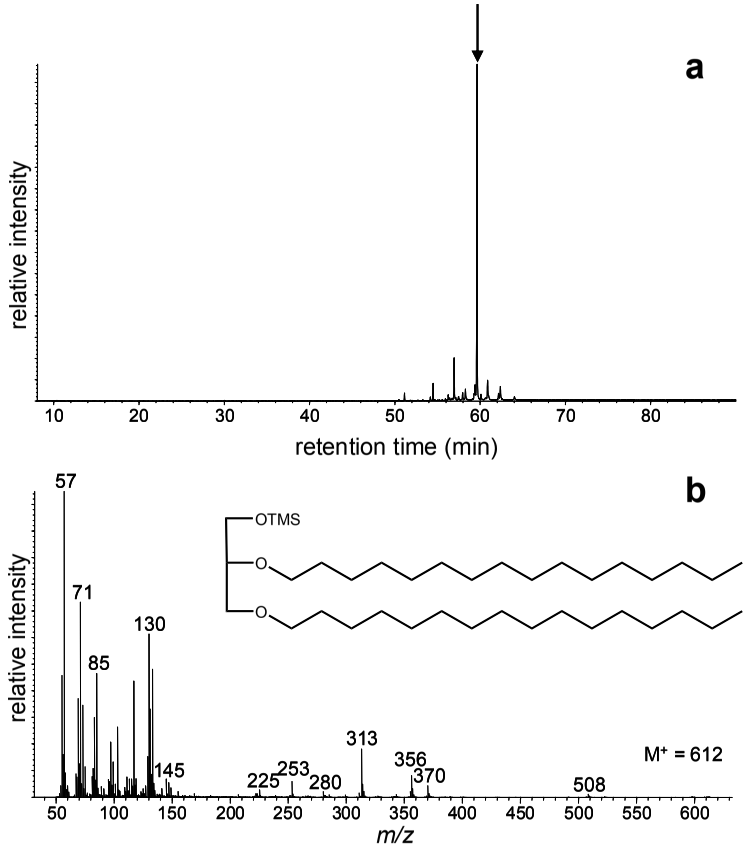

Figure 5-4: a) Chromatogram of *m/z* 133 (diethers) from the alcohol fraction of sample 3862-1219. b) Spectrum of the largest peak in (a) eluting at 59.7 minutes. Mass spectrum and RI are consistent with C_{35} diether with two nC_{16} alkyl groups (structure shown as tms derivative).

Figure 5-4 shows the *m/z* 133 chromatogram of tms-derivatives of the alcohol (F4) fraction of sample 3862-1219. The largest peak, at 59.7 minutes has the spectrum shown in Figure 5-4b. The spectrum and Kovats retention index of this peak (RI = 3722) are consistent with the identity of this peak being a C_{35} diether that is substituted with two *n*-C_{16} alkyl groups, presumably on the *sn*-1 and *sn*-2 positions (Figure 5-4b). This interpretation was confirmed by analysis of an authentic (racemic) C_{35} gylcerol diether standard, which had an identical retention index and spectrum.

From this information, we infer that the most abundant peaks in the GC-MS chromatogram and in the peak in the HPLC-ESI-MS^n chromatogram correspond to the same compound. The spectra in each case are consistent with a this compound being a diether lipid with a C_{35} core. The GC-MS data gives relevant information concerning the structure of the side chains inferred to be at *sn*-1 and *sn*-2, while the HPLC-ESI-MS^n data suggests that this same compound has a diglyco- headgroup.

A study by Pancost et al. (2001) provides the basis for interpretation of the structures of these diethers. That study defined diethers in three series: Series I contains an *iso*- or *anteiso*- branched C_{15} alkyl moiety at the *sn*-2 position, Series II contains a cyclopropyl C_{17} alkyl moiety at the *sn*-2 position, and Series III contain a C_{15} straight-chain alkyl moiety at the *sn*-2 position and another straight-chain alkyl moiety at the *sn*-1 position.

All three of these series are detected in Lost City carbonates (Table 5-2). Identification of these series is by analysis of the mass spectrum and Kovats retention index (Kissin et al., 1986) of the intact diethers. The diether mass spectrum contains the information necessary to discern the size of the side chains at the *sn*-1 and *sn*-2 positions, while the Kovats retention index can be used to infer the presence and type of methylation in one or both of the side chains. In some cases the retention index may indicate that the methylation pattern differs between the two alkyl substituents. In those cases the retention index alone can not determine which chain has which pattern. This information may be inferred in cases where ether cleavage experiments exclude the presence of certain alkyl chains. This is not always

Table 5-2: Kovats Retention index, molecular ion (as tms derivative), isotopic, and putative structural information for the diether core lipids analyzed in this study. Mass spectra for these compounds can be found in Appendix 3.

				carbon number				branching		
	RI	**M^+**	**C#**	***sn*-1**	***sn*-2**	**Group**	**$\delta^{13}C$**	***sn*-1**	***sn*-2**	**ID #**
3862-1219	3428	570	C_{32}	15	14	III		n	n	6
	3454	584	C_{33}	15	15	Id		i	i	7
	3477	584	C_{33}	15	15	If		ai	ai	9
	3489	584	C_{33}	16	14			i	n	11
	3525	584	C_{33}	14	16		-4.9	n	n	14
	3563	598	C_{34}	16	15	I		ai	ai	16
	3597	598	C_{34}	16	15	I	-8.9	n	i	20
	3621	598	C_{34}	16	15	III	-2.5	n	n	22
	3696	610	$C_{35:1}$	16:1	16			cp	ai	25
	3703	610	$C_{35:1}$	16	16:1			n	cp	27
	3722	612	C_{35}	16	16	III	-4.7	n	n	29
	3756	626	C_{36}	17	16		-8.5	i	ai	31
	3795	640	C_{37}	17	17	IV		ω7-Me	ω7-Me	34
	3813	624	C_{36}	17	16		-4.2	n	n	36
	3822	624	$C_{36:1}$	16	17:1	IIc		n	cp	38
	3899	638	$C_{37:1}$	18:1	16		-7.4	cp	ai	40
	3911	640	C_{37}	18	16	III	-5.4	n	n	41
	4020	652	$C_{38:1}$	19:1?	16?			cp	n	43
3867-1225	3460	584	C_{33}	15	15	Id	-6.4	i	i	7
	3483	584	C_{33}	15	15	If	-7.9	ai	ai	9
	3515	582	$C_{33:1}$	16:1	14			cp	ai	12
	3526	582	$C_{33:1}$	16:1	14		-5.0	n	cp	13
	3530	584	C_{33}	14	16			n	n	14
	3567	598	C_{34}	16	15	I	-4.9	ai	ai	16
	3587	596	$C_{34:1}$	16:1	15	I		cp	i	18
	3603	598	C_{34}	16	15	I	-5.4	n	i	20
	3629	612	C_{35}	17	15	IV	-3.4	ω7-Me	i	23
	3692	608	$C_{35:2}$	16:1	16:1			?	?	24
	3711	610	$C_{35:1}$	16	16:1			n	cp	27
	3717	608	$C_{35:2}$	16:1	16:1		-6.0	cp	cp	28
	3724	612	C_{35}	16	16	III		n	n	29
	3760	626	C_{36}	17	16		-10.1	i	ai	31
	3815	624	C_{36}	17	16		-7.6	n	n	36
	3824	624	$C_{36:1}$	16	17:1	IIc		n	cp	38
	3885	636	$C_{37:2}$	18:1	16:1			?	?	39
	3899	638	$C_{37:1}$	18:1	16		-9.0	cp	ai	40
	4006	652	$C_{38:1}$	19:1?	16?			cp	n	43

				carbon number				branching		
	RI	**M^+**	**C#**	***sn*-1**	***sn*-2**	**Group**	**$\delta^{13}C$**	***sn*-1**	***sn*-2**	**ID #**
3867-1228	3285	556	C_{31}	15	13		-6.8	ai	ai	1
	3297	556	C_{31}	14	14			n	i	2
	3333	556	C_{31}	14	14	III	-2.3	n	n	3
	3370	570	C_{32}	15	14	Ia	-5.6	ai	i	4
	3405	570	C_{32}	14	15	Ic	-5.5	n	ai	5
	3431	570	C_{32}	15	14	III	-7.5	n	n	6
	3455	584	C_{33}	15	15	Id	-3.9	i	i	7
	3466	584	C_{33}	15	15	Ie		i	ai	8
	3479	584	C_{33}	15	15	If	-6	ai	ai	9
	3486	582	$C_{33:1}$	16:1	14		-1.8	cp	i	10
	3512	582	$C_{33:1}$	16:1	14			cp	ai	12
	3527	582	$C_{33:1}$	16:1	14		-2.0	cp	n	15
	3565	598	C_{34}	16	15	I		ai	ai	16
	3572	596	$C_{34:1}$	16:1	15	I		?	?	17
	3584	596	$C_{34:1}$	16:1	15	I	-6.2	cp	i	18
	3594	596	$C_{34:1}$	16:1	15	Ig	-8.8	cp	ai	19
	3618	596	$C_{34:1}$	16:1	15	I	-3.7	cp	n	21
	3628	612	C_{35}	17	15	IV	-1.3	ω7-Me	i	23
	3691	608	$C_{35:2}$	16:1	16:1			?	?	24
	3717	608	$C_{35:2}$	16:1	16:1		-3.5	cp	cp	28
	3753	624	$C_{36:1}$	17	16:1		-1.9	ω7-Me	?	30
	3765	624	$C_{36:1}$	17	16:1			?	?	32
	3778	624	$C_{36:1}$	?	?			?	?	33
	3796	640	C_{37}	17	17	IV		ω7-Me	ω7-Me	34
	3803	622	$C_{36:2}$	18:1	16:1			?	?	35
	3820	622	$C_{36:2}$	16:1	17:1		-4.6	cp	cp	37
	3885	636	$C_{37:2}$	18:1	16:1		-7.7	?	?	39
	3896	636	$C_{37:1}$	18:1	16		-7.5	cp	ai	40
	3927	636	$C_{37:2}$	17:1	17:1	IId	-5	ch	cp	42
3869-1404	3479	584	C_{33}	15	15	If	0.8	ai	ai	9
	3511	582	$C_{33:1}$	16:1	14		-1.1	cp	ai	12
	3523	582	$C_{33:1}$	16:1	14		3.6	cp	n	13
	3565	598	C_{34}	16	15	I	3.6	ai	ai	16
	3573	596	$C_{34:1}$	16:1	15	I	-3.8	?	?	17
	3584	596	$C_{34:1}$	16:1	15	I	0	cp	i	18
	3595	596	$C_{34:1}$	16:1	15	Ig	-10.6	cp	ai	19
	3627	612	C_{35}	17	15	IV	2.2	ω7-Me	i	23
	3690	608	$C_{35:2}$	16:1	16:1		-5.3	?	?	24
	3702	608	$C_{35:2}$	16:1	16:1			?	?	26
	3707	610	$C_{35:1}$	16	16:1			n	cp	27
	3713	608	$C_{35:2}$	16:1	16:1		0.1	cp	cp	28
	3720	612	C_{35}	16	16	III		n	n	29
	3759	626	C_{36}	17	16		-1.2	i	ai	31
	3797	640	C_{37}	17	17	IV	1.4	ω7-Me	ω7-Me	34
	3813	626	C_{36}	17	16		0.3	n	n	36
	3886	636	$C_{37:2}$	18:1	16:1		-9.3	?	?	39
	3898	638	$C_{37:1}$	18:1	16		-11.2	cp	ai	40

				carbon number				branching		
	RI	**M^+**	**C#**	***sn*-1**	***sn*-2**	**Group**	**$\delta^{13}C$**	***sn*-1**	***sn*-2**	**ID #**
3869-1446	3454	584	C_{33}	15	15	Id	-2.2	i	i	7
	3477	584	C_{33}	15	15	If	-3.3	ai	ai	9
	3522	582	$C_{33:1}$	16:1	14		+2.6	cp	n	13
	3563	598	C_{34}	16	15	I		ai	ai	16
	3583	596	$C_{34:1}$	16:1	15	I		cp	i	18
	3595	596	$C_{34:1}$	16:1	15	Ig		cp	ai	19
	3598	598	C_{34}	16	15	I	-4.9	n	i	20
	3626	612	C_{35}	17	15	IV		ω7-Me	i	23
	3704	610	$C_{35:1}$	16	16:1			n	cp	27
	3712	608	$C_{35:2}$	16:1	16:1		-1.4	cp	cp	28
	3718	612	C_{35}	16	16	III		n	n	29
	3754	626	C_{36}	17	16			i	ai	31
	3795	640	C_{37}	17	17	IV		ω7-Me	ω7-Me	34
	3812	624	C_{36}	17	16	??		n	n	36
	3821	624	$C_{36:1}$	16	17:1	IIc	-0.9	n	cp	38
	3884	636	$C_{37:2}$	18:1	16:1			?	?	39
	3897	638	$C_{37:1}$	18:1	16			cp	ai	40
	3911	640	C_{37}	18	16	III		n	n	41
	3927	636	$C_{37:2}$	17:1	17:1	IId		ch	cp	42
3876-1133	3702	608	$C_{35:2}$	16:1	16:1		-22.1	?	?	26
	3759	626	C_{36}	17	16		-17.3	i	ai	31
	3796	640	C_{37}	17	17	IV		ω7-Me	ω7-Me	34
authentic standard	3721	612	C_{35}	16	16			n	n	

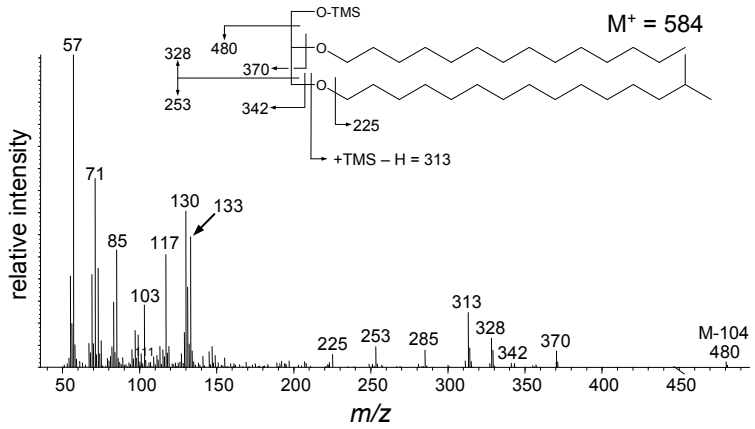

Figure 5-5: Mass spectrum and structure for a C_{33} diether in 3862-1219

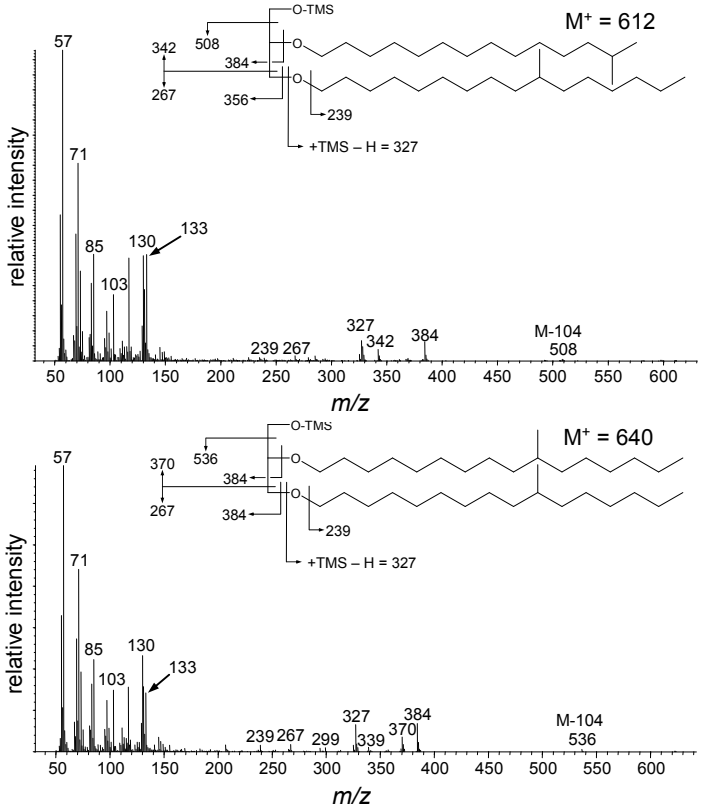

Figure 5-6: Spectra and putative structures of two nonisoprenoidal diethers with methyl groups at the ω7 position.

applicable however, and in some compounds the identification of *n*-alkyl, *iso*-, and *anteiso*-chains are interchangeable.

In addition to the three series of diethers described by Pancost et al. (2001), the Lost City carbonates contain diverse diethers that are structurally similar but do not readily conform with that classification scheme. At least forty-three distinct diether compounds can be detected in Lost City carbonates. Most are similar to the three series detected by Pancost et al. (2001) and contain *n*-alkyl, *iso*-, and *anteiso*- branched alkyl substituents, but with a wider variety of carbon numbers. For example in sample 3862-1219 we detect a C_{33} diether that contains a C_{16} alkyl moiety at the *sn*-1 position and a C_{14} alkyl moiety at the *sn*-2 position (Figure 5-5). Examination of the diether spectra from samples at Lost City revealed that they have alkyl substituents that range in size from C_{13} to C_{18}, with carbon numbers from 14 to 17 being most common. Some of these chains are unsaturated, although the presence of an unsaturation is limited to those side chains with carbon numbers of 16 and greater. The retention indices of unsaturated diethers are largely consistent with the presence of cyclopropyl and cyclohexyl groups, as described by Pancost et al. (2001).

GC-MS data regarding diether compounds are listed in Table 5-2. Small inconsistencies exist in retention indexes among our samples. In particular, compounds in sample 3867-1225 in many cases have a retention index that is 5-8 units higher than the same compound in other samples. We attribute this to slight variations in analytical conditions between samples, which were analyzed over the span of several months. Additionally we note that the retention index we report for many compounds is in many cases 5-8 units earlier than that reported by Pancost et al. (2001), including that we measure for the diether standard. This is also likely due to slight differences in analytical conditions.

While most of the diethers we detected are generally similar to the three series reported by Pancost et al. (2001), differing only in the carbon numbers of their side chains, several of the new diethers had retention times that suggested that their structures might be distinct. Two compounds, one a C_{35} diether and the other a C_{37} diether, stood out by virtue

of RIs that were 100 and 125 units smaller, respectively, than would expected for Series III compounds of identical mass. These compounds have fully saturated side chains, and have been designated series IV. The retention times are consistent with C_{17} side chains that are methylated at the ω7 position. The C_{35} diether elutes with a RI of 3628, consistent with a C_{17} alkyl chain methylated at the ω7 position, and an *iso*-C_{15} alkane at the *sn*-2 position. The C_{37} diether has a RI of 3796, consistent with each of the side chains consisting of a C_{17}ω7 alkyl moiety. (Figure 5-6, Table 5-2). Cleavage of the ether-bonded side chains with boron tribromide, and reduction of the resulting bromides to hydrocarbons with lithium triethylborohydride yields 7-methyl hexadecane. This is consistent with the methylation of the side-chains at the ω7 position. Ether cleavage products include the other expected structures, including 5-methylhexadecane and 6-methylhexadecane, which result from the presumed 11,12-methylenehexadecyl moiety previously described (Pancost et al., 2001).

Both odd- and even-numbered carbon chains contain methylation at the *iso*- position, as reported at other sites (Pancost et al., 2001). Lost City samples also are methylated at *anteiso*- positions in both odd and even carbon numbers. Products with these methylation patterns are predicted by the RIs of the diethers, and their presence is confirmed by examination of ether-cleavage products. Methylated chains with even carbon numbers are probably unusual. In methylated fatty acids, the presence of even chain-length methylated moieties is unusual, as it requires a slightly different synthetic pathway. Even-chain methylated ethers are likely to be similar. In fatty acid synthesis, methylation is introduced by incorporation of methylmalonyl-CoA instead of malonyl-CoA during chain elongation (Kaneda, 1991; Michal, 1999). The 'extra' carbon thus incorporated forms the methyl group. The expectation is that mono-branched fatty acids (and by analogy, alcohols), which are usually elongated from acetyl-CoA as a starting molecule, will predominantly be of odd carbon number. To generate even carbon numbered methylated alkyl chains, propionyl-CoA must be substituted for acetyl-CoA as the primer (Michal, 1999). In culture studies, odd-carbon numbered monomethyl fatty acids are indeed observed to predominate, but the

presence of even-carbon number monomethyl fatty acids in some cultured sulfate reducers (Rutters et al., 2001) shows that this process is not unknown.

5.3.3 Nonisoprenoid ether-linked glycolipids

Together these data suggest that the abundant diethers in Lost City carbonates are glycolipids containing previously undetected alkyl moieties. Both of these results expand the diversity of lipids that are synthesized by bacteria.

The initial report of diether lipids in *Thermodesulfobacterium commune* (Langworthy et al., 1983) was suggestive of the presence of glycolipid diethers. The glycolipid fraction in that report likely contained diethers, but a detailed analysis confirming the presence of diethers was performed only on the phospholipid fraction. While glycolipids are common in many bacteria (Shaw, 1970), glycolipid diethers have been confirmed only in archaea.

The glycolipids detected at Lost City have masses that are inconsistent with the presence of phytanyl side chains. GC-MS analysis of the diether fractions reveals compounds that are identical to, or closely resemble compounds previously described as non-isoprenoidal diethers (Pancost et al., 2001). Ether cleavage of the diether side chains does not reveal the presence of isoprenoidal hydrocarbons other than phytane, which is derived from archaeol. Nonisoprenoidal diether lipids are also detected at Lost City sites where 16S rDNA surveys do not detect the Lost City *Methanosarcinales* phylotype (Brazelton et al., 2006). Lipid extracts at these sites lack archaeol, and ether cleavage of the diether fraction of these extracts lack phytane. All this evidence is consistent with these diether compounds having nonisoprenoidal side chains.

Archaeal diversity is very limited in Lost City carbonates, with one predominant phylotype related to Methanosarcinales (Brazelton et al., 2006; Kelley et al., 2005; Schrenk et al., 2004). In carbonates in which this archaeal strain is detected, we detect archaeol, along with *sn*-2 hydroxyarchaeol and dihydroxyarchaeol, and the relative proportions of these samples is nearly invariant between samples (Chapter 3). This is highly suggestive

that the Lost City Methanosarcinales produce these compounds. The nonisoprenoidal diethers are therefore likely to derive from bacteria. A specific bacterial source for these lipids is unknown, as none of the bacterial families detected at Lost City (Brazelton et al., 2006) are known to synthesize diether lipids.

Diether lipids are common in carbonate crusts at cold seeps where anaerobic oxidation of methane (AOM) occurs. Previous studies (Bouloubassi et al., 2006; Pancost et al., 2001) have demonstrated that at least three series of such diethers occur in these environments. In these environments, nonisoprenoidal diether lipids are likely to derive from bacteria in the *Desulfosarcina*/*Desulfococcus* group (Blumenberg et al., 2004). Nonisoprenoidal diethers are most closely associated with environments in which AOM is carried out by ANME-1 archaea. In environments dominated by ANME-2 archaea, the associated bacteria predominantly produce fatty acids with similar carbon skeletons to the diether skeletons (Blumenberg et al., 2004). For example, *Desulfosarcina*/*Desulfococcus* bacteria associated with ANME-2 archaea commonly produce an *ai*15:0 fatty acid (Blumenberg et al., 2005; Blumenberg et al., 2004) and in some cases produce a cy17:0w5,6 fatty acid (Nauhaus et al., 2007) similar to the 11,12-methylenehexadecyl moiety in diethers associated with ANME-1 archaea (Pancost et al., 2001).

The ω7 methylated C_{17} alkyl moieties detected in diether lipids at Lost City have carbon backbones that are structurally similar to 10-methylhexadecanoic acid, which is a common fatty acid substituent in sufate-reducing δ-proteobacteria bacteria such as *Desulfobacter*, *Desulfobacterium* (Dowling et al., 1986; Londry et al., 2004), *Geobacter* (Lovley et al., 1993) *Desulfosarcina* and *Desulforhabdus* (Rutters et al., 2001). We also detect other alkyl substituents, such as *ai*15:0 and 11,12-methylenehexadecyl, that have previously been described from ether lipids associated with sulfate-reducing proteobacteria (Bouloubassi et al., 2006; Pancost et al., 2001). These alkyl chains are also known as ester-linked fatty acids in δ –proteobacterial cultures (Dowling et al., 1986; Londry et al., 2004; Lovley et al., 1993; Rutters et al., 2001), and in environments where sulfate-reducing δ

–proteobacteria are presumed to play a key role (Blumenberg et al., 2004; Ringelberg et al., 1989). In most of these studies these alkyl chains are components of phospholipids. The diversity of glycolipids in sulfate-reducing δ –proteobacteria remains unclear due to the limited number of cultures studied to date.

In any case it is noteworthy that such unusual methylated and cyclized carbon moities are maintained across a wide range of environments, and even when other fundamental aspects of lipid synthesis (ether vs. ester bonds, phospholipids vs. glycolipid) are altered. The physiological function of these methylated and cyclized chains remains unknown. It has been hypothesized that the differences between these and straight-chain moieties may play a role in modulating the phase-transition temperature of lipid membranes (Kaneda, 1991). This remains untested. One intriguing possibility is that in anaerobic environments it may be physiologically less costly to modulate membrane fluidity by altering the methylation pattern of the membrane compared to introducing a double bond.

5.3.4 Origin of nonisoprenoidal diether lipids at Lost City

One of the more confounding aspects of the abundant nonisoprenoidal diether lipids at Lost City is the lack of an obvious source for them. While the lipid assemblage consisting of both isoprenoidal and nonisoprenoidal diethers invites comparison to that found at AOM sites (Blumenberg et al., 2004), the dominant archaea at Lost City are methanogens, not methanotrophs. Furthermore, methanotrophic communities typically have a δ–proteobacterial sulfate-reducing partner in the consortium, but none of the usual partners are detected at Lost City (Brazelton et al., 2006). In AOM environments these sulfate reducers are the presumed source of nonisoprenoidal diethers. Other potential sources for diether lipids include bacteria related to *Thermodesulfobacterium* (Langworthy et al., 1983) or *Aquifex* (Huber et al., 1992), but these organisms are also undetected in Lost City carbonates (Brazelton et al., 2006).

The most common sulfate-reducing bacterium detected in Lost City carbonates

is a Clostridium similar to *Desulfotomaculum*. Clostridia are not known to make diether lipids with the one known exception of *Ammonifex* (Huber et al., 1996). Many Clostridia do produce ether-ester plasmalogens in their lipid membrane (Goldfine, 1997), which could in principle be detected as glycerol monoethers. However, these are known only as phospholipids (Goldfine, 1997). *Desulfotomaculum* is not reported to make ether lipids (Londry et al., 2004; Pikuta et al., 2000), but the studies that have examined its lipid content specifically examined fatty acids. It is unclear whether ether lipids would have been detected had they been present. Most Clostridia also do not make methylated fatty acids, but there are a few exceptions (Kaneda, 1991). One study of the fatty acid methyl esters of *Desulfotomaculum acetoxidans* did not reveal the presence of any *iso*-, *anteiso*-, ω7-Me, or cyclopropyl moieties (Londry et al., 2004). However other investigations have dectected small amounts of *iso*-C_{15} moieties in *D. acetoxidans* (Dowling et al., 1986), and both *iso*-C_{17} and *anteiso*-C_{17} in *Desulfotomaculum alkaliphilum* (Pikuta et al., 2000), which is closely related to the Lost City phylotype . The presence of similar alkyl moieties in the fatty acid fraction is promising, but inconclusive.

The abundance of glycolipids compared to phospholipids at Lost City invites ecological and evolutionary speculation. In oligotrophic environments some bacteria have the capability to conserve phosophorus by utilizing alternate lipid polar headgroups (Van Mooy et al., 2006). The fluid chemistry at Lost City is both high in pH and precipitates brucite. Brucite quantitatively removes phosphorus from fluids at high pH. This reaction is so effective that it is a standard quantitative analytical protocol for removal and analysis of phosphorus concentrations in seawater (Karl and Tien, 1992). We therefore speculate that Lost City hydrothermal fluids are low in phosphate, and that the synthesis of glycolipids is a phosphorus-conservation strategy. If Lost City is indeed a good analogue for an environments in which early life may have flourished, we might further specultate that glycolipids were an evolutionary predecessor to phospholipids.

Whatever the source of the nonisoprenoidal ether lipids at Lost City, its lipid synthetic

pathway is interesting from the point of view of the evolutionary development of lipid synthesis. These nonisoprenoidal diethers have an unprecedented combination of bacterial (nonisoprenoidal chains) and archaeal (diether glycolipid) traits. It has been speculated that Lost City might be an attractive analogue for the environment in which life originated (Kelley et al., 2001; Kelley et al., 2005; Russell, 2003; Skophammer et al., 2007). The Lost City ecosystem is dominated by Firmicutes and archaea that may be related to organisms inhabiting the deepest branches of the tree of life (Ciccarelli et al., 2006; Skophammer et al., 2007). Identification of the source of nonisoprenoidal lipids at Lost City will advance our understanding of the evolutionary and ecological role of these organisms.

5.4 Conclusions

Abundant diether lipids at Lost City are derived from archaea, principally Methanosarcinales, and unidentified bacteria. Nonisoprenoidal diether core lipids are more structurally diverse at Lost City than in any previously desribed environment. Analysis of the intact polar lipids reveals that the nonisoprenoidal diethers have glycosyl headgroups, which is unprecedented in bacteria. Lost City vent fluids are likely to be phosphorus-poor, and synthesis of glycolipids instead of phospholipids may be a phosphorus conservation strategy.

5.5 References

Blumenberg, M., Seifert, R., Nauhaus, K., Pape, T., Michaelis, W., 2005. In vitro study of lipid biosynthesis in an anaerobically methane-oxidizing microbial mat. Applied and Environmental Microbiology 71(8), 4345-51.

Blumenberg, M., Seifert, R., Reitner, J., Pape, T., Michaelis, W., 2004. Membrane lipid patterns typify distinct anaerobic methanotrophic consortia. Proceedings of the National Academy of Sciences of the United States of America 101(30), 11111-11116.

Bouloubassi, I., Aloisi, G., Pancost, R.D., Hopmans, E., Pierre, C., Sinninghe Damste, J.S., 2006. Archaeal and bacterial lipids in authigenic carbonate crusts from eastern Mediterranean mud volcanoes. Organic Geochemistry 37(4), 484-500.

Brazelton, W.J., Schrenk, M.O., Kelley, D.S., Baross, J.A., 2006. Methane- and sulfur-metabolizing microbial communities dominate the lost city hydrothermal field ecosystem. Applied and Environmental Microbiology 72(9), 6257-6270.

Ciccarelli, F., D., Doerks, T., von Mering, C., Creevey Christopher, J., Snel, B., Bork, P., 2006. Toward automatic reconstruction of a highly resolved tree of life. Science 311(5765), 1283-7.

De Rosa, M., Gambacorta, A., Huber, R., Lanzotti, V., Nicolaus, B., Stetter, K.O., Trincone, A., 1988. A new 15,16-dimethyl-30-(glyceryloxy)triacontanoic acid from lipids of Thermotoga maritima. Journal of the Chemical Society, Chemical Communications (19), 1300-1.

Dowling, N.J.E., Widdel, F., White, D.C., 1986. Phospholipid ester-linked fatty acid biomarkers of acetate-oxidizing sulfate-reducers and other sulfide-forming bacteria. Journal of General Microbiology 132(7), 1815-25.

Goldfine, H., 1997. Structure, biosynthesis, physical properties, and functions of the polar lipids of Clostridium. Advances in Lipobiology 2, 109-142.

Huber, R., Rossnagel, P., Woese, C.R., Rachel, R., Langworthy, T.A., Stetter, K.O., 1996. Formation of ammonium from nitrate during chemolithoautotrophic growth of the extremely thermophilic bacterium *Ammonifex degensii* gen. Nov. sp. nov. Systematic and Applied Microbiology 19, 79-93.

Huber, R., Wilharm, T., Huber, D., Trincone, A., Burggraf, S., Konig, H., Rachel, R., Rockinger, I., Fricke, H., Stetter, K.O., 1992. Aquifex pyrophilus gen. nov. sp. nov., Represents a Novel Group of Marine Hyperthermophilic Hydrogen-Oxidizing Bacteria. System. Appl. Microbiol. 15, 340-351.

Kaneda, T., 1991. Iso- and anteiso-fatty acids in bacteria: biosynthesis, function, and taxonomic significance. Microbiol Rev FIELD Full Journal Title:Microbiological reviews 55(2), 288-302.

Karl, D.M., Tien, G., 1992. MAGIC: a sensitive and precise method for measuring dissolved phosphorus in aquatic environments. Limnology and Oceanography 37(1), 105-16.

Kelley, D.S., Karson, J.A., Blackman, D.K., Fruh-Green, G.L., Butterfield, D.A., Lilley, M.D., Olson, E.J., Schrenk, M.O., Roe, K.K., Lebon, G.T., Rivizzigno, P., 2001. An off-axis hydrothermal vent field near the Mid-Atlantic Ridge at 30 degrees N. Nature 412(6843), 145-149.

Kelley, D.S., Karson, J.A., Fruh-Green, G.L., Yoerger, D.R., Shank, T.M., Butterfield,

D.A., Hayes, J.M., Schrenk, M.O., Olson, E.J., Proskurowski, G., Jakuba, M., Bradley, A., Larson, B., Ludwig, K., Glickson, D., Buckman, K., Bradley, A.S., Brazelton, W.J., Roe, K., Elend, M.J., Delacour, A., Bernasconi, S.M., Lilley, M.D., Baross, J.A., Summons, R.E., Sylva, S.P., 2005. A Serpentinite-Hosted Ecosystem: The Lost City Hydrothermal Field. Science 307(5714), 1428-1434.

Kissin, Y.V., Feulmer, G.P., Payne, W.B., 1986. Gas chromatographic analysis of polymethyl-substituted alkanes. Journal of Chromatographic Science 24(4), 164-9.

Koga, Y., Kyuragi, T., Nishihara, M., Sone, N., 1998. Did Archaeal and Bacterial Cells Arise Independently from Noncellular Precursors? A Hypothesis Stating That the Advent of Membrane Phospholipid with Enantiomeric Glycerophosphate Backbones Caused the Separation of the Two Lines of Descent. Journal of Molecular Evolution 46, 54--63.

Koga, Y., Nishihara, M., Morii, H., Akagawa-Matsushita, M., 1993. Ether polar lipids of methanogenic bacteria: structures, comparative aspects, and biosyntheses. Microbiological reviews 57(1), 164-82.

Langworthy, T.A., Holzer, G., Zeikus, J.G., Tornabene, T.G., 1983. Iso- and anteiso-branched glycerol diethers of the thermophilic anaerobe Thermodesulfobacterium commune. System. Appl. Microbiol. 4, 1-17.

Londry, K.L., Jahnke, L.L., Des Marais, D.J., 2004. Stable Carbon Isotope Ratios of Lipid Biomarkers of Sulfate-Reducing Bacteria. Applied and Environmental Microbiology 70(2), 745-751.

Lovley, D.R., Giovannoni, S.J., White, D.C., Champine, J.E., Phillips, E.J., Gorby, Y.A., Goodwin, S., 1993. Geobacter metallireducens gen. nov. sp. nov., a microorganism capable of coupling the complete oxidation of organic compounds to the reduction of iron and other metals. Arch Microbiol FIELD Full Journal Title:Archives of microbiology 159(4), 336-44.

McLafferty, F.W., Turecek, F., 1993. *Interpretation of Mass Spectra*. University Science Books, Sausalito.

Michal, G., 1999. Biochemical Pathways: an atlas of biochemistry and molecular biology, pp. 277. Wiley, New York.

Nauhaus, K., Albrecht, M., Elvert, M., Boetius, A., Widdel, F., 2007. In vitro cell growth of marine archaeal-bacterial consortia during anaerobic oxidation of methane with sulfate. Environmental Microbiology 9(1), 187-196.

Nishihara, M., Morii, H., Koga, Y., 1989. Heptads of Polar Ether Lipids of an Archaebacterium, Methanobacterium thermoautotrophicum: Structure and Biosynthetic Relationship. Biochemistry 28, 95-102.

Nishihara, M., Nagahama, S., Ohga, M., Koga, Y., 2000. Straight-chain fatty alcohols in the hyperthermophilic archaeon Pyrococcus furiosus. Extremophiles 4(5), 275-277.

Orphan, V.J., Hinrichs, K.U., Ussler, W., III, Paull, C.K., Taylor, L.T., Sylva, S.P., Hayes, J.M., Delong, E.F., 2001. Comparative analysis of methane-oxidizing archaea and sulfate-reducing bacteria in anoxic marine sediments. Applied and Environmental Microbiology 67(4), 1922-1934.

Pancost, R.D., Bouloubassi, I., Aloisi, G., Sinninghe Damste, J.S., Party, M.S.S., 2001.

Three series of non-isoprenoidal dialkyl glycerol diethers in cold-seep carbonate crusts. Organic Geochemistry 32, 695-707.
Pereto, J., Lopez-Garcia, P., Moreira, D., 2004. Ancestral lipid biosynthesis and early membrane evolution. Trends in Biochemical Sciences 29(9), 469-477.
Pikuta, E., Lysenko, A., Suzina, N., Osipov, G., Kuznetsov, B., Tourova, T., Akimenko, V., Laurinavichius, K., 2000. Desulfotomaculum alkaliphilum sp. nov., a new alkaliphilic, moderately thermophilic, sulfate-reducing bacterium. International Journal of Systematic and Evolutionary Microbiology 50(1), 25-33.
Poulter, C.D., Aoki, T., Daniels, L., 1988. Biosynthesis of isoprenoid membranes in the methanogenic archaebacterium Methanospirillum hungatei. J. Am. Chem. Soc. 110(8), 2620-2624.
Ringelberg, D.B., Davis, J.D., Smith, G.A., Pfiffner, S.M., Nichols, P.D., Nickels, J.S., Henson, J.M., Wilson, J.T., Yates, M., et al., 1989. Validation of signature polarlipid fatty acid biomarkers for alkane-utilizing bacteria in soils and subsurface aquifer materials. FEMS Microbiology Ecology 62(1), 39-50.
Russell, M.J., 2003. The importance of being alkaline. Science 302, 580-581.
Rutters, H., Sass, H., Cypionka, H., Rullkotter, J., 2001. Monoalkylether phospholipids in the sulfate-reducing bacteria Desulfosarcina variabilis and Desulforhabdus amnigenus. Archives of Microbiology 176(6), 435-442.
Schouten, S., Hopmans, E.C., Pancost, R.D., Damste, J.S.S., 2000. Widespread occurrence of structurally diverse tetraether membrane lipids: Evidence for the ubiquitous presence of low-temperature relatives of hyperthermophiles. Proceedings of the National Academy of Sciences of the United States of America 97(26), 14421-14426.
Schrenk, M., O., Kelley Deborah, S., Bolton Sheryl, A., Baross John, A., 2004. Low archaeal diversity linked to subseafloor geochemical processes at the Lost City Hydrothermal Field, Mid-Atlantic Ridge. Environmental Microbiology 6(10), 1086-95.
Shaw, N., 1970. Bacterial glycolipids. Bacteriol Rev FIELD Full Journal Title:Bacteriological reviews 34(4), 365-77.
Sinninghe Damste, J., S., Rijpstra, W.I.C., Hopmans, E.C., Schouten, S., Balk, M., Stams, A.J.M., 2007. Structural characterization of diabolic acid-based tetraester, tetraether and mixed ether/ester, membrane-spanning lipids of bacteria from the order Thermotogales. Archives of Microbiology 188, 629-641.
Skophammer, R.G., Servin, J.A., Herbold, C.W., Lake, J.A., 2007. Evidence for a Gram Positive, Eubacterial Root of the Tree of Life. Molecular Biology and Evolution 24(8), 1761-1768.
Sturt, H.F., Summons, R.E., Smith, K., Elvert, M., Hinrichs, K.-U., 2004. Intact polar membrane lipids in prokaryotes and sediments deciphered by high-performance liquid chromatography/electrospray ionization multistage mass spectrometry—new biomarkers for biogeochemistry and microbial ecology. Rapid Communications in mass spectrometry 18, 617-628.
Van Mooy, B.A.S., Rocap, G., Fredricks, H.F., Evans, C.T., Devol, A.H., 2006. Sulfolipids dramatically decrease phosphorus demand by picocyanobacteria in oligotrophic marine environments. Proceedings of the National Academy of

Sciences of the United States of America 103(23), 8607-12.
Wachtershauser, G., 2003. From pre-cells to Eukarya - a tale of two lipids. Molecular Microbiology 47(1), 13-22.

THIS PAGE INTENTIONALLY LEFT BLANK

Chapter 6

Analysis of insoluble residues from carbonates of the Lost City Hydrothermal Field

Abstract

Recalcitrant organic material from carbonate chimneys at the Lost City Hydrothermal Field is associated with acid-insoluble mineral residues. Residues comprise up to 11.1 mg per gram of rock and are composed of between 2.5 and 30.8 wt% organic carbon. Organic carbon in residues is more highly enriched in ^{13}C than total organic carbon in carbonates; residue $\delta^{13}C_{organic}$ values are as high as -0.3‰ vs. VPDB. There is a strong negative correlation between the $\delta^{13}C$ and the $\delta^{15}N$ of residues, suggesting a mixture of two end members from marine and vent organisms. The $\delta^{15}N$ of vent organic matter approaches 0‰, suggesting that hydrothermal primary producers are fixing nitrogen. Biomarker lipids suggest that the main primary producers at Lost City are methanogenic archaea, and we propose that these organisms are fixing nitrogen.

Catalytic hydropyrolysis of residues yielded a range of hydrocarbons consistent with structures previously reported for isoprenoidal and nonisoprenoidal diethers. The main organisms inhabiting vent chimneys produce diether lipids. MRM experiments revealed a series of hopanes, including 3-methylhopanes. This result suggests that aerobic methanotrophy, in addition to anaerobic methanogenesis, plays a role in Lost City ecosystems. Analysis of residues by in-line pyrolysis-GC-MS resulted in the production of mostly aromatic products, most of which are likely derived from proteins.

6.1 Introduction

Organic carbon from carbonate chimneys at the Lost City hydrothermal field is surprisingly enriched in ^{13}C, likely due to the limited availability of dissolved inorganic carbon to the organisms inhabiting that ecosystem (Chapter 3). Extractable lipids from

Lost City carbonates have provided information about the nature of carbon cycling at Lost City, suggesting that the main archaeal phylotype is a methanogen.

Much of the organic material in ancient rocks is insoluble in organic solvents. This material, called kerogen, is a geopolymer that is thermally broken down over time. The formation of kerogen is not well understood, but selective preservation of non-hydrolysable biopolymers resistant to biodegradation is thought to play a role (Tegelaar et al., 1989). Upon dissolution of Lost City carbonates in acid, we noted the presence of a non-hydrolysable residue with filamentous character that we considered a possible biological product. We characterized the content of organic carbon and nitrogen in this residue and attempted to determine its nature.

6.2 Materials and Methods

6.2.1 Collection and residue isolation

Carbonate samples were collected and extracted as described previously. Extracted carbonate powders were placed in a 250 ml Erlenmeyer flask, and covered in a small volume (10 – 20 ml) of pre-extracted DI water. To this volume we slowly added concentrated HCl, at rate of 5 to 10 ml per hour. The total volume of HCl added was calculated to be less than what was necessary to dissolve the carbonate in its entirety, and the pH of the solution was monitored to ensure that it remained near neutral after several hours equilibration between acid and carbonate.

After 24 hours of equilibration between acid and carbonate, the liquid, along with an insoluble residue and minor amounts of carbonate, was poured off into a glass centrifuge tube. This mixture was extracted three times with dicholoromethane (approximately a 2:1 volume of acidified water: DCM). During the extraction we noted a solid residue that accumulated at the boundary between the organic and aqueous phases. After the third extraction of the carbonate and residue mixture, the aqueous phase along with the residue was transferred to a centrifuge tube, and centrifuged for 10 minutes at 2000 rpm. The

aqueous phase was then poured off. Because some residue was lost during this process, the reported concentrations of residues are considered minima. To the remaining solid residue we added 20 ml of pre-extracted DI water and sonicated for 10 minutes, then centrifuged again and poured off the water. This process was repeated twice more in order to remove residual $CaCl_2$. The residue was then freeze dried and weighed. Each dried residue was then re-acidified with 5 ml of 2N pre-extracted HCl to remove any remaining carbonate. After 30 minutes reaction time, the samples were centrifuged and washed as before, and then freeze-dried a second time. This cycle of acidification, washing and freeze-drying was repeated a third time, at which point we detected no remaining reaction with HCl and inferred that all remaining carbonate had been removed.

6.2.2. Elemental analysis

Elemental analysis of residues was undertaken with a Fisons NA 1500 Elemental Analyzer coupled with helium dilution to a Finnigan MAT DeltaPlus XP isotope ratio-monitoring mass spectrometer. The elemental analyzer was operated with the oxidation furnace at 1030 ºC and the reduction furnace at 650 ºC. Typically between 0.5 and 5 mg of dry residue was required to obtain sufficient carbon and nitrogen peak areas for analysis. The mass spectrometer was operated with Isodat 2.0 software and its precision was periodically monitored with international standards, and found to be better than 0.3‰ (1σ). Each sample was measured at least in triplicate to determine $\delta^{13}C$ and $\delta^{15}N$, and peak areas were integrated and calibrated with a known standard to calculate total organic carbon (%C) and nitrogen (%N) contents.

6.2.3. Hydropyrolysis and GC-MS

Two residues were mixed with an aqueous solution of ammonium dioxydithiomolybdate . in proportions such that molybdenum constituted 2 wt% of the total mass. The ammonium dioxydithomolybdate decomposes under pyrolysis conditions

to yield a sulfided molybdenum phase that is catalytically active for hydropyrolysis (HyPy). HyPy was performed in an open-system temperature-programmed reactor configuration (Love et al., 1995). The catalyst-loaded samples were initially heated in a stainless steel reactor tube to 250 ^{o}C at a rate of 300 ^{o}C per minute, then to 520 ^{o}C at 8 ^{o}C per minute, with a hydrogen pressure of 15 MPa and a constant hydrogen gas flow of 6 L min^{-1} through the reactor bed. Products were collected in a silica gel trap cooled with dry ice. Between samples the HyPy apparatus cleaning run was heated to 520 ^{o}C under high hydrogen pressure to clean the apparatus. Experimental blanks, using clean silica gel in the reactor tube instead of a sample, were regularly analyzed and the products monitored and quantified to ensure that trace organic contamination levels were acceptably low.

Hydropyrolysates were separated by silica gel adsorption chromatography into aliphatics (saturated alkanes plus alkenes), aromatics and polars (or N, S, O compounds) by sequential elution with hexanes, hexanes:dichloromethane (3:1 v/v) and dichloromethane:methanol (3:1 v/v), respectively. Elemental sulfur was removed from the extracts by passing over a column of activated copper. Hydrocarbons were identified using a HP 6890 gas chromatograph fitted with a PTV injector operated in splitless mode and equipped with a Varian CP-Sil-5 (60-m length, 0.32 mm inner diameter, and 0.25-um film thickness) fused silica capillary column and coupled to an Agilent 5973 mass-selective detector for full-scan analyses or to an AutoSpecQ for MRM analyses.

6.2.4 In-line Pyrolysis and GC-MS

In-line pyrolysis experiments were performed with a CDS (Chemical Data System, Oxford, Pennsylvania, USA) Pyroprobe 5150. Each sample was loaded into a quartz tube and pyrolyzed at 650 ^{o}C for 10 seconds in a helium flow of 15 – 25 ml per minute. The transfer line was held at 320 ^{o}C and was coupled to a HP 6890 gas chromatograph equipped with a DB-1 (60-m length, 0.32 mm inner diameter, and 0.25-um film thickness) fused silica capillary column. The GC oven was initially set to 60 ^{o}C, where it was held for 2

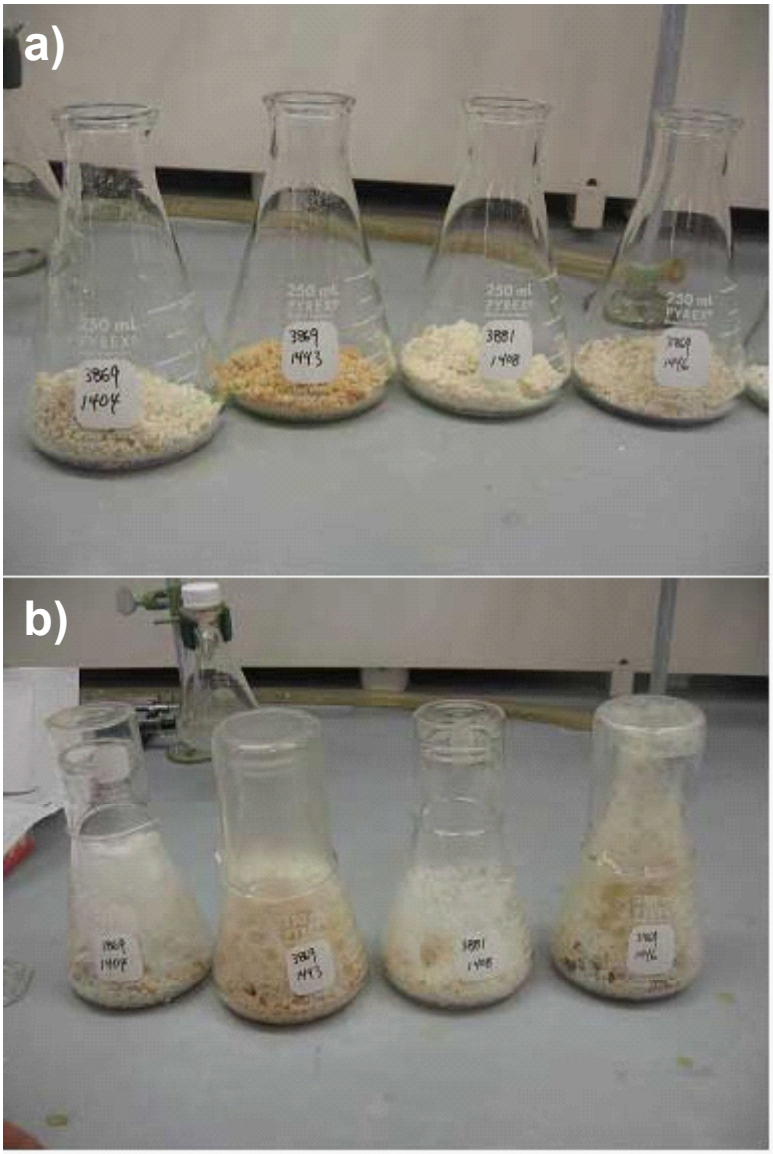

Figure 6-1: Photo of flasks with Lost City carbonates. a) undissolved carbonates; b) dissolution process showing development of rich foam.

Figure 6-2: Filaments on carbonate chimney at Lost City Hydrothermal Field

Table 6-1: Residue data. "Residue": '+/-': standard error; 'mg/g': mg of residue per gram of dry rock; 'C/N': molar ratio of carbon to nitrogen, calculated from wt% data. "Whole Rock": 'TOC': total organic carbon in dry Lost City carbonates; "Residue C (%)": percent contribution to the whole dry rock weight of residue-bound organic carbon.

		Residue										Whole Rock	
marker	residue	$\delta^{13}C$	+/-	$\delta^{15}N$	+/-	wt% C	+/-	wt% N	+/-	mg/g	C/N	TOC (%)	Residue C (%)
C	LC 3869-1404	-0.3	0.3	0.8	0.5	5.2	1.4	0.4	0.1	8.82	16.2	0.22	0.046
2	LC 3864-1524	-4.7	0.3	4.5	0.3	4.5	0.1	2.2	0.1	2.68	2.4	0.11	0.012
H	LC 3881-1228	-12.3	0.6	6.3	0.2	7.1	0.3	3.2	0.1	0.46	2.6	0.09	0.003
C	LC 3869-1443	-3.7	0.2	5.4	0.2	30.8	4.5	12.4	1.3	0.59	2.9	0.47	0.018
C	LC 3869-1446	-6.8	0.2	5.3	0.2	17.5	0.4	7.3	0.4	1.92	2.8	0.34	0.034
X1	LC 3876-1133	-13.8	0.1	6.8	0.2	12.1	2.0	5.3	0.9	3.87	2.7	0.15	0.047
3	LC 3881-1408	-8.6	0.1	3.9	0.2	15.9	2.2	5.7	0.6	0.16	3.3	0.13	0.002
X2	LC 3880-1557	-23.1	0.7	9.9	0.5	2.5	1.0	1.1	0.5	11.11	2.7	0.11	0.028

minutes, and then heated at 10 °C per minute to 100 °C followed by an increase of 4 °C to 320 °C where it was held for 20 minutes. The GC was coupled to an AutoSpecQ operated in full scan mode.

6.3 Results and Discussion

6.3.1 Elemental and Isotope analysis

Upon treatment with acid, Lost City carbonates reacted violently and the aqueous phase developed into a rich foam (Figure 6-1**)** that in our experience with carbonates is unusual. In addition, the removal of the carbonate matrix revealed an insoluble residue with a filamentous appearance. These resembled filaments observed on actively venting structures at Lost City (Figure 6-2). The amount of residue recovered from the carbonates comprised up to slightly more than 1% of the total dry weight of the rock, although we estimate that the actual weight percent of residue is slightly higher than this, since recovery was imperfect **(**Table 6-1).

Isolated residues showed wide variation in their organic content. Elemental analysis revealed that residues consist of between 2.5 and 30.8 weight percent carbon, and 0.4 to 12.4 weight percent nitrogen. While Lost City carbonates are up to 0.6% total organic carbon, the carbon in insoluble residues apparently accounts for near 0.05% of the dry rock weight. This accounts for near 30% of the total organic carbon (TOC) in the rocks in the two fissure samples, collected at sites X1 and X2, and near 20% of the TOC from sample 3869-1404. At the other sites, carbon from recovered residue accounts for approximately 11% of TOC or less.

The residues are unusual in that the ratio of carbon to nitrogen is remarkably low. Of the eight residues examined, seven have a C/N ratio between 2.4 and 3.3, with a mean of 2.8 (Figure 6-3). One residue (3869-1404) does not fit this pattern and has C/N = 16.2, although the nitrogen content in this sample was anomalously low. These ratios are low when compared to the canonical C/N ratio observed in marine phytoplankton, defined by

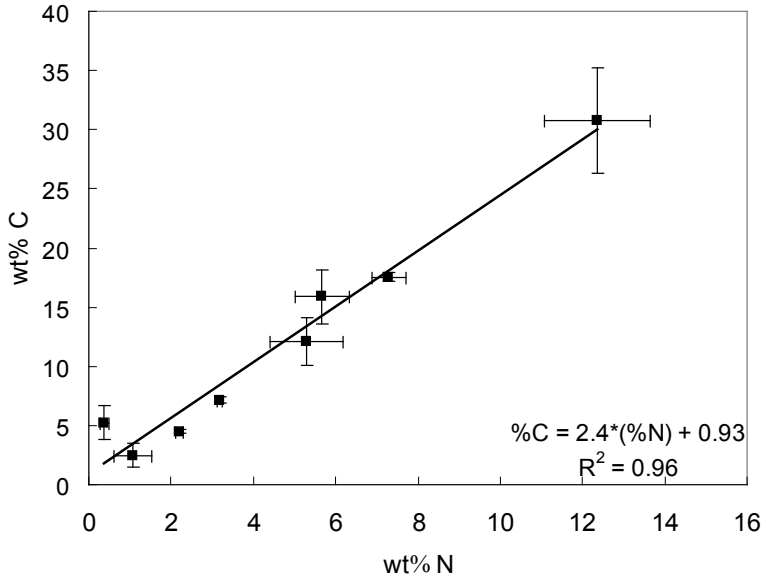

Figure 6-3: Correlation of wt% carbon and wt% nitrogen showing consistent C/N ratio of 2.4. This equates to a molar C/N ratio of 2.8.

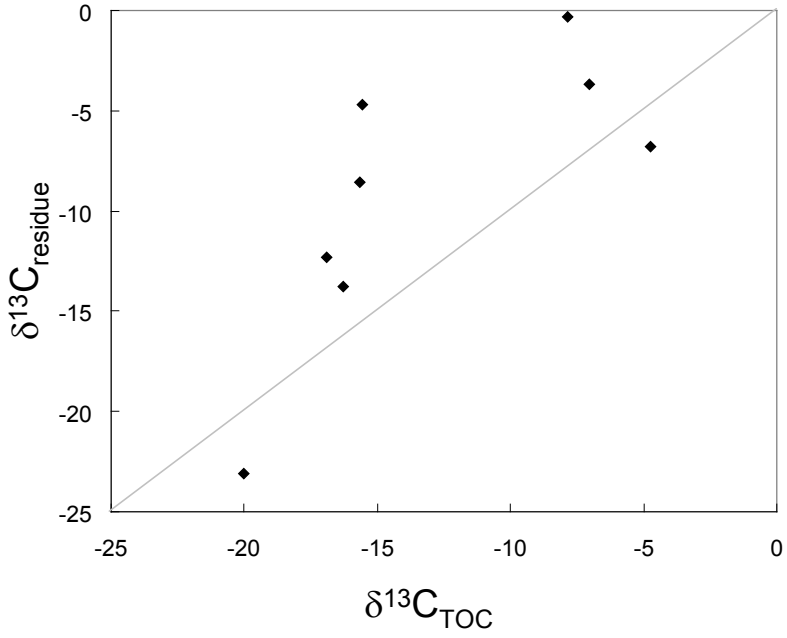

Figure 6-4: Relationship of $\delta^{13}C$ of carbon associated with insoluble residue to that of total organic carbon. Grey line is the predicted 1:1 relationship. Residues are slightly enriched in ^{13}C relative to TOC.

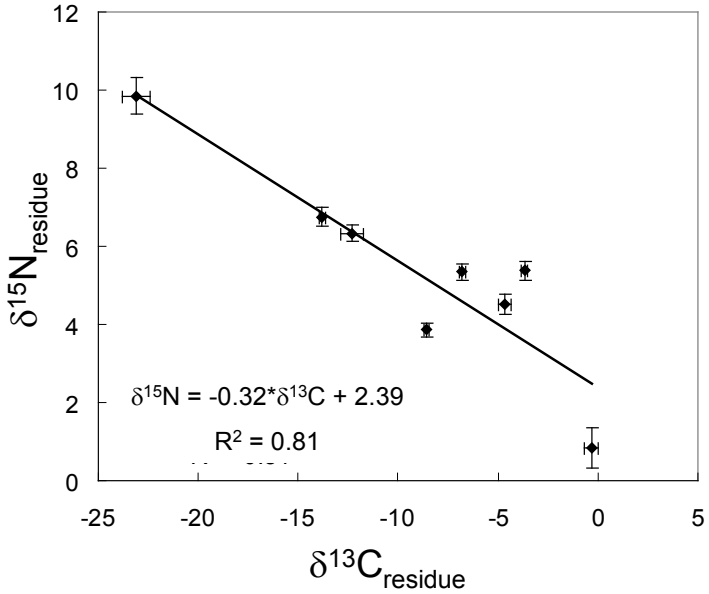

Figure 6-5: Relationship of $\delta^{13}C$ and $\delta^{15}N$ in residue organic material, showing strong anticorrelation, with marine end member at upper left and vent end member lower right.

the Redfield ratio of 106:16 (C/N ~ 6.6) (Arrigo, 2005). Lower ratios of carbon to nitrogen might be expected if the organic material is proteinaceous, or contains abundant nucleic acids. Nucleic acids are soluble in aqueous media and would be expected to be removed by the extraction process. Proteins would be water-soluble after hydrolysis, and the extent of their exposure during the acid treatment would determine whether they were removed. One possible explanation for this problem is that the residue consists of proteins that are acid-resistant or adsorbed to an inorganic matrix. The wt% carbon of the residue suggests that large proportions of it are inorganic. For example, the 20 standard protein-forming amino acids are between 34% and 73% carbon, a range higher than the 2.5 to 30.8 wt% carbon range of the residues.

The $\delta^{13}C$ of the organic carbon in residues roughly parallels the $\delta^{13}C$ of total organic carbon (Figure 6-4**)**. In general the organic carbon in the residues is slightly enriched in ^{13}C relative to total organic carbon. Values for $\delta^{13}C$ of total organic carbon at Lost City can be

approximated to lie on a mixing line between ^{13}C depleted detrital input from the marine water column ($\delta^{13}C \sim -20‰$ at 30ºN latitude (Goericke and Fry, 1994)) and ^{13}C enriched input from carbon-limited autotrophs inhabiting the carbonates ($\delta^{13}C \sim 0‰$) (Chapter 3). If residues were to derive primarily from vent organisms, a $\delta^{13}C$ near the vent end-member would be predicted. A strong correlation between $\delta^{13}C_{TOC}$ and $\delta^{13}C_{residue}$ would be expected if inorganic material bound organic material without preference to whether it was derived from the vent or the water column. This is the correspondence we observe, but the enrichment of ^{13}C in the residues relative to TOC suggests a slight preference for the incorporation of vent organic material over water-column material, albeit with significant scatter in the data.

Residue $\delta^{15}N$ is strongly anticorrelated with $\delta^{13}C$ (Figure 6-5)**.** Such anticorrelations are rare, although correlations between $\delta^{15}N$ and $\delta^{13}C$ have been noted in marine sediments and are explained by mixing between end member terrestrial and marine carbon (Peters et al., 1978). At Lost City mixing is likely to be the explanation for anticorrelation. In the inferred marine end-member, with $\delta^{13}C \sim -20‰$, $\delta^{15}N$ is near +10‰. This value is very close to the marine end-member $\delta^{15}N$ observed in the North Pacific (Peters et al., 1978), although it is slightly higher than that observed in sediments in the subtropical North Atlantic (~ +6‰, (Altabet, 2006)). The other end-member, which has $\delta^{15}N$ near +2‰ represents organic material from the hydrothermal vent. This is similar to the $\delta^{15}N$ value that would be expected in an assemblage of organisms that included N_2-fixers. Seawater in equilibrium with atmospheric N_2 has $\delta^{15}N$ of approximately +0.7‰, and the fractionation imposed by fixation is small, typically less than 2‰ (Altabet, 2006), so that marine diazotrophs typically have $\delta^{15}N$ values near 0‰. Nitrogen fixation by autotrophic methanogens in hydrothermal settings has been observed in *Methanocaldococcus jannaschii* at Axial Volcano on the Juan de Fuca Ridge (Mehta and Baross, 2006). The methanogens at Lost City are closely related to *Methanosarcina*, which is also an archaeal diazotroph (Raymond et al., 2004) . Isotopic evidence suggests that the process of thermophilic nitrogen fixation may be underway at Lost City.

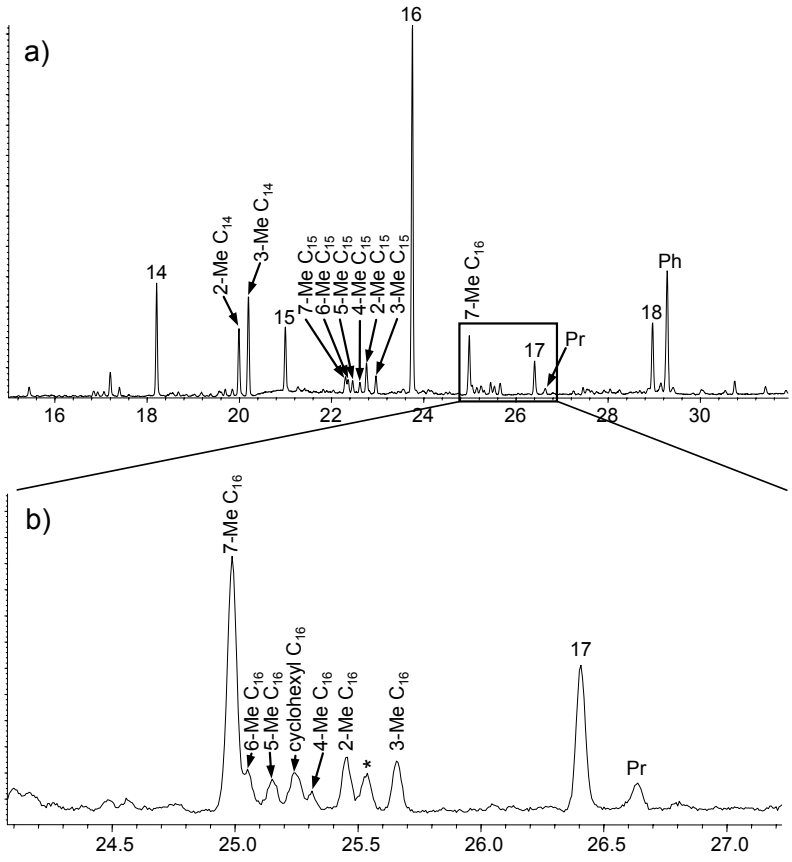

Figure 6-6: A total ion current chromatogram from GCMS analysis (full scan data) of saturated hydrocarbon fraction of the hypropyrolysate of sample 3867-1228. a)full scan chromatogram showing the major *n*-alkanes and methylated alkanes. b) enlarged view of the region between 24.5 and 28 minutes, showing methyl-branched alkanes and C_{16} alkylcyclohexane. Peak marked with * is C_{17} alkylbenzene.

Nitrogen fixation activity would suggest that an adequate supply of fixed nitrogen is lacking. Hydrothermal fluids at mid-ocean ridges commonly have low concentrations of nitrate, which is consumed as an electron acceptor (Butterfield et al., 2004). At Lost City, the highly reducing conditions during serpentinization are likely to reduce any nitrate in the fluids. Loss of nitrate can be partially compensated by production of ammonia (Butterfield et al., 2004). Abiotic nitrogen fixation in hydrothermal settings can supply ammonia, but maximum fluids temperatures at Lost City are around 150 ºC (Kelley et al., 2005; Proskurowski et al., 2006), which is too low for abiotic nitrogen fixation to be a significant reaction (Brandes et al., 1998).

6.3.2. Hydropyrolysis

Hydropyrolysis of two samples revealed that the dominant products were likely derived from bacterial and archaeal diether lipids. Figure 6-6 shows the trace of the aliphatic fraction of the hydropyrolysate of sample 3867-1228. Straight chain *n*-alkanes with lengths of 14 to 18 carbons were detected, along with numerous methyl-branched compounds. The most abundant of the methyl-branched alkanes are 2-methyl and 3-methyl tetradecane. These are consistent with the presence of *iso*- and *anteiso*- branched C_{15} moieties in the diether compounds, as reported previously (Chapter 5).

Five isomers of methylpentadecane are detected, with the methyl branch occurring at positions 2 through 7. These occur in near-equal abundance, but methylation at the 2- and 3- positions is slightly favored. Similar results are reported in the C_{17} series, with detection of six isomers of methylhexadecane. We note that 7-methyl hexadecane is particularly abundant. This is unsurprising, as among previously reported diether structures we noted the appearance of an abundant diether with a mass of 640 Da, and a retention time suggesting the presence of two 7-methyl heptadecane moieties. The appearance of methyl branches positions 4, 5, and 6 in the hydropyrolysates are likely derived from cyclopropyl moieties in side chains of non-isoprenoidal diethers. Cyclopropyl unsaturations are

commonly detected in bacterial diethers (Pancost et al., 2001) and would be expected to produce mid-chain methyl alkanes as pyrolysates. We also detect small amounts of C_{16} alkylcyclohexane. This is also a common moiety in nonisoprenoidal diethers, and is likely the desaturated side chain detected in some of the diethers at Lost City. The same suite of hydrocarbons was detected in the hydropyrolysate of 3876-1104, with additional detection of C_{12}-C_{14} *n*-alkanes.

Small amounts of pristane and larger amounts of phytane are also detected in the hydropyrolysate of sample 3867-1228. Pristane is commonly considered a diagenetic product of the oxidative degradation of phytol. In this sample both pristine and phytane are likely to derive from the phytanyl side chains of archaeal diethers. In the hydropyrolysate of 3876-1104 (not shown) pristine and phytane were not detected, suggesting that the relative input of archaeal biomass was smaller in this sample than in 3867-1228. This interpretation is consistent with the $\delta^{13}C$ of total organic carbon previously reported. Sample 3867-1228 is relatively enriched in ^{13}C ($\delta^{13}C \sim$ -7‰ vs. VPDB) reflecting abundant input of ^{13}C-enriched archaea, while 3876-1104 is more ^{13}C depleted ($\delta^{13}C \sim$ -18‰) suggesting it contains largely marine inputs. The lack of phytane implies that the marine input does not contain abundant chlorophylls or that the component with $\delta^{13}C$ near -20‰ is not associated with debris from marine phytoplankton.

Analysis of hydropyrolysates with MRM experiments shows that they contain small amounts of steranes and hopanes. Hopanes are present with carbon numbers from C_{30}–C_{35} (Figure 6-7). The MRM trace also reveals the presence of gammacerane, the hydropyrolysis product tetrahymanol, which is presumably derived from ciliates. Hopanes with carbon numbers C_{27} to C_{29} are lacking, consistent with a thermally immature source. Thermal immaturity of hopanes is confirmed by their stereochemistry, which is dominantly the biological (but thermally unstable) 17β,21β isomer for all except for C_{30} hopane.

Small amounts of 3-methylhopanes (C_{31}-C_{34}) are also present. Although functionalized hopanoids were not detected, the presence of 3-methylhopanes is usually

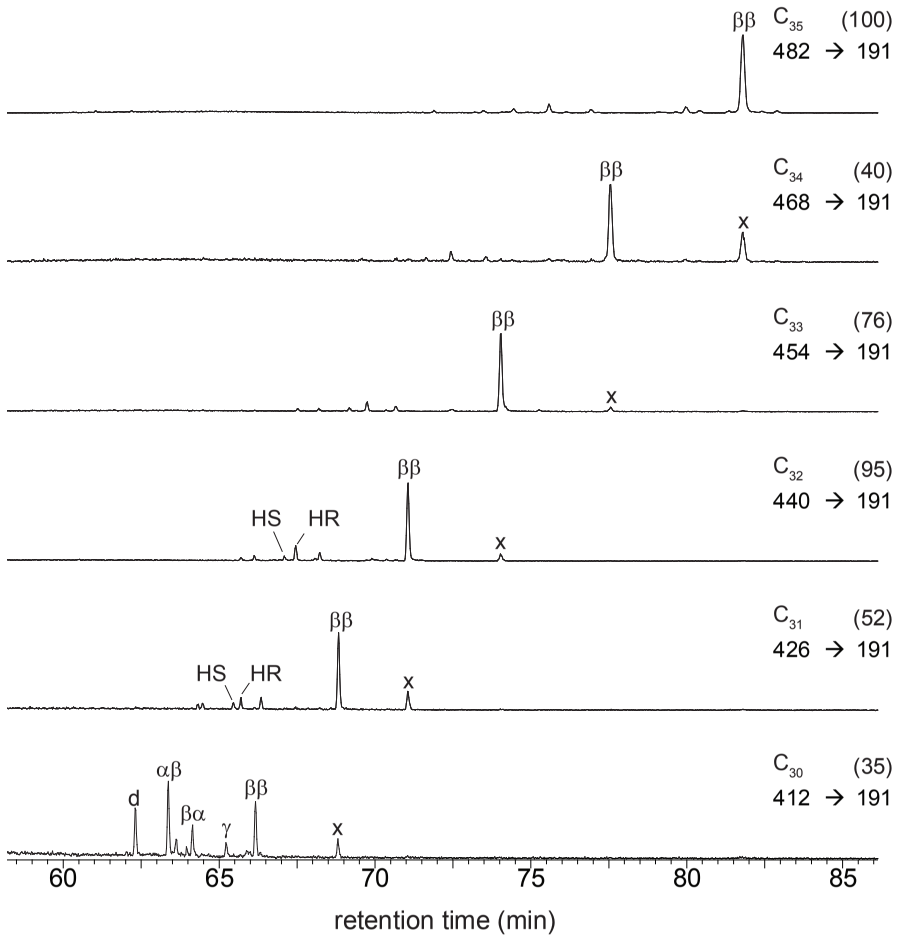

Figure 6-7: MRM chromatograms showing the hopane series from hydropyrolysis of sample 3867-1228. Each chromatogram is identified by its carbon number, relative height (abundance) of the largest peak, and the mass transition yielding that chromatogram. Hopanes are present almost exclusively as the 17β,21β isomer, except for the C_{30} hopane series. γ = gammacerane, d = diahopane, x = ghost peak (electronic cross-talk from overlying chromatogram).

taken as a marker for the presence of aerobic Type I methanotrophs (Brocks and Summons, 2004). This is consistent with results from 16S rDNA studies which show the presence of *Methylobacter* in many of the carbonate chimneys (Brazelton et al., 2006). These organisms presumably live in contact with aerobic seawater and consume methane produced by the archaea within the carbonates.

6.3.3 Pyrolysis-GC-MS

Pyrolysis-GC-MS experiments produced a range of mainly aromatic compounds. Figure 6-8 shows a typical product profile, consisting mainly of aromatic compounds. Most of these compounds are likely to be derived from amino acids (Stankiewicz et al., 1997). These are summarized in Table 6-2. Toluene may also be derived from thermal rearrangement of lipids. Several diketopiperazine compounds are also detected, derived from peptide bonds between amino acids. The predominance of peaks potentially derived from peptides suggests that the residue material consists largely of protein.

6.4 Conclusions

Insoluble residues from Lost City carbonates are partially biological, but largely inorganic. The organic residue that remains is a mixture of products from vent biota and the water column. Hydropyrolysis confirmed the structures of the alkyl moieties of diether lipids, and suggested that aerobic methanotrophy plays a role in carbon cycling at Lost City. Pyrolysis-GC-MS suggests that the residues largely consist of protein material, which may help explain their high nitrogen content. The ratio of the isotopes of nitrogen in this residue strongly suggests that vent biota is supported by nitrogen fixation. In combination, we suggest that archaeal methanogens in Lost City vent carbonates are actively fixing nitrogen.

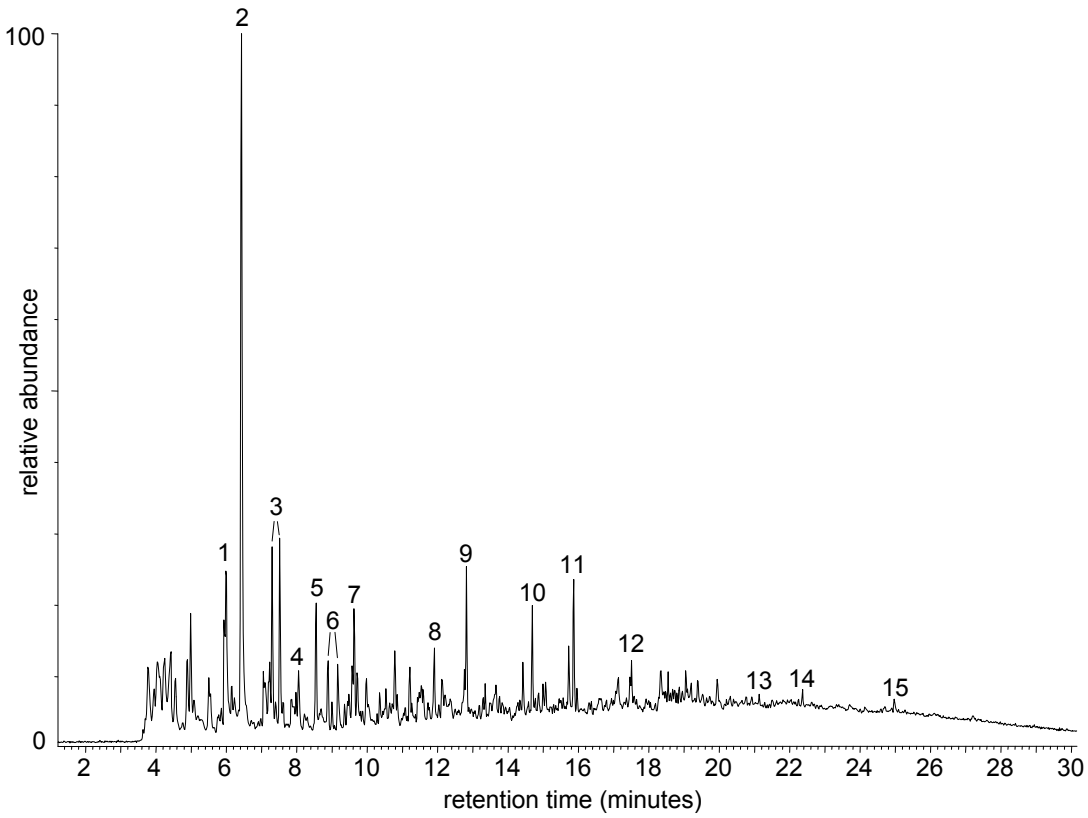

Figure 6-8: Chromatogram of pyrolysate products from in-line-pyrolysis-GC-MS experiment (Sample number 3881-1228). Numbers refer to compounds denoted in Table 6-2.

Peak #	Compound	Precursor(s)
1	pyrrole	Proline
2	toluene	Phenylalanine
3	methylpyrrole	Proline, Hydroxyproline
4	ethylbenzene	Phenylalanine
5	styrene	Phenylalanine
6	dimethylpyrrole	Diketopiperazine
7	benzaldehyde	unknown
8	methylphenol	Tyrosine
9	ethylcyanobenzene	Phenylalanine
10	propylcyanobenzene	Phenylalanine
11	indole	Tryptophan
12	methylindole	Tryptophan
13	diketopiperazine	Pro-Ala
14	diketodipyrrole	Hydroxyproline
15	diketopiperazine	Pro-Pro

Table 6-2: Identities of the peaks in the chromatogram in Figure 6-8, along with their presumed sources.

6.5 References

Altabet, M.A., 2006. Isotopic tracers of the marine nitrogen cycle: present and past. In: J.K. Volkman (Ed.), *Marine Organic Matter: Biomarkers, Isotopes, and DNA*, *The Handbook of Environmental Chemistry*, pp. 251-293. Springer-Verlag, Berlin Heidelberg.

Arrigo, K.R., 2005. Marine microorganisms and global nutrient cycles. Nature (London, United Kingdom) 437(7057), 349-355.

Brandes, J.A., Boctor, N.Z., Cody, G.D., Cooper, B.A., Hazen, R.M., Yoder Jr., H.S., 1998. Abiotic nitrogen reduction on the early Earth. Nature 395, 365-367.

Brazelton, W.J., Schrenk, M.O., Kelley, D.S., Baross, J.A., 2006. Methane- and sulfur-metabolizing microbial communities dominate the lost city hydrothermal field ecosystem. Applied and Environmental Microbiology 72(9), 6257-6270.

Brocks, J.J., Summons, R.E., 2004. Sedimentary hydrocarbons, biomarkers for early life. In: W.H. Schlesinger (Ed.), *Biogeochemistry 8*, *Treatise on Geochemistry*, pp. 63-116. Elsevier, Oxford.

Butterfield, D.A., Roe, K.k., Lilley, M.D., Huber, J.A., Baross, J.A., Embley, R.W., Massoth, G.J., 2004. Mixing, Reaction and Microbial Activity in the Sub-seafloor Revealed by Temporal and Spatial Variation in Diffuse Flow Vents at Axial Volcano. In: W.S.D. Wilcock, E.F. DeLong, D.S. Kelley, J.A. Baross, S.C. Cary (Eds.), *The Subseafloor Biosphere at Mid-Ocean Ridges*, *Geophysical Monograph Series*. American Geophysical Union, Washington D.C.

Goericke, R., Fry, B., 1994. Variations of marine plankton d13C with latitude, temperature, and dissolved CO2 in the world ocean. Global Biogeochemical Cycles 8(1), 85-90.

Kelley, D.S., Karson, J.A., Fruh-Green, G.L., Yoerger, D.R., Shank, T.M., Butterfield, D.A., Hayes, J.M., Schrenk, M.O., Olson, E.J., Proskurowski, G., Jakuba, M., Bradley, A., Larson, B., Ludwig, K., Glickson, D., Buckman, K., Bradley, A.S., Brazelton, W.J., Roe, K., Elend, M.J., Delacour, A., Bernasconi, S.M., Lilley, M.D., Baross, J.A., Summons, R.E., Sylva, S.P., 2005. A Serpentinite-Hosted Ecosystem: The Lost City Hydrothermal Field. Science 307(5714), 1428-1434.

Love, G.D., Snape, C.E., Carr, A.D., Houghton, R.C., 1995. Release of covalently-bound alkane biomarkers in high yields from kerogen via catalytic hydropyrolysis. Organic Geochemistry 23(10), 981-6.

Mehta, M.P., Baross, J.A., 2006. Nitrogen fixation at 92 degrees C by a hydrothermal vent archaeon. Science 314(5806), 1783-6.

Pancost, R.D., Bouloubassi, I., Aloisi, G., Sinninghe Damste, J.S., Party, M.S.S., 2001. Three series of non-isoprenoidal dialkyl glycerol diethers in cold-seep carbonate crusts. Organic Geochemistry 32, 695-707.

Peters, K.E., Sweeney, R.E., Kaplan, I.B., 1978. Correlation of carbon and nitrogen stable isotope ratios in sedimentary organic matter. Limnology and Oceanography 23(4), 598-604.

Proskurowski, G., Lilley, M.D., Kelley, D.S., Olson, E.J., 2006. Low temperature volatile production at the Lost City Hydrothermal Field, evidence from a hydrogen stable isotope geothermometer. Chemical Geology 229(4), 331-343.

Raymond, J., Siefert, J.L., Staples, C.R., Blankenship, R.E., 2004. The natural history of

nitrogen fixation. Molecular Biology and Evolution 21(3), 541-554.
Stankiewicz, B.A., Hutchins, J.C., Thomson, R., Briggs, D.E.G., Evershed, R.P., 1997. Assessment of Bog-body Tissue Preservation by Pyrolysis-Gas Chromatography/ Mass Spectrometry. Rapid Communications in mass spectrometry 11, 1884-1890.
Tegelaar, E.W., De Leeuw, J.W., Derenne, S., Largeau, C., 1989. A reappraisal of kerogen formation. Geochimica et Cosmochimica Acta 53(11), 3103-6.

THIS PAGE INTENTIONALLY LEFT BLANK

Chapter 7

Composition of biomass in hydrothermal Pink Streamer Communities: Isotopes and Lipids

Abstract

Biomass of streamer communities from alkaline hot springs in Yellowstone National Park has a wide range of values in its stable isotope ratios of carbon and nitrogen. Some biomass is surprisingly enriched in ^{13}C, with $\delta^{13}C_{biomass}$ as high as -2.4‰. Analysis of the total lipid extracts of these streamer communities shows that they are composed of archaea and bacteria, a result supported by parallel 16S rRNA surveys being undertaken by coworkers. Analysis of intact polar lipid structures shows that the degree of cyclization of archaeal lipids is independent of the polar headgroup. It also shows that in hot-spring runoffs streams the relative contribution of bacteria to the microbial community increases downstream with decreasing temperature and increasing pH. The values of $\delta^{13}C_{biomass}$ also decrease downstream.

Ether lipids derived from Aquificales are enriched in ^{13}C relative to archaeal ether lipids. This result conflicts with reports from other alkaline hotspring environments, and suggests that in these environments Aquificales can operate either as heterotrophs or autotrophs.

Microbial biomass with $\delta^{13}C$ values near 0‰ appears to be a common feature of alkaline hydrothermal systems, a result that should be considered when the ^{13}C content of organic carbon is employed as a biosignature.

7.1 Introduction

Bacterial and archaeal thermophiles occupy the deepest roots of the 16S rDNA tree of life (Barns et al., 1996; Ciccarelli et al., 2006; Stetter, 1996), and it has been postulated the universal common ancestor of life on Earth inhabited a hydrothermal environment

(Nisbet and Sleep, 2001). These are among the reasons that thermal ecosystems have been intensively investigated as potential analogues for early ecosystems on Earth or for microbial processes elsewhere in the solar system (Bock and Goode, 1996).

Putative fossils of microbes in ancient hydrothermal systems have been reported from rocks as old as 3.2 Ga (Duck et al., 2007; Rasmussen, 2000; Zang, 2007). Most reports of possible fossilized microbes in Archaean hydrothermal deposits are millimeter-scale filamentous structures (Duck et al., 2007; Rasmussen, 2000; Reysenbach and Cady, 2001). These structures preserve morphology, but evidence for their phylogenetic placement or metabolic strategies can only be inferred. Indeed the very biogenicity of these fossils is subject to challenge (Brasier et al., 2006). Demonstrably biogenic fossils are present in Phanerozoic deposits, including the siliceous sinters of the Devonian Rhynie Chert, best known for plant fossils but also preserving microbial fossils (Trewin, 1996) and from Devonian to Carboniferous sinter deposits in the Drummond Basin of Australia (Walter et al., 1996).

Information about microbes in early hydrothermal systems could conceivably be understood through examination of recalcitrant biomarker lipids. Lipid biomarkers have been detected in siliceous sinter precipitates in modern New Zealand hot springs (Pancost et al., 2005), suggesting that such deposits may hold the potential to be preserved over long time periods. Examination of lipid structures and their isotopic composition in modern hot springs can provide context by which ancient hot springs might be better understood.

Modern systems are not perfect analogues to understanding hydrothermal ecosystems on early Earth. The organisms inhabiting modern hydrothermal systems have deep phylogenetic roots, but are adapted to modern – not Archaean – environments. Perhaps most significantly, organisms such as Aquificales, which are deeply rooted on the 16S rDNA tree of life, are obligate aerobes. Prior to 2.2 Ga atmospheric pO_2 was likely less than 10^{-5} the present atmospheric level (Farquhar et al., 2007; Pavlov and Kasting, 2002) and availability of suitable electron acceptors would have been far more restricted than in modern

environments. It is also possible that to some degree the bacterial inhabitants of modern terrestrial hot springs are supported by carbon or nutrients derived from the surrounding ecosystem. For example, in Yellowstone National Park hot springs exist in the presence of a rich assembly of flora and fauna, including insects and animals that are capable of transporting material between hot springs, and of contributing their own biomass and waste to hot spring environments. Evidence supports the notion that thermophilic microbes have evolved to benefit from this coexistence. For example the bacterial thermophile lineage Thermotogales, which is common in Yellowstone hot springs, is deeply rooted on the tree of life (Stetter, 1996), but at least one representative of this genus contains numerous genes involved in pathways that can be used to degrade polysaccharides and sugars derived from plants (Nelson et al., 1999). If terrestrial hot springs supported life during the Archaean era, the organisms in them and their metabolic strategies must have differed from their modern analogues. Utilization of modern terrestrial hot springs as Archaean analogues must be undertaken with great care to avoid spurious comparisons. This can be approached by a thorough understanding of the chemical, physical, and genetic controls on any signal observed in modern environments and inferred to be analogous to ancient ones.

Pink streamer communities are commonly observed in alkaline terrestrial hot springs in Yellowstone (Brock, 1978; Reysenbach et al., 1994; Setchell, 1903) and elsewhere around the world (Jones et al., 2001; Konhauser et al., 2001). The microbes comprising streamer communities are often filamentous, but also include associated non-filamentous types. The term 'streamer' has been applied to these communities (Walter et al., 1996), and we use it here to refer to a flow-oriented accumulation of millimeter to centimeter long strands of microbial and other biomass and silica. The term 'filament' has sometimes been used to refer these accumulations as well as to filamentous cell morphologies, but the term 'streamer' avoids this confusion. Streamers are rapidly encrusted by silica, a process which destroys most morphological taxonomic information (Jones et al., 2001), but suggests a mechanism for potentially enhanced preservation of organic material. Streamer-forming

and associated microbes could be entrained in the silica and preserved as the filamentous organic fossils.

Macroscopic filamentous communities of hyperthermophiles are common in the outflow streams of alkaline hot springs in Yellowstone National Park, USA. These communities form distinctive morphological streamer forms that attach to rocks or other hard surfaces in outflow streams (Figure 7-1**)**. A report of the sequences of 16S rDNA recovered from pink streamer communities (PSC) at Octopus Spring indicated that they consist mainly of bacteria related to the deeply-branching Aquificales and Thermotogales. Archaeal contributions were undetected (Reysenbach et al., 1994). However, subsequent studies of the constituents of alkaline hot springs have reported archaea related to *Thermoproteus*, *Thermosphaera*, and several groups of Desulfurococcales (Meyer-Dombard et al., 2005). While none of these archaea are filaments - *Thermoproteus* is a rod, *Thermosphaera* and other Desulfurococcales are coccoid – they are reported to be the main archaeal constituents of streamer communities at Bison Pool (Meyer-Dombard et al., unpublished).

Study of the carbon isotopic compositions of pink streamer biomass and lipids has suggested that Aquificales at Octopus Spring are heterotrophs consuming formate (Jahnke et al., 2001). That report also noted a discrepancy between ^{13}C content measured in PSC biomass and the ^{13}C content of Aquificales biomass predicted from *in situ* lipid $\delta^{13}C$. This discrepancy could be accounted for by suggesting the presence of a second, undetected component of the pink streamer community, predicted to have $\delta^{13}C$ near -5‰. One possibility that might account for this 'missing' biomass that it is derived from archaea. Examination of the ^{13}C content of ether lipids from archaea can test this hypothesis.

7.2 Methods

7.2.1. Sample collection and preparation

Streamer biomass was collected in the outflow channels of hot springs in Yellowstone

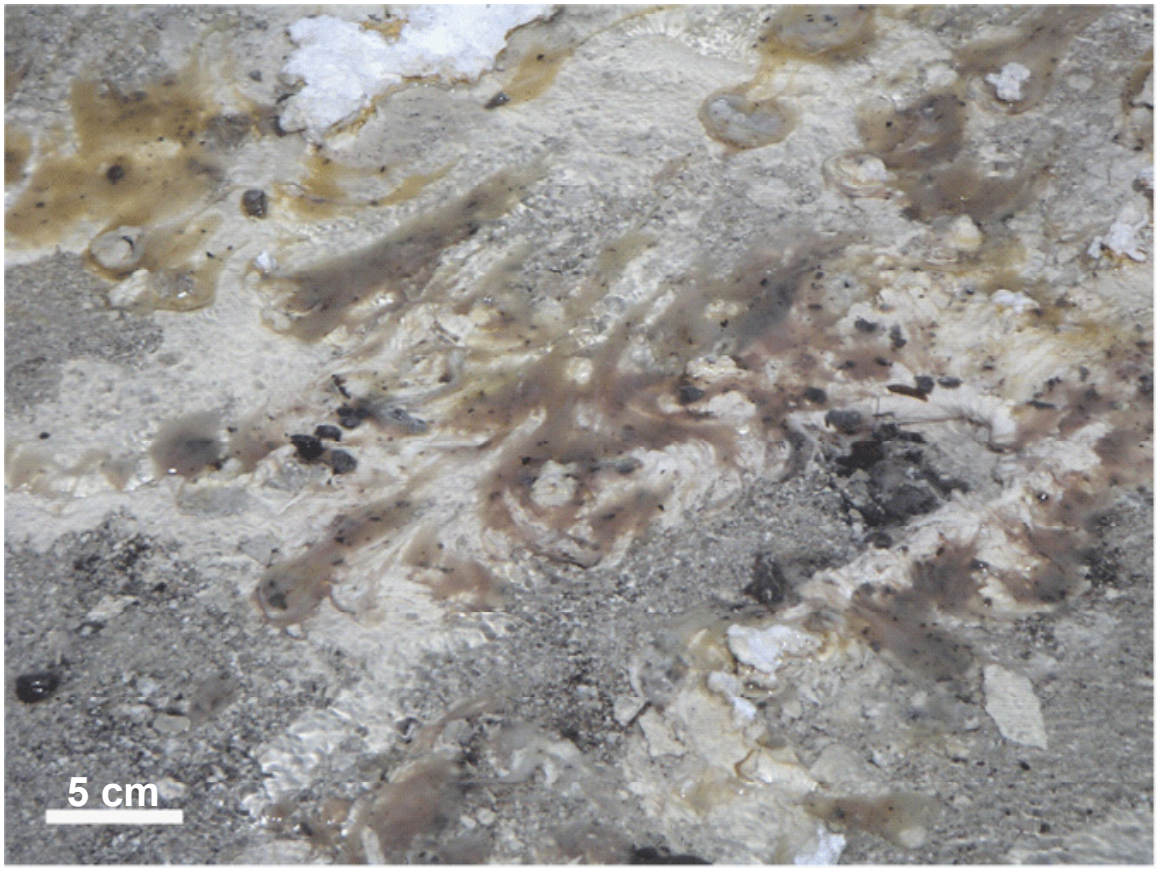

Figure 7-1: Pink streamers communities in the runoff stream at Bison Pool, Yellowstone National Park.

National Park during summer field seasons in 2003-2005. Sample locations included hot springs in the Lower Geyser Basin and Sylvan springs area. Streamers were sampled with forceps, placed in Whirlpak sample bags, and frozen at -20 ºC within 4 hours of collection. Frozen samples were shipped on dry ice to MIT and immediately transferred to a -20 ºC freezer upon arrival. At one location (informally named 'Bison Pool') in the Sentinel Meadows area of the Lower Geyser Basin, we temporarily located a web of cotton string in the outflow stream, designed to facilitate colonization of streamer communities. Experience had suggested that this setup would allow the rapid development of fresh biomass (D. Meyer-Dombard, pers. comm.), which might limit contribution of detrital biomass from upstream locations. Each mesh apparatus was put in place in July 2005 and collected in August 2005 at the three locations shown in Figure 7-2. The pair of apparatus (04A, 04B) placed most proximally to the source were bathed in stream water with a temperature near 78 ºC. A third apparatus (05) was at approximately 75 ºC. Water temperatures above 74 ºC are greater than the highest known temperatures at which photosynthetic growth is known to occur in thermophilic environments(Brock, 1978), and these three samples were placed with the expectation of the growth of chemosynthetic organisms only. A fourth apparatus (06) was placed at 66 ºC, where growth of organisms with photosynthetic pigments could be visually observed. Each apparatus is shown in Figure 7-3 after 3 days and 6 weeks of growth. Aliquots of the collected biomass were lyophilized and ground to a fine powder using a pre-combusted mortar and pestle. Dry biomass was then either combusted for elemental analysis and bulk isotope data, or extracted for lipid analysis. The *Sulfolobus* sample was obtained courtesy of Linda Jahnke.

7.2.2. Elemental analysis

Elemental analysis of dry biomass was undertaken with a Fisons NA 1500 Elemental Analyzer coupled with helium dilution to a Finnigan MAT DeltaPlus XP isotope-ratio-monitoring mass spectrometer. The elemental analyzer was operated with the oxidation

furnace at 1030 ºC and the reduction furnace at 650 ºC. Typically between 2 and 5 mg of dry, crushed streamer biomass was required to obtain sufficient carbon and nitrogen peak areas for analysis. The mass spectrometer was operated with Isodat 2.0 software and its precision was periodically monitored with international standards, and found to be better than 0.3‰ (1σ). Each sample was measured at least in triplicate to determine $\delta^{13}C$ and $\delta^{15}N$, along with total organic carbon (TOC) and nitrogen (TON) contents.

7.2.3. Lipid extraction

Lipids were extracted with a modified Bligh and Dyer method (Bligh and Dyer, 1959). Dried crushed biomass (200 to 500 mg) was placed in a solvent-cleaned 50 ml Teflon centrifuge tube, along with 19 ml of 10:5:4 methanol:dichloromethane:water. The mixture was vigorously shaken for 5 minutes and subsequently sonicated for 30 minutes, then centrifuged at 5000 rpm using a Eppendorf 5804 centrifuge. The supernatant was decanted into precombusted 60 ml glass vials. A two-phase mixture was obtained by adding 5 ml of chloroform and 5 ml of water to each vial, and the organic phase was removed with a Pasteur pipette and added to a new vial. This extraction procedure was repeated three times in total. A modified Bligh and Dyer mixture was used for the third extract, in which the water was replaced with 1% trichloroacetic acid in water. The organic phases from the three extracts were pooled, and dried under a stream of N_2. Elemental sulfur was removed from the extracts by passing over a column of activated copper, followed by filtration of the extract through a combusted glass Buchner funnel (poresize ~40 μm). Total lipid extracts were weighed and yields are reported as μg of lipid per gram of dry biomass extracted.

7.2.4. HPLC-MS

Lipid extracts were analyzed by analytical high-performance liquid chromatography-mass spectrometry following methods previously established (Sturt et al., 2004). Briefly, lipids were separated on a LiChrospher® Diol column (125 mm x 2mm, 5μm) with a linear

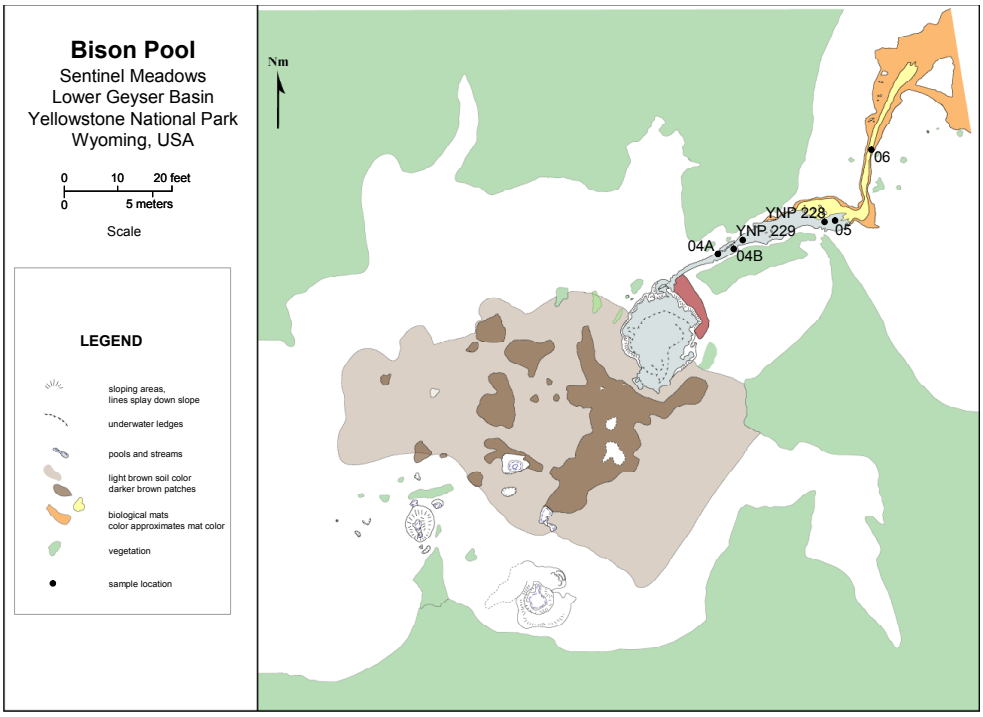

Figure 7-2: Schematic of Bison Pool and its runoff stream with sample collection locations, Lower Geyser Basin, Yellowstone National Park.

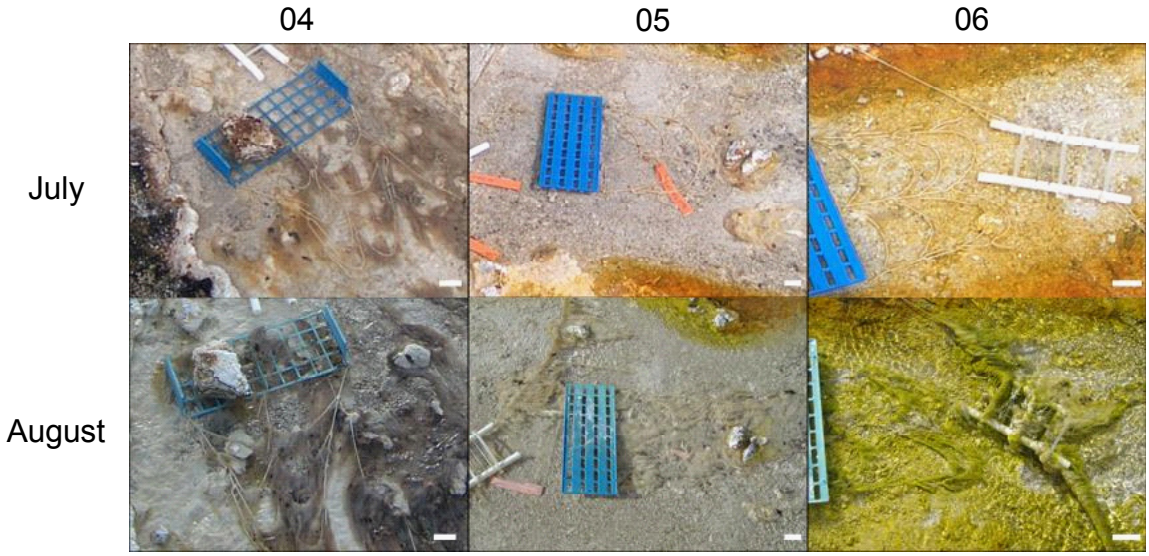

Figure 7-3: Colonization apparatus at three locations in the Bison Pool runoff stream, in July and in August, 2005.

solvent gradient and the HPLC was coupled to a ThermoFinnigan LCQ Deca XP ion-trap mass spectrometer. Solvents contained ammonia and formic acid, which form adducts with polar lipids to enhance ionization. The mass spectrometer scanned m/z 500 – 2000 and performed MS^n experiments in a data-dependent acquisition mode where the base peak was fragmented up to MS^3 in both positive and negative ion modes. The MS^n data provided information about the masses of the headgroup and core lipid by reference to standards previously published (Sturt et al., 2004).

7.2.5. GC-MS

Aliquots of lipid extracts were analyzed as their trimethylsilyl ethers and esters by reacting with *N,O*-bis(trimethylsilyl)trifluoro-acetamide (BSTFA + 1% TMCS) in pyridine at 60°C for thirty minutes. The remainder of the total lipid extract was separated over silica gel into five fractions using an elution scheme of solvents of increasing polarity: aliphatic hydrocarbons 1⅜ dead column volume (DV) hexane, aromatic hydrocarbons 2 DV 4:1 hexane:DCM, ketones 2 DV DCM, alcohols 2 DV 4:1 DCM:ethyl acetate, fatty acids and diols 2 DV 7:3 DCM:methanol. Individual lipids were identified using a HP 6890 gas chromatograph fitted with a PTV injector operated in splitless mode and equipped with a Varian CP-Sil-5 (60-m length, 0.32 mm inner diameter, and 0.25-um film thickness) fused silica capillary column and coupled to an Agilent 5973 mass-selective detector. Lipids were identified by comparisons of mass spectra and retention times with authentic standards or samples where these compounds have previously been characterized. Diether lipids were identified by comparison to similar authentic standards, and we report their mass without attempting to solve their structure. Lipid abundances were quantified relative to a coinjected standard.

7.2.6. Ether cleavage

Side chains of ether lipids were cleaved by reaction with 1.0 M boron tribromide

(BBr_3, Aldrich) in dichloromethane (DCM). Approximately 200 µl BBr_3 was added to lipid extracts in dry vials under a stream of argon, after which vials were sealed and heated to 60 ºC for 2 hours. After the reaction was complete, the resulting bromides were reduced to hydrocarbons by adding the DCM solution containing bromides to approximately 1 ml of Super-Hydride solution (1.0 M lithium triethylborohydride in tetrahydrofuran, Aldrich) in dry vials under a stream of argon and reacting at 60 ºC for 2 hours. This procedure was tested in parallel on an ether lipid standard to confirm quantitative cleavage of side chains to hydrocarbons.

7.2.7. GC-irMS

Stable carbon isotopic compositions of individual lipids were determined using a Thermo TraceGC gas chromatograph fitted with a programmable temperature vaporizing (PTV) injector and equipped with a Varian DB-1 (60-m length, 0.32 mm inner diameter, and 0.25-um film thickness) fused silica capillary column and coupled to a ThermoFinnigan Deltaplus XL isotope ratio monitoring mass spectrometer via a combustion interface operated at 850°C. Column temperatures were programmed from 60°C at a constant flow of 2.5 ml/min and a temperature gradient of 10°C per minute to 100°C, followed by a temperature gradient of 4°C per minute to 320°C then isothermal for 20 minutes. Stable carbon isotope ratios were determined relative to an external CO_2 standard that was regularly calibrated relative to a reference mixture of n-alkane (Mixture B) provided by Arndt Schimmelmann (Indiana University). Reported values for the isotopic compositions of lipids were corrected by mass balance for the carbon present in the TMS derivative where applicable.

7.3. Results and Discussion

7.3.1. Elemental analysis

Figure 7-4, Table 7-1 shows the distribution of ^{13}C and ^{15}N contents of bulk biomass

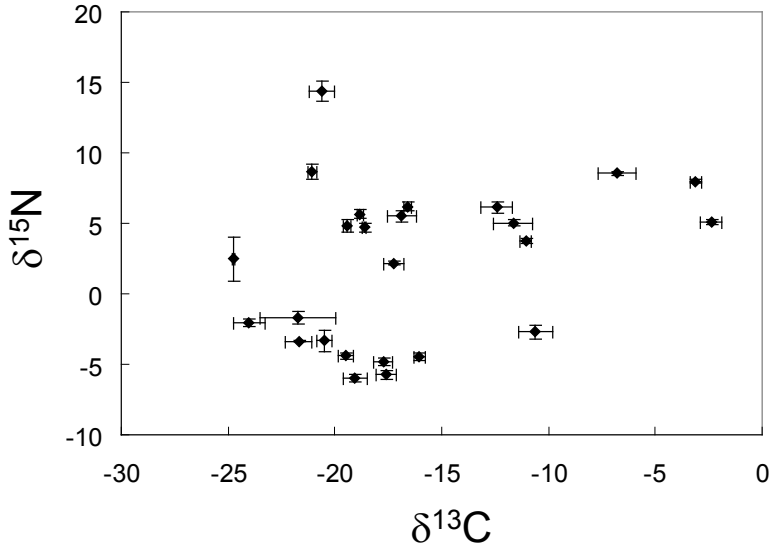

Figure 7-4: Carbon and nitrogen isotope compositions of bulk streamer biomass

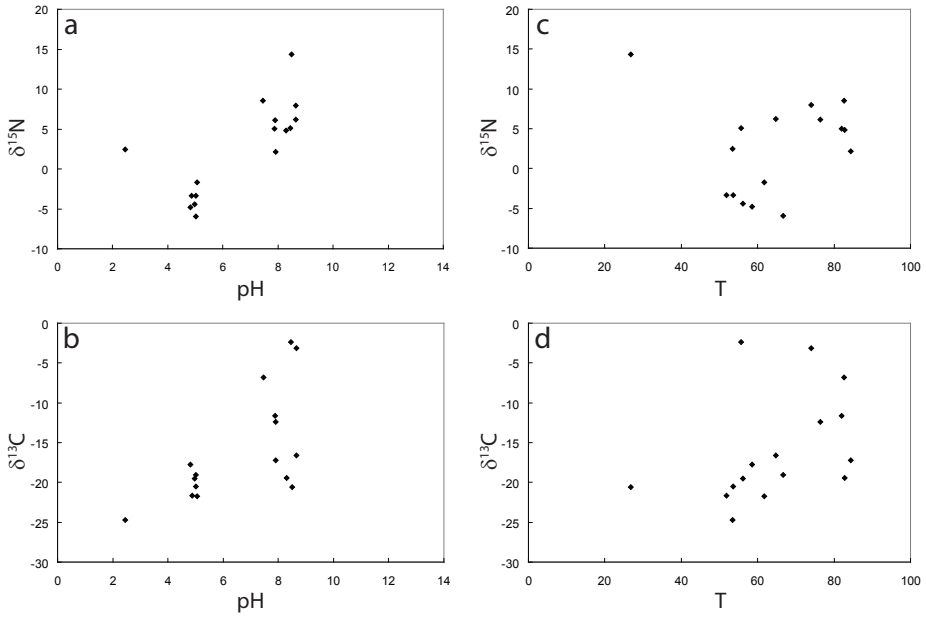

Figure 7-5: Carbon and nitrogen isotope compositions of bulk streamer biomass plotted vs. pH and T

Sample no.	Easting	Northing	Formal/Informal Location Name	pH	T	$\delta^{13}C$	+/-	$\delta^{15}N$	+/-	%C	+/-
YNP 001	0516135	4931005	Octopus Spring	7.9	84.3	-17.2	0.4	2.2	0.1	9.1	1.3
YNP 006	0516139	4930830	pool behind 5 sisters PF6	8.3	82.7	-19.4	0.2	4.8	0.4	1.5	0.0
YNP 018	n/a	n/a	Sylvan Springs/ Goldilocks source pool	2.5	53.4	-24.8	0.0	2.5	1.5	0.2	0.0
YNP 023	n/a	n/a	Avacado Pool outflow	8.5	26.8	-20.6	0.6	14.4	0.7	1.6	0.1
YNP 026	0511969	4932412	Mitch's Last Stand outflow	8.5	55.7	-2.4	0.5	5.1	0.2	4.0	0.4
YNP 031	0512460	4933742	Boulder Spring outflow	8.7	64.7	-16.6	0.2	6.2	0.3	7.2	0.5
YNP 042	n/a	n/a	downstream of Skippy's Bathtub			-16.1	0.3	-4.5	0.2	2.1	0.1
YNP 045	n/a	n/a	edge of Skippy's Bathtub	5.1	61.7	-21.8	1.8	-1.7	0.5	1.3	0.2
YNP 046	n/a	n/a	Figure 8 Pool runoff stream	5.0	66.7	-19.0	0.5	-6.0	0.3	2.3	0.2
YNP 048	n/a	n/a	Ojo Caliente runoff	7.5	82.6	-6.8	0.9	8.6	0.1	16.1	0.5
YNP 142	0510715	4934945	Bison Pool	7.9	82.0	-11.7	0.9	5.0	0.2	8.9	0.5
YNP 145	n/a	n/a	Bison Pool	7.9	76.4	-12.4	0.7	6.1	0.4	4.4	0.3
YNP 150	n/a	n/a	Bison Pool			-18.6	0.1	4.7	0.3	4.8	0.2
YNP 201	0544632	4939632	Skippy's Outflow 2	4.9	51.9	-21.7	0.6	-3.4	0.0	2.3	0.6
YNP 205	0544632	4932666	Skippy's Outflow 2	5.0	53.6	-20.5	0.4	-3.3	0.8	1.2	0.5
YNP 206	0544626	4939655	Skippy's Outflow 1	5.0	56.2	-19.5	0.3	-4.4	0.2	1.4	0.5
YNP 207	0544618	4939652	Skippy's Bathtub	4.8	58.6	-17.7	0.4	-4.8	0.3	1.1	0.4
YNP 208	n/a	n/a	Skippy's bathtub			-17.6	0.5	-5.7	0.3	1.4	0.4
YNP 215	0544625	4939577	Spotted Grizzly Pool			-24.0	0.7	-2.1	0.3	24.6	0.4
YNP 218	0544596	4939577	Green Cheese			-10.6	0.8	-2.7	0.5	9.2	2.4
YNP 227	0510790	4934956	Bison Spring			-21.1	0.2	8.6	0.5	6.3	1.0
YNP 228	0510787	4934951	Bison Spring			-16.9	0.7	5.5	0.4	3.4	0.4
YNP 229	0510782	4934954	Bison Spring			-11.1	0.3	3.8	0.2	16.4	0.4
YNP 231	0510895	4934820	Flat Cone Spring	8.7	74.0	-3.1	0.3	8.0	0.1	12.1	0.9
YNP 239	0518640	4949503	Avacado Outflow			-18.8	0.2	5.7	0.3	3.9	0.1

Table 7-1: Location, stable carbon and nitrogen compositions, and %C of bulk streamer biomass from several locations in Yellowstone National Park. UTM Coordinates are listed as NAD27, zone 12T. n/a = not available.

in chemotrophic streamer communities from a variety of locations in Yellowstone. These communities have $\delta^{13}C$ values ranging from -24.8‰ to -2.4‰ vs. VPDB and $\delta^{15}N$ ranging from -6.0‰ to +14.4‰ vs. air N_2. There is no apparent correlation between the values of $\delta^{13}C$ and $\delta^{15}N$.

Figure 7-5 shows $\delta^{13}C$ and $\delta^{15}N$ plotted vs. temperature and pH at the collection locations. There is no clear relationship of $\delta^{13}C$ with either temperature or pH, but $\delta^{15}N$ correlates with pH ($R^2 = 0.54$; Figure 7-5a). We note that the heaviest enrichments ($\delta^{13}C >$ -15‰ and $\delta^{15}N >$ +3‰) all occur at only where conditions are alkaline.

We sampled biomass from multiple locations in the outflow stream of Bison Pool in 2004 and 2005. Within this outflow stream both $\delta^{13}C$ and $\delta^{15}N$ are correlated with distance from the spring source, with proximal samples most enriched in ^{13}C and depleted in ^{15}N (Figure 7-6)**.**

Previous reports have shown that pink streamer communities at Octopus Spring have bulk biomass near -15‰ (Jahnke et al., 2001), and similar ^{13}C contents are reported from biomass inhabiting vent communities at Mammoth Hot Springs (Zhang et al., 2004). The latter report also indicated that ^{13}C content of biomass decreased with distance from the source at Mammoth Hot Springs. The wide range of $\delta^{13}C$ values can be partially explained by variation in community composition and of metabolic strategies among the community members that make up pink streamer samples. Fixation of inorganic carbon via the Calvin-Benson and acetyl-CoA cycles normally impart a greater discrimination against ^{13}C than carbon fixation by the reductive tricarboxylic acid cycle (rTCA) or 3-hydroxypropionate cycle (Hayes, 2001). If the relative abundance of organisms using the Calvin cycle versus rTCA increases with distance from the source, that would result in the a decrease in net community $\delta^{13}C$. Such a change was suggested to explain the variation in travertine systems (Zhang et al., 2004) and may be applicable in alkaline siliceous sytems as well.

Biomass $\delta^{15}N$ is greater than 0‰ and increases with distance from the source at Bison Pool. If nitrogen fixation were dominant, then organic $\delta^{15}N$ would be expected to be

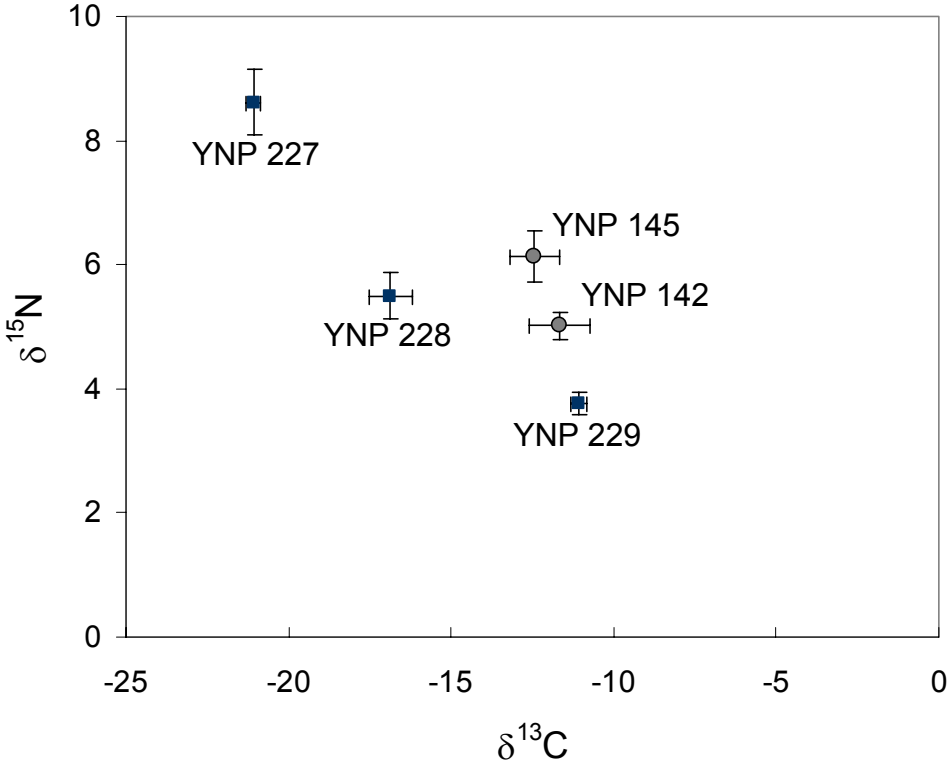

Figure 7-6: Carbon and nitrogen isotope compositions of bulk streamer biomass from Bison Pool, showing decreasing $\delta^{13}C$ and increasing $\delta^{15}N$ with distance from source

near 0‰. However this is unlikely, since the high temperature microbial communities are dominated by Crenarchaea, Aquificales, and Thermodesulfobacteria (Meyer-Dombard et al., 2005), none of which are known to be dizaotrophs (Raymond et al., 2004). The data suggest that the biological source of nitrogen is supplied in the form of ammonia. The equilibrium between ammonia gas and dissolved ammonium ion associated with a large isotopic fractionation (~34‰ at 25 ºC). Evaporative loss of volatile ammonia results in increasing $\delta^{15}N$ of residual dissolved ammonium. This effect is predicted to be smaller in fluids with a pH below the p*K* of ammonium (9.24). Figure 7-5a shows the $\delta^{15}N$ of biomass samples from hot spring outflows in Yellowstone with a wide range of pH. These data are consistent with ammonium being an important source of organic nitrogen, and show that biomass from lower pH outflow streams generally have lower $\delta^{15}N$ values.

7.3.2. Intact Polar Lipid Analysis

7.3.2.1. Archaeal lipids

We analyzed the intact polar lipid (IPL) composition of streamer communities at several locations along the outflow stream at Bison Pool and Ojo Caliente. Intact polar lipids are derived from living cells, and analysis of both the polar headgroup and core lipid provides more taxonomic information about the source organism than the core lipid alone (Sturt et al., 2004).

Figure 7-7 shows lipid density maps for lipid extracts from the four colonization sites at Bison Pool. In this presentation of LCMS data, time is represented on the horizontal axis and molecular ion mass is represented on the vertical axis. This presentation is convenient because it allows the simultaneous display of coeluting compounds with different molecular masses. Peak areas are represented by the intensity of the spot for each compound. This method allows rapid qualitative comparison of the differences between the IPL profiles of two or more samples. Figure 7-7 shows only the molecular ion of each compound. Also collected, but not shown, are the multidimensional MS-MS spectra, which along with

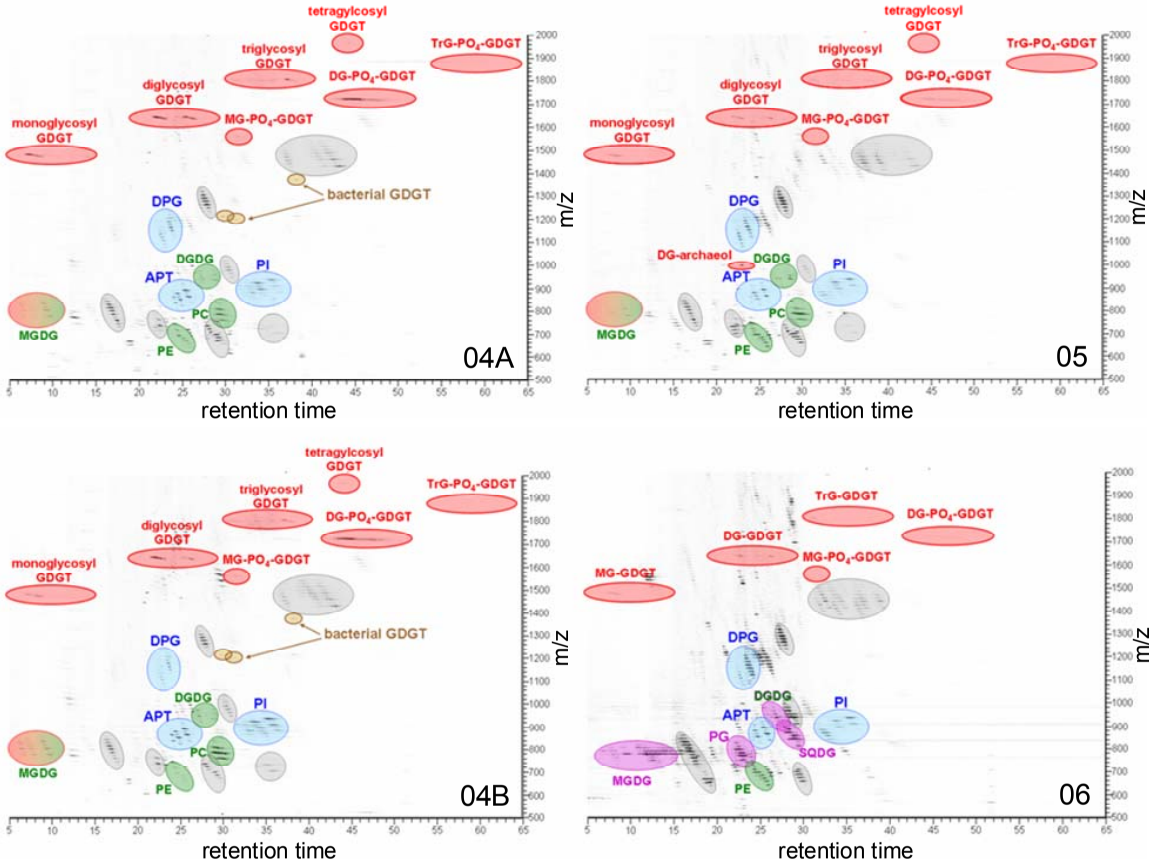

Figure 7-7: Density maps of IPLs from colonization experiments. The horizontal axis on each density map is retention time; the vertical axis is the *m/z* of the molecular ion. Groups of ions are circled, the abbreviation denotes their identity (see abbreviation explanation in caption to Table 3). The fill color of each circle denotes their presumed source; red: archaea, blue: Aquificales, green: other bacteria, brown: unknown bacteria (GDGTs), purple: cyanobacteria, grey: unidentified. Analyses courtesy of Helen Fredricks and Kai Hinrichs.

retention time is used to identify the headgroup and core lipid of each compound.

Figure 7-7 shows the wide range of IPL types present in the streamer community at Bison Pool. Polar archaeal tetraethers are dominated by glycosylated forms, including monogycosyl, digylcosyl, triglycosyl, and trace tetragylcosyl variants. Lipids that contain both phosphatidyl and glycosyl headgroups are also present (Figure 7-8)**.** Within each polar group, we detect archaeal tetraethers with 0-4 rings. Tetraethers with more than four rings are not detected. Schouten et al. (2007) report that archaea that synthesize GDGTs with more than four rings are primarily found within the orders Sulfolobales and Thermoplasmatales, which primarily grow at low pH. Therefore it is unsurprising that organisms in alkaline thermophilic environments produce GDGTs with up to only four rings (Schouten et al., 2007).

We calculated degree of cyclization (Uda et al., 2001) for the tetraethers associated with each polar headgroup in each sample. These results are reported in Table 7-2. In general, differences in degree of cyclization were smaller between polar headgroups than between samples. The sample that was collected *in situ* at higher temperature (YNP 229), and those allowed to colonize the string web at the same site (04A, 04B all had degrees of cyclization around 1.3 – 1.4 when integrated for all lipid headgroups. This result was very consistent among all samples and across all headgroups, with the exception of the digylcosylated GDGTs in 04B. Experiments with archaea grown in laboratory cultures have suggested that an increasing degree of cyclization in GDGTs accompanies an increase in growth temperature (Gliozzi et al., 2002; Uda et al., 2001). Lipids extracted from hydrothermal settings have not supported this relationship (Schouten et al., 2007). One report has suggested that crenarchaeol abundance is strongly affected by temperature, with a maximum at 40 ºC (Zhang et al., 2006), but subsequent investigations dispute this (Schouten et al., 2007). We did not detect crenarchaeol in our samples. Figure 7-9 shows degree of cyclization of each sample plotted versus the temperature and pH measured at the time of collection. These data suggest a decrease in degree of cyclization with increasing

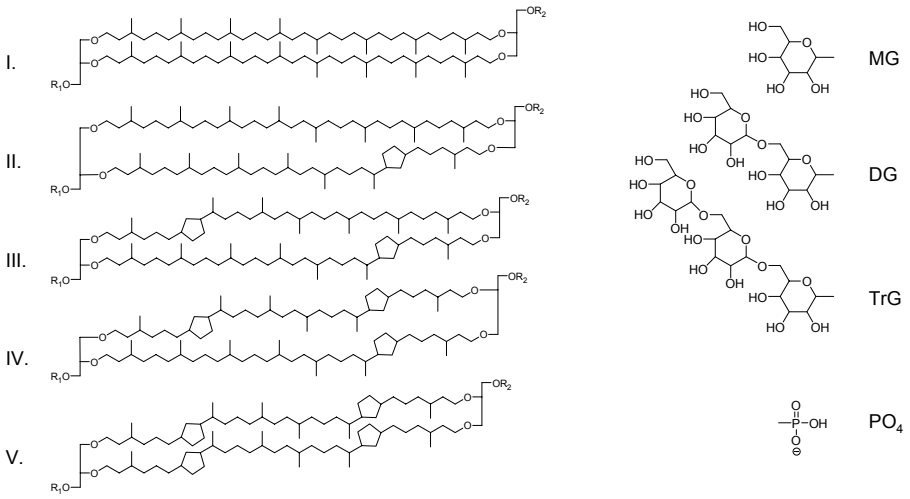

Figure 7-8: Structures of archaeal tetraether lipids detected in Bison Pool runoff. Core lipids with 0-4 rings are shown on the left. Monoglycosyl (MG), digylcosyl (DG), trigylcosyl (TrG) and phosphate (PO_4) headgroups are shown on the right.

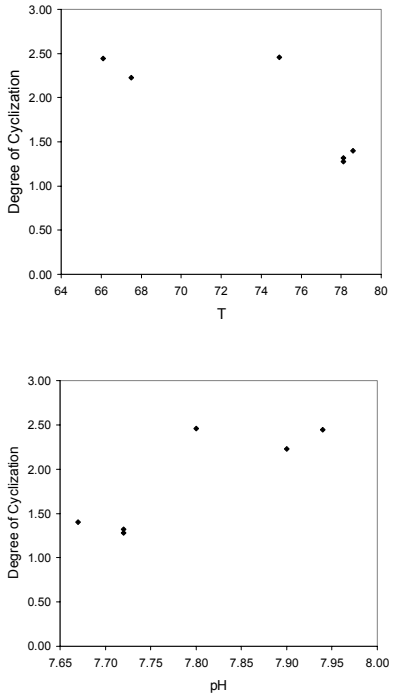

Figure 7-9: Overall degree of cyclization for tetraether lipids in Bison Pool runoff plotted vs. T and pH

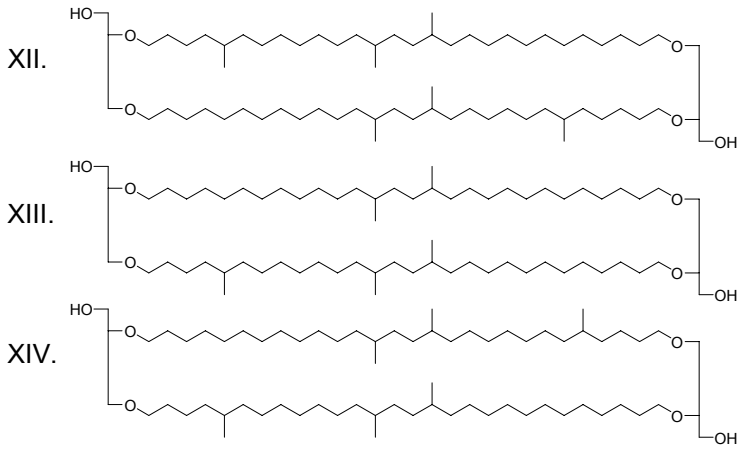

Figure 7-10: Core lipid structures of bacterial GDGTs XII, XIII, and XIV (Schouten et al., 2007). Monogylcosyl functionalized lipids with the core lipid masses corresponding to these structures were detected in Bison Pool runoff, although the positions of the methyl groups has not been confirmed.

	T	pH	monoglycosyl	digylcosyl (1)	digylcosyl (2)	trigylcosyl	P-monoglycocyl	P-diglycosyl	Sum
DMD-04A	78.1	7.7	1.46	1.24	1.40	0.91	1.36	1.34	1.32
DMD-04B	78.1	7.7	1.97	1.09	2.31	1.33	1.39	1.19	1.28
DMD-05	74.9	7.8	2.78	1.97	2.64	2.49	-	2.44	2.46
DMD-06	66.1	7.9	2.85	2.25	2.23	2.35	-	2.32	2.45
YNP 229	78.6	7.7	1.54	1.29	1.52	1.04	-	-	1.40
YNP 228	67.5	7.9	2.23	-	-	-	-	-	2.23
YNP 101	79.0	8.2	1.52	0.94	0.99	0.57	1.24	0.90	1.04
YNP 048	82.6	7.5	1.90	1.20	0.99	0.74	1.21	0.99	1.12

Table 7-2: Degree of cyclization of archaeal GDGTs, overall and categorized by polar headgroup. Calculated after the manner of Uda et al., (2001): Degree of cyclization = (%monocyclic + 2 x %bicyclic + 3 x %tricyclic+ 4 x %tetracyclic)/100. 'Sum' is the degree of cyclization of the weighted integration of all tetraethers.

growth temperature, but the number of data points collected is too few to rigorously support this conclusion.

Archaeol with monoglycosyl headgroups is detected in samples 04A, 04B, and 05, and digylcosyl archaeol is detected only in sample 05.

7.3.2.2. Bacterial lipids

We detect trace amounts of bacterial tetraether lipids in the biomass collected at the highest temperature locations. These are functionalized with monoglycosyl and digylcosyl headgroups. Monoglycosyl bacterial GDGTs contained 5 or 6 methyl groups (corresponding to GDGTs XII, XIII, and XIV in the nomenclature of Schouten et al., 2007), while diglycosyl bacterial GDGTs were detected only with five methyl groups (XIII) **(**Figure 7-10**)**.

Monoglycosyl diesters are not abundant in the high temperature sites, but are detected in the low temperature (photosynthetic) sample, along with digylcosyl diesters.

Lipids with aminopentanetetrol (APT) headgroups are abundant in all samples, and relatively more abundant in samples collected at higher temperature. Diether, diester, and mixed ether/ester lipid cores are associated with APT headgroups, and contain acid and alcohol moieties of 18 and 20 carbons with up to two unsaturations. APT is associated with Thermodesulfobacteria and Aquificales (Sturt et al., 2004), as well as the archaeal order Methanomicrobiales (Garcia et al., 2006). Diphosphatidylgylcerol lipids, exclusively with three acyl chains are present. Side chains range from C_{16} to C_{20} and typically are present with two unsaturations among them. The most common diphosphatidylglycerol lipids at the higher temperature sites contains three C_{18} moieties, but the tri-C_{16} and tri-C_{20} are also present. At the photosynthetic site the C_{16}, C_{18}, C_{18} diphosphatidylglycerol is the most abundant variant.

Phosphatidylethanolamine is most abundant as the 16,16 diacyl variety and is most abundant in the photosynthetic samples. Phosphatidylgylcerol displays a similar pattern, with greatest relative abundance in the photosynthetic zone. A 16,18 fatty acid

	04A	04B	05	06
Archaeal tetraethers				
MG-GDGT	5.9	3.2	5.9	1.1
DG-GDGT - 1	10.7	13.3	5.2	0.9
DG-GDGT - 2	6.0	2.6	3.7	0.8
TrG-GDGT	2.9	3.0	1.6	0.1
MG-PO4-GDGT	0.9	0.8	0.0	0.8
DG-PO4-GDGT	24.3	29.7	9.6	0.0
Total archaeal GDGT	**50.6**	**52.7**	**26.0**	**3.8**
Bacterial tetraethers				
MG-nonisoprenoidal GDGT	1.8	0.9	0.0	0.0
DG-nonisoprenoidal GDGT	0.7	0.4	0.0	0.0
Archaeal diethers				
MG-archaeol	0.3	0.5	0.0	0.0
Bacterial lipids				
MG	2.5	6.4	1.3	0.2
APT	10.9	10.9	16.7	5.5
PE	7.6	5.4	10.1	1.7
PC	6.2	12.3	30.6	0.0
PI	18.8	10.5	10.8	4.1
PG	0.5	0.3	2.2	17.3
SQDG	0.0	0.0	0.0	66.2
Total bacterial lipids*	**46.6**	**45.8**	**71.7**	**95.1**
Archaea	51.0	53.2	26.0	3.8
Bacteria	49.0	47.1	71.7	95.1

*excluding bacterial tetraethers

Table 7-3: Relative abundance of major polar headgroups in Bison Pool colonization experiment, showing increasing bacterial contribution with decreasing temperature (sample 04A,B =highest T; 06 = lowest T). Relative abundance is semiquantitative, and is determined by integrated peak area compared to total integrated peak area of all identified lipids without correction for response factor.

Abbreviations:
MG-GDGT: monogylcosyl glycerol dibiphytanyl glycerol tetraether
DG-GDGT-1: diglycosyl glycerol dibiphytanyl glycerol tetraether (peak 1)
DG-GDGT-2: diglycosyl glycerol dibiphytanyl glycerol tetraether (peak 2)
TrG-GDGT: triglycosyl glycerol dibiphytanyl glycerol tetraether
MG-PO4-GDGT: monogylcosyl phosphatidyl glycerol dibiphytanyl glycerol tetraether
DG-PO4-GDGT: digylcosyl phosphatidyl glycerol dibiphytanyl glycerol tetraether
MG-nonisoprenoidal GDGT: monogylcosyl glycerol nonisoprenoidal dialkyl glycerol tetraether
DG-nonisoprenoidal GDGT: digylcosyl glycerol nonisoprenoidal dialkyl glycerol tetraether
MG-archaeol: monoglycosyl archaeol
MG: monoglycosyl
APT: aminopentanetetrol
PE: phosphatidylethanolamine
PC: phosphatidylcholine
PI: phosphatidylinositol
PG: phosphatidylglycerol
SQDG: sulfoquinovosyldiacylglycerol

configuration is dominant in that lipid type. Sulfoquinovosyldiacylglycerol (SQDG) lipids appear in the photosynthetic sample only, and have saturated side chains with a total of 34 or 36 carbons.

Variations in the proportions of headgroups making up the lipid extract are apparent in the data presented in Table 7-3. The streamers sampled at the highest temperature (04A, and 04B) contain the highest proportion of archaeal tetraethers, the bulk of which are functionalized as digylcosyl lipids or digylcosyl-phosphatidyl lipids. In addition, small amounts of bacterial tetraethers are present at the highest temperature sites. The headgroups phosphatidylcholine, phosphatidylinositol and aminopentanetetrol are most abundant on the diacyl and diether bacterial lipids at these sites. In the lower temperature site, which appears to contain abundant photosynthetic biomass, the most abundant lipids are SQDG lipids. SQDG is a common lipid in photosynthetic organisms, and is localized to thylakoid membranes (Ohta et al., 1997).

At least two significant unidentified lipid groups appear in the density maps in Figure 7-7. The first elutes near 28 minutes in all four samples and is a pseudohomologous series with molecular ions of 1262, 1276, 1290, and 1304 Da. In positive ion MS-MS each of these loses 269 Da in the first mass transition. This mass loss probably corresponds to the mass of the unidentified polar headgroup (Sturt et al., 2004). The second group of abundant unidentified lipids elutes between 40 and 45 minutes, but contains only one dominant molecular ion with a mass of 1722 Da. Positive ion MS-MS suggests that this lipid contains a digylcosyl polar headgroup and a core lipid mass of 1380 Da.

7.3.3. Ether cleavage products

Cleavage and reduction of lipid ether bonds is a useful way to generate GC-amenable hydrocarbons that can be easily analyzed mass-spectrometrically and isotopically.

Ether cleavage products were generated from several sets of samples, including samples collected *in situ* from Ojo Caliente and grown on the colonization apparatus at

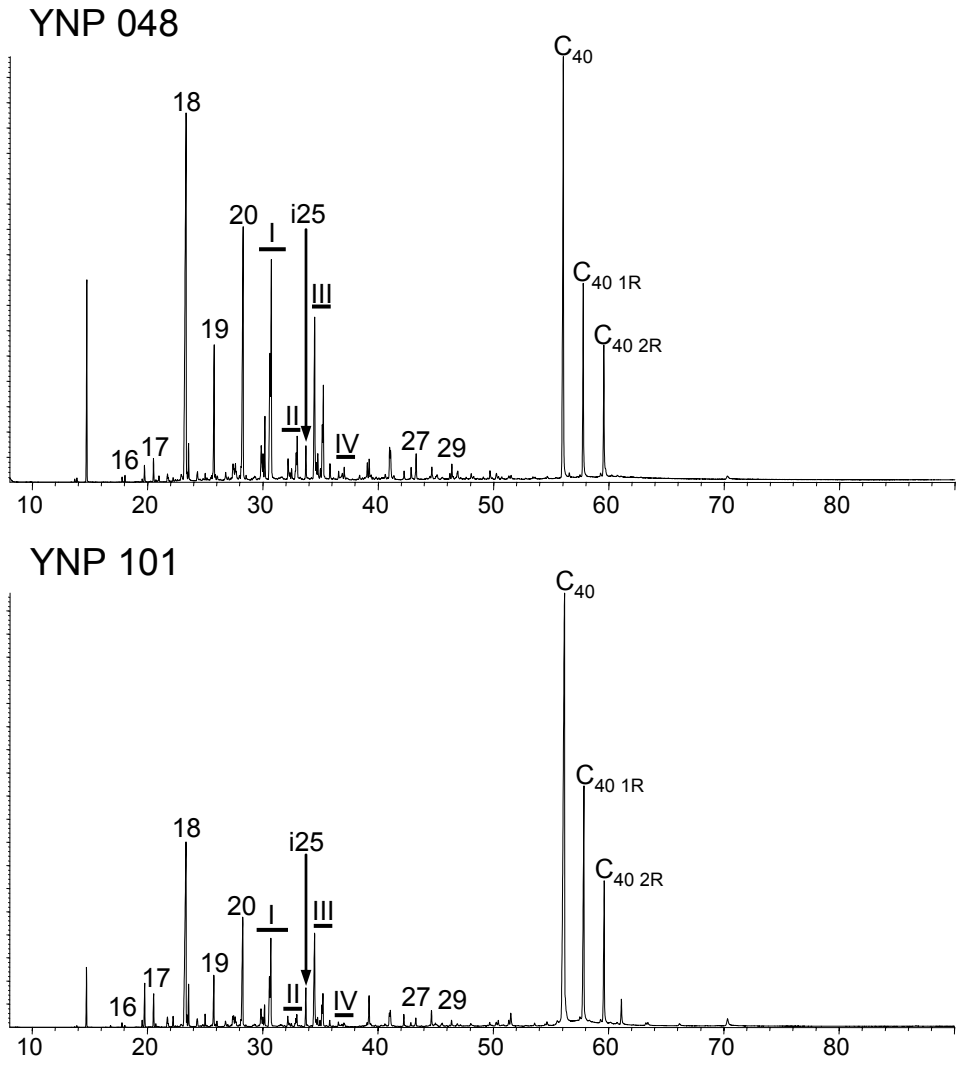

Figure 7-11: Hydrocarbons derived from ether cleavage of lipids from Ojo Caliente. Numbers refer to chain lengths of *n*-alkanes. Isoprenoids are i25: C_{25} regular isoprenoid; C_{40}: biphytane; $C_{40\ 1R}$: biphytane with one pentacyclic ring; $C_{40\ 2R}$: biphytane with two pentacyclic rings. Groups denoted I-IV are methyl-branched alkanes.

Bison Pool. The ether cleavage products shown in Figure 7-11 from Ojo Caliente reveal that there is limited variation in the year-to-year distribution of ether lipids sampled from the same location. The C_{40} products from GDGTs show similar distributions, although the sample collected in 2003 has a slightly higher degree of cyclization than that collected in 2004, which consistent with the LCMS data.

Among the products with carbon chains shorter than C_{40} we detected straight chain hydrocarbons with chain lengths primarily C_{18} to C_{20}. Ether lipids in Aquificales contain alkyl side chains predominantly of these lengths (Jahnke et al., 2001) ; Aquificales are the likely source for these lipids. We detected several groups (labeled I-IV, Figure 7-11) of methyl branched alkanes, but we are unable to specify their sources other than to identify them as bacterial. The Bison Pool samples have a relatively abundant peak monounsaturated hydrocarbon eluting immediately after nC_{25}. A C_{25} regular isoprenoid was detected in each sample, and is presumed to be archaeal.

We detected several unexpected products with hydrocarbon chain lengths greater than C_{40}. Figure 7-12 shows the portion of the chromatogram of YNP 101 that includes the

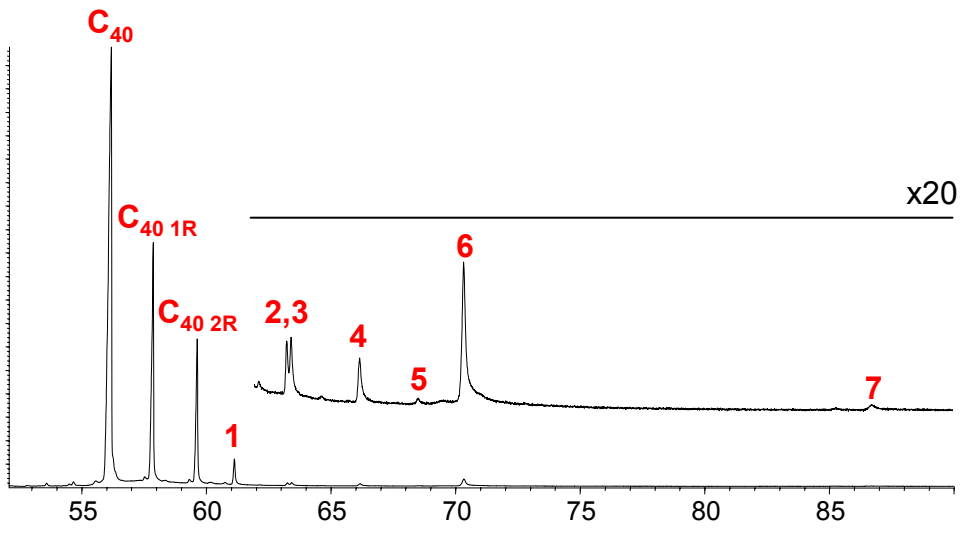

Figure 7-12: Magnified view of hydrocarbons eluting after 50 minutes derived from ether cleavage of YNP 101 lipid extract. Unknown compounds are numbered 1-7.

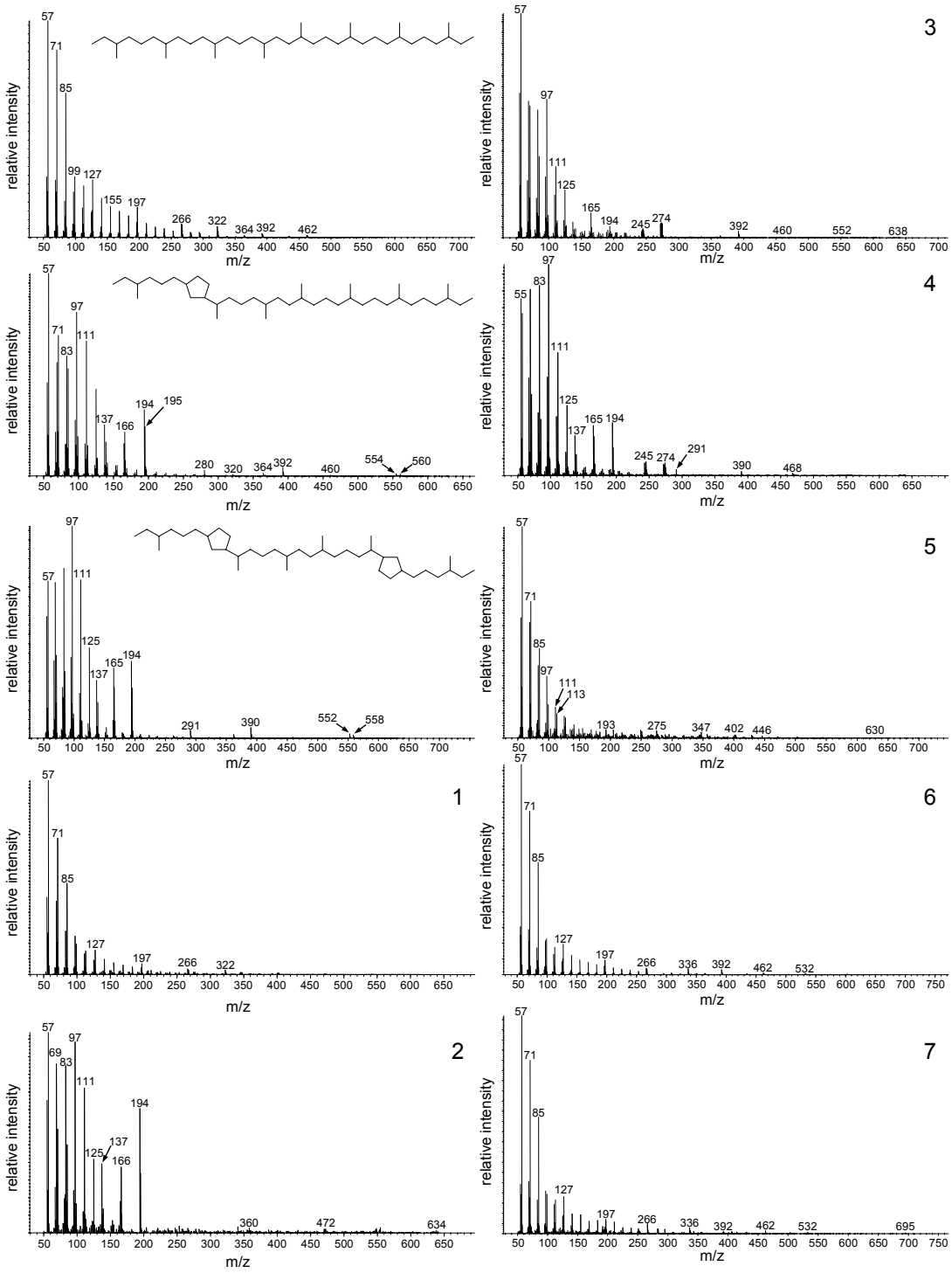

Figure 7-13: Mass spectra of compounds in the chromatogram in Figure 12. Strucutures for C_{40}, $C_{40\ 1R}$, and $C_{40\ 2R}$ are shown. Unknown structures are labeled 1-7.

C_{40} products. The first three peaks in this area of the chromatogram are readily identifiable as biphytane and biphytane derivatives with one and two pentacyclic rings (Figure 7-13**)**. However seven peaks that elute after this, with the spectra shown in Figure 7-13. These structures remain unidentified, but they share features with biphytanes. Unknown compounds 1, 5, 6, and 7 are likely acyclic isoprenoids, while unknowns 2, 3, and 4 are isoprenoids which almost certainly contain at least one ring, likely a cyclopentane ring. Although unknown peak 1 elutes at approximately the time expected for the tricyclic isoprenoid derived from crenarchaeol (DeLong et al., 1998; Schouten et al., 1998; Schouten et al., 2000), its mass spectrum excludes that structure from consideration. Due to their late elution times, each of these compounds probably contains more than 40 carbon atoms. Since they are not detected in the total lipid extracts, but released only upon cleavage of ether bonds, they could be diether or tetraether compounds, most likely tetraethers due to their large size. However the corresponding intact polar lipids have not been detected in our LCMS data to date. This may be simply a function of concentration; these compounds are far less abundant than the C_{40} compounds, and their corresponding tetraethers might well be below detection limits. Understanding the physiological function of these lipids is problematic. GDGTs are thought to span a lipid membrane, forming a monolayer that is of approximately equal dimension to conventional membrane-forming lipid bilayers. Additional methylene units would change the thickness of that bilayer. Therefore it seems probable that higher homologues of GDGTs are not in the bilayer.

Streamers growing in the chemosynthetic zone, as shown by their proliferation on the colonization apparatus in Bison Pool yielded similar products to the *in situ* streamers in Ojo Caliente (Figure 7-14). We detected abundant C_{40} isoprenoids and higher homologues in the high-temperature samples. Lower temperature samples were notably different, with much lower concentrations of C_{40} isoprenoids.

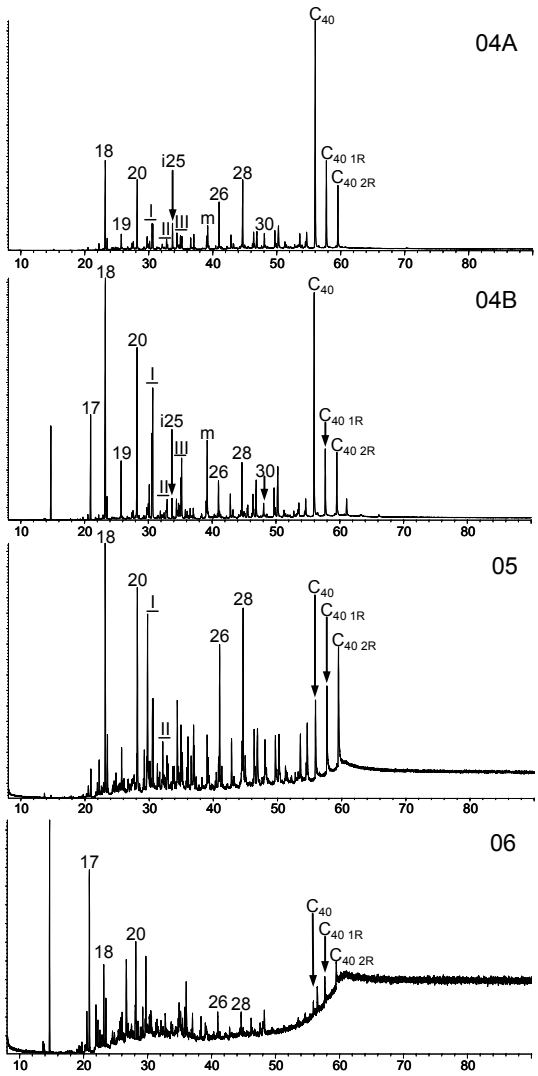

Figure 7-14: Hydrocarbons derived from ether cleavage of lipids from Bison Pool runoff stream colonization experiment. Abundances of isoprenoidal hydrocarbons relative to non-isoprenoidal hydrocarbons decrease with decrease temperature and distance from the source pool.

Peak	YNP 048	YNP 101	04A	04B	05
C18	-3.5	-2.8	-2.2	-0.4	-6.0
C19	-6.2	-7.6	-8.2	-4.3	-15.1
C20	-2.5	-1.3	-3.7	-0.1	-4.5
Grp I -1	-7.3	-4.5	-11.5	-7.9	-18.6
Grp I -2	-5.3	-2.6	-5.2	-1.2	-14.1
Grp I -3	-4.3	-2.2	-2.3	-0.4	-6.1
Grp I -4	-3.0	-1.4	-3.4		
Grp I -5	-2.9	-2.7	-2.0	0.8	-7.4
Grp II -1	-7.3	-7.1	-16.0		
Grp II -5	-5.9	-7.1	-10.4	-3.4	-16.6
iC25	-21.6	-21.2	-15.2	-15.1	
Grp III -1	-1.3	0.5	-4.2	-1.6	-5.7
Grp III -2	-3.0	-0.3	-8.9	-2.9	-15.5
Grp III -3	-4.0	-0.8	-6.2	-1.5	-29.8
Grp III -5	-3.0	-0.9	-3.9	-0.3	-9.4
IV			-3.5	-1.9	-27.7
C24			-34.9	-31.6	-26.4
C25			-31.0	-26.8	-28.4
monounsaturated hydrocarbon			-3.3	0.6	-11.4
C26			-35.6	-33.8	-34.0
iC30?		-24.9			
C27			-33.7	-30.5	-30.9
C28			-35.2	-33.9	-33.3
C29			-36.7	-34.7	-34.9
V			-33.9	-33.3	-32.3
C30			-36.9	-36.6	-33.5
C31			-34.5	-33.1	-32.1
VI			-33.3	-29.0	
biphytane	-16.0	-14.9	-12.2	-12.5	-13.8
C40 1R	-19.1	-17.3	-12.9	-12.8	-13.2
C40 2R	-22.4	-21.5	-15.5	-15.0	-16.7
C40 unknown @ 61 minutes		-18.5			

Table 7-4: Stable carbon isotope compositions of hydrocarbons derived from ether cleavage reactions from Bison Pool and Ojo Caliente. Roman numerals refer to groups of methyl-branched alkanes; within each group the carbon number of the alkanes are the same. There are up to 5 isomers within each group (e.g. Group I-1 – I-5).

7.3.4. GC-irms

We analyzed the compound-specific ^{13}C contents of hydrocarbons derived from ether cleavage reactions and the results are reported in Table 7-4. Samples from Ojo Caliente and from Bison Pool are consistent in that the same hydrocarbons show similar $\delta^{13}C$ values. C_{18} to C_{20} *n*-alkanes are relatively enriched in ^{13}C with $\delta^{13}C$ values between 0‰ and -8‰ in the high temperature samples. In sample 05, nC_{19} is more depleted in ^{13}C with $\delta^{13}C$ = -15.1‰.

Archaeal lipids are more depleted in ^{13}C than *n*-alkanes. The C_{25} regular isoprenoid, detected in all the ether cleavage fractions has $\delta^{13}C$ near -21‰ at Ojo Caliente, and near -15‰ in Bison Pool runoff. C_{40} isoprenoids are more variable in their ^{13}C contents. In all samples biphytane is the C_{40} lipid most enriched in ^{13}C, and ^{13}C content decreases with increasing number of rings. This pattern was strongest in the high temperature samples, where the difference between biphytane and the $C_{40\ 2R}$ (the C_{40} isoprenoid with two rings) was greater than 6‰. This pattern is not expected if each of these compounds derives from the same source organism. Although the biosynthesis of C_{40} lipids is not well understood, it is thought that a C_{86} tetraether core is first synthesized as two C_{43} diethers that are subsequently joined (Koga and Morii, 2007). The introduction of rings into large molecules such as this is unlikely to be associated with a large isotopic fractionation. In ether-cleavage products of a *Sulfolobus* culture (Figure 7-14, Table 7-5), the $\delta^{13}C$ of C_{40} isoprenoids differed by less than 2‰.

At Ojo Caliente the groups of unidentified branched alkanes (denoted I-IV in Figure 7-11), which derive from an unknown source, had $\delta^{13}C$ that were greater than -8‰. These values resembled the *n*-alkanes derived from Aquificales. However, in the Bison Pool outflow some of these branched alkanes were much more depleted in ^{13}C, suggesting that they might derive from multiple sources.

As a general pattern, in both the *in situ* streamer communities at Ojo Caliente and in the streamers that colonized the apparatus at Bison Pool, bacterial lipids were enriched in ^{13}C relative to archaeal lipids. The Aquificales products at these locations were also

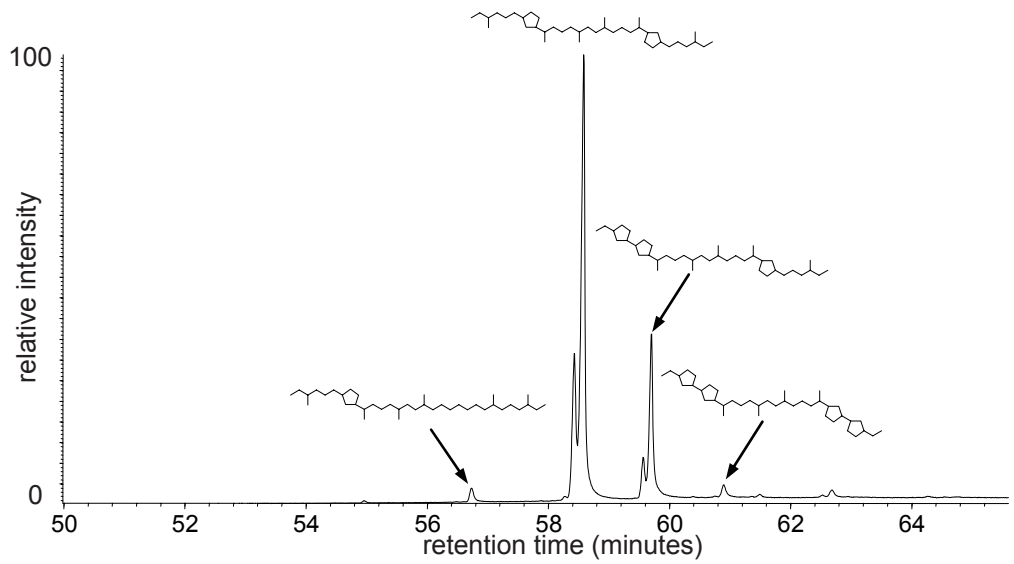

Figure 7-15: Hydrocarbons derived from ether cleavage of lipids from *Sulfolobus*.

Compound	$\delta^{13}C$
$C_{40\ 1R}$	-16.3
$C_{40\ 2R}$ (1)	-13.1
$C_{40\ 2R}$ (2)	-14.0
$C_{40\ 3R}$ (1)	-12.4
$C_{40\ 3R}$ (2)	-14.3
$C_{40\ 4R}$	-16.3

Table 7-5: Stable carbon isotope compositions of hydrocarbons derived from ether cleavage reactions from *Sulfolobus* culture

enriched in ^{13}C relative to the Aquificales from Octopus Spring (Jahnke et al., 2001). However that study examine ester-linked lipids, while this study examines ether-linked lipids. A comprehensive study of both ether- and ester-linked lipids should be undertaken for a better understanding of carbon cycling in these environments. Jahnke et al. (2001) report that Aquificales at Octopus Spring likely consume formate as their carbon substrate, but Aquificales are also capable of autotrophic growth via the reductive tricarboxylic acid cycle (rTCA). Such growth normally produces biomass depleted by 4-13‰ relative to

CO_2(aq) (Hayes, 2001), although Jahnke et al. (2001) observed only a 3‰ between CO_2 and the biomass of *Thermocrinus ruber* in culture.

The $\delta^{13}C$ values of Aquificales at Ojo Caliente and Bison Pool are consistent with the fractionation seen in autotrophic growth of *Thermocrinus*. The discrepancy between these results and that from Octopus Spring (Jahnke et al., 2001) suggests that there variability in metabolic strategy between similar streamer communities in various hot springs. Future studies trageting the full range of lipid products may shed light on this hypothesis.

7.4. Conclusions

The presence of isotopic variability between compounds and of organic carbon that is highly enriched in ^{13}C is not unprecedented. Values of δ_{org} vary by as much as 25‰ in alkaline hot springs in New Zealand and contain Aquificales-derived lipids with $\delta^{13}C$ as high as +3.9‰ (Pancost et al., 2006). Microbial mats in Yellowstone hot springs containing *Chloroflexus* communities have been reported to contain lipids with $\delta^{13}C$ as high as -8.9‰ (van der Meer et al., 2000). In each case the extraordinary enrichment of ^{13}C has been attributed to the pathway of carbon fixation. *Chloroflexus* operates primarily as an autotroph in these environments, fixing carbon by the 3-hydroxypropionate pathway, and the Aquificales are likely to be rTCA autotrophs. In deep sea alkaline thermal environments at the Lost City hydrothermal field, similar isotopic compositions have been reported in the lipids derived from methanogens (Kelley et al., 2005). In that case the ^{13}C enrichment has been attributed to carbon-limitation (Chapter 3). In terrestrial environments that are in constant contact with atmospheric CO_2, limitation of available carbon seems unlikely. This suggests that speciation of DIC, controlled by pH and temperature may be crucial. As temperatures and pH rise the speciation of DIC is driven away from CO_2 and towards bicarbonate and carbonate. At high temperatures and pH the amount of inorganic carbon available as CO_2 is small. The role of changes in DIC concentration and $\delta^{13}C$ due to disequilibrium concentrations in vent fluids is not well constrained. Studies in other alkaline

thermal environments have suggested that CO_2 is oversaturated in high temperature fluids and rapidly degasses as waters cool. The magnitude of equilibrium isotope fractionation between CO_2 and carbonate is inversely correlated with temperature, so degassing as fluids cool produces increased enrichments in ^{13}C of residual DIC. At Mammoth Hot Springs degassing produces an enrichment in δ_{DIC} of about 5‰ (Fouke et al., 2000). At Bison Pool the largest enrichments in $\delta^{13}C$ of organic are seen in high temperature samples. This result is not likely to be produced by the effects of degassing, and may reflect a combination of three processes: speciation of DIC away from CO_2, $\delta^{13}C$ of CO_2 that is close to that of DIC at high temperatures, and the processes by which organisms assimilate carbon.

These results invite the question of how frequently biomass and individual lipids with high $\delta^{13}C$ values occur in alkaline thermal environments. This is a relevant line of inquiry for students of geobiology. In Archaean rocks including hydrothermal deposits, organic carbon with $\delta^{13}C$ near -25‰ has been proposed to be biological in origin (Duck et al., 2007; Rosing, 1999). However, ^{13}C depletion is not sufficient for a claim of biogenicity (Brasier et al., 2004) because similar depletions may be produced abiotically (McCollom and Seewald, 2006). It has usually been implicitly assumed that a ^{13}C depletion similar in magnitude to that imposed by known carbon assimilation pathways is necessary to infer that ancient carbon is biological; carbon lacking this depletion would be interepreted as abiotic. In modern hydrothermal systems, unmistakably biological carbon lacking the ^{13}C depletion typically imposed by carbon assimilation pathways shows that such assumptions are not always valid.

7.5. References

Barns, S.M., Delwiche, C.F., Palmer, J.D., Pace, N.R., 1996. Perspectives on archaeal diversity, thermophily and monophyly from environmental rRNA sequences. Proceedings of the National Academy of Sciences of the United States of America 93(17), 9188-9193.

Bligh, E.G., Dyer, W.J., 1959. A rapid method of total lipid extraction and purification. Canadian journal of biochemistry and physiology 37(8), 911-7.

Bock, G.R., Goode, J.A., 1996. Evolution of hydrothermal ecosystems on Earth (and Mars?), pp. 334. Wiley, Chichester.

Brasier, M., Green, O., Lindsay, J., Steele, A., 2004. Earth's oldest (approximately 3.5 Ga) fossils and the 'Early Eden hypothesis': questioning the evidence. Origins of life and evolution of the biosphere : journal of the International Society for the Study of the Origin of Life 34(1-2), 257-69.

Brasier, M., McLoughlin, N., Green, O., Wacey, D., 2006. A fresh look at the fossil evidence for early Archean cellular life. Philosophical Transactions of the Royal Society of London, Series B: Biological Sciences 361(1470), 887-902.

Brock, T.D., 1978. *Thermophilic Microorganisms and Life at High Temperatures*. Springer-Verlag, New York.

Ciccarelli, F., D., Doerks, T., von Mering, C., Creevey Christopher, J., Snel, B., Bork, P., 2006. Toward automatic reconstruction of a highly resolved tree of life. Science 311(5765), 1283-7.

DeLong, E.F., King, L.L., Massana, R., Cittone, H., Murray, A., Schleper, C., Wakeham, S.G., 1998. Dibiphytanyl Ether Lipids in Nonthermophilic Crenarchaeotes. Applied and Environmental Microbiology 64(3), 1133-1138.

Duck, L.J., Glikson, M., Golding, S.D., Webb, R.E., 2007. Microbial remains and other carbonaceous forms from the 3.24 Ga Sulphur Springs black smoker deposit, Western Australia. Precambrian Research 154(3-4), 205-220.

Farquhar, J., Peters, M., Johnston, D.T., Strauss, H., Masterson, A., Wiechert, U., Kaufman, A.J., 2007. Isotopic evidence for Mesoarchaean anoxia and changing atmospheric sulphur chemistry. 449(7163), 706-709.

Fouke, B.W., Farmer, J.D., Des Marais, D.J., Pratt, L., Sturchio, N.C., Burns, P.C., Discipulo, M.K., 2000. Depositional facies and aqueous-solid geochemistry of travertine-depositing hot springs (Angel Terrace, Mammoth Hot Springs, Yellowstone National Park, U.S.A.). Journal of sedimentary research. Section A, Sedimentary petrology and processes : an international journal of SEPM (Society for Sedimentary Geology) 70(3), 565-85.

Garcia, J.-L., Ollivier, B., Whitman, W.B., 2006. The order Methanomicrobiales. In: M. Dworkin, S. Falkow, E. Rosenberg, K.-H. Schleifer, E. Stackebrandt (Eds.), *The Prokaryotes 3*, pp. 208-230. Springer, New York.

Gliozzi, A., Relini, A., Chong, P.L.-G., 2002. Structure and permeability properties of biomimetic membranes of bolaform archaeal tetraether lipids. Journal of Membrane Science 206(1-2), 131-147.

Hayes, J.M., 2001. Fractionation of carbon and hydrogen isotopes in biosynthetic processes. Reviews in Mineralogy & Geochemistry 43, 225-277.

Jahnke, L.L., Eder, W., Huber, R., Hope, J.M., Hinrichs, K.-U., Hayes, J.M., Des

Marais, D.J., Cady, S.L., Summons, R.E., 2001. Signature Lipids and Stable Carbon Isotope Analyses of Octopus Spring Hyperthermophilic Communities Compared with Those of Aquificales Representatives. Applied and Environmental Microbiology 67(11), 5179-5189.

Jones, B., Renaut, R.W., Rosen, M.R., 2001. Taphonomy of Silicified Filamentous Microbes in Modern Geothermal Sinters--Implications for Identification. Palaios 16(6), 580-592.

Kelley, D.S., Karson, J.A., Fruh-Green, G.L., Yoerger, D.R., Shank, T.M., Butterfield, D.A., Hayes, J.M., Schrenk, M.O., Olson, E.J., Proskurowski, G., Jakuba, M., Bradley, A., Larson, B., Ludwig, K., Glickson, D., Buckman, K., Bradley, A.S., Brazelton, W.J., Roe, K., Elend, M.J., Delacour, A., Bernasconi, S.M., Lilley, M.D., Baross, J.A., Summons, R.E., Sylva, S.P., 2005. A Serpentinite-Hosted Ecosystem: The Lost City Hydrothermal Field. Science 307(5714), 1428-1434.

Koga, Y., Morii, H., 2007. Biosynthesis of ether-type polar lipids in archaea and evolutionary considerations. Microbiol Mol Biol Rev FIELD Full Journal Title:Microbiology and molecular biology reviews : MMBR 71(1), 97-120.

Konhauser, K.O., Phoenix, V.R., Bottrell, S.H., Adams, D.G., Head, I.M., 2001. Microbial-silica interactions in Icelandic hot spring sinter: possible analogues for some Precambrian siliceous stromatolites. Sedimentology 48(2), 415-433.

McCollom, T.M., Seewald, J.S., 2006. Carbon isotope composition of organic compounds produced by abiotic synthesis under hydrothermal conditions. Earth and Planetary Science Letters 243(1-2), 74-84.

Meyer-Dombard, D.R., Shock, E.L., Amend, J.P., 2005. Archaeal and bacterial communities in geochemically diverse hot springs of Yellowstone National Park, USA. Geobiology 3(3), 211-227.

Nelson, K.E., Clayton, R.A., Gill, S.R., Gwinn, M.L., Dodson, R.J., Haft, D.H., Hickey, E.K., Peterson, J.D., Nelson, W.C., Ketchum, K.A., McDonald, L., Utterback, T.R., Malek, J.A., Linher, K.D., Garrett, M.M., Stewart, A.M., Cotton, M.D., Pratt, M.S., Phillips, C.A., Richardson, D., Heidelberg, J., Sutton, G.G., Fleischmann, R.D., Eisen, J.A., Fraser, C.M., 1999. Evidence for lateral gene transfer between Archaea and bacteria from genome sequence of Thermotoga maritima. Nature 399(6734), 323-9.

Nisbet, E.G., Sleep, N.H., 2001. The habitat and nature of early life. Nature 409(6823), 1083-1091.

Ohta, H., Shimojima, M., Awai, K., Masuda, T., Takamiya, K., 1997. Glycolipids in chloroplast thylakoid membrane. The mechanism for the biosynthesis and evolutionary origin. Tanpakushitsu Kakusan Koso 42(16), 2601-2612.

Pancost, R.D., Pressley, S., Coleman, J., M., Benning, L.G., Mountain, B.W., 2005. Lipid biomolecules in silica sinters: indicators of microbial biodiversity. Environmental Microbiology 7(1), 66-77.

Pancost, R.D., Pressley, S., Coleman, J.M., Talbot, H.M., Kelly, S.P., Farrimond, P., Schouten, S., Benning, L., Mountain, B.W., 2006. Composition and implications of diverse lipids in New Zealand geothermal sinters. Geobiology 4(2), 71-92.

Pavlov, A.A., Kasting, J.F., 2002. Mass-Independent Fractionation of Sulfur Isotopes in Archean Sediments: Strong Evidence for an Anoxic Archean Atmosphere.

Astrobiology 2(1), 27-41.
Rasmussen, B., 2000. Filamentous microfossils in a 3,235-million-year-old volcanogenic massive sulphide deposit. Nature 405, 676-697.
Raymond, J., Siefert, J.L., Staples, C.R., Blankenship, R.E., 2004. The natural history of nitrogen fixation. Molecular Biology and Evolution 21(3), 541-554.
Reysenbach, A.-L., Cady, S.L., 2001. Microbiology of ancient and modern hydrothermal systems. Trends in Microbiology 9(2), 79-86.
Reysenbach, A.L., Wickham, G.S., Pace, N.R., 1994. Phylogenetic analysis of the hyperthermophilic pink filament community in Octopus Spring, Yellowstone National Park. Applied and Environmental Microbiology 60(6), 2113-9.
Rosing, M.T., 1999. 13C-depleted carbon microparticles in >3700-Ma sea-floor sedimentary rocks from West Greenland. Science (Washington, D. C.) 283(5402), 674-676.
Schouten, S., Hoefs, M.J.L., Koopmans, M.P., Bosch, H.-J., Sinninghe Damste, J.S., 1998. Structural characterization, occurrence and fate of archaeal ether-bound acyclic and cyclic biphytanes and corresponding diols in sediments. Organic Geochemistry 29(5-7), 1305-1319.
Schouten, S., Hopmans, E.C., Pancost, R.D., Damste, J.S.S., 2000. Widespread occurrence of structurally diverse tetraether membrane lipids: Evidence for the ubiquitous presence of low-temperature relatives of hyperthermophiles. Proceedings of the National Academy of Sciences of the United States of America 97(26), 14421-14426.
Schouten, S., van der Meer, M.T.J., Hopmans, E.C., Rijpstra, W.I.C., Reysenbach, A.-L., Ward, D.M., Damste, J.S.S., 2007. Archaeal and bacterial glycerol dialkyl glycerol tetraether lipids in hot springs of Yellowstone National Park. Applied and Environmental Microbiology 73(19), 6181-6191.
Setchell, W.A., 1903. The upper temperature limits of life. Science 17, 934-937.
Stetter, K.O., 1996. Hyperthermophiles in the history of life. In: G. Bock, J. Goode (Eds.), *Evolution of hydrothermal ecosystems on Earth (and Mars?)*, pp. 1-18. Wiley, Chichester.
Sturt, H.F., Summons, R.E., Smith, K., Elvert, M., Hinrichs, K.-U., 2004. Intact polar membrane lipids in prokaryotes and sediments deciphered by high-performance liquid chromatography/electrospray ionization multistage mass spectrometry—new biomarkers for biogeochemistry and microbial ecology. Rapid Communications in mass spectrometry 18, 617-628.
Trewin, N.H., 1996. The Rhynie cherts: an early Devonian ecosystem preserved by hydrothermal activity. In: G. Bock, J. Goode (Eds.), *Evolution of hydrothermal ecosystems on Earth (and Mars?)*, pp. 131-149. Wiley, Chichester.
Uda, I., Sugai, A., Itoh, Y.H., Itoh, T., 2001. Variation in molecular species of polar lipids from Thermoplasma acidophilum depends on growth temperature. Lipids 36(1), 103-105.
van der Meer, M.T., Schouten, S., de Leeuw, J.W., Ward, D.M., 2000. Autotrophy of green non-sulphur bacteria in hot spring microbial mats: biological explanations for isotopically heavy organic carbon in the geological record. Environmental Microbiology 2(4), 428-35.

Walter, M.R., Desmarais, D., Farmer, J.D., Hinman, N.W., 1996. Lithofacies and biofacies of mid-Paleozoic thermal spring deposits in the Drummond Basin, Queensland, Australia. Palaios FIELD Full Journal Title:Palaios 11, 497-518.

Zang, W.-L., 2007. Deposition and deformation of late Archaean sediments and preservation of microfossils in the Harris Greenstone Domain, Gawler Craton, South Australia. Precambrian Research 156(1-2), 107-124.

Zhang, C., L., Pearson, A., Li, Y.-L., Mills, G., Wiegel, J., 2006. Thermophilic temperature optimum for crenarchaeol synthesis and its implication for archaeal evolution. Applied and Environmental Microbiology 72(6), 4419-22.

Zhang, C.L., Fouke, B.W., Bonheyo, G.T., Peacock, A.D., White, D.C., Huang, Y., Romanek, C.S., 2004. Lipid biomarkers and carbon-isotopes of modern travertine deposits (Yellowstone National Park, USA): Implications for biogeochemical dynamics in hot-spring systems. Geochimica et Cosmochimica Acta 68(15), 3157-3169.

Appendix 1

'Reverse methanogenesis' as a hypothesis for archaeal methanotrophy

A1.1 'Reverse Methanogenesis'

'Reverse methanogenesis' has been the primary hypothesis invoked to explain the anaerobic oxidation of methane. This hypothesis suggests that ANME consortia are supported by interspecies hydrogen transfer between methanotrophic archaea and sulfate reducing bacteria (Valentine and Reeburgh, 2000). In this model, CH_4 is oxidized by methanotrophic archaea to CO_2 and H_2. This reaction can proceed only if it is thermodynamically favored. Thermodynamic favorability is achieved if H_2 is continually removed by a sulfate-reducing syntroph. Environmental genomics supports this hypothesis (Hallam et al., 2004), showing that ANME-1 archaeal methanotrophs possess nearly the same suite of genes as methanogens for encoding enzymes along the pathway between CO_2 and CH_4 (ANME-1 lack only *mer*) and could, in principle, operate as methanogens in reverse.

If this hypothesis is correct, then the millimolar hydrogen concentrations in Lost City vent fluids would be expected to exclude anaerobic methanotrophy. However, several reports have suggested that the interspecies hydrogen transfer hypothesis may be incorrect. Addition of H_2 to AOM enrichments does not significantly increase the sulfate reduction rate (Nauhaus et al., 2005). This may be inconsistent with the interspecies hydrogen transfer hypothesis, because the sulfate-reducing syntroph would be expected to be a H_2 consumer. More recently an isotope-tracer experiment showed that addition of H_2 to AOM enrichments decreases the rate of methane oxidation, but does not halt it (Moran et al., 2007). Because high hydrogen levels would be expected to thermodynamically inhibit methanotrophy under the 'reverse methanogenesis' hypothesis, this was proposed as evidence that the intermediate was a substance other than H_2.

Moran et al. (2007) propose methyl sulfide (MeSH) as an alternative intermediate metabolite, and showed that addition of methyl sulfides to AOM enrichements results in

a decrease in methane oxidation rates (Moran et al., 2007). Methyl-sulfide is an attractive option for the intermediate, because it is easily derived from methyl-S-CoM, which would be the first product formed from methane by a methanogen operating in reverse (Hallam et al., 2004). However, the evidence presented by Moran et al. (2007) is unconvincing for several reasons.

First, the magnitude of the decrease in rate of methanotrophy is similar upon addition of methyl sulfide as it is with addition of hydrogen. Moran et al. (2007) report that addition of hydrogen resulted in a 33% decrease in CH_4 oxidation over 60 days, with all of the decrease in rate occurring in the first week. When dosed with MeSH, the methane oxidation rates are reported to drop 68%. However, it is not clear that this calculation is valid. Figure 3 of Moran et al. (2007) indicates that the culture that was dosed with MeSH on day 14 of the experiment was already growing more slowly than the control culture, even before MeSH addition. The report of a 68% drop in methane oxidation rate in the experimental culture compared to the control does not account for the reduced growth rate of the experimental culture. If this were taken into account the true reduction in growth rate may be closer to 50%.

This 50% reduction in methane oxidation rate is attributed to the inhibitory effects of supplying the enrichment culture with the metabolic intermediate between archaea and bacteria. It is subject to question whether a 50% reduction in methane oxidation rate with supply of MeSH is sufficient evidence for thermodynamic inhibition by this substrate when a 33% reduction with supply of hydrogen has been presented as evidence that hydrogen is *not* the intermediate. Both compounds result in a decrease in methane oxidation rate that is of similar magnitude, so it is unclear why the interpretations should differ.

Second, no evidence is presented that the reduction in methane oxidation rate upon MeSH addition is due to thermodynamic inhibition. There are a number of ways that MeSH might inhibit methane oxidation. MeSH might be toxic to methanogens, or it could act to inhibit an enzyme involved in methane oxidation. No evidence has been presented that

excludes these possibilities.

Third, if MeSH is the intermediate, its addition should promote a large increase in sulfate reduction rates. This could be dectected as an increase in the sulfide concentration, but no such data is reported.

Methyl sulfide is an attractive candidate for the metabolic intermediate in AOM consortia, but its identification as the intermediate has not been adequately demonstrated. Both MeSH and hydrogen addition result in large decreases in methane oxidation rates, but questions remain about both. The nature of the metabolic intermediate remains an open question.

A1.2 References

Hallam, S., J., Putnam, N., Preston Christina, M., Detter John, C., Rokhsar, D., Richardson Paul, M., DeLong Edward, F., 2004. Reverse methanogenesis: testing the hypothesis with environmental genomics. Science 305(5689), 1457-62.

Moran, J.J., Beal, E.J., Vrentas, J.M., Orphan, V.J., Freeman, K.H., House, C.H., 2007. Methyl sulfides as intermediates in the anaerobic oxidation of methane. Environmental Microbiology, doi:10.1111/j.1462-2920.2007.01441.x.

Nauhaus, K., Treude, T., Boetius, A., Kruger, M., 2005. Environmental regulation of the anaerobic oxidation of methane: a comparison of ANME-I and ANME-II communities. Environmental Microbiology 7(1), 98-106.

Valentine, D.L., Reeburgh, W.S., 2000. New perspectives on anaerobic methane oxidation. Environmental Microbiology 2(5), 477-484.

THIS PAGE INTENTIONALLY LEFT BLANK

Appendix 2

Dissolved Inorganic Carbon at the Lost City Hydrothermal Field

A2.1 Introduction

Several questions remain outstanding regarding dissolved inorganic carbon in Lost City Vent fluids. The foremost of these is the concentration of DIC. Kelley et al. (2005) report that "carbonate alkalinity is less than one-third of seawater values". We use this and other information about vent fluids to evaluate this interpretation, to better understand the precipitation of carbonate at Lost City, and to evaluate the potential for carbon-limitation of microbial growth.

A2.2 Background

Aliquots of hydrothermal vent fluids were not collected at the Lost City Hydrothermal Field with the specific intention to preserve them and analyze their DIC contents (Kelley et al., 2005). For this reason, fluid samples collected for sulfur isotope analyses were also used for DIC analysis. Initial attempts lead to errors (Kelley et al., 2005), the final result is reported only with respect to carbonate alkalinity ("less than one-third of seawater values").

A2.3 Carbonate Precipitation

Carbonate towers precipitate at Lost City because calcium carbonate is oversaturated in some mixture of vent fluids and seawater. This precipitation may be biologically mediated or influenced. Several lines of evidence suggest that this precipitation occurs when vent fluids are mixed with seawater. These include:

A2.3.1 $\Delta^{14}C$ of carbonate:

Actively venting structures give modern radiocarbon ages. This indicates that

carbonate is directly derived from seawater, and may contain bomb radiocarbon. (Früh-Green et al., 2003)

A2.3.2 Sr isotopes:

Active vent structures contain $^{87}Sr/^{86}Sr$ carbonate = 0.7070 to 0.7075 This can be compared to seawater and mantle end-members (seawater = 0.7091, mantle = 0.7025). The $^{87}Sr/^{86}Sr$ of carbonate suggests that precipitation of aragonite and brucite is derived from mixing of hydrothermal fluids (assumed to equilibrate at mantle $^{87}Sr/^{86}Sr$) in an approximately 27:73 ratio with seawater. (Fruh-Green et al., 2003)

A2.3.3 $\delta^{18}O$:

Older vent structures have $\delta^{18}O$ values in the range of +1‰ to +3‰ vs. VPDB. Fruh-Green et al. (2003) suggest that this is consistent with precipitation from glacial waters, but note that other samples are strongly enriched in ^{18}O. The range of $\delta^{18}O$ in vents is -7‰ to +5‰ (Kelley et al., 2005). If these precipitated in equilibrium with water with $\delta^{18}O_{H2O}$ = 0‰ vs. VSMOW, it indicates precipitation temperatures of up to 42 ˚C (Zhou and Zheng, 2003). However the $\delta^{18}O$ values above +2‰ vs. VPDB can not be explained by equilibrium precipitation, and must reflect ^{18}O enrichment, presumably due to water-rock interaction, and precipitation at ambient temperatures.

One active structure has $\delta^{18}O$ = +2.2‰vs. VPDB (Fruh-Green et al., 2003). Assuming that carbonates are precipitating from water with $\delta^{18}O_{H2O}$ = +0‰ vs. VSMOW, this indicates a precipitation temperature of about 2.7 ˚C, although fluids at this site are 75 ˚C (Fruh-Green et al., 2003). This seemingly indicates a dominance of seawater over vent fluid in the mixture from which carbonate precipitates. Basement fissures have $\delta^{18}O$ = -14.2‰ to -16.8‰, suggesting precipitation at temperatures of 115 ˚C to 135 ˚C.

A2.3.4 Ca concentrations

High T fluids have higher Ca (normalized to zero Mg) than low T fluids This indicates that carbonate is precipitating (lowering Ca) upon seawater mixing (Kelley et al., 2001)

A2.3.5 Magnesium

Active vent structures contain up to 27 wt% magnesium. If vent fluids contain zero Mg, then the Mg in carbonate must be derived from seawater, suggesting mixing during precipitation. Most extinct vents have equilibrated with seawater and contain < 1 wt% Mg (Kelley et al., 2005; Ludwig et al., 2006).

A2.4 Fluid Chemistry

A2.4.1 Saturation state

A summary of bulk fluid chemistry is shown in Table A2-1. At the conditions measured for end-member vent fluids, carbonate should be oversaturated in vent fluids. This is consistent with the apparent precipitation of high temperature carbonate in fracture fills, but does not explain why carbonate towers precipitate only upon mixing with seawater.

There are two possible explanations for why carbonate precipitation mainly occurs only upon mixing with seawater. First, carbonate precipitation can be kinetically inhibited in many of the vent fluids. This occurs in surface seawater where calcium carbonate is oversaturated, but presumably because of the presence of 53 mM Mg^{2+}, which forms ion-

Vent fluid T	40 ºC - 90 ºC
pH	9 - 11
$[CH_4]$	1 - 2 mM
$[H_2]$	1 - 15 mM
$[Ca^{2+}]$	10 - 30 mM
$[Mg^{2+}]$	0
CA	< 1/3 seawater

Table A2-1: Bulk properties of Lost City vent fluids

pairs with CO_3^{2-}, effectively lowering CO_3^{2-} activity and poisoning calcium carbonate precipitation. However, Lost City vent fluids contain zero Mg^{2+}. Without the presence of the major kinetic inhibitor, kinetic inhibition of carbonate precipitation is unlikely.

The second possibility is that one or more parameters have been measured incorrectly. The most likely culprit is the DIC concentration, which is not directly reported at all. Since carbonate oversaturation increases with temperature, precipitation of calcium carbonate at ambient temperatures suggests that seawater must provide a key ingredient for carbonate precipitation. This suggests that DIC in fluid waters is actually less than the equivalent of one-third of seawater carbonate alkalinity.

A simple fluid mixing model suggests that if DIC concentrations are low, both seawater and vent fluids are undersaturated or near saturated with respect to calcium carbonate, but that the mixed fluid is massively oversaturated (Figure A2-1). Addtionally, the mixed fluid have lower magnesium ion concentrations than seawater, depressing this kinetic barrier to precipitation. This model assumes that total alkalinity, temperature, cations (Mg^{2+}, Ca^{2+}) and DIC undergo conservative mixing, and and iteratively calculates calculates pH, carbonate speciation, and saturation state for the mixed fluid.

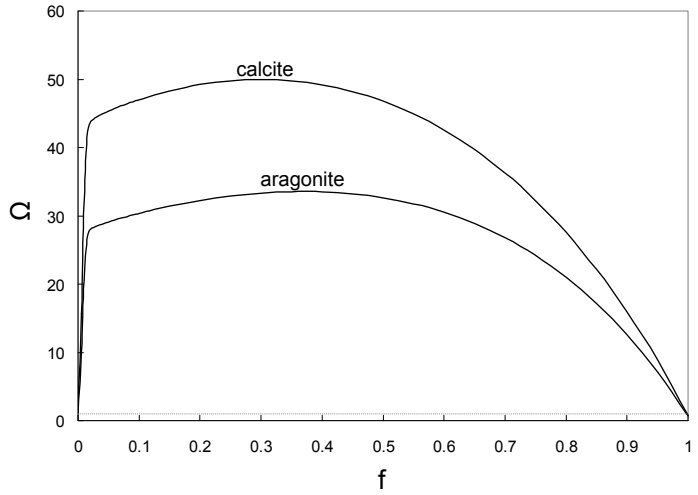

Figure A2-1: Calcite and aragonite saturation state attained by mixing two end member fluids. Seawater end member pH = 8.1, T = 7 ºC, S = 35, total alkalinity (TA) = 2.2 mmol kg^{-1}, carbonate alkalinity (CA) = 2.125 mmol kg^{-1}, DIC = 2.1 mmol kg^{-1}, [Ca^{2+}] = 10.4 mmol kg^{-1}. Hydrothermal end member pH = 11, T = 70 ºC, S = 35.5, TA = 183 mmol kg^{-1}, CA = 0.02 mmol kg^{-1}, DIC = 0.01 mmol kg^{-1}, [Ca^{2+}] = 30 mmol kg^{-1}. f = fraction hydrothermal fluid in mixture.

A2.4.2 Controls on $\delta^{18}O_{carbonate}$

If mixed fluids are precipitating aragonite, we could make the assumption that they are in equilibrium with the precipitating carbonate. If that is true, the $\delta^{18}O_{carbonate}$ should reflect the ^{18}O contents of the mixed fluids and the temperature of precipitation, and those mixed fluids are a mass balance between the two end members. If we assume a mixture of seawater ($\delta^{18}O$ = 0‰, 7 ˚C) and vent fluid ($\delta^{18}O$ = +2‰, 70 ˚C), the aragonite precipitated in equilibrium will fall near the curve denoted in Figure A2-2.

Most values of $\delta^{18}O_{aragonite}$ fall close to 0‰ vs. VPDB, but a few range as low as -7‰ and as high as +13‰ (Kelley et al., 2005). The higher values are interpreted to reflect enrichment during fluid/rock interaction, presumably after precipitation. The lower values are consistent with precipitation at high temperature.

However, the assumption of isotope equilibrium during precipitation may not be valid. Equilibration of ^{18}O between carbonate and H_2O occurs only via hydration or hydroxylation of CO_2 (Zeebe and Wolf-Gladrow, 2001). In the high temperature, high pH vent fluids, CO_2 is almost non-existent, and even in the mixed fluids its concentration is very low. The time required to achieve ^{18}O equilibrium in these fluids is probably on the order of 10^4 minutes

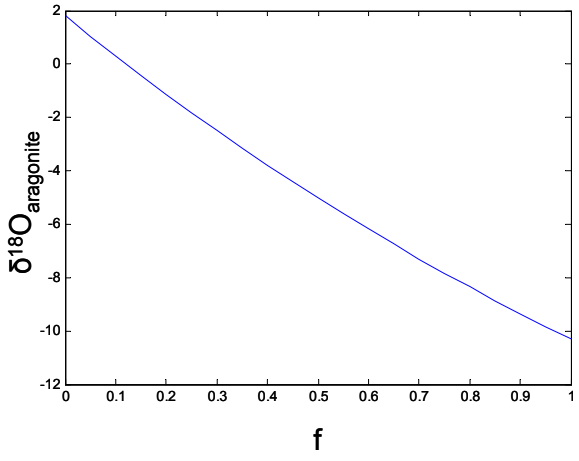

Figure A2-2: $\delta^{18}O$ of calcium carbonate precipitated in equilibrium with fluid mixture as a function of f (fraction vent fluid). End member compositions as described in main text.

(Zeebe and Wolf-Gladrow, 2001), while the precipitation rate is likely to be very fast – several 10's of μmol per square meter per hour (Zhong and Mucci, 1993). If precipitation is fast enough that equilibrium can not be attained, then the $\delta^{18}O_{aragonite}$ should still reflect a pseudo-equilibrium, because hydrothermal fluid $\delta^{18}O_{aragonite}$ should be in equilibrium with vent fluid temperatures, and seawater $\delta^{18}O_{carbonate}$ should be in equilibrium with seawater temperatures. The input of hydrothermal carbonate to the precipitated aragonite should add an ^{18}O-depleted component to the bulk precipitate. In this case $\delta^{18}O$ can be considered a mass balance between hydrothermal and seawater carbonate contributions, and not a temperature proxy. This could only be avoided if hydrothermal water were heavy with regard to $\delta^{18}O$ in the correct amount to exactly offset the temperature effect (which seems extremely unlikely) or if there is some measure of equilibrium occurring, which is difficult at high pH. If $\delta^{18}O_{carbonate}$ reflects a mass balance of hydrothermal and seawater inputs, then in most cases at Lost City it supports an extremely low input of hydrothermal carbonate into the carbonate that is precipitated.

A2.4 Reaction and Diffusion

In high pH environments, the relative abundance of CO_2 is very small (Table A2.1). For organisms that require CO_2 (those that can not utilize bicarbonate), CO_2 can be limiting under some conditions, even when DIC concentrations are millimolar or more (Riebesell et al., 1993; Wolf-Gladrow and Riebesell, 1997). The reason for this is that at pH higher than 7 only a small percentage of DIC is available as CO_2. The remainder is bicarbonate and carbonate. As CO_2 is depleted at a cell surface, it must be replenished. The resupply of CO_2 comes from two sources: i) diffusion of CO_2 towards the cell surface, and ii) conversion of bicarbonate to CO_2.

The layer surrounding the cell that has depleted CO_2 concentrations is the diffusive boundary layer (DBL). The thickness of this layer is determined by the size of the cell; for bacteria and archaea it is typically ~1 μm. The rate at which CO_2 permeates this layer is

determined by the diffusion coefficient for CO_2 (a function of temperature and salinity).

The conversion of bicarbonate to CO_2 is determined by kinetic coefficients. Two reactions play a role. The first, the hydration of CO_2, is most important at low pH:

$$CO_2 + H_2O \leftrightarrow H^+ + HCO_3^-$$

The second, the hydroxylation of CO_2, is predominant at high pH:

$$CO_2 + OH^- \leftrightarrow HCO_3^-.$$

The relative importance of the diffusive supply of CO_2 and the reaction supply of CO2 is determined by the square root of the ratio of the diffusion coefficient to the combined reaction rate (pH-dependent) of the CO_2-forming reactions. This ratio has length units and is denoted as the reacto-diffusive length scale (a_k) (Wolf-Gladrow and Riebesell, 1997; Zeebe and Wolf-Gladrow, 2001).

The reacto-diffusive length scale can be compared to the size of the DBL. When ak is greater than the DBL, diffusion is the most important process. Under these conditions CO_2 is not formed by reaction at an appreciable rate, and cells can become CO_2 limited if they fix CO_2 at a rate that matches the diffusive supply.

When the reacto-diffusive length scale is less than or equal to the thickness of the DBL, conversion of bicarbonate to CO_2 can make an appreciable contribution to the CO_2 supply. Assuming suffient bicarbonate, cells will not become limited under these conditions.

Figure A2-3 shows contours of the reacto-diffusive length scale (in μm) for a range of temperatures and pH. The length at a temperature of 70 ºC and pH of 11 – typical of the Lost City fluids is ~1 μm – similar to the size of microbial cells and to the thickness of the DBL. Under these conditions, carbon limitation because of insufficient conversion between bicarbonate at CO_2 is unlikely. At slightly lower pH and temperature a_k is on the order of a few 10's of μm. Under these conditions diffusion-limited carbon limitation might

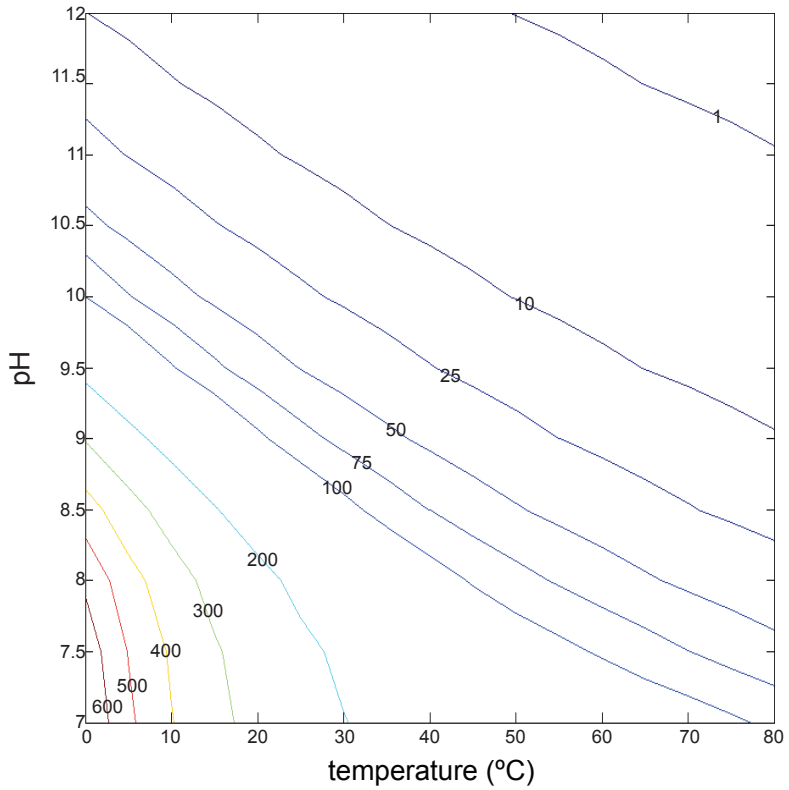

Figure A2-3: Contours of the effective reacto-diffusive length scale (a_k) in μm as a function of temperature and pH.

play a role if CO_2 is the only carbon source.

A2.5 Conclusions

Our analysis suggests that a number of lines of evidence are consistent with the hypothesis that DIC concentrations in Lost City vent fluids may in many cases be smaller than have been previously reported. We also suggest that sluggish conversion between bicarbonate and CO_2 can not be responsible for carbon limitation, and therefore high $\delta^{13}C$ of organic material. Carbonic anhydrase may allow fixation of bicarbonate directly. Although bacarbonate concentrations are also very low in hydrothermal fluids, the rate of equilibrium between bicarbonate and carbonate is six to seven orders of magnitude faster than the equilibrium between bicarbonate and CO_2. Sluggish equilibrium can be ruled out as a factor limiting carbon availability to microbes, leaving low concentrations as the most likely explanation for carbon limitation.

pH	8.1	9	9	9	9	9	9	10	10	10	10	11	11	11	11
S	35	35	35	35	35	35	35	35	35	35	35	35	35	35	35
T	4	4	4	40	70	40	70	40	70	40	70	40	70	40	70
DIC	2.10	2.10	0.55	0.44	0.40	0.44	0.40	0.38	0.37	0.38	0.37	0.37	0.37	0.37	0.37
CA	2.21	2.82	0.74	0.74	0.74	0.74	0.74	0.74	0.74	0.74	0.74	0.74	0.74	0.74	0.74
% CO_2	0.79%	0.07%	0.07%	0.02%	0.00%	0.02%	0.00%	0.00%	0.00%	0.00%	0.00%	0.00%	0.00%	0.00%	0.00%
% HCO_3^-	93.07%	65.56%	65.56%	31.55%	15.08%	31.55%	15.08%	4.41%	1.74%	4.41%	1.74%	0.46%	0.18%	0.46%	0.18%
% CO_3^{2-}	6.14%	34.37%	34.37%	68.44%	84.92%	68.44%	84.92%	95.59%	98.26%	95.59%	98.26%	99.54%	99.82%	99.54%	99.82%
$[Ca^{2+}]$	10.4	10.4	10.4	10.4	10.4	30	30	10.4	10.4	30	30	10.4	10.4	30	30
$\Omega_{calcite}$	2.7	14.9	3.9	7.0	10.0	20.2	28.7	8.4	10.7	24.3	31.0	8.6	10.8	27.8	31.2
$\Omega_{aragonite}$	1.7	9.5	2.5	4.9	8.1	14.2	23.5	5.9	8.8	17.0	25.3	6.0	8.9	17.4	25.5

Table A2-2: Carbonate speciation and saturation state of calcite and aragonite for a variety of temperature, pH, and DIC concentration states. First column on the left is seawater, others represent theoretical vent fluids.

A2.6 References

Fruh-Green, G.L., Kelley, D.S., Bernasconi, S.M., Karson, J.A., Ludwig, K.A., Butterfield, D.A., Boschi, C., Proskurowski, G., 2003. 30,000 years of hydrothermal activity at the Lost City vent field. Science 301(5632), 495-498.

Kelley, D.S., Karson, J.A., Blackman, D.K., Fruh-Green, G.L., Butterfield, D.A., Lilley, M.D., Olson, E.J., Schrenk, M.O., Roe, K.K., Lebon, G.T., Rivizzigno, P., 2001. An off-axis hydrothermal vent field near the Mid-Atlantic Ridge at 30 degrees N. Nature 412(6843), 145-149.

Kelley, D.S., Karson, J.A., Fruh-Green, G.L., Yoerger, D.R., Shank, T.M., Butterfield, D.A., Hayes, J.M., Schrenk, M.O., Olson, E.J., Proskurowski, G., Jakuba, M., Bradley, A., Larson, B., Ludwig, K., Glickson, D., Buckman, K., Bradley, A.S., Brazelton, W.J., Roe, K., Elend, M.J., Delacour, A., Bernasconi, S.M., Lilley, M.D., Baross, J.A., Summons, R.E., Sylva, S.P., 2005. A Serpentinite-Hosted Ecosystem: The Lost City Hydrothermal Field. Science 307(5714), 1428-1434.

Ludwig, K.A., Kelley, D.S., Butterfield, D.A., Nelson, B.K., Frueh-Green, G., 2006. Formation and evolution of carbonate chimneys at the Lost City Hydrothermal Field. Geochimica et Cosmochimica Acta 70(14), 3625-3645.

Riebesell, U., Wolf-Gladrow, D.A., Smetacek, V., 1993. Carbon dioxide limitation of marine phytoplankton growth rates. 361(6409), 249-251.

Wolf-Gladrow, D., Riebesell, U., 1997. Diffusion and reactions in the vicinity of plankton: A refined model for inorganic carbon transport. Marine Chemistry 59, 17-34.

Zeebe, R.E., Wolf-Gladrow, D., 2001. *CO_2 in Seawater: Equilibrium, Kinetics, Isotopes*. Elsevier, Amsterdam.

Zhong, S., Mucci, A., 1993. Calcite precipitation in seawater using a constant addition technique: A new overall reaction kinetic expression. Geochimica et Cosmochimica Acta 57(7), 1409-17.

Zhou, G.T., Zheng, Y.F., 2003. An experimental study of oxygen isotope fractionation between inorganically precipitated aragonite and water at low temperatures. Geochimica et Cosmochemica Acta 67, 387-399.

Appendix 3

Mass spectra and putative structures of nonisoprenoidal diethers

This supplement contains the information used to deduce the structures of nonisoprenoidal diethers in Lost City carbonates.

Figure A3-1 shows a generalized structure of a nonisoprenoidal diethers, and the major fragment ions derived from it.
The tables give the major ion masses that are helpful in deciphering the identity of a nonisoprenoidal diether

Table A3-1 shows the molecular ion (as TMS derivative) for a nonisoprenoidal diether of common masses. It is often easier to identify the carbon number of the diether by examining the spectrum and finding the M-104 ion.

Table A3-2 shows the fragment ions for important fragments. These fragments are shown in Figure 1. The fragments described as "*sn*-2 major ion," *sn*-2 minor ion" and "*sn*-1 + OTMS –H" are commonly among the most abundant ions of mass >133 in the chromatogram. They are particularly useful for identification of the masses of the *sn*-1 and *sn*-2 alkyl chains.

The diether spectrum does not generally distinguish the various side chain isomers. The spectrum is identical whether side chains are *n*-alkyl, iso-, anteiso, or ω7-Me. These isomers are inferred by the Kovats retention index (RI) (Kissin and Feulmer, 1986; Kissin et al., 1986), a practice that has previously been demonstrated to be applicable to nonisoprenoidal diethers (Pancost et al., 2001).

References

Kissin, Y.V., Feulmer, G.P., 1986. Gas chromatographic analysis of alkyl-substituted parrafins. Journal of Chromatographic Science 24, 53-59.

Kissin, Y.V., Feulmer, G.P., Payne, W.B., 1986. Gas chromatographic analysis of polymethyl-substituted alkanes. Journal of Chromatographic Science 24(4), 164-9.

Pancost, R.D., Bouloubassi, I., Aloisi, G., Sinninghe Damste, J.S., Party, M.S.S., 2001. Three series of non-isoprenoidal dialkyl glycerol diethers in cold-seep carbonate crusts. Organic Geochemistry 32, 695-707.

Figure A3-1

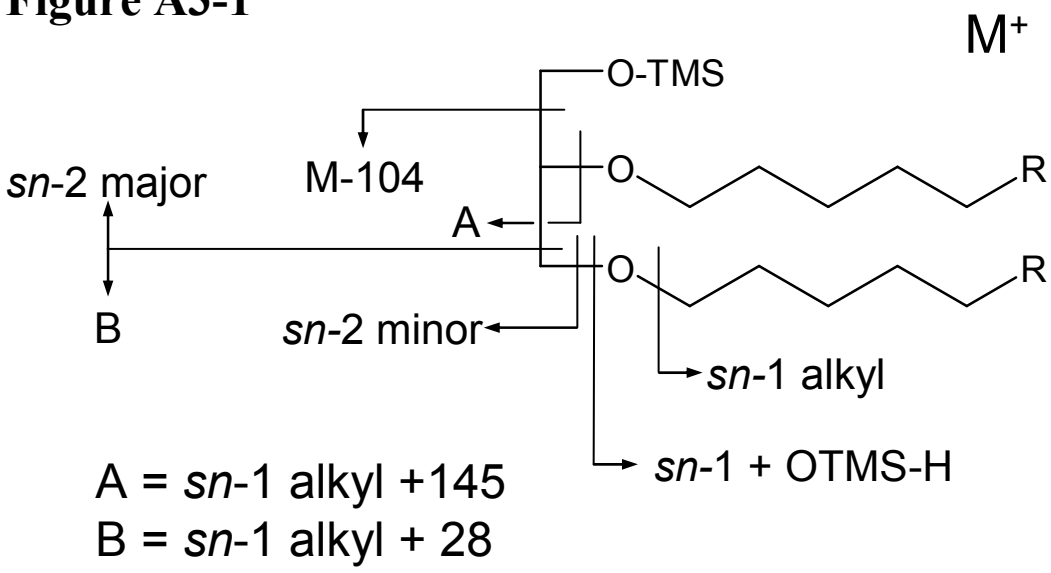

Table A3-1

Carbon number	M+	M-104
31	556	452
32	570	466
33	584	480
34	598	494
35	612	508
36	626	522
37	640	536
38	654	550
39	668	564
40	682	578

Table A3-2

Carbon number	alkyl	*sn*-1 + OTMS -H	*sn*-2 major ion	*sn*-2 minor ion
13	183	271	314	328
14	197	285	328	342
15	211	299	342	356
16	225	313	356	370
17	239	327	370	384
18	253	341	384	398
19	267	355	398	412
20	281	369	412	426
21	295	383	426	440
22	309	397	440	454

ID	ID #	Pancost ID
RI	Kovats RI	
M^+	M^+	Carbon #
***sn*-1**	C# *sn*-1 chain	structure *sn*-1*
***sn*-2**	C# *sn*-2 chain	structure *sn*-2*

* indicates that structures could be interchanged between *sn*-1 and *sn*-2

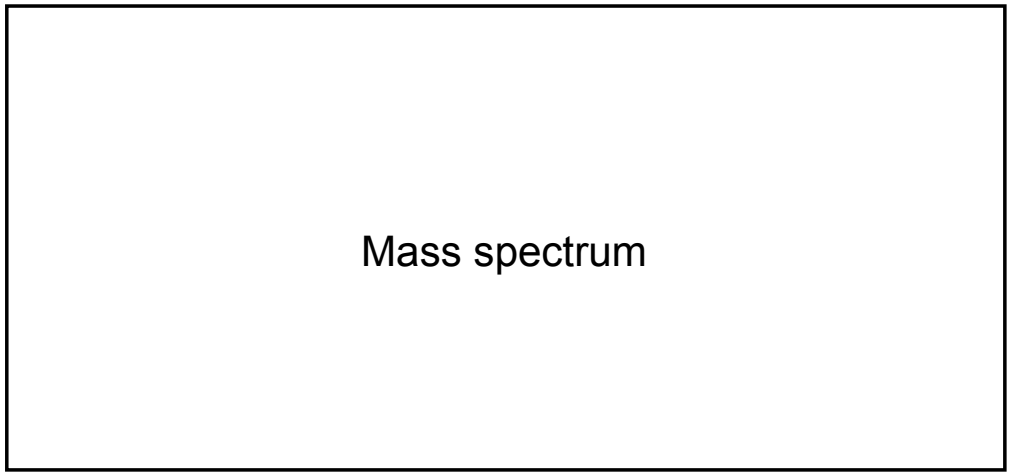

Format of the data in Appendix 3

ID	1	
RI	3285	
M^+	556	C31
***sn*-1**	15	ai
***sn*-2**	13	ai

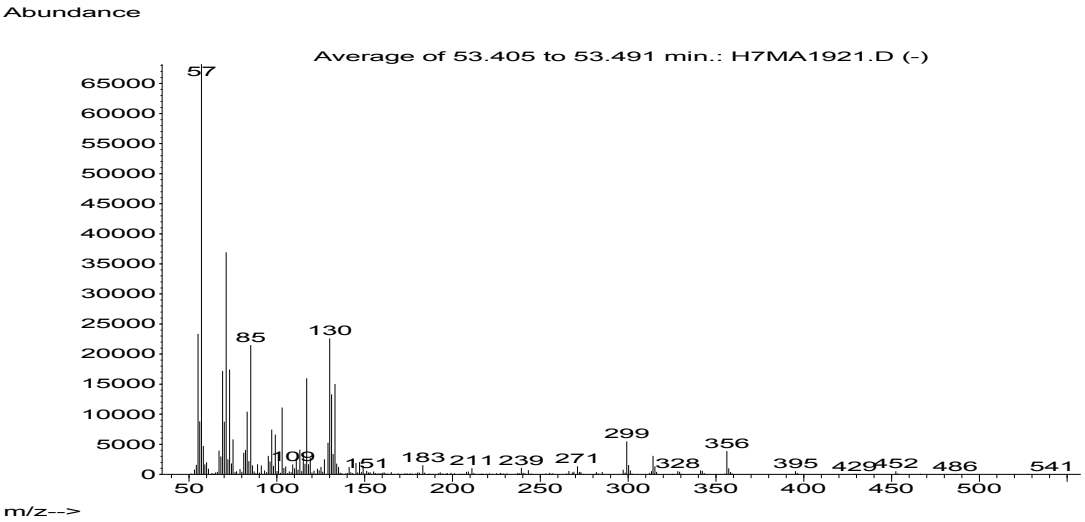

ID	2	
RI	3297	
M^+	556	C31
***sn*-1**	14	n
***sn*-2**	14	i

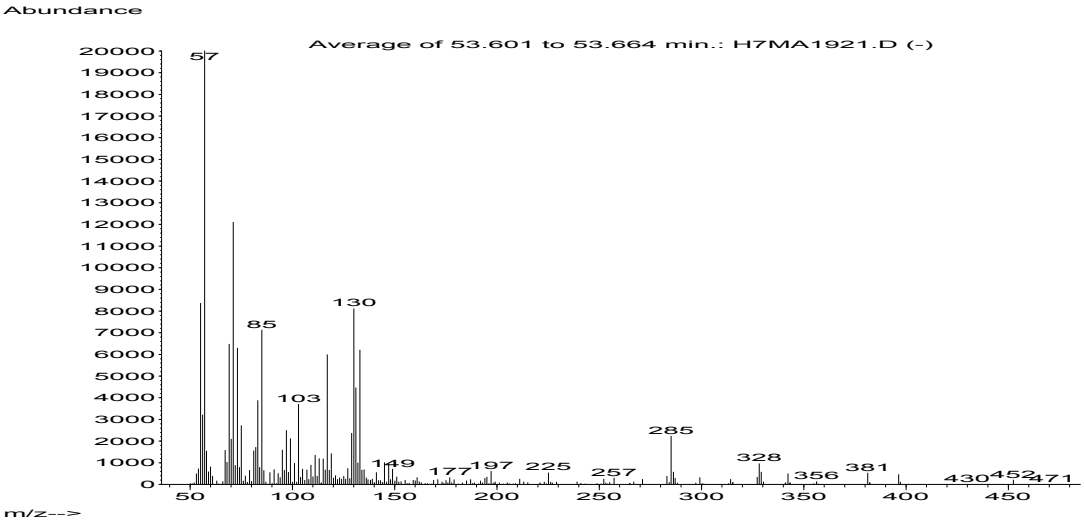

ID	3	
RI	3333	
M^+	556	C31
***sn*-1**	14	n
***sn*-2**	14	n

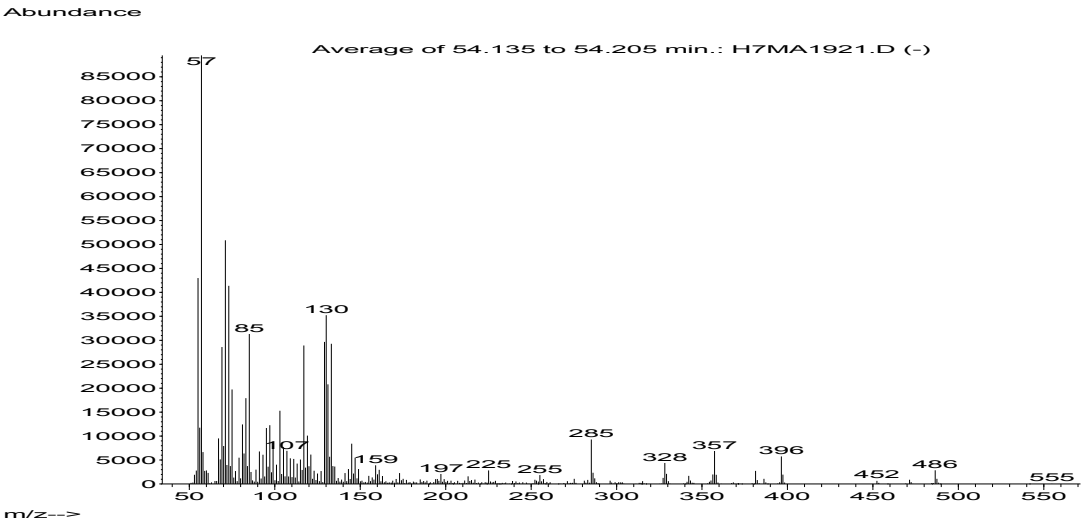

ID	4	**Ia**
RI	3370	
M^+	570	C32
***sn*-1**	15	ai
***sn*-2**	14	i

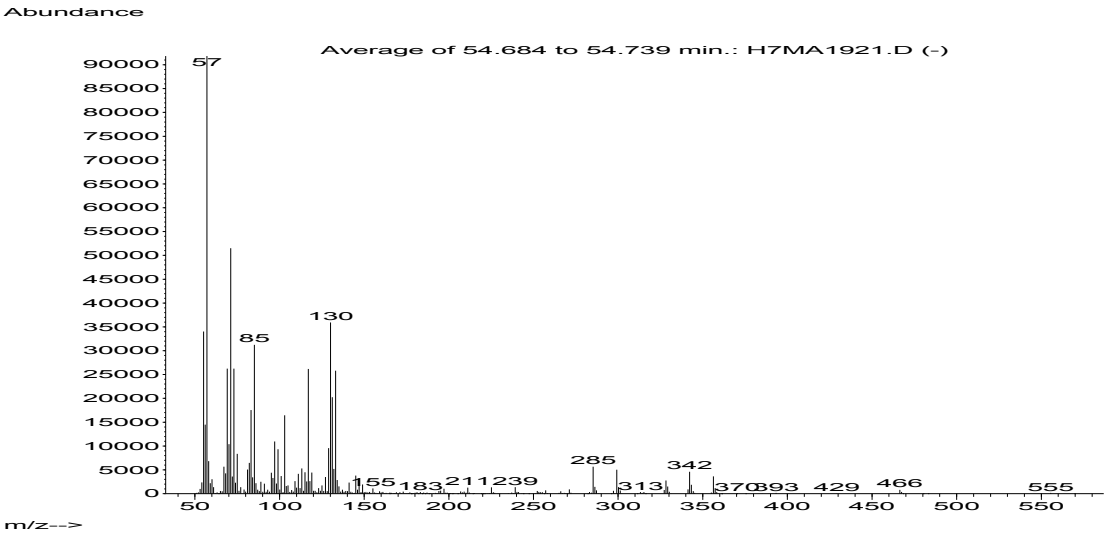

ID	5	**Ic**
RI	3405	
M^+	570	C32
***sn*-1**	14	n
***sn*-2**	15	ai

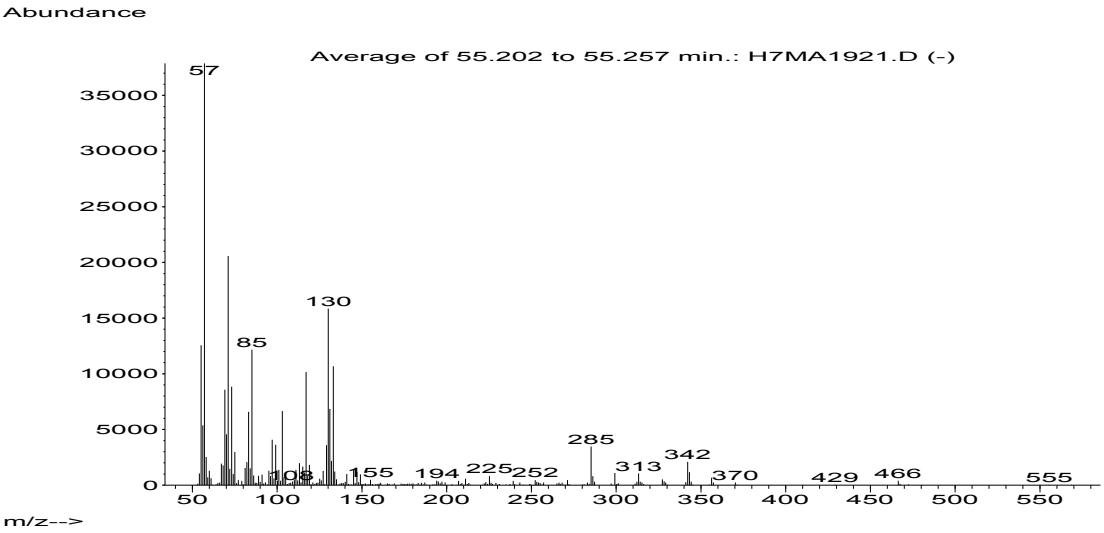

ID	6	
RI	3431	
M^+	570	C32
***sn*-1**	15	n
***sn*-2**	14	n

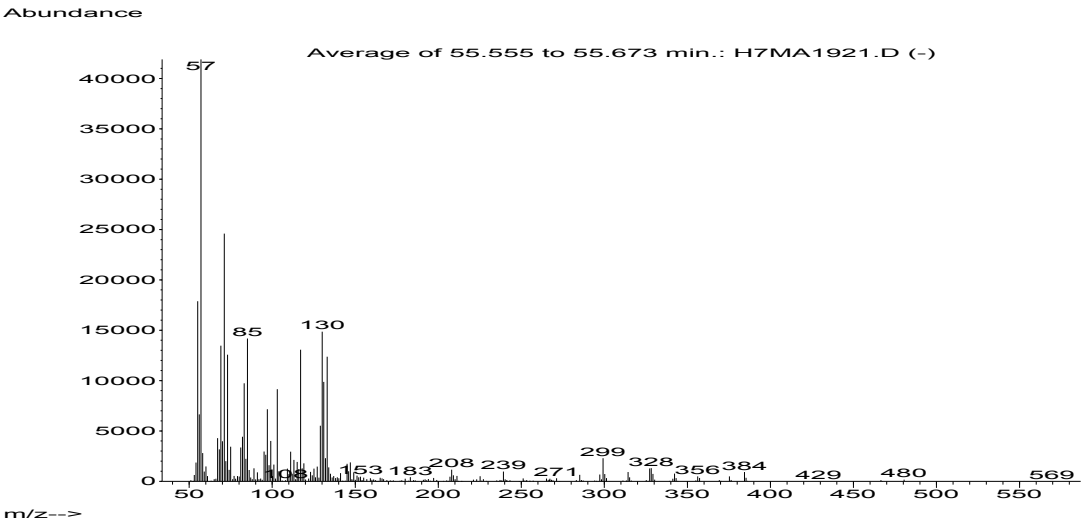

ID	7	**Id**
RI	3455	
M^+	584	C33
***sn*-1**	15	i
***sn*-2**	15	i

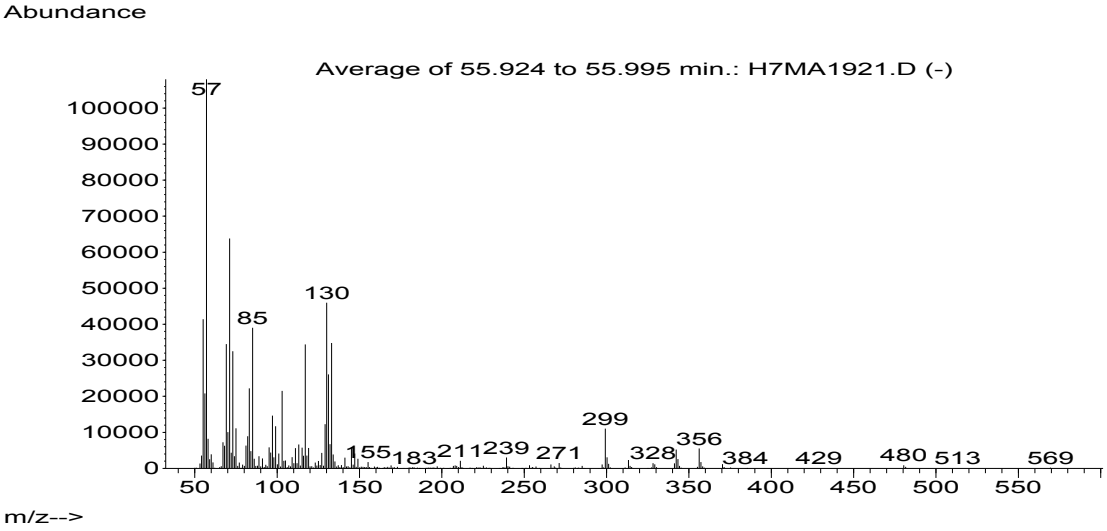

ID	8	**Ie**
RI	3466	
M^+	584	C33
***sn*-1**	15	i*
***sn*-2**	15	ai*

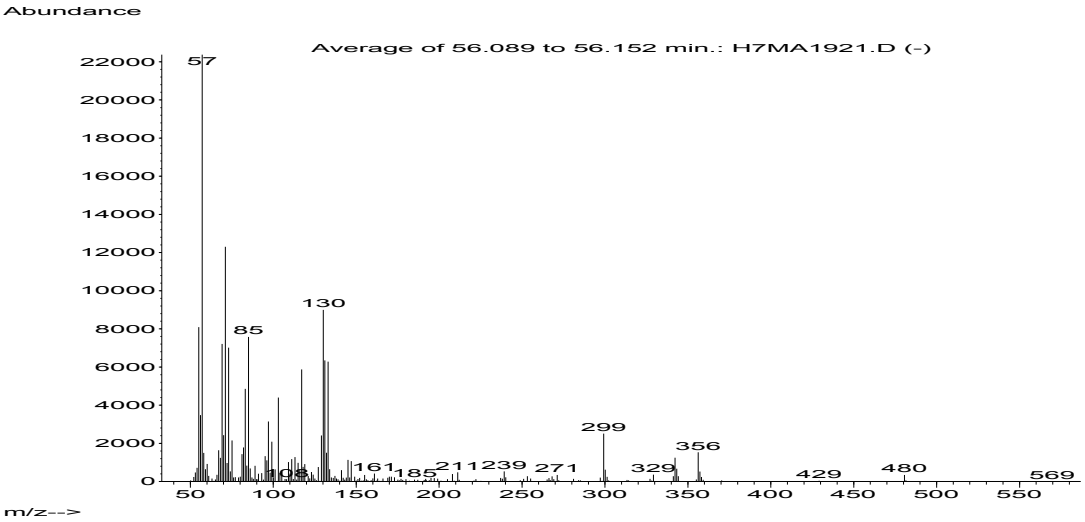

ID	9	**If**
RI	3479	
M^+	584	C33
***sn*-1**	15	ai
***sn*-2**	15	ai

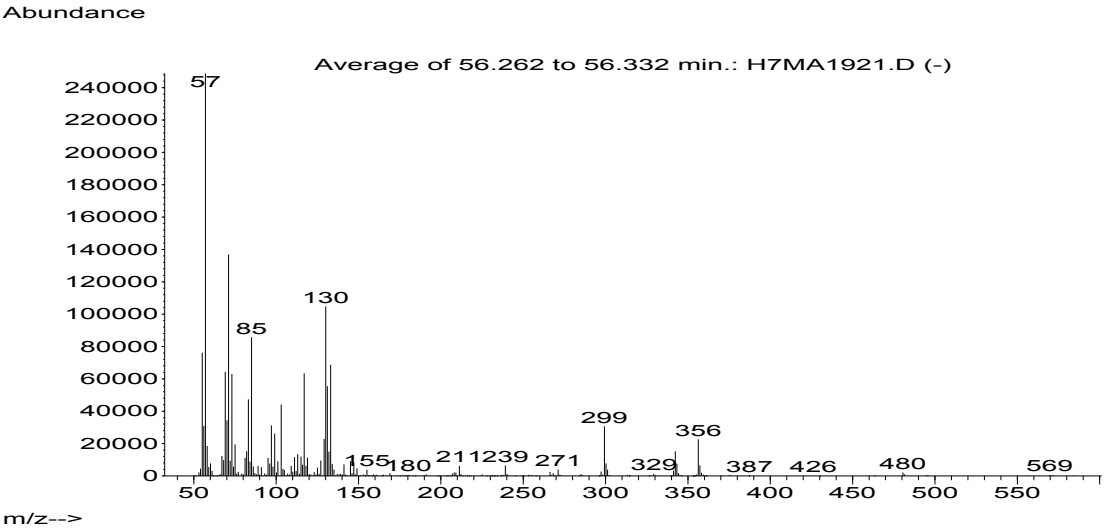

ID	10	
RI	3486	
M^+	582	C33:1
***sn*-1**	16:1	cp
***sn*-2**	14	i

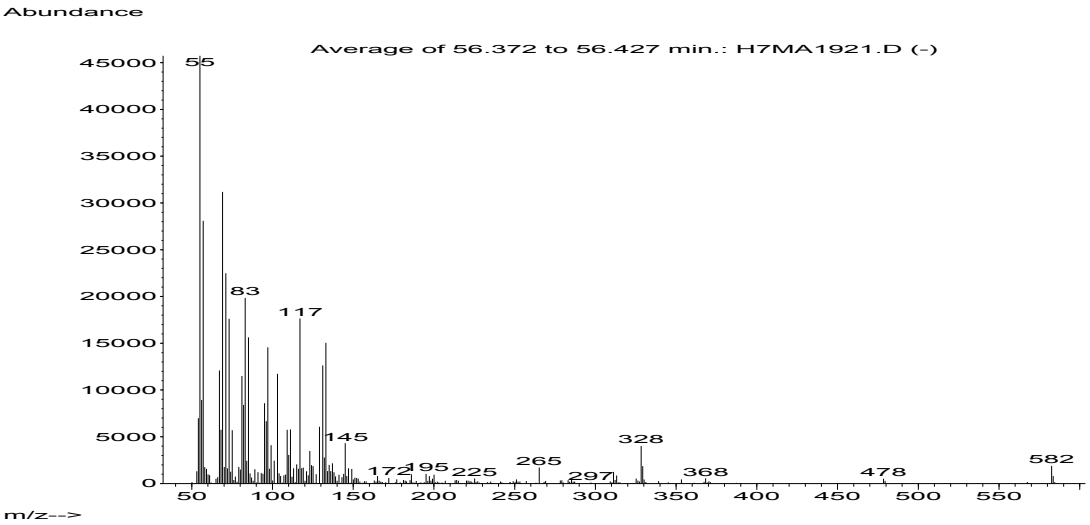

ID	11	
RI	3489	
M^+	584	C33
***sn*-1**	16	i*
***sn*-2**	14	n*

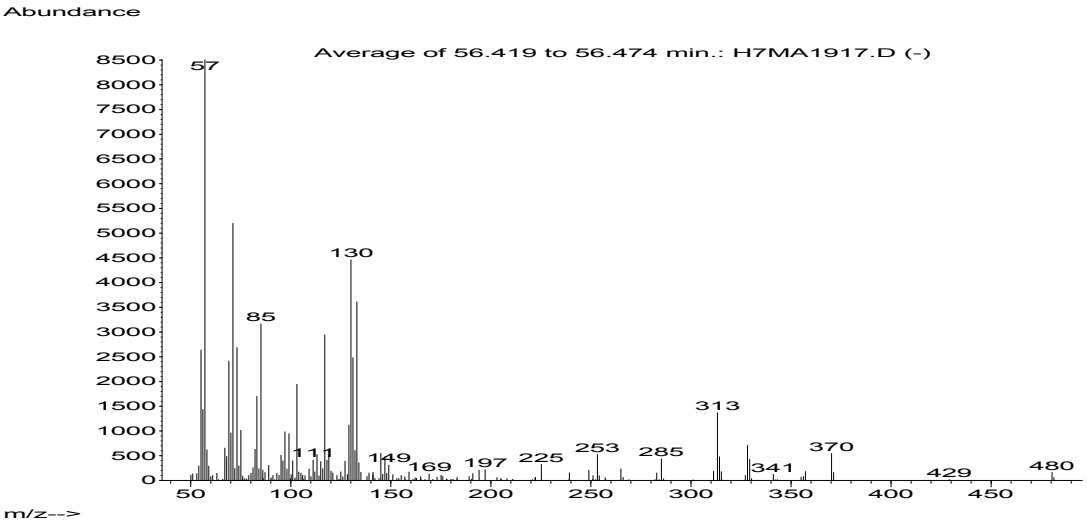

ID	12	
RI	3512	
M^+	582	C33:1
***sn*-1**	16:1	cp
***sn*-2**	14	ai

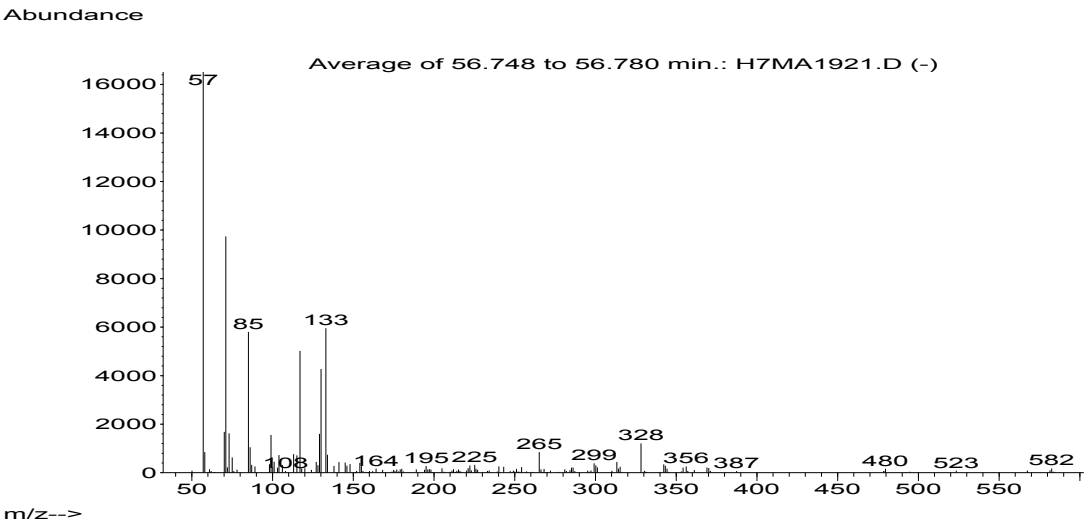

ID	13	
RI	3522	
M^+	582	C33:1
***sn*-1**	16:1	cp
***sn*-2**	14	n

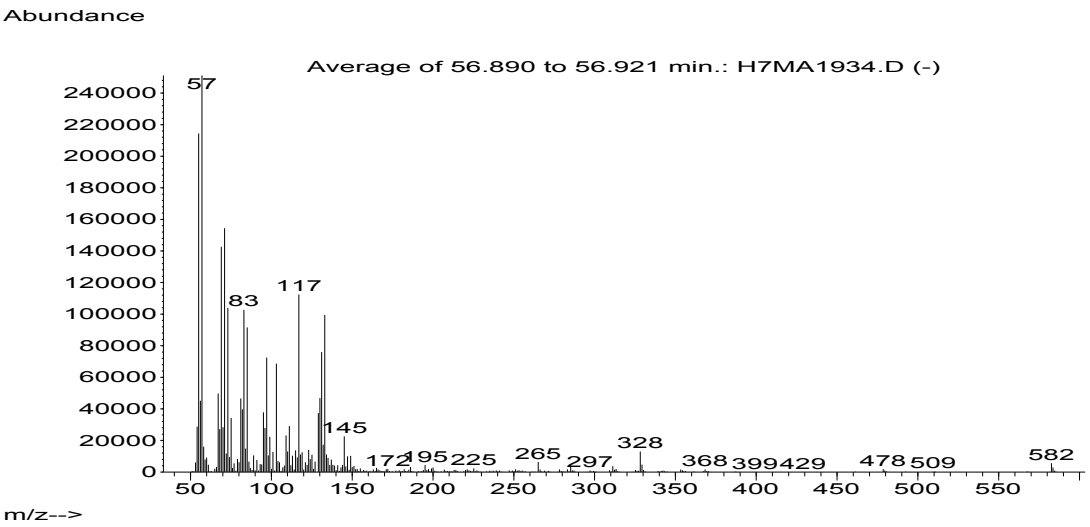

ID	14	
RI	3525	
M^+	584	C33
***sn*-1**	14	n
***sn*-2**	16	n

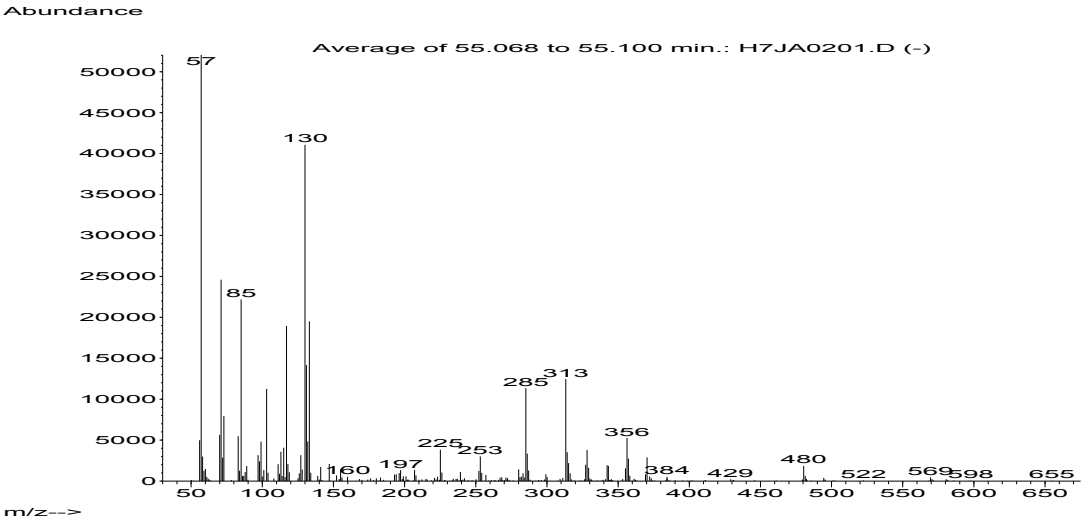

ID	15	
RI	3527	
M^+	582	C33:1
***sn*-1**	16:1	cp
***sn*-2**	14	n

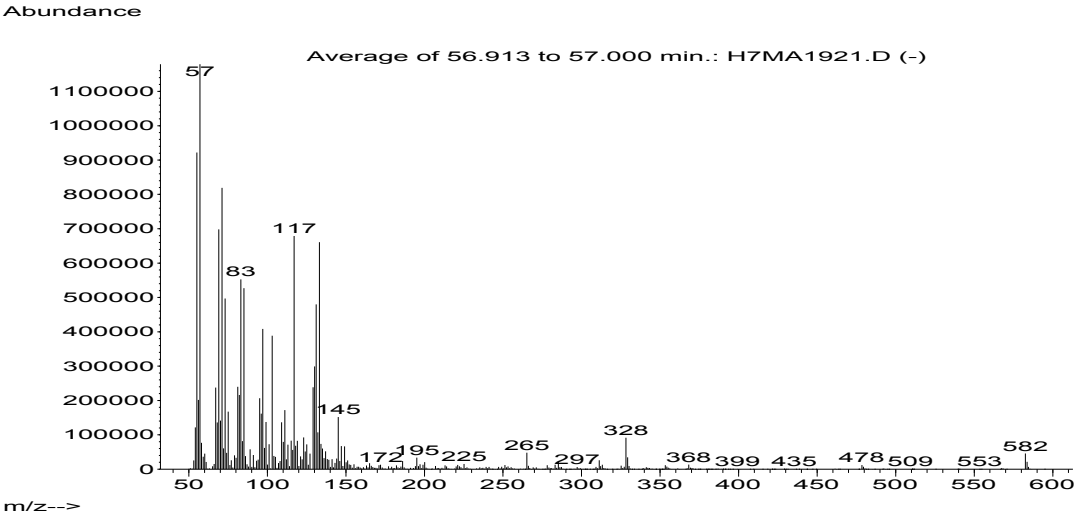

ID	16	**I**
RI	3565	
M^+	598	C34
***sn*-1**	16	ai
***sn*-2**	15	ai

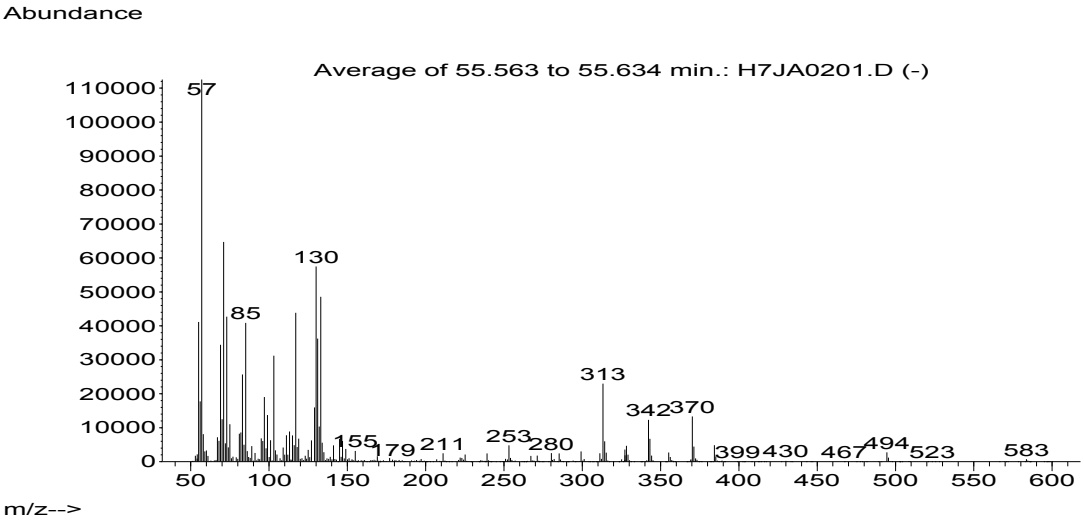

ID	17	**I**
RI	3565	
M^+	596	C34:1
***sn*-1**	16:1	?
***sn*-2**	15	?

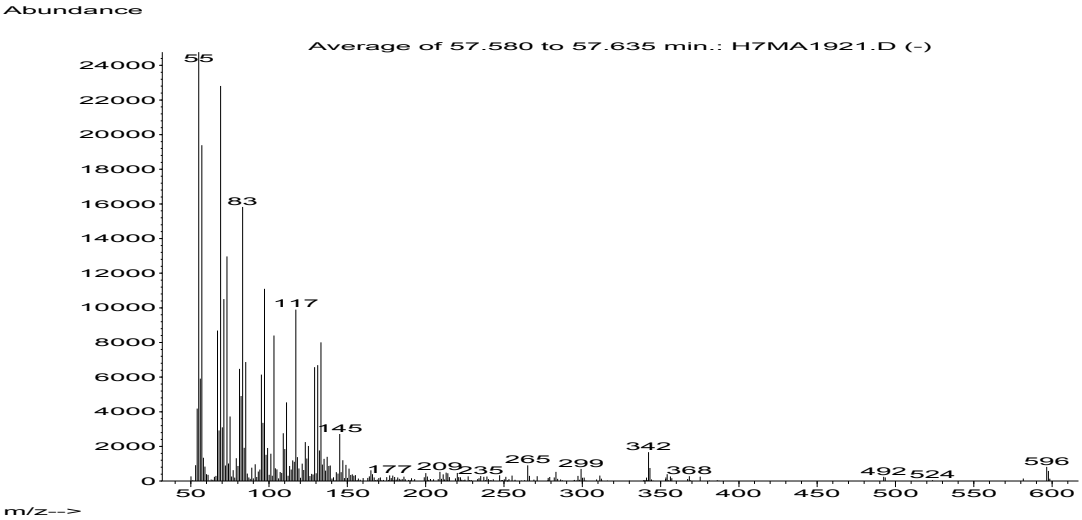

ID	18	**I**
RI	3584	
M^+	596	C34:1
***sn*-1**	16:1	?
***sn*-2**	15	?

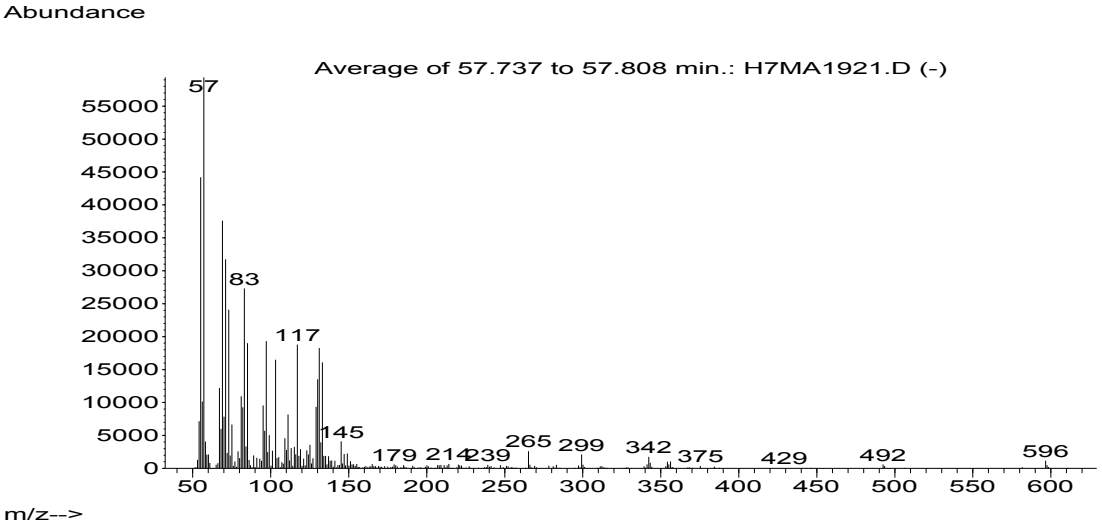

ID	19	**Ig**
RI	3594	
M^+	596	C34:1
***sn*-1**	16:1	cp
***sn*-2**	15	ai

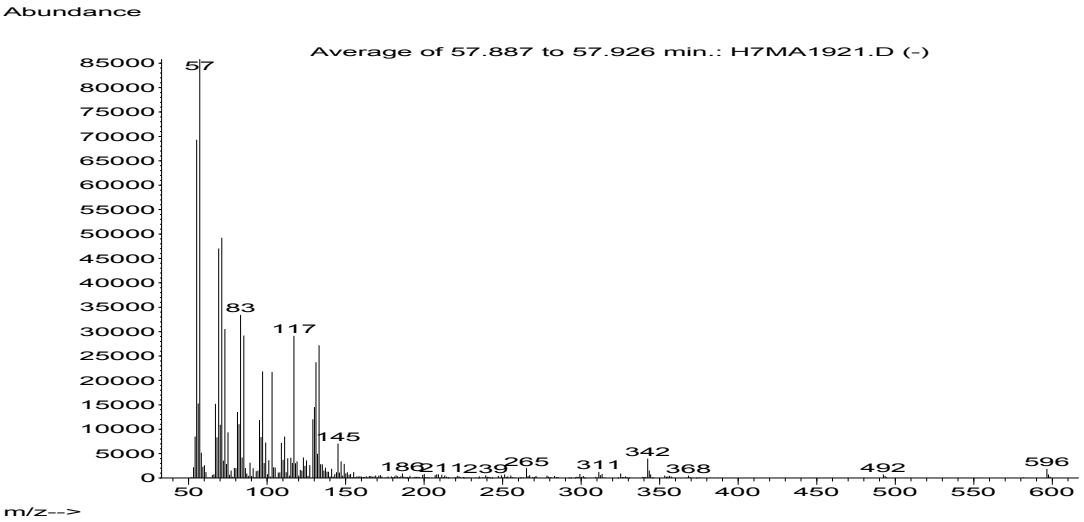

ID	20	**I**
RI	3565	
M^+	598	C34
***sn*-1**	16	i
***sn*-2**	15	i

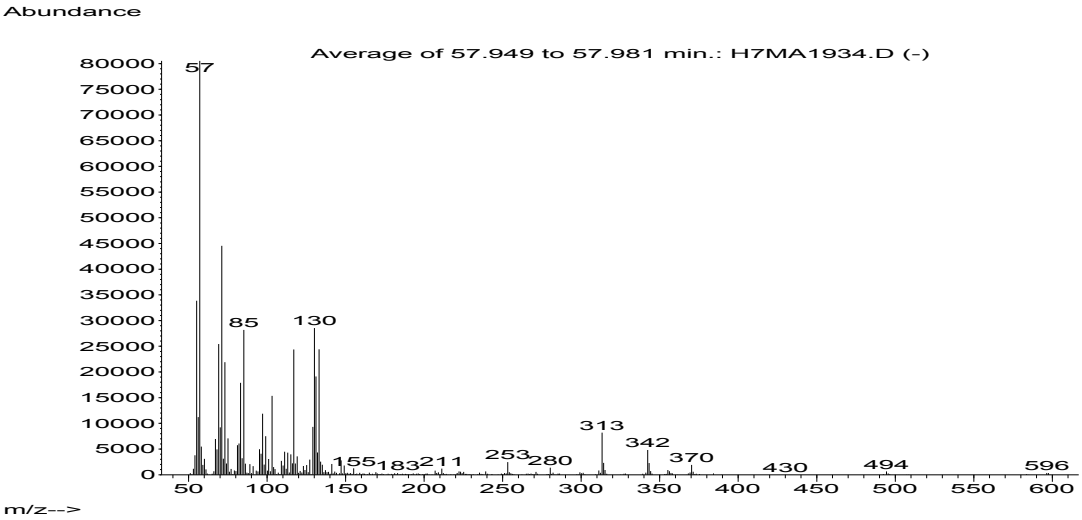

ID	21	**I**
RI	3618	
M^+	596	C34:1
***sn*-1**	16:1	cp
***sn*-2**	15	n

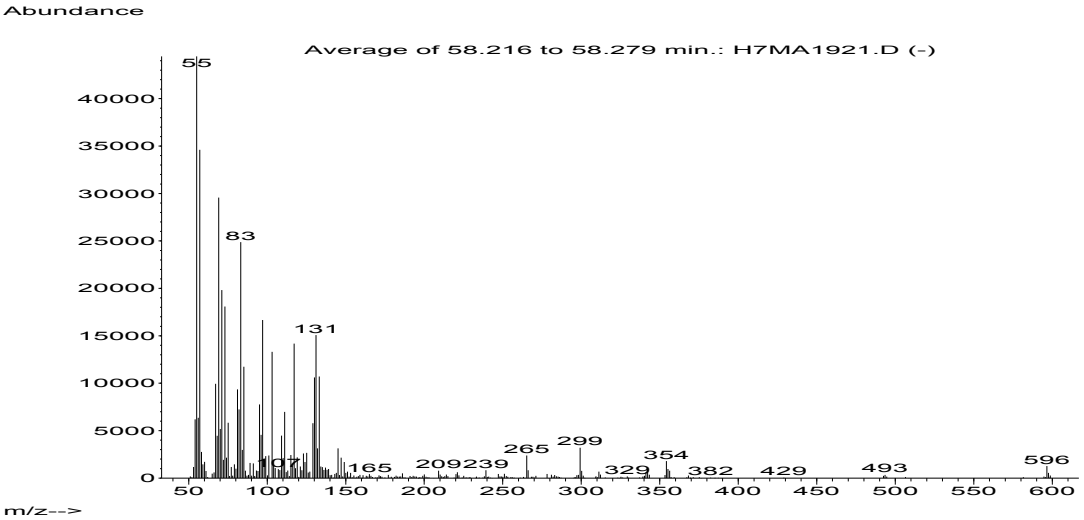

ID	22	
RI	3621	
M^+	598	C34
***sn*-1**	16	n
***sn*-2**	15	n

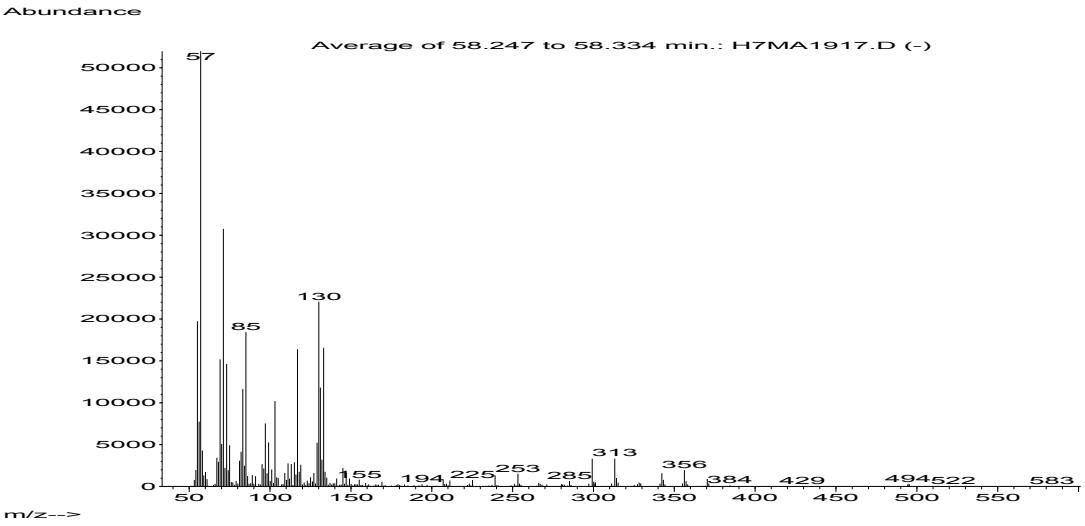

ID	23	**IV**
RI	3628	
M^+	612	C35
***sn*-1**	17	i
***sn*-2**	15	ω7-Me

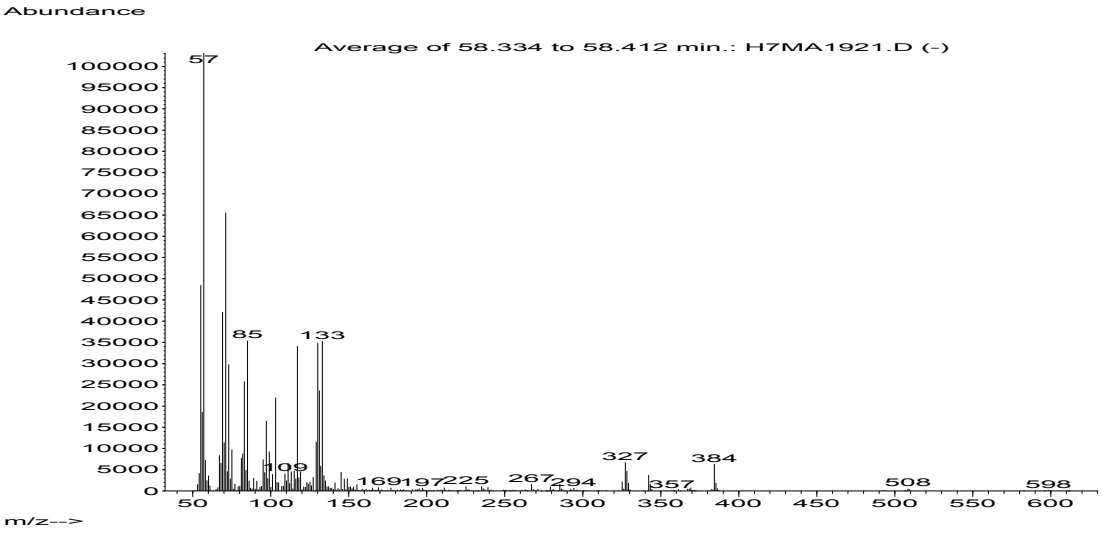

ID	24	
RI	3691	
M^+	608	C35:2
***sn*-1**	16:1	?
***sn*-2**	16:1	?

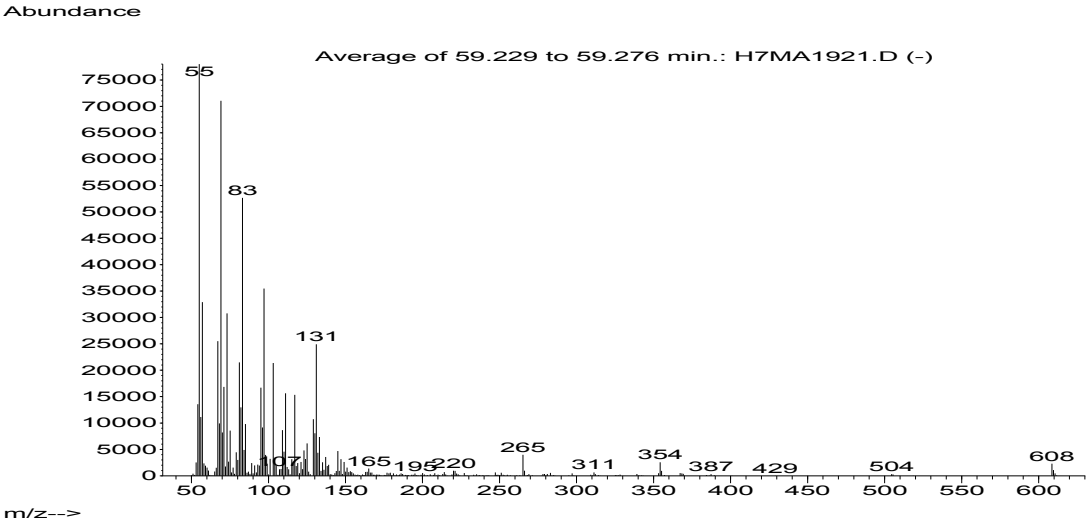

ID	25	
RI	3696	
M^+	610	C35:1
***sn*-1**	16:1	cp
***sn*-2**	16	ai

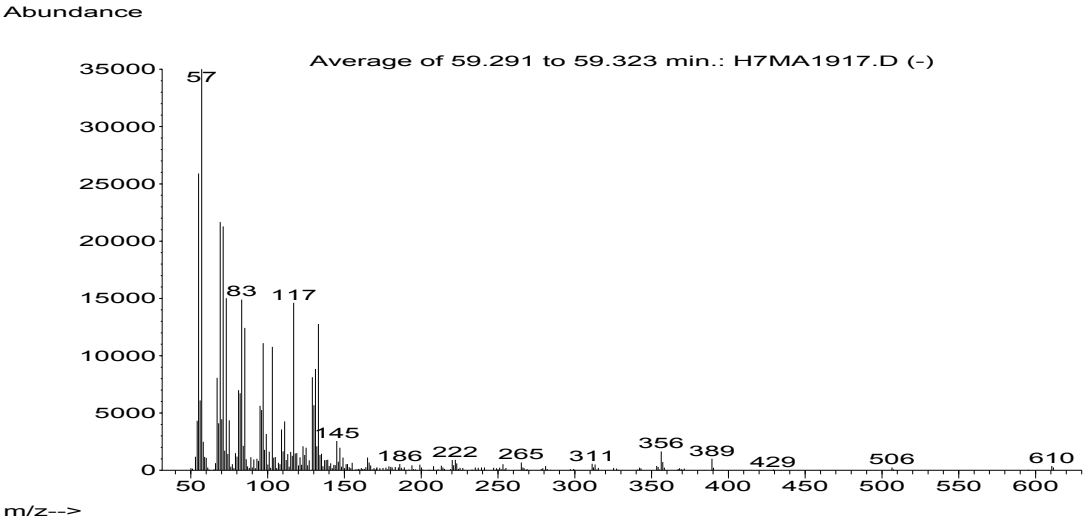

ID	26	
RI	3702	
M^+	608	C35:2
***sn*-1**	16:1	?
***sn*-2**	16:1	?

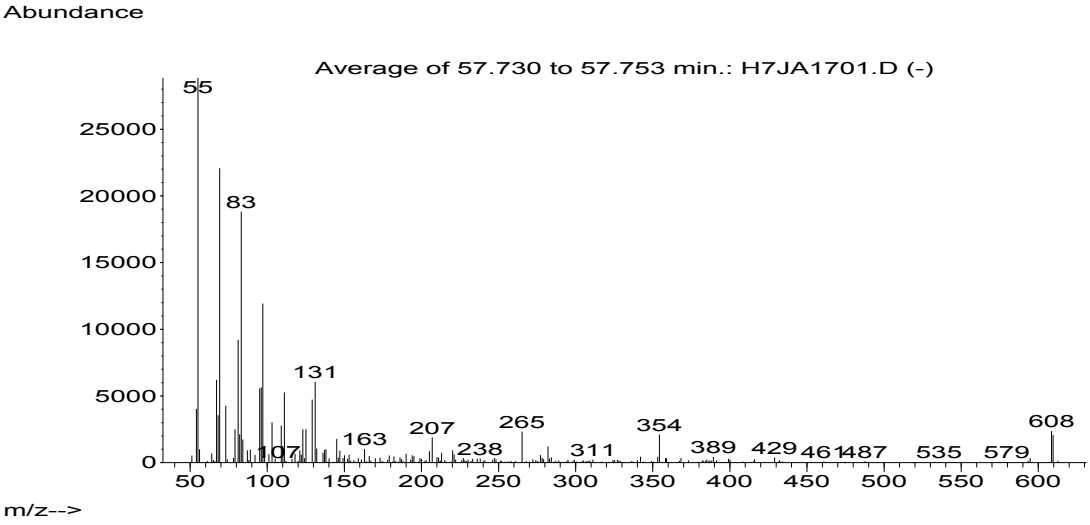

ID	27	
RI	3704	
M^+	610	C35:1
***sn*-1**	16	n
***sn*-2**	16:1	cp

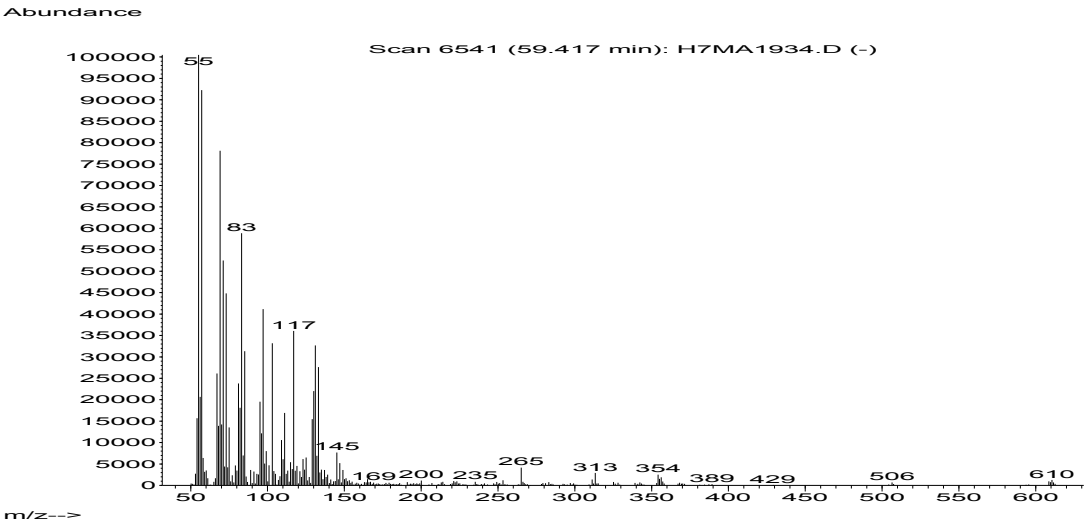

ID	28	
RI	3712	
M^+	608	C35:2
***sn*-1**	16:1	cp
***sn*-2**	16:1	cp

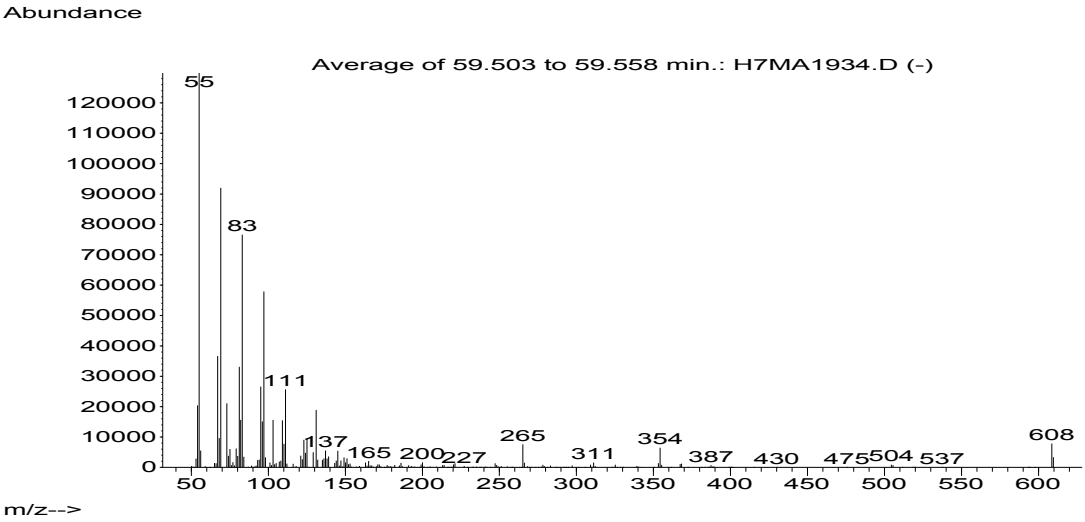

ID	29	
RI	3721	
M^+	612	C35
***sn*-1**	16	n
***sn*-2**	16	n

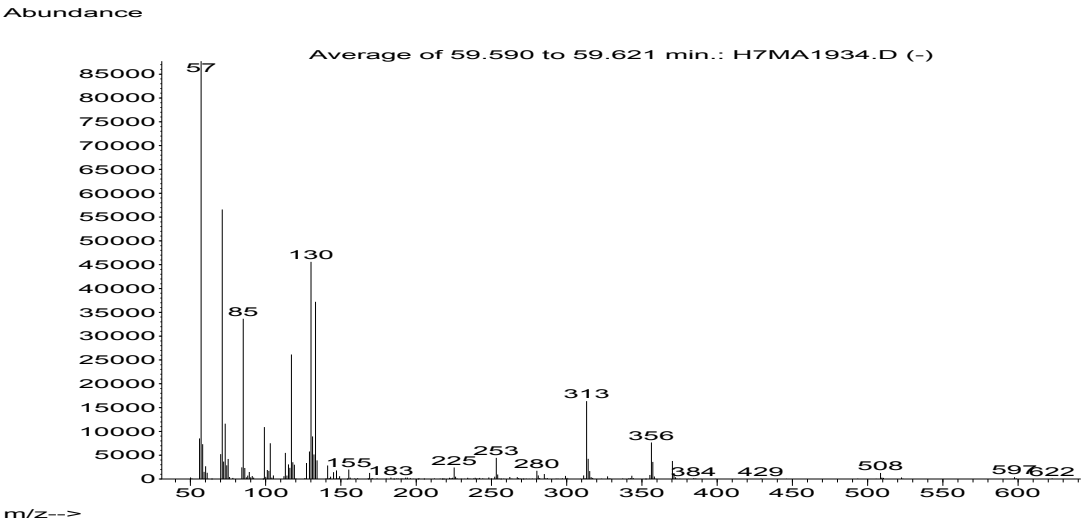

ID	30	
RI	3753	
M^+	624	C36:1
***sn*-1**	17	ω7-Me
***sn*-2**	16:1	?

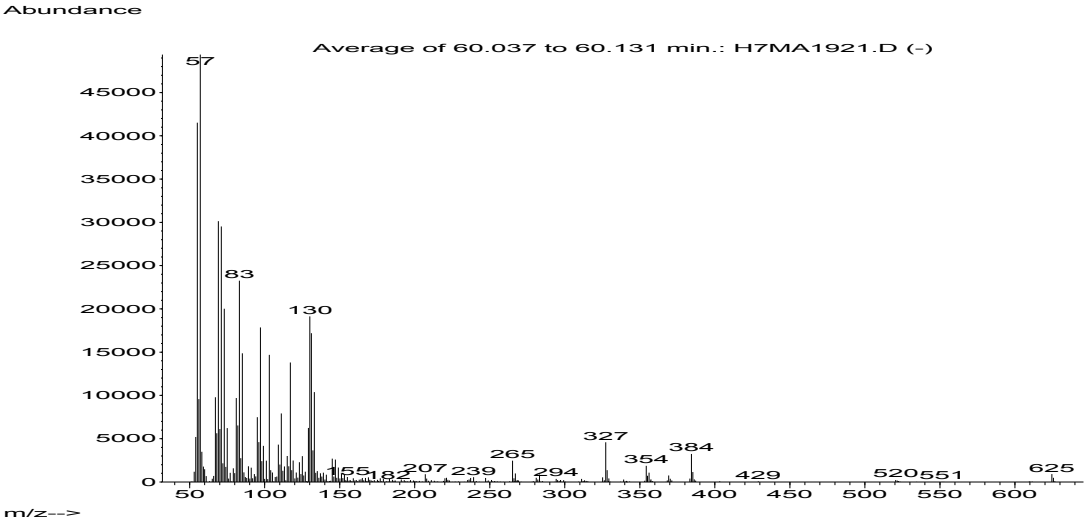

ID	31	
RI	3759	
M^+	626	C36
***sn*-1**	17	i*
***sn*-2**	16	ai*

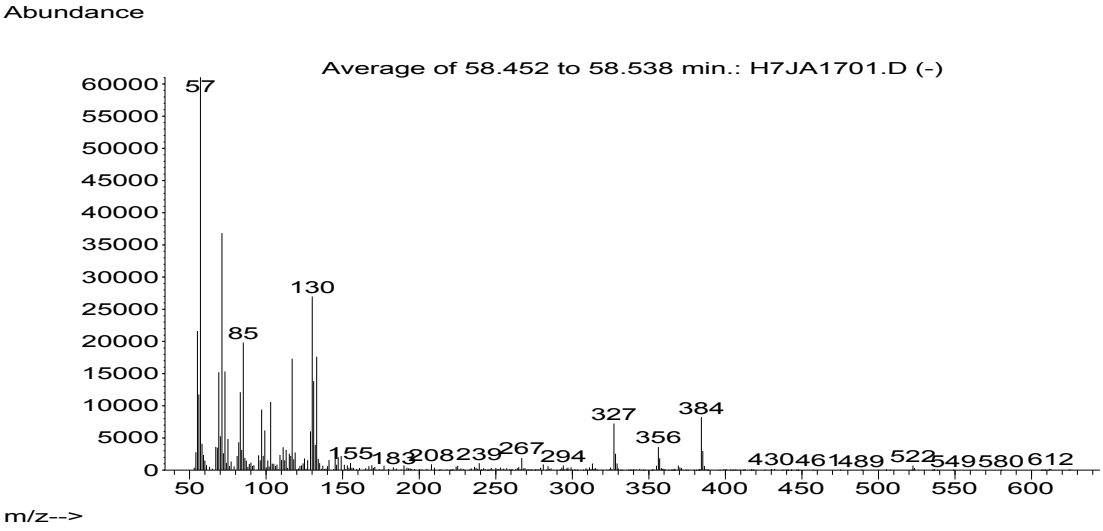

ID	32	
RI	3765	
M^+	624	C36:1
***sn*-1**	17	?
***sn*-2**	16:1	?

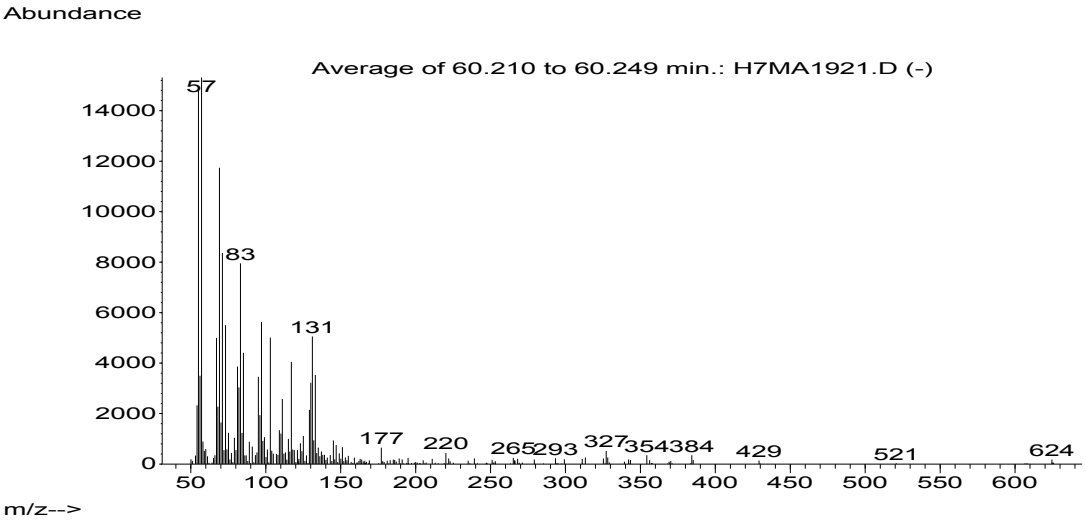

ID	33	
RI	3778	
M^+	624	C36:1
***sn*-1**	?	?
***sn*-2**	?	?

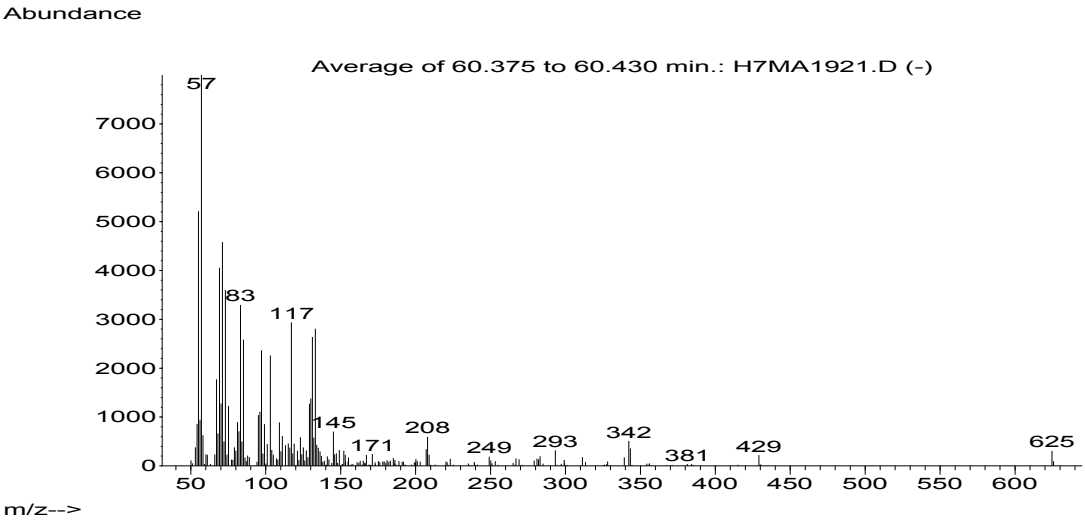

ID	34	**IV**
RI	3796	
M^+	640	C37
***sn*-1**	17	ω7-Me
***sn*-2**	17	ω7-Me

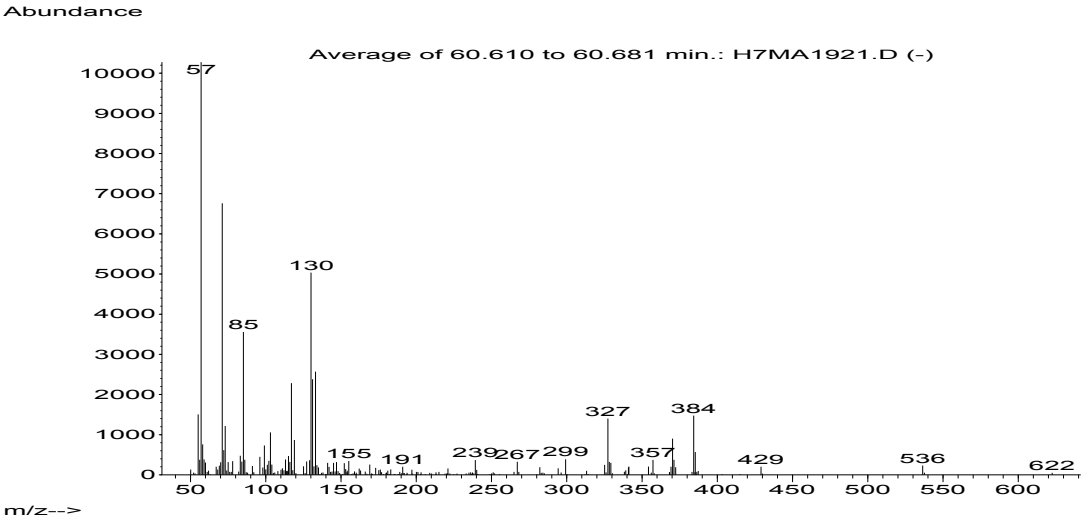

ID	35	
RI	3803	
M^+	622	C36:2
***sn*-1**	18:1	?
***sn*-2**	16:1	?

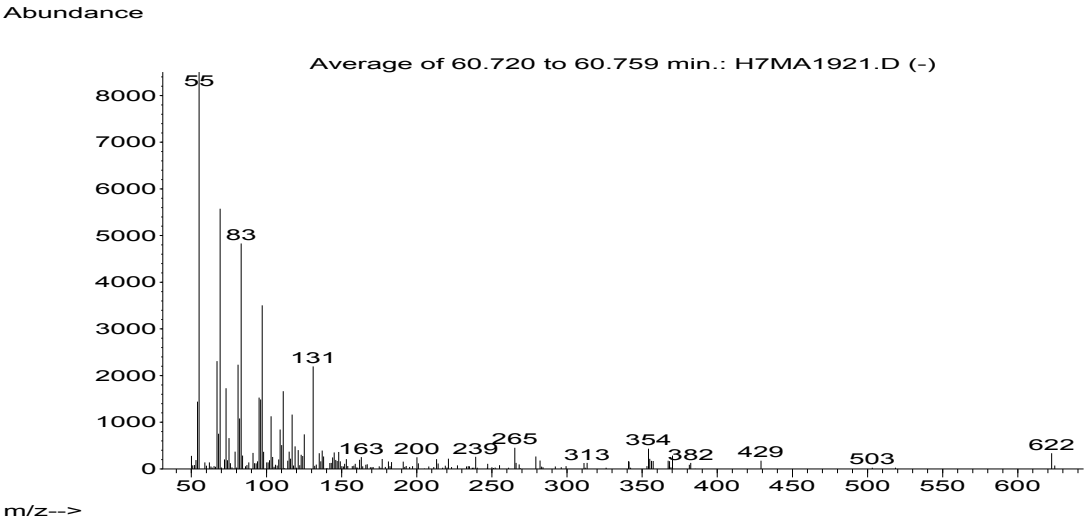

ID	36	
RI	3813	
M^+	626	C36
***sn*-1**	17	n
***sn*-2**	16	n

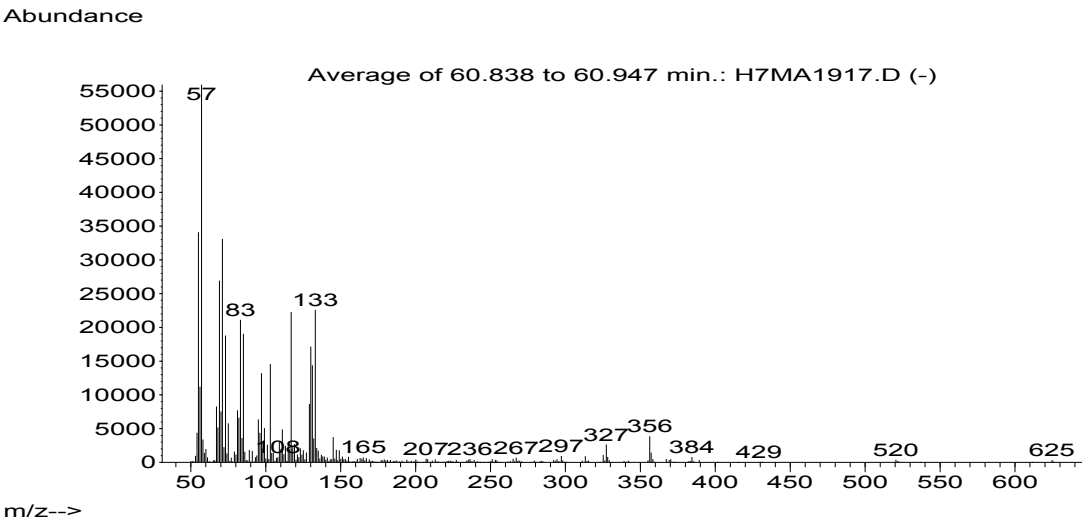

ID	37	
RI	3820	
M^+	622	C36:2
***sn*-1**	16:1	cp
***sn*-2**	17:1	cp

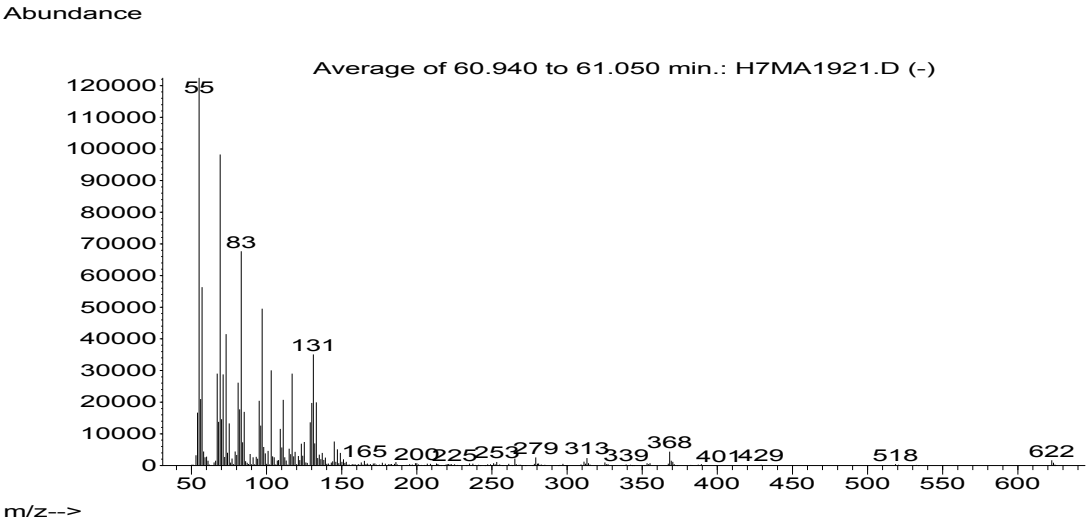

ID	38	**IIc**
RI	3821	
M^+	624	C36:1
***sn*-1**	16	n
***sn*-2**	17:1	cp

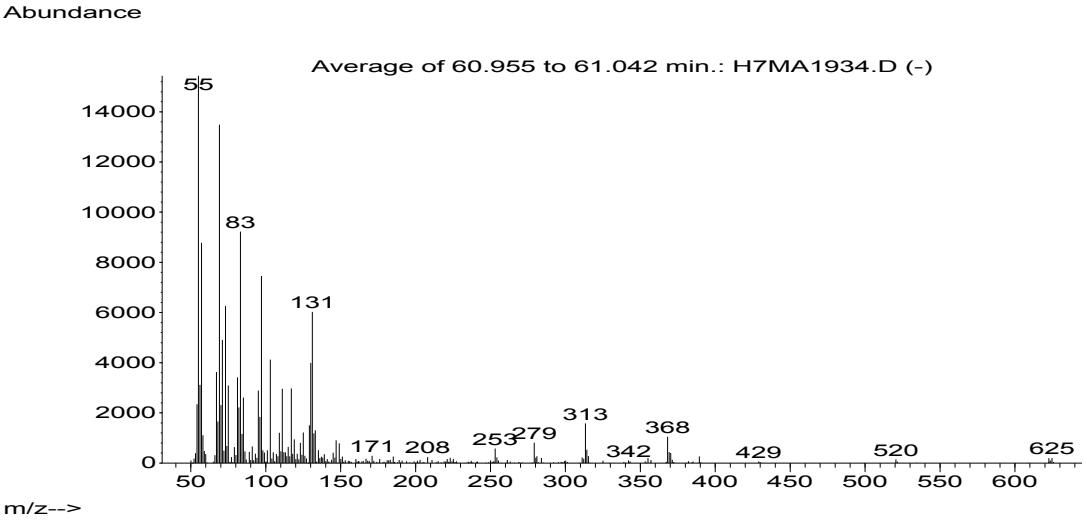

ID	39	
RI	3885	
M^+	636	C37:2
***sn*-1**	18:1	?
***sn*-2**	16:1	?

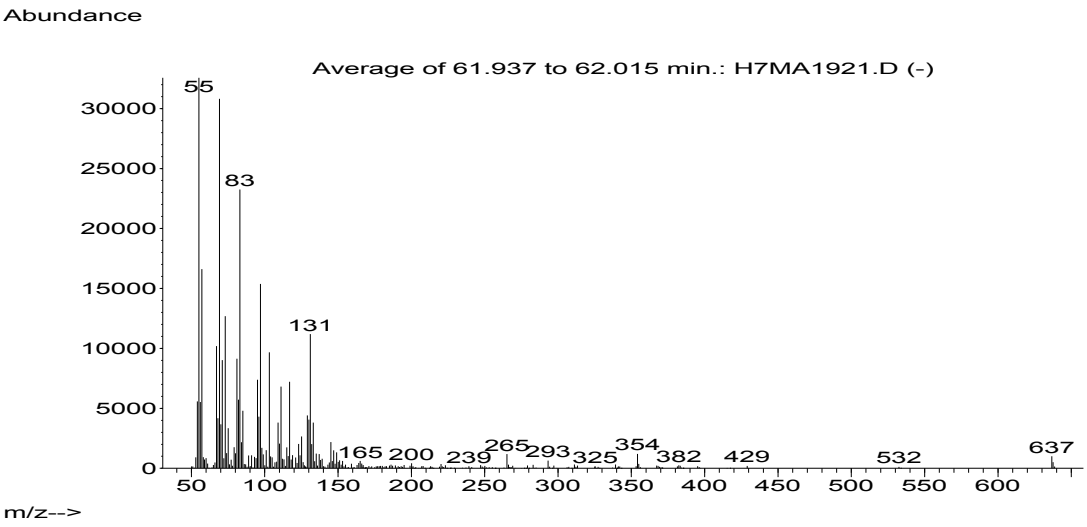

ID	40	
RI	3898	
M^+	638	C37:1
***sn*-1**	18:1	cp
***sn*-2**	16	ai

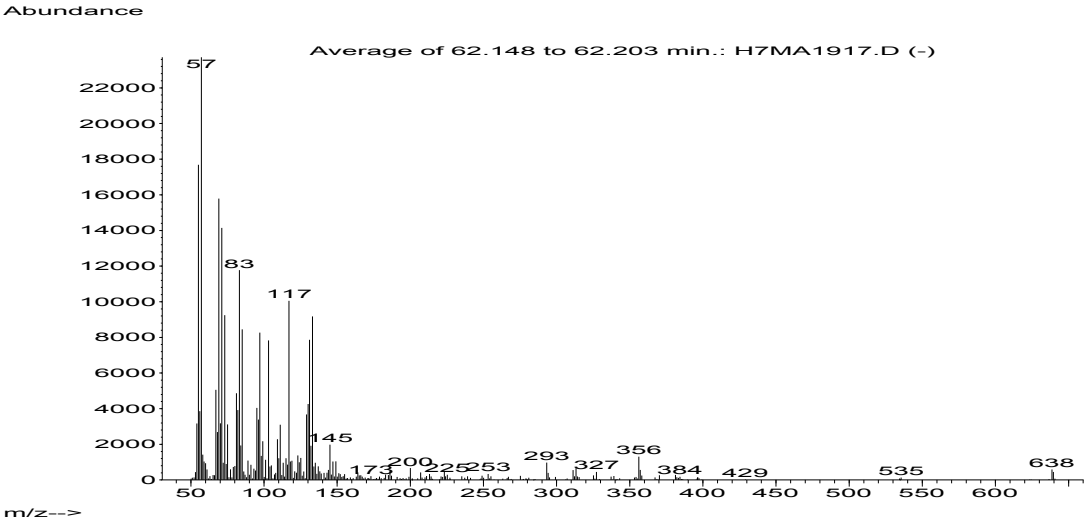

ID	41	
RI	3911	
M^+	640	C37
***sn*-1**	18	n
***sn*-2**	16	n

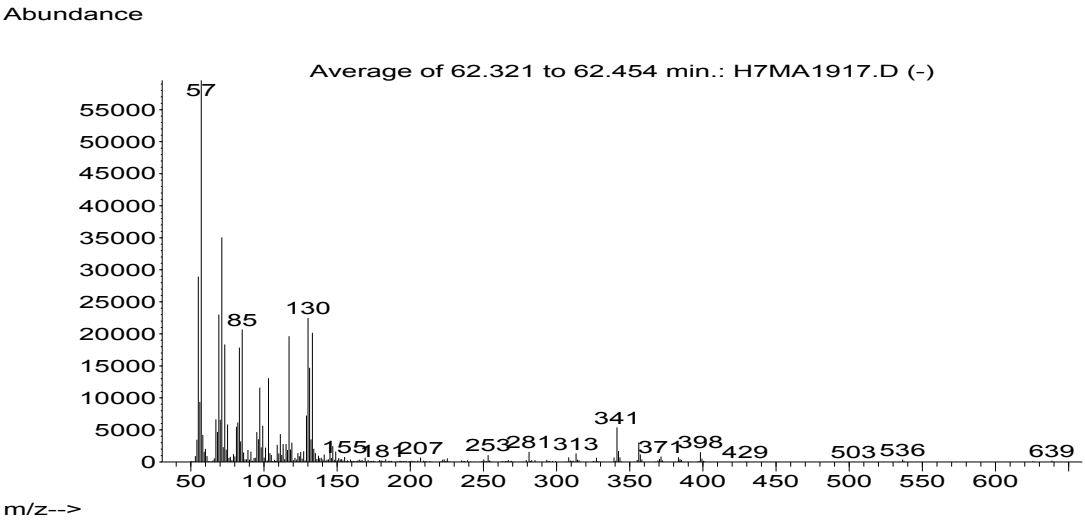

ID	42	
RI	3927	
M^+	636	C37:2
***sn*-1**	17:1	ch
***sn*-2**	17:1	cp

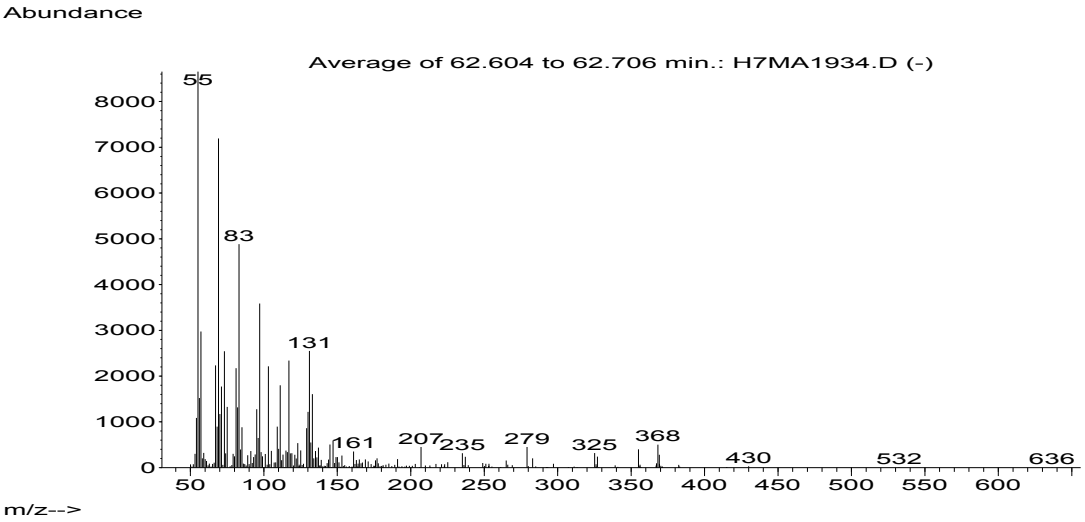

ID	43	
RI	4013	
M^+	652	C38:1
***sn*-1**	19:1?	cp
***sn*-2**	16?	n

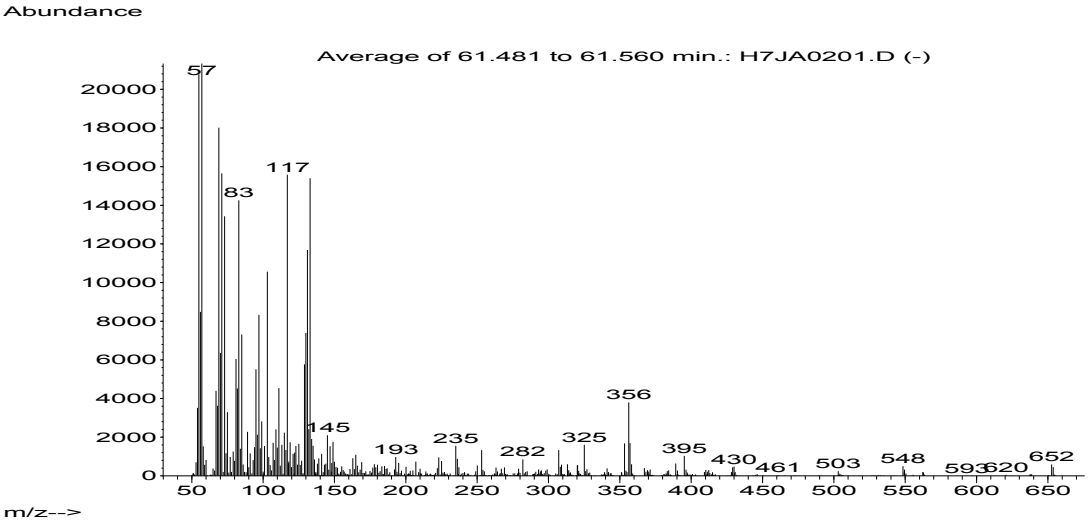

ID	authentic standard	
RI	3721	
M^+	612	C35
***sn*-1**	16	n
***sn*-2**	16	n